12-2023

Nanobubble Technology for the Removal of MIB and Geosmin From Drinking Water

Meryem Soyluoglu
Clemson University, msoyluo@g.clemson.edu

NANOBUBBLE TECHNOLOGY FOR THE REMOVAL OF MIB AND GEOSMIN FROM DRINKING WATER

A Dissertation

Presented to

the Graduate School of

Clemson University

In Partial Fulfillment

of the Requirements for the Degree

Doctor of Philosophy

Environmental Engineering and Earth Sciences

by

Meryem Soyluoglu

December 2023

Accepted by:

Dr. Tanju Karanfil, Committee Chair

Dr. Alex Chow

Dr. Cindy M. Lee

Dr. Onur G. Apul

ABSTRACT

The presence of taste and odor (T&O) compounds in drinking water has been historically a major challenge for water utilities. They are difficult to remove using conventional water treatment processes, a combination of coagulation, flocculation, sedimentation, filtration, and chlorination. However, activated carbon (AC) adsorption, advanced oxidation processes, and biofiltration can be effective. The seasonal nature of T&O events makes it difficult to justify installing dedicated treatment technologies. Additionally, incorporating these technologies into existing water treatment plants can be expensive and require significant upgrades. Therefore, water utilities are always interested in exploring new approaches to minimize the occurrence and removal of T&O compounds in drinking water.

Nanobubbles (NBs) can provide innovative solutions to T&O problems in water supplies and water treatment. The main objectives of this dissertation were to conduct a comprehensive investigation to systematically examine (i) the characterization and stability of oxygen and ozone NBs in typical freshwater and drinking water treatment conditions and ii) the removal efficiency and mechanisms of geosmin and 2-methylisoborneol (MIB), the major and most common T&O compounds in freshwaters, by NBs.

First, the stability of oxygen NBs was investigated under the representative key natural water chemistry conditions and constituents, including pH, Ca^{2+}, Na^{+}, natural organic matter (NOM) and temperature. The half-lives of oxygen NBs followed the order

Ca^{2+} < Na^{+} < pH 3 < high $SUVA_{254}$ NOM < pH 5 < 30 ˚C. Calcium was the most influential parameter significantly decreasing NBs levels among all parameters investigated. The main disappearance pathway of the negatively charged oxygen NBs in water was found to be coalescence, which was promoted greatly by cations (i.e., Ca^{2+}, Na^{+} and low pH) and adsorption of NOM with high aromaticity onto the surface of oxygen NBs. The impact of higher temperatures became more noticeable after longer storage periods, where higher temperatures increase the kinetic energy of oxygen NBs, making them more likely to collide and coalesce. Therefore, when oxygen NBs are released or used in freshwater, high calcium, high $SUVA_{254}$ NOM, and low pH would significantly reduce their availability and residence times.

Second, removal of geosmin and MIB from water by oxygen NBs was investigated. Initially, comparisons of nitrogen, air, and oxygen NBs showed higher removal percentages of geosmin and MIB as the oxygen content in NBs increased. Using oxygen NBs, volatilization was the dominant mechanism for the removal of geosmin (~40%) and MIB (~20%), while oxidation by reactive oxygen species (ROS) brought additional removal of up to 15%. The formation of hydroxyl (•OH) radicals was promoted when NBs were mixed with microbubbles (MBs). Formation of singlet oxygen and superoxide radicals did not appear to play a role for removal of target compounds by oxygen NBs. Alkalinity decreased the removal percentages of both geosmin and MIB by scavenging •OH radicals and inhibiting the oxidative removal pathway, while pH in the range of 3 to 10 had no significant impact on the geosmin and MIB removal. Geosmin and MIB removals were higher at higher temperatures due to increased volatilization and oxidative

processes, where they decreased in the presence of either NOM or hardness. Under all tested conditions, geosmin removal efficiency was consistently higher than MIB due to the difference in their physicochemical properties (i.e., hydrophobicity or Log Kow, Henry's law constant, functional groups, and steric hindrance of the MIB structure). Overall, the use of oxygen NBs resulted in less than 15% enhancement in removal of geosmin and MIB through the oxidative pathway.

Third, the characterization of ozone NBs, their stability and •OH radical formation from ozone decomposition were examined under freshwater conditions. Ozone NBs were more stable than oxygen NBs because of their higher negative surface charge (i.e., −32.0 mV and −23.6 mV, respectively). Ozone NBs generated at a higher dissolved ozone concentration (12.5 mg/L) exhibited greater stability (and higher negative surface charge) than those generated at a lower dissolved ozone concentration (1 mg/L) during long-term storage, which showed that ozone NBs generation conditions affect their stability and physicochemical properties. The stability of ozone NBs (generated at 12.5 mg/L dissolved ozone) were investigated under different pH, NOM, alkalinity, calcium, and temperature of freshwater conditions, for an extended storage time (i.e., 255 days). The half-lives of ozone NBs followed the order of 3 mM Ca^{2+} < pH 3 < high $SUVA_{254}$ NOM (4.1 L/mg.m) < pH 7 < pH 9, while the effects of carbonate (or alkalinity) and temperature on the stability of ozone NBs were insignificant. Thus, ozone NBs would be stable for up to several months in natural waters depending on the water hardness and aromaticity of NOM. The formation of •OH radicals in ozone NBs solutions was 2 – 3 times higher than conventional ozonation during the same reaction time. A rapid disappearance of ozone NBs in the presence of 3

mM Ca^{2+} led to almost no additional •OH radical formation and the overall concentration of •OH radicals in that solution was comparable to conventional ozonation. The presence of carbonate ions lowered the formation of •OH radicals, but it was not enough to stop the continuous generation of radicals. However, NBs concentrations were not affected by the presence of carbonate in the background water.

Fourth, the removal efficiencies of geosmin and MIB were investigated by ozone NBs and compared side-by-side with conventional ozonation. The primary mechanism of geosmin and MIB removal by both conventional ozonation and ozone NBs was oxidative degradation via •OH radicals. Ozone NBs were more effective at removing geosmin and MIB (i.e., 80% and 73%, respectively) than conventional ozonation (i.e., 69% and 54%, respectively) in a 10-minute contact time at 20°C in distilled and deionized (DDI) water, which was due to the higher •OH radical formation in ozone NB water. Furthermore, in natural waters, ozone NBs maintained its performance with 85% and 74% removal of geosmin and MIB, respectively, which is more than 10% higher than conventional ozone at 20 °C. Increasing temperature from 20 to 30 °C enhanced the removal efficiencies of geosmin and MIB for ozone NBs (i.e., up to 15 %) and conventional ozonation (up to 6%) in DDI and natural waters. Reducing the initial ozone dose from 1.0 (O_3/DOC= 0.43 mg/mg) to 0.5 mg/L (O_3/DOC= 0.22 mg/mg) at 20 °C widened the gap in removal efficiencies (i.e., up to 20%) between ozone NBs and conventional ozonation in natural water, demonstrating that the effectiveness of ozone NBs was less impacted by lowering the ozone dose. This can be explained by the presence of the same amount of ozone NBs in solutions for 0.5 and 1.0 mg/L ozone even though ozone level was reduced. While the

addition of calcium (300 mg/L as $CaCO_3$) reduced the ozone NBs concentration, it did not impact the geosmin and MIB removal by ozone NBs. On the other hand, the presence of background alkalinity (250 mg/L as $CaCO_3$) decreased the removal efficiencies of geosmin and MIB, but its impact on ozone NBs (i.e., 7-10%) was less than conventional ozonation (11-13%). Lastly, bromate formation in the presence of 250 µg/L bromide was not significantly different between ozone NBs and conventional ozone, and the bromate level was below the USEPA regulatory limit of 10 µg/L. The results showed that the use of ozone NBs is more efficient and performs better than conventional ozonation during water treatment, which will reduce the cost and the environmental impact of the treatment process.

Overall, this research showed that oxygen NBs will be more effective for oxygen transfer applications (e.g., aeration) especially in low hardness waters with long term stability of oxygen NB, while the oxidative capabilities of oxygen NBs are rather much less important due to lower amount of ROS (mainly •OH) formation. On the other hand, ozone NBs, with their •OH formation, are more effective in the abiotic degradation of organic compounds than conventional ozonation. Ozone NBs, depending on the generation conditions, carry a higher negative surface charge than oxygen NBs, giving them longer stability in water, except increasing calcium levels significantly reduce both NBs stability.

DEDICATION

I dedicate my dissertation

To my family...

ACKNOWLEDGMENTS

I would like to express my deepest gratitude to my dissertation advisor, Dr. Tanju Karanfil for his guidance, support, and mentorship throughout this journey. I would also like to thank my committee members, Dr. Alex Chow, Dr. Cindy M. Lee, and Dr. Onur G. Apul, for their valuable feedback and support.

My sincere thanks to Dr. Daekyun Kim and Dr. Yeakub Zaker for their help and support throughout my PhD studies.

I am also grateful to the Water Research Foundation for providing financial support for my research.

Finally, I would like to thank my family and friends for their love and support throughout this journey. I am especially grateful to my parents, Canan and Mustafa Mete Soyluoglu, and sisters, Seda Bahar and Damla Soyluoglu, for always believing in me. I am especially grateful to Cagri Utku Erdem, for being my biggest cheerleader. I could not have done it without them.

Last but not least, I would like to thank all EEES staff for their help and friendship.

TABLE OF CONTENTS

LIST OF TABLES

LIST OF FIGURES

CHAPTER 1

INTRODUCTION

1.1. Introduction and Motivation

Nanobubbles (NBs) are spherical packages of gas within liquid that are operationally defined as having diameters less than 1000 nm, though typically, the average size is around 100 nm (Atkinson et al., 2019). Recently, superior characteristics of NBs (improving the mass transfer in the gas-liquid interface, stability up to a couple of weeks, forming reactive oxygen species (ROS) with high oxidative potential) have been suggested to promise great potential for addressing a variety of challenges in water treatment (Atkinson et al., 2019; Temesgen et al., 2017). Application of NBs in water treatment processes has gained significant attention in recent decades (Atkinson et al., 2019). Various lab-scale studies have tested their potential for aeration in biological water treatment, water disinfection, membrane defouling, and groundwater and sediment remediation (Ahmed et al., 2018a; Lyu et al., 2019; Wang et al., 2021; Xue et al., 2022; S. Zhou et al., 2022; Zhu et al., 2016). These studies aimed to downsize facilities and reduce operational time and operational and maintenance costs of water-treatment plants, while achieving greater contaminant removal efficiency.

The stability and reactivity of NBs depend on several factors, such as the bubble size, zeta potential, and interfacial characteristics (Calgaroto et al., 2014; M. Chen et al., 2020; Sun et al., 2016; Temesgen et al., 2017; Zhang et al., 2020). NBs characteristics also highly depend on solution properties, infilled gas type, and the energy provided to the system to generate NBs (Meegoda et al., 2018). Solution properties such as temperature, pressure, ion type, ion concertation, pH, presence of organic matter or impurities, presence of surfactants, and saturated

gas concentrations play an important role (Ahmed et al., 2018b; Bui et al., 2019; Guo et al., 2019; Temesgen et al., 2017). The infilled gas type and its solubility and reactivity can also impact the properties of NBs (Guo et al., 2019; Jadhav and Barigou, 2020; Meegoda et al., 2018).

Recently, a few studies have evaluated the possibility of scaling up from bench-scale to full-scale and application of NBs to an industrial level. The successful integration of NBs technology into drinking water treatment can lead to a technological revolution by significantly improving the efficiency of micropollutant abatement and membrane fouling control, downsizing treatment facilities, and reducing operational times and costs. However, our current knowledge of NBs applications in drinking water treatment is very limited. The influence of complex water composition in various types of freshwaters on the generation and stability of NBs is not well-known.

One area of drinking water treatment that is worth considering is the removal of taste and odor (T&O) compounds due to several factors. These factors include the increasing prevalence of T&O compounds in natural water sources, heightened public concerns regarding drinking water safety, and the inherent challenges associated with removing these compounds from water (Mustapha et al., 2021a). Algal blooms are an issue for the world's water supply because they frequently occur in freshwater and marine environments (Chapra et al., 2017; Paerl et al., 2018). Concentrations of algae in large reservoirs in the U.S. are likely to rise due to climate change-induced water temperature increases and nutrient loading, further intensified by population growth. This phenomenon, known as algal growth, raises significant ecological and water quality concerns (Botana, 2016; Chapra et al., 2017; Ger et al., 2014; Lehman et al., 2017; Lewitus et al., 2012; Lürling et al., 2017; Mustapha et al., 2021a; Wells et al., 2015; Wickham et al., 2019). During an algal bloom, two semi-volatile compounds, 2-methylisoborneol (MIB) and geosmin, are released

from cyanobacteria (blue-green algae) cells (Jüttner and Watson, 2007; Kim and Park, 2021a; Mustapha et al., 2021a; Watson et al., 2008; Wert et al., 2014). These compounds have a very strong earthy taste and odor with very low odor threshold concentrations (OTCs) from 4 to 20 ng/L (Antonopoulou et al., 2014; Watson et al., 2008). The resulting taste and odor problems in drinking water are perceived as safety concerns by the public.

NBs technology can offer a cost-effective non-reagent approach that generates reactive oxygen species (ROS), including hydroxyl radicals (•OH), superoxide anion radicals (O_2^-), and singlet oxygen ($^1O_2$), during the process of NBs collapse (Liu et al., 2016). These reactive species are characterized by high reaction rate constants with MIB/geosmin. For example, measured rate constants for the reactions with hydroxyl radicals were between 3×10^9 and 10^{10} $M^{-1}s^{-1}$, while the reaction rate constants for MIB and geosmin with ozone were 0.10 ± 0.03 and 0.35 ± 0.06 $M^{-1}s^{-1}$, respectively (Peter and von Gunten, 2007). Oxygen and ozone delivered by NBs can generate a higher concentration of free radicals compared to conventional methods, effectively enhancing the removal of MIB and geosmin from water. In addition, as semi-volatile compounds, MIB and geosmin can be removed through volatilization.

Clearly, the combination of oxidation and gas transfer processes indicates the viability of emerging NBs technology as an alternative treatment option for removing MIB and geosmin from drinking water. However, there is currently no research on the topic in literature. Additionally, previous studies have reported promising results for the removal of organic contaminants (i.e., polyvinyl alcohol, phenol, oxytetracycline, grease etc.) using NBs or microbubbles for ROS generation (Li et al., 2009; Takahashi et al., 2007; L. Wang et al., 2020; Wu et al., 2021). The effectiveness has yet to be evaluated for generated ROS under the influence of various types of freshwaters with complex matrices.

1.2. Research Objectives

The main objective of the research is to investigate the NBs technology for water treatment applications. The investigation is especially important to address the increasing challenges of water scarcity and treatment technologies without high chemical demand. The hypotheses, objectives and approaches of four phases of this study were

Hypothesis 1: The stability, size distribution, and zeta potential of oxygen NBs will exhibit significant changes over time under varying natural water conditions. Understanding the behavior of oxygen NBs in drinking water conditions will facilitate their application in various water treatment processes.

Objective 1: Systematically examine the stability of oxygen NBs under various conditions which are closely related to a typical freshwater or drinking water treatment.

Approach 1: The change of NBs concentration, size distribution and zeta potential changes in time was observed under various natural water conditions (e.g., soft and hard water, organic matter with a low and high specific ultraviolet absorbance ($SUVA_{254}$), pH, temperature, ionic strength, and the presence of an oxidant) during the study. Also, the formation of hydroxyl radical (•OH) was investigated using disodium terephthalate which forms fluorescent adducts with •OH in the presence of oxygen NBs under the selected conditions.

Hypothesis 2: The removal of geosmin and MIB from drinking water using oxygen NBs will be significantly influenced by NB generation conditions (i.e., gas types and flowrates) and natural water background parameters (i.e., pH, DOC, $SUVA_{254}$, etc.).

Objective 2: Investigate (i) the removal efficiency of geosmin and MIB by oxygen NBs under various conditions (e.g., gas flowrate, gas type, pH, alkalinity, hardness, and temperature)

in DDI water and natural water matrices, and (ii) the removal mechanisms of geosmin and MIB from water using oxygen NBs.

Approach 2: To explore the effect of NBs' generation conditions; oxygen, air and nitrogen gas were used for the removal of geosmin and MIB. The effect of natural water background parameters was tested at their low and high levels to evaluate the efficiency of oxygen NBs' performance under various conditions. Finally, the removal mechanisms of geosmin and MIB were examined for volatilization and oxidation with different radical scavengers.

Hypothesis 3: Water quality parameters of natural waters such as pH, hardness, alkalinity, NOM, and temperature will impact the stability and radical formation of ozone NBs. Understanding such phenomena will be critical for the applications of ozone NBs in natural waters and engineered treatment systems.

Objective 3: Investigate the characteristics and effects of key water chemistry parameters in freshwaters (e.g., pH, natural organic matter (NOM), carbonate, calcium, and temperature) on the stability of ozone NBs for a relatively long storage period (i.e., 255 days) and ozone decomposition rate.

Approach 3: Various parameters and their values were carefully selected since ozone is reactive and unstable in water. The concentration, size, size distribution and surface charge of ozone NBs was monitored during the NBs storage time. Also, decomposition of ozone and formation of •OH radicals were examined under different conditions and compared by conventional ozonation.

Hypothesis 4: Ozone NBs, with their longer stability in water and higher •OH radical formation, will be more effective than dissolved ozone to remove MIB and geosmin during water treatment.

Objective 4: Investigate the removal efficiency of geosmin and MIB in DDI and natural waters under various conditions by ozone NBs and a side-by-side comparison with conventional ozone application. Also, mass transfer of ozone was investigated and compared with conventional ozone application.

Approach 4: To explore the effectiveness of ozone NBs on geosmin and MIB removal in DDI and natural water, various conditions were tested and compared side by side with conventional ozonation. The effect of temperature, alkalinity, and hardness on the ozone decomposition, and geosmin and MIB removal performance were evaluated. Ozone doses were determined based on the background organic matter level in natural water experiments to further evaluate the effect of ozone NBs and comparison with previous studies.

CHAPTER 2

LITERATURE REVIEW

2.1. Nanobubbles Generation and Characteristics

NBs are microscopic gas-filled spheres with a diameter less than 1000 nm, typically around 100 nm in size (Atkinson et al., 2019). The study of bubbles and their behavior has been ongoing since the early 1900s, but the concept of NBs was first proposed to explain the under-predicted attractive forces observed between hydrophobic surfaces in water in the 1990s (Alheshibri et al., 2016; Hansen et al., 2023). However, the existence of NBs cannot be explained by the classic Laplace pressure bubble catastrophe theory because decreasing the size of fine bubbles below the water surface leads to high internal pressure inside the bubbles, which is directly proportional to the bubble's diameter (Alheshibri et al., 2016; Attard, 2014; Manning, 2020; Matsumoto and Tanaka, 2008; Zhou et al., 2021). The relationship between pressure and diameter is expressed by the Young–Laplace equation (Equation 2.1):

$$P=P_L+\frac{4\sigma}{d_b} \qquad \text{Equation 2.1}$$

where P is the gas pressure, P_L is the liquid pressure, σ is the surface tension of the liquid and d_b is the bubble diameter. According to Equation 2.1, the inside pressure of NBs would be very high, and thus the NBs lifetime should be short. For example, a microbubble with diameter (db) of 1 μm has a ΔP ($=P-P_L$) of 1.4 bar, while a NBs with a db of 10 nm has a ΔP of 140 bar (Agarwal et al., 2011; White et al., 2011). Thus, NBs should not exist. The existence of these NBs has remained a topic of debate for several years, which creates a discrepancy with experimental results. To further explain the NBs formation and stability, some modifications to the Young-

Laplace equation focus on the higher-order curvature terms (Equation 2.2) and electrostatic force (Equation 2.3) (Yildirim et al., 2022).

$$\Delta p = \frac{2\gamma}{R} - \frac{C}{R^2} \qquad \text{Equation 2.2}$$

where Δp is pressure differences between inside and outside of bubbles, γ is the surface tension, R is the principal radii of curvature of the liquid–gas interface, and C is the curvature coefficient. The equation is second order, and, as stated above, higher curvature terms can be added. More terms can be added to the right-hand side of the equation.

$$\Delta p = \frac{2\gamma}{R}\left(1 - \frac{\delta_e^3}{R^3}\right) \qquad \text{Equation 2.3}$$

where $\delta_e^3 = n^2e^2/64\pi^2\varepsilon_0\varepsilon$

where n is the number of elementary charges (e) on the surface of the NBs, ε_0 is vacuum permittivity, ε is the dielectric constant of the liquid (Manning, 2020; Yildirim et al., 2022)

Tyrrell and Attard (2002) obtained the first image of nanoscale bubbles using atomic force microscopy and proving experimentally the existence of NBs. Since then, the research about NBs has gained gradual interest, and significant research attention has been devoted to the fundamental characterization of NBs, including their generation processes and physicochemical surface properties (Lyu et al., 2019).

Apart from their unique size, NBs also differ from other types of bubbles in terms of their longevity, negative surface charge, low buoyancy, high gas solubility, and capability to generate free radicals (Temesgen et al., 2017; Yasui et al., 2018). Indeed, the characteristics of the novel NBs technology (i.e., an improved mass transfer in the gas-liquid interface, stability up to a month, formation of negatively charged surface, high oxidative potential reactive oxygen species) indicate

a great potential for applications in water treatment (**Figure 2.1**) (Atkinson et al., 2019; Temesgen et al., 2017).

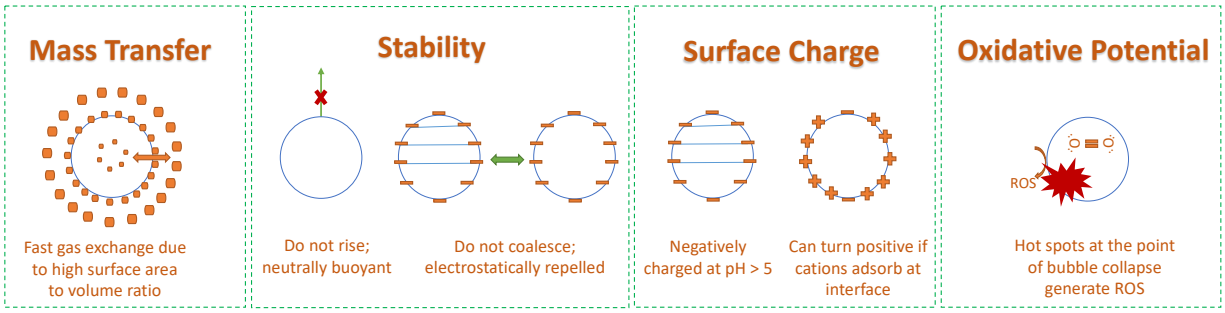

Figure 2.1.Unique physicochemical characteristics of NBs (adapted from Atkinson et al., 2019).

2.2. Application of NBs in Water Treatment

2.2.1. Production of ROS for abatement of micropollutants

NBs technology can offer a cost-effective nonreagent approach that generates numerous reactive oxygen species (ROS), including hydroxyl radicals (•OH), superoxide anion radicals (O_2^-), and singlet oxygen ($^1O_2$), during NBs collapse. Liu et al. 2016 showed using a sensitive fluorescent probe, 3'-p-(aminophenyl) fluorescein, that without any stimuli (such as H_2O_2, metals, etc.), NBs water continually produced ROS. The collapse of NBs was used to explain the formation of free radicals characterized by electron spin resonance (ESR) spectra (Minamikawa et al., 2015). Various species of ROS, such as superoxide anion radical ($O_2•^-$), hydrogen peroxide (H_2O_2), hydroxyl radical (•OH), and singlet oxygen ($^1O_2$) were identified in oxygenated NBs water (Liu et al., 2016). However, in another study (Li et al., 2009), it was indicated that the concentrations of free radicals were too low to react with some contaminant; spiking the water with H_2O_2 and some metal catalysts increased •OH formation in the NBs systems. For example, the collapse of oxygen

microbubbles under acidic conditions was observed to enhance both the generation of •OH and the degradation of the refractory compound, polyvinyl alcohol (Li et al., 2009).

2.2.2. Enhanced mass transfer for aeration

Aeration plays a major role in delivering oxygen, which is an important life-sustaining component for aquatic species and a biochemical reaction substrate in the aerobic environment (Temesgen et al., 2017). In gas–liquid reactors, mass transfer can be characterized by measuring the volumetric mass transfer coefficient, as it is an important parameter for evaluating the performance of the aeration system and aeration tank (Bouaifi and Roustan, 1998). It is the product of the liquid mass-transfer coefficient "k_l" and the interfacial surface area "a" (Temesgen et al., 2017). The liquid mass-transfer coefficient is a function of the turbulence and liquid parameters. The interfacial area depends on the size distribution of the bubbles, which is a function of the gas flow rate, sparger and nozzle design, shear rate, fluid properties (liquid viscosity and gas density), and other design and operating parameters (Temesgen et al., 2017).

Enhanced mass transfer using air or oxygen NBs results in the improvement of biological matter degradation and microbial growth rate. In conventional wastewater treatment systems, mechanical aerators or diffusers, which are typically used, require high electrical input and frequent mechanical maintenance, resulting in high operating costs. Therefore, oxygen NBs can enhance aeration efficacy and reduce operating costs. For example, an investigation on the aeration of groundwater by NBs showed that the mass transfer rate of oxygen to the water was 125 times faster than the macro bubbled water (H. Li et al., 2014).

2.2.3. Application of ozone NBs

The application of ozone for disinfection and oxidation of drinking water is used worldwide due to its effectiveness in the inactivation of microorganisms, the removal of organic pollutants, and taste and odor control (von Gunten, 2003a). Ozone is a selective oxidant, and reaction rate constants between ozone and some refractory pollutants (e.g., MIB and geosmin) are relatively low (Peter and von Gunten, 2007; Westerhoff et al., 2006). During the ozonation process, the ozone molecule can also react with hydroxide to produce •OH radicals, which are the strongest non-selective oxidant in water treatment (von Gunten, 2003a).

As an oxidative gas, the application of ozone into water treatment is limited by the mass transfer from gas to liquid phase. The diffusion of gas into water depends on several factors, such as gas solubility, temperature, gas concentration, solution pressure, and internal gas pressure. At 25 °C, ozone solubility in water is 109 mg/L, which is thirteen times greater than oxygen (von Sonntag and von Gunten, 2012). However, when ozone gas is supplied as micro- and macrobubbles, the bubbles can rapidly leave the solution due to high buoyancy. The result is a short contact time for dissolution in water. In contrast, ozone NBs remain in the solution much longer than micro- and macrobubbles due to the low buoyancy of NBs. Experimental results and theoretical calculations show that the use of NBs leads to faster diffusion and higher ozone concentration compared to the use of conventional bubbles (Batagoda et al., 2019). Therefore, ozone NBs technology is expected to reduce the operational cost for ozone applications.

The enhanced mass transfer caused by ozone NBs means that the high ozone concentration in the liquid phase may lead to elevated levels of •OH radicals formed from the decomposition of ozone (Temesgen and Han, 2021). Ozone micro-nanobubbles/nanobubbles (MNBs/NBs) have been investigated for the i) remediation of contaminated sediments and groundwater (Aluthgun

Hewage et al., 2021; Batagoda et al., 2019; Hu and Xia, 2018; Meegoda et al., 2017; Meegoda and Batagoda, 2016; Xia and Hu, 2015), ii) removal of model compounds and micropollutants in water and wastewater (Batagoda et al., 2018; Fan et al., 2021a, 2020; Farid et al., 2022; Hashimoto et al., 2021; Hutagalung et al., 2023; Jiang et al., 2018; Kim et al., 2021; Kwon et al., 2020; Lee et al., 2023; Maie et al., 2022, 2020; Menendez and Flores, 2017; Pal et al., 2022; Ponce-robles et al., 2023; Sakr et al., 2022; Salguero and Flores, 2017; Tekile et al., 2017; Wei et al., 2023; Wu et al., 2022; Xia and Hu, 2018; Xie et al., 2023; Y. Zhou et al., 2022; Zhu et al., 2022), iii) reduction of bacterial pathogens and disinfection in freshwater, wastewater and aquaculture system (Benazir Abate and Flores, 2017; Cruz and Flores, 2017; Dien et al., 2022; Epelle et al., 2022; Huang et al., 2023; Jhunkeaw et al., 2021, 2020; Linh et al., 2022, 2021; Ng et al., 2023; Nghia et al., 2022; Saijai et al., 2019; Seridou and Kalogerakis, 2021; Yang et al., 2023), and iv) antimicrobial effectiveness on fresh vegetables (He et al., 2015; Ushida et al., 2017). More than 50 peer-reviewed articles on various applications of ozone MNBs or NBs were reviewed and summarized in **Table A1**. NBs generation and characterization methods, stability of ozone NBs, ROS characterization and quantification, and comparisons of conventional ozone with ozone MNBs/NBs were summarized based on publications between 2011 and 2023 in **Table A1**.

The studies employed a variety of MNBs/NBs generators, including venturi-type, ultrasonication, nozzle, orifice plate, and membrane-based generators (Agarwal et al., 2011; Aluthgun Hewage et al., 2021, 2020; Batagoda et al., 2019; Hutagalung et al., 2023; Jhunkeaw et al., 2021; Maie et al., 2020). Information that is missing from the literature includes Information on the operational conditions, limitations of the technologies, commercial availability, feasibility to apply in a full-scale treatment, and ozone resistance of generators it is crucial to have that type of information for a comprehensive understanding of ozone NB technology.

Additionally, NanoSight (NS300, NS500, or LM-10), Delsa™ Nano C, microscopy, ZetaView and Zetasizer were the most commonly used instruments to characterize bubble size, concentration, and size distribution (Agarwal et al., 2011; Aluthgun Hewage et al., 2021, 2020; Batagoda et al., 2019; Cruz and Flores, 2017; Epelle et al., 2022; Farid et al., 2022; Hashimoto et al., 2021; Hu and Xia, 2018; Jhunkeaw et al., 2020, 2021; Lee et al., 2023; Maie et al., 2022; Xia and Hu, 2018; Zhu et al., 2022). While NanoSight instruments can also measure bubble concentration, the Zetasizer used in the reviewed studies were only capable of measuring bubble size. Another important characteristic of bubbles is their surface charge, which was monitored using Zetasizer and Delsa™ Nano C, using the technique of dynamic light scattering (DLS), in previous studies.

Furthermore, the concentration change in time or longer-term stability of ozone NBs was not investigated in any of the studies reviewed. Only one study monitored the stability of ozone NBs in ultrapure water at pH 7-7.5, and the longest storage time was 14 days (Farid et al., 2022), suggesting that the stability of ozone NBs in natural water conditions is not well understood and requires further research.

The most important factor to consider when studying ozone is how many •OH radicals are created in the NBs solution. The factor is crucial because •OH radicals are highly reactive and can be used to disinfect water and degrade organic pollutants. However, only a few studies detected •OH radicals in ozone NBs applications. The radicals were detected using electron paramagnetic resonance (EPR), para-chlorobenzoic acid (pCBA), fluorescent probes, or formaldehyde capture methods. While EPR only showed the signal in the presence of radicals (without identification or quantification), degradation of pCBA was used to calculate •OH radical exposure in some of the studies. Additionally, formaldehyde and 7-hydroxycoumarin production was used to estimate •OH

radicals in ozone NBs studies. However, assumptions, limitations, and the effects of environmental and experimental conditions were not clarified for the measurement of •OH radicals. Since •OH radicals are the most significant nonselective strong oxidant in ozone applications, their determination and quantification should be a top priority for ozone NBs researchers. Therefore, further investigation and development are still needed in the area.

Ozone NBs technology offers several advantages over conventional ozonation, including higher ozone solubility, enhanced mass transfer, and improved disinfection and oxidation efficiency, according to current theoretical information and experimental results from some studies. However, there is no comprehensive understanding of the various effects of environmental and operational conditions on the performance of ozone NBs. Therefore, side-by-side comparisons are needed to evaluate the advantages and limitations of ozone NBs over conventional ozone and ozone with macro- or microbubbles. Although some studies in the review showed the performance of ozone NBs, they did not compare it with conventional ozonation for the removal of target compounds (Batagoda et al., 2019; Hu and Xia, 2018; Jhunkeaw et al., 2021, 2020; Maie et al., 2020). For these reasons, there are knowledge gaps in the literature to comprehensively understand and apply ozone NBs technology for various areas.

The following topics need to be investigated and addressed for a fundamental understanding of ozone NBs:

- **Characterization and stability of ozone NBs:** The effect of each parameter on the behavior of ozone NBs should be investigated individually because it will provide valuable insights into the underlying mechanisms. For example, understanding how ozone NBs interact with different types of organic matter and inorganic particles in water will be crucial for optimizing their performance in natural water applications. By thoroughly

characterizing and understanding the behavior of ozone NBs, researchers and engineers can develop more effective and efficient ways to use them for water and wastewater treatment. Such knowledge could lead to significant improvements in water quality and public health.

- **Measurement of ozone NBs in natural water:** New methods must be developed to measure ozone NBs in real water conditions with background particles, which is essential for assessing the efficiency and fate of ozone NBs applications in natural water and wastewater applications.

- **Formation and quantification of ROS:** The formation and quantification of ROS, especially •OH radicals, should be investigated under various conditions and compared to conventional ozone under the same experimental conditions. Since there is no direct measurement of •OH radicals, the current methods should be assessed, and a quantitative measurement of •OH radicals should be provided with the most accurate and appropriate methods to further evaluate the technology and its limitations.

- **Ozone mass transfer and decomposition rate:** Ozone mass transfer and decomposition rates should be tested and compared for each specific NBs generation system and conventional ozonation, as there is a lack of understanding regarding the impact of different generator types, operating pressures, and gas flowrates on ozone NBs characteristics and reactivity. Additionally, the effect of NBs concentration and size on ozone dissolution in water should be specifically investigated to assess the capacity of each system.

- **Effect of experimental and environmental conditions:** The experimental and environmental conditions for each experiment should be clearly defined, as ozone is highly

sensitive to changes in water parameters. The information will facilitate comparisons between studies and generate novel ideas for future research objectives.

- **Assessment of ozone NBs performance in natural water with real water pollutants:** The removal of target compounds by ozone NBs in ultrapure water is not a representative study to assess the limitations or advantages of the technology. Testing ozone NBs in real water with background organic matter, alkalinity, and other constituents will demonstrate their realistic performance for further evaluation. Additionally, comparing ozone NBs to conventional ozone under the same experimental conditions will be beneficial for evaluating their performance.

- **The accurate classification of bubbles (NBs, MBs or MNBs):** NBs and MBs should be distinguished from each other, as they have different physicochemical and chemical properties. Compared to MBs, ozone NBs persisted in water for a long period of time and prolonged oxidation efficiency for the remediation of both organic and inorganic contaminants.

Fundamental understanding and application of ozone NBs technology is critical to significantly enhancing ozonation efficiency and effectiveness, reducing cost and chemical use, and providing opportunities for the development of innovative treatment approaches.

2.3. NBs Generation and Detection Techniques

Various techniques including electrolysis, ultrasonic cavitation, venturi, nozzle and diffuser system, and membranes have been used to generate NBs of different gases such as air, oxygen, nitrogen, carbon dioxide, hydrogen, or helium (Bu and Alheshibri, 2021; Favvas et al., 2021; Gurung et al., 2016; Khan et al., 2020; Pourkarimi et al., 2017; Zhou et al., 2021; Zhu et al., 2016). These systems are, in general, controlled by hydrodynamic forces, and most NBs generators are spiral liquid-flow, diffuser-nozzle, plate diffusers or membrane systems. The performance, evaluation and comparison of these techniques and their applications in freshwaters and water treatment settings are still open to discussion since most published studies have been conducted in lab-scale experiments.

One area of study that has been greatly overlooked is the ability to accurately measure NBs in natural waters in the presence of ubiquitous background particles. NBs in water can be detected using different methods: nanoparticle tracking analysis (NTA), dynamic light scattering (DLS), and electrical sensing zone (ESZ) (Ulatowski et al., 2019; Wang et al., 2019; Zhou et al., 2021). The NTA method captures the movement of all scattering particles in the solution with a field microscopy. It analyzes and differentiates bubbles that are moving due to Brownian motion with 10-1000 nm size. It has been shown that the sensitivity of DLS and ESZ is less than NTA in the presence of polydisperse particles in solution (Fan et al., 2021b; Zhou et al., 2021). Compared to DLS and ESZ, NTA provides higher resolution and sensitivity for small particles. Also, NTA has the capability to measure 10-1000 times less concentrated samples than DLS and ESZ (Fan et al., 2021b; Nobbmann, 2016). While NTA provides both the number and size of particles

in solution, DLS measures the size of particles in solution (Nobbmann, 2016). However, all these methods have a common shortcoming, the presence of background particles limits the sensitivity and accuracy of the analysis.

2.4. ROS Detection and Quantification Methods

NBs have been reported to generate various ROS, including hydroxyl radicals (•OH), superoxide anion radicals ($O_2^{\bullet-}$), and singlet oxygen ($^1O_2$). However, for ROS from ozone NBs, limited studies have been conducted.

The most significant key parameter for ozone studies is the detection and quantification of •OH radicals formed in the NBs solution. •OH radicals are highly reactive and short-lived, making direct quantification impossible. However, there are a number of indirect methods, with different chemical probes, that are used to characterize •OH radicals in ozone microbubbles (MBs) or NBs solutions [e.g., disodium terephthalate (Chu et al., 2007; Sun et al., 2020), *p*-chlorobenzoic acid (*p*-CBA) (Achar et al., 2020; John et al., 2022; Khuntia et al., 2015; Temesgen and Han, 2021; Yang et al., 2021), *tert*-butyl alcohol (TBA) (Fan et al., 2021a, 2020; Khuntia et al., 2014), and iso-propyl alcohol (IPA) (Jabesa and Ghosh, 2016)]. However, there is no literature available to characterize other reactive oxygen species in ozone MBs/NBs solution including superoxide anion radicals (O_2•−), hydrogen peroxide (H_2O_2), singlet oxygen ($^1O_2$) and carbonate radical (CO_3•).

Disodium terephthalate (TP) was used as a probe molecule for the measurement of •OH radicals (Chu et al., 2007; Sun et al., 2020) in ozone MBs solutions, which resulted in 1.29 µg/L of •OH concentration. TP produces 2-hydroxy terephthalate (TPOH) with •OH

radical which is fluorescence active. The reaction yield of TPOH has been known to be 35%, which can be used to quantify the •OH radicals in the solution (Žerjav et al., 2020).

As an indirect method, *p*-CBA has been used for the detection of •OH in ozone MBs/NBs solutions (Achar et al., 2020; John et al., 2022; Khuntia et al., 2015; Temesgen and Han, 2021; Yang et al., 2021). pCBA is used as a probe compound for hydroxyl radical exposure calculation because it has a low reaction rate constant with ozone ($k_{O_3+pCBA} \leq 0.15$ $M^{-1}s^{-1}$) but a significantly higher reaction rate constant with •OH radicals ($k_{\cdot OH+pCBA} = 5 \times 10^9$ M^{-1} s^{-1}) (Buxton et al., 1988; Fischbacher geb Jarocki, 2017; Khuntia et al., 2015; Neta et al., 1988). The formation of the •OH radical was calculated by the degradation of *p*-CBA in the solution. Using the *p*-CBA method, very low levels (i.e., nM) of •OH radicals have been reported in ozone MBs/NBs solutions. It is a promising and widely used method for conventional ozone studies, but water quality parameters can impact measurements, as ozone decay is sensitive to the presence of organic matter, alkalinity, and various pH values (Fischbacher geb Jarocki, 2017). Therefore, main conclusions should be made with caution when using the method, especially when there are significant differences in water quality.

Other radical quenchers such as TBA and IPA have also been used to quantify the ROS formation in ozone MBs solutions (Jabesa and Ghosh, 2016; Khuntia et al., 2014). In addition, a colorimetric method, where formaldehyde was produced from TBA by •OH radical oxidation, has been deployed to quantify •OH radicals in ozone MBs/NBs system (Fan et al., 2020, 2021a). However, the presence of ozone in the solution can lead to the formation of superoxide radicals, which can increase the yield of •OH radicals. Thus, in the presence of ozone, formaldehyde can be formed from other reactions besides the

reaction with •OH radicals (Fischbacher geb Jarocki, 2017; Ulanski and von Sonntag, 1999), which can lead to an overestimation of the yield of •OH radicals.

Today, there is no comprehensive study available in the literature showing the characterization and quantification of various ROS (•OH, $O_2^{\bullet-}$, and $^1O_2$) in ozone NBs systems. Electron spin resonance (ESR) spectra have been used as direct evidence of •OH radical formation (Michailidi et al., 2020; Minamikawa et al., 2015; Yamaguchi et al., 2021) but the signals of •OH radicals can be blended with other types of radicals coming from organic contaminants, thus it may be difficult to distinguish and quantify specific ROS concentrations by the method (Michailidi et al., 2020; Pei et al., 2020). Further, since ESR depends on the intensity of the adduct compound during the detection of the •OH radicals; sometimes complex reactions or false positive signals can be detected (Pei et al., 2020). The chemical instability of spin adducts makes the ESR method weak, and the commonly used spin trap, DMPO, is known to be a highly cytotoxic compound (Hosokawa et al., 2002). Moreover, sometimes complex reactions or false positive signals can be detected because of the instability of spin adducts (Pei et al., 2020). Furthermore, trapping products are continuously formed and transformed, which may change the ESR intensity. Therefore, the stability of the trapping product, reaction time, and the residual concentrations of ozone and ROS in the collected sample can have an impact on the ESR intensity. Therefore, •OH radicals' measurement with ESR method needs to be supported by other methods to quantify the formed radicals in the solution.

2.5. MIB and Geosmin Removal

Significant research efforts have been directed to control the level of MIB and geosmin in drinking water. Although conventional treatment processes, such as coagulation, sedimentation and chlorination, are ineffective for the removal of MIB/geosmin, activated carbon (AC) adsorption, advanced oxidation process, and biofiltration have been shown to be effective (Beniwal et al., 2018; Kim and Park, 2021b; Liang et al., 2007; Peter and von Gunten, 2007; Srinivasan and Sorial, 2011; Westerhoff et al., 2006; Xie et al., 2015). The seasonal nature of taste and odor manifestations precludes the installation of treatment technologies exclusively for treating taste and odor. Furthermore, the incorporation of these techniques requires retrofitting the treatment train within the water treatment facility, significantly increasing the treatment costs.

Previous studies have shown the occurrence of MIB and geosmin in surface water reservoirs worldwide due to the seasonal algal bloom, which is due to the metabolism of the *Cyanobacteria* known as blue-green algae and *Cyanophyta* (Westerhoff et al., 2005; Jüttner and Watson, 2007; Kim and Park, 2021; Watson et al., 2008; Wert et al., 2014). The maximum concentration of MIB can approach 100 ng/L in reservoirs serving as the major water supply system for Phoenix, AZ (Westerhoff et al., 2005). Another study indicated maximum concentrations of geosmin (19 ng/L) and MIB (3 ng/L) in three Swiss lakes due to their different nutrient levels from eutrophic to oligotrophic (Peter et al., 2009). Another survey of 59 drinking water treatment plants in the Great Lakes region showed that the occurrence of the two taste/odor compounds was widespread, with a significant number (20%) of utilities reporting annual outbreaks during the summer months with even

a higher number (27%) experiencing sporadic episodes (Watson et al., 2008). In addition to seasonal algal blooms, reuse of wastewater effluent can increase the input of MIB and geosmin to drinking water sources. For example, median concentrations of MIB (11 ng/L) and geosmin (27 ng/L) were reported in municipal wastewater secondary effluent (Agus et al., 2011). **Table 2.1** summarizes physico-chemical properties of MIB and geosmin.

Table 2.1. Chemical and physical properties of MIB and geosmin

Property	**MIB**	**Geosmin**	**References**
Chemical Formula	$C_{11}H_{12}O$	$C_{12}H_{22}O$	(Hafuka et al., 2019; Mustapha et al., 2021a)
Molecular Weight (g/mole)	168.28	182.31	
Density (g/cm^3)	0.929	0.949	
Solubility in water	194.5	150.2	
Hydrophobicity (Log K_{ow})	3.1	3.7	
Second order rate constant, $k_{O3}(M^{-1}\ s^{-1})$	1	7.5	(Westerhoff et al., 2006)
Second order rate constant, $k_{\cdot OH}(M^{-1}\ s^{-1})$	8.2×10^9	1.4×10^{10}	

CHAPTER 3

MATERIALS AND METHODS

In this chapter, an overall description of experimental materials and methods used in the research will be provided. Since different samples and methods were involved in different phases of the study, in each chapter there will be a short experimental materials and methods section to list the experimental matrix conducted for a particular chapter.

3.1. NBs Generation

NBs were generated in distilled and deionized (DDI) water using a commercially available NBs generator (Nano Bubble Technologies (NBT), Sydney, Australia). The NBT NBs generator has a ceramic membrane for the generation of NBs (**Figure 3.1**). A 70-L metal container was used for the NBs generating system filled with 65 L water while supplying different types of gas such as oxygen, nitrogen, air and ozone. A stainless-steel system was needed to conduct experiments with ozone. The manufacturer recommended operational parameters for the optimum gas feed pressure of 60 psi and the gas flowrate ranged from 1-10 L/min (LPM). The water flowrate was 87 L/min.

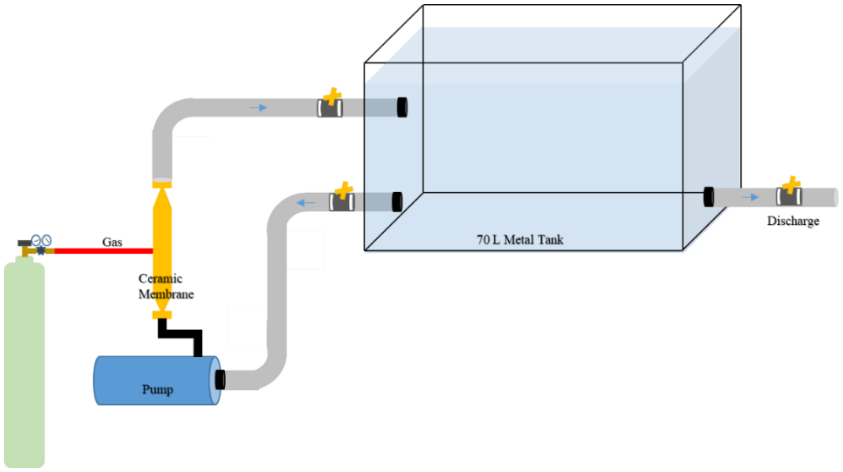

Figure 3.1. Illustration of NBs generation system

For most experiments, the NBs generator was operated for 6 hours. When the pump was turned on, a rotameter was fully closed (i.e., gas flow is zero), and suction and discharge valves connected to the water container were opened. Before injecting gas, water in the tank was circulated for about two minutes which allowed about 5 cycles of water circulation, and then the background samples (i.e., control samples at time=0) were taken from 2-3 inches below the water surface using vials rinsed with circulated water three times. Vial caps were screwed below the water surface to ensure that there was no headspace in the vials. The control samples were analyzed on a NanoSight NS300 for NBs, which is described below. After collecting the control samples, the gas supply to NBs generator was turned on. The bubble generator was run until the solution reached the gas saturation point, then samples were collected at different time intervals. Collected NBs solutions were analyzed on NS300 for bubble size and concentration. To distinguish NBs in a solution from other particles in the background water, a control sample was always

used for comparison with a sample containing NBs. In addition, to obtain a sufficient NBs density for reproducible NanoSight results, oxygen NBs samples were collected after dissolved oxygen reached the supersaturation level and water was circulated at least 10 more cycles.

3.2. Nanobubble Characterization: Particle Size Distribution

To quantify the bubble numbers and sizes, a NanoSight NS300 (Malvern Instruments Ltd., UK), which was developed based on a noninvasive technique, i.e., nanoparticle tracking analysis (NTA), was used (**Figure 3.2**). To obtain particle size distributions of samples in liquid suspension, properties of both light scattering and Brownian motion are utilized. A laser beam is passed through a prism-edged glass flat (optical flat) within the sample chamber. Green laser light with a 532 nm wavelength was used to characterize NBs during the study. NBs in the path of the beam scatter light and can be easily visualized via a long working distance (×20 magnification) microscope. A charge-coupled device (CCD), electron multiplied CCD, or high-sensitivity CMOS camera is mounted on the microscope and operated at 30 frames per second on the NSS300. The CCD or CMOS captures a video file of NBs moving under Brownian motion. Therefore, NBs can be indirectly tracked, and their Brownian motion analyzed in real time. Based on the information, size distribution and concentration of NBs from 10 nm to 2000 nm can be determined with the NS300. The NanoSight instrument works with particle concentrations in the range of ~10^7– 10^9 particles/mL, which is approximately 20–100 particles in the field of view. Camera level, focus and detection threshold are three important parameters during

the analysis. These parameters are adjusted based on the sample's characteristics. Mono vs. polydisperse samples have different behavior and characteristics.

Figure 3.2. NanoSight NS 300 (Malvern Instruments Ltd., UK).

Before determining the particle size distribution of generated NBs, the NanoSight analysis chamber was flushed with 1-2 mL of DDI water to remove any contaminants. After the flush, the syringe was carefully removed while holding the end of the injection line, and 2-3 drops of DDI water were added to the injection line connector to create a water seal that is required to prevent the introduction of larger bubbles when switching between the DDI rinse syringe and the 1 mL NBs sample syringe. If large bubbles are introduced, they would be trapped in the analysis chamber and impact the accuracy of the NanoSight analysis. Then the camera was turned on so that the view of the analysis chamber was visible on the monitor. Focus and the camera level were adjusted based on the characteristics of the sample. If the screen appeared to have significant background noise, the analysis chamber needed to be disassembled and cleaned. Finally, after adjusting

the quick or standard measurements parameters (number or captures and duration), the measurement of NBs was started.

The parameters used to characterize nano-sized bubbles are given in

Table 3.1. Longer measurements increased the accuracy and reproducibility of the data. The particle concentration standard deviation can be used as an indication of the accuracy of the NanoSight analysis. Typically, standard deviations that are less than 15% of the particle concentration are acceptable for NanoSight analysis. After measuring the samples, the analysis chamber was cleaned with DDI (or a solution of up to 10% ethanol, if needed), and then the optical flat was wiped gently with a soft dry tissue to remove any streaks from the optical surface and dried with compressed air. **Figure 3.3** shows an example of the particle size distribution and size/intensity data of NBs generated in DDI water. The highest peaks were observed around a bubble size of 100 nm.

Table 3.1. NanoSight analysis parameters

Capture Settings	
Camera Level	13 - 16
Pump Speed	25
Camera Gain	1
Number of Captures	5
Capture Duration	60 Seconds
Focus Specifications	
Camera Type	CMOS
Laser Type	Green
Slider Shutter	1300
Slider Gain	512
Temperature	Default
Viscosity	(Water)
Analysis Settings	
Threshold	9- 20
Blur size	Auto

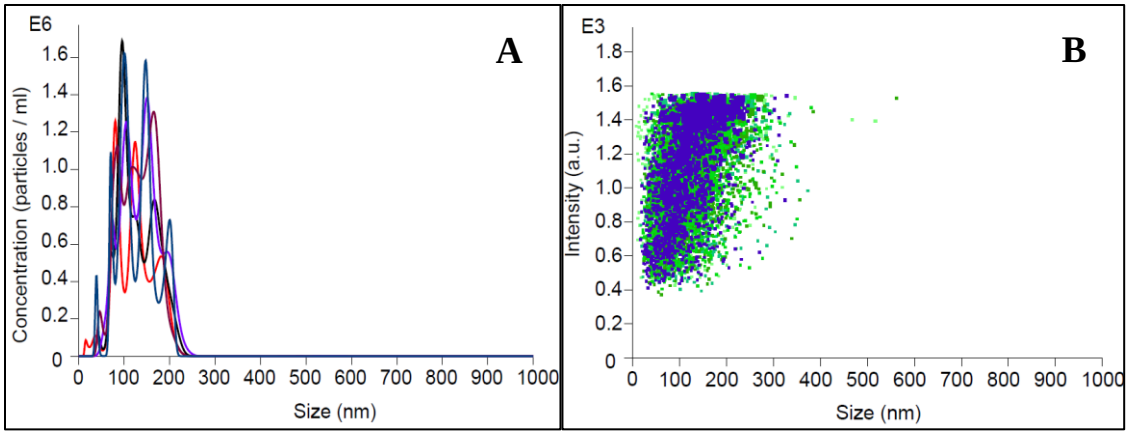

Figure 3.3. (A) Particle size distributions of NBs in the unit of million particles/mL and (B) intensity in the unit of a.u with five measurements per sample (each color representing one measurement).

To test and confirm the detectable range and reproducibility of NBs measurements using a NanoSight instrument, standard calibration solutions in the range of ~10^7– 10^9 particles/mL were prepared with highly uniform polystyrene latex spheres (100 nm), as recommended by the manufacturer, by diluting with DDI. **Table 3.2** and **Figure 3.4** show the results of calculated and measured concentrations and particle size of the latex standard particles. Nano-sized particle concentrations measured using NanoSight are linearly correlated with calculated concentrations with R^2=0.997. **Table 3.3** shows the results of reproducibility tests with 100 nm latex standard solution at 2.3 × 10^8 particles/mL. NanoSight provided relatively consistent particle concentrations for 10 repeated measurements of the same latex standard sample with about 2.3% relative standard deviation.

The background nano-sized particle level in the DDI water from the laboratory ranged from 1.6 to 2.0 × 10^7 particles/mL for multiple measurements. The concentration of NBs in my samples have always been at least 4-5 times higher than the background levels and the NBs concentrations were always determined in the study by subtracting background particles.

Table 3.2. NanoSight calibration test results conducted with 100 nm Latex standard solutions.

Calculated concentration (particles/mL)	**Measured concentration (particles/mL)**	**Mode size (nm)**	**Mean size (nm)**
2.15E+07	3.28E+07	108	138
4.30E+07	4.30E+07	119	139
8.60E+07	8.00E+07	119	135
2.15E+08	2.70E+08	107	117
4.30E+08	4.72E+08	100	107
1.08E+09	1.37E+09	97	100
2.15E+09	2.60E+09	80	83

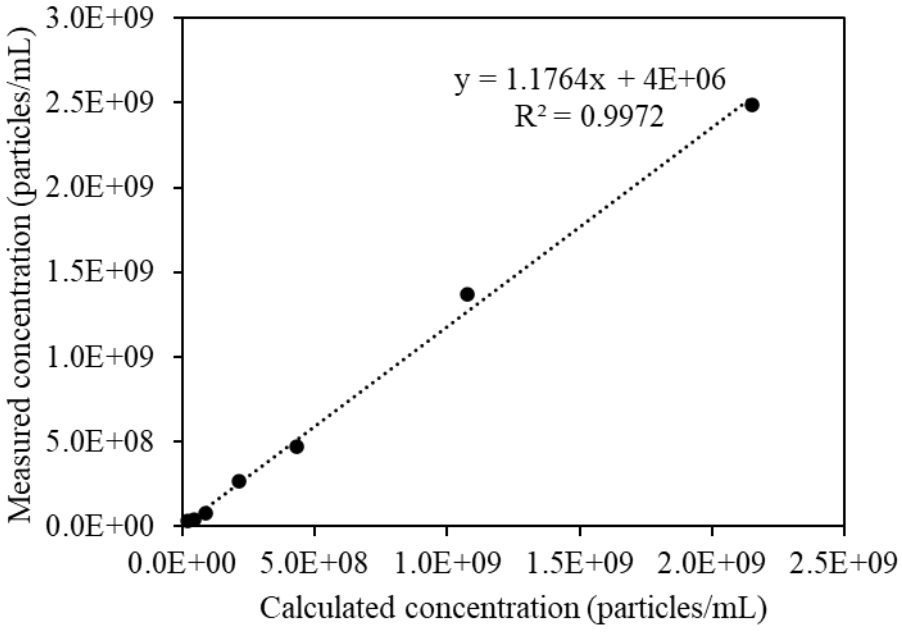

Figure 3.4. Calibration curve obtained with 100 nm Latex standard solutions.

Table 3.3. Reproducibility of the NanoSight measurement with a 100 nm Latex standard solution

Measurement number	Mode size (nm)	Mean size (nm)	Concentration (particles/mL)	Std. Dev.
1	115	125	2.49E+08	3.16E+06
2	123	133	2.38E+08	3.54E+06
3	118	130	2.30E+08	3.53E+06
4	115	130	2.33E+08	3.72E+06
5	127	134	2.37E+08	3.85E+06
6	124	134	2.34E+08	3.91E+06
7	116	131	2.33E+08	3.70E+06
8	115	131	2.36E+08	3.50E+06
9	114	129	2.39E+08	5.85E+06
10	114	129	2.42E+08	5.94E+06
Average	118	131	**2.37E+08**	
Std. dev.	4.7	2.8	**5.43E+06**	
Coefficient of variations			**2.29E-02**	
Relative std. dev. (%)			**2.3**	

3.3. NBs Characterization: Zeta Potential Measurements

To investigate the gas−water interfacial electrical charge of NBs, the zeta potential, which is the electrical potential at the slipping plane between the bulk liquid and gas, was measured using a Brookhaven 90Plus Particle Size Analyzer (**Figure 3.5**). An increase of negative zeta potential value indicated an increase in the NBs stability (Hewage et al., 2021; Meegoda et al., 2018). In general, NBs have a high zeta potential, meaning their

interaction with surrounding colloidal particles is stable compared to larger bubbles (i.e., microbubbles and macrobubbles). A fundamental zeta potential (ζ) calculation method for NBs is the application of the Smoluchowski equation (Equation 3.1) (Takahashi, 2005):

$$\upsilon_E = 4\pi\varepsilon_0\varepsilon_r \frac{\zeta}{6\pi\mu}(1+\kappa r) \qquad \text{Equation 3.1}$$

where υ_E is their mobility; ε_0 and ε_r are the relative dielectric constant and the electrical permittivity of a vacuum, respectively; μ is the solution viscosity; r is the particle radius; and $\kappa = (2n_0z^2e^2/\varepsilon_r\varepsilon_0k_BT)^{1/2}$ is the Debye–Hückel parameter; n_0 is the bulk ionic concentration; z is the valence of the ion; e is the charge of an electron; k_B is the Boltzmann constant; and T is the absolute temperature. The instrument detects the electrophoretic mobility (horizontal speed in the recorded image) of the bubble at the stationary plane in the measurement cell, and the zeta potential is then calculated from the recorded speed.

Figure 3.5. Brookhaven 90Plus particle size analyzer.

For zeta potential measurements, 1.6 mL of NBs sample was added to the sample cell and the electrodes were fully inserted into the cell. Any sample spilled over the surface

of the cell was removed with a tissue. The cable terminated connector on instrument was plugged to the connector of the electrodes and the cell was placed into the sample cell holder. Then the sliding door was closed. After adjusting measurement parameters such as pH, water type, viscosity, temperature, etc., the run time and cycle time were properly selected. Before each sample measurement, a known specific zeta potential was checked with a BI-ZR5 standard solution with a mean zeta potential value of –44 (±8) mV and conductance of 320 µS ± 10%.

3.4. Reactive Oxygen Species (ROS) Measurement

•OH radical is one of the major species that plays an important role in the degradation mechanism of NBs solutions. However, direct measurement of •OH is very difficult because of its high reactivity resulting in an extremely short lifetime (often 10^{-9} s) (Ishibashi et al., 2000). Therefore, indirect methods are often used to assess the radical's contribution in the degradation processes. In these indirect techniques, a probe molecule is added into the reaction medium as a radical trap that reacts with •OH radicals to form stable hydroxyl radical adducts detectable with a well-established method. Terephthalate or terephthalic acid (TP) is a slightly fluorescent probe molecule that yields highly fluorescent adducts upon reacting with •OH (Hirano and Kobayashi, 2016; Ishibashi et al., 2000; Page et al., 2010) as shown in Scheme 1. TP can selectively react with hydroxyl radicals in the bulk solution (Song and O'Shea, 2007).

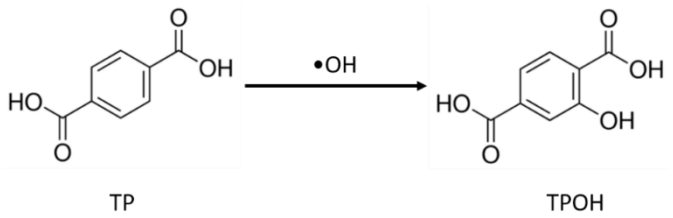

Scheme 1.TP reacts with •OH and forms fluorescent 2-hydroxyterepthalate (TPOH).

3.4.1. Measurement of •OH in liquid phase using TP trap

Disodium terephthalate was used to scavenge •OH and to produce TPOH with a percent yield of 35 % (Fang et al., 1996; Matthews, 1980; Žerjav et al., 2020). Terephthalic acid can be used also for the •OH radicals trap, but it has a low solubility in water (i.e., 0.017 g/L) at acidic and neutral pH, dissolving only at pH 10-11 (Hayashi et al., 2016; Matuszek et al., 2020). Therefore, disodium terephthalate, the dianion of terephthalic acid, was used for experiments with its higher solubility (i.e., 130 g/L) (Hayashi et al., 2016; Rezazadeh et al., 2021). In a typical experiment, 40 µL of 50 mM TP aqueous solution was transferred to a centrifuge tube and mixed with a 3.96 mL aliquot of NBs solution taken at a specific time to make 4 mL total volume for spectrofluorometric analysis. TPOH was excited at 315 nm to emit fluorescence at 425 nm, which was measured on a Shimadzu RF5301PC spectrofluorometer. The instrument was calibrated against a series of standard TPOH concentrations ranging from 1 to 1000 nM (1, 10, 50, 100, 250, 500, 750, and 1000 nM). By using the fluorescence intensity of TPOH at 425 nm, a calibration curve was plotted with a linear trendline going through the origin (**Figure 3.6**). The slope of the

equation was 0.6083 with an R^2 value of 0.9997. The calibration curve equation was used to calculate the concentration of •OH in the NBs solution.

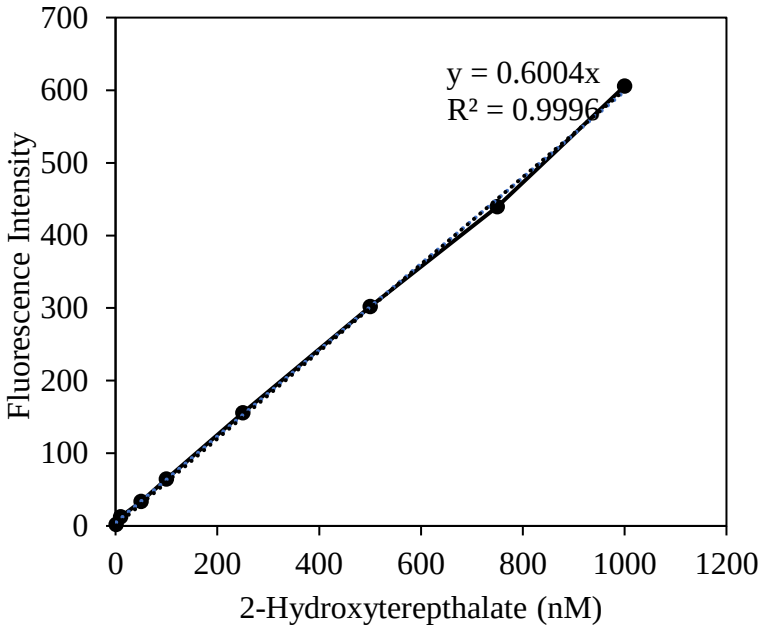

Figure 3.6. The calibration curve for TPOH, 1-1000 nM

The initial concentration at time =0 and decay of TP were measured with UV-Vis optical spectra using a Shimadzu 1800 spectrometer. The instrument was calibrated against a series of standard TP concentrations ranging from 1 to 100 μM (1, 10, 25, 50, and 100 μM). The spectra of TP are shown in **Figure 3.7** with an absorption peak at 240 nm, which is the characteristic peak for TP (Caire-Maurisier et al., 2019; Pirillo et al., 2021; Ravichandran et al., 2016).

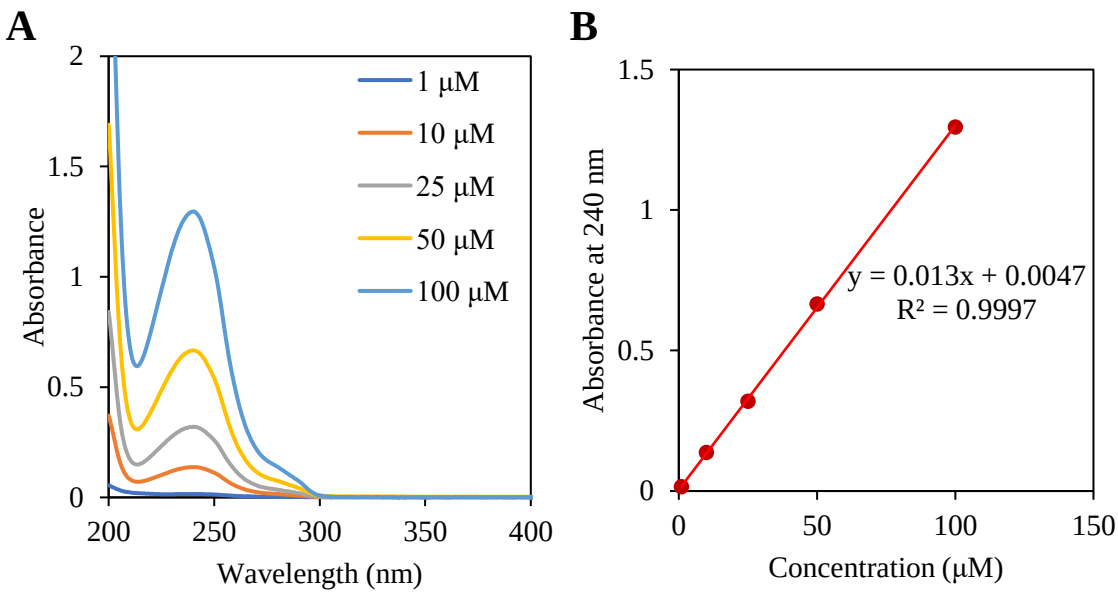

Figure 3.7. (A) UV-Vis optical spectra of TP and (B) calibration curve for TP

3.5. Other Analytical Methods and Minimum Reporting Levels (MRLs)

A summary of all other analytical methods and MRLs used in the project is presented in **Table 3.4**.

Table 3.4. Other analytical methods and minimum reporting levels

Parameter	Unit	Measurement method	Equipment	MRL or Accuracy[a]
Dissolved Organic Carbon (DOC)[b]	(mg/L)	SM[c] 5310B	TOC-V_{CHS}, Shimadzu Corp.	0.1
Dissolved Nitrogen (DN)	(mg-N/L)	High Temp. Combustion	Shimadzu TOC-V_{CHS} & TNM-1,	0.1
UV Absorbance[d]		SM 5910	Varian Carry 50	±0.004[a]
Cl^-, Br^-, BrO_3^-, NO_2^-, NO_3^-	(µg/L)	USEPA Method 300	ICS 2100, Dionex Corp.	$Cl^-/Br^-/BrO_3^-$=5, NO_3^-=10, NO_2^-=20
pH		SM 4500-H^+	VWR Symphony	±0.01[e, a]
Dissolved Oxygen (DO)	(mg/L)	Sensor method	Thermo Scientific Orion 5-Star Meter	±0.1[a]
Ozone	(mg/L)	SM 4500-O3	HACH Test Kit	0.02
Residual Free/Combined Chlorine	(mg/L)	SM 4500-Cl F	N/A[f]	0.05

[a]: as reported by the manufacturer. **[b]**: reagent grade potassium hydrogen phthalate was used to prepare external standards. Precision ranged from 0.05 to 0.15 mg/L. **[c]**: Standard Methods ("5310 Total Organic Carbon," n.d., "5910 UV-Absorbing Organic Constituents," n.d.; American Public Health Association, American Water Works Association, 2023) . **[d]**: measured at wavelengths of 254 nm using a 1 cm cell. **[e]**: Accuracy (pH units). **[f]**: Not applicable

CHAPTER 4

STABILITY OF OXYGEN NANOBUBBLES UNDER FRESHWATER CONDITIONS

4.1. Introduction

Nanobubbles are spherical packages of gas within liquid and are operationally defined as having diameters less than 1000 nm, though typically, the average size is around 100 nm (Atkinson et al., 2019). Superior characteristics of NBs to larger bubbles (e.g., improving the mass transfer in the gas-liquid interface, being stable up to a couple of weeks, and forming reactive oxygen species (ROS) with high oxidative potential) have been suggested to promise great potential for addressing a variety of challenges in water treatment in recent decades (Atkinson et al., 2019). Various lab-scale studies have tested their potential for aeration in biological water treatment, water disinfection, membrane defouling, and groundwater and sediment remediation. These studies aimed to downsize facilities and reduce operational time and maintenance costs of water-treatment plants, while achieving greater contaminant removal efficiency (Agarwal et al., 2011; Batagoda et al., 2019; Hu and Xia, 2018; Rosa and Rubio, 2018). The NBs technology has also been examined in many other sectors such as agriculture (Wu et al., 2019) and medical science (Hayakumo et al., 2014; Lukianova-Hleb et al., 2014; Yin et al., 2012).

Although NBs are attracting significant attention due to their unique physiochemical characteristics, their existence and stability have been questioned since the

pressure inside a bubble is higher than the outside liquid pressure due to surface tension. Such excess pressure which is called Laplace pressure, can be expressed as $2\sigma/R$, where σ is surface tension and R is a bubble radius. A bubble with R=100 nm (surface tension = 72 mN/m and atmospheric pressure in the surrounding water = 105 N/m^2) would give an internal pressure of 1.5 MPa (Attard, 2014; Millero, 2001). Thus, such a bubble is expected to be immediately dissolved into the surrounding liquid with a driving force between the gas interface and the liquid interface. Nevertheless, the existence of NBs has been reported in various experimental observations with lifetimes of NBs reported to be days to months (Duval et al., 2012; Liu et al., 2016; Nirmalkar et al., 2018a; Ushikubo et al., 2010a). The stability of NBs has often been attributed to a high negative zeta potential (Hewage et al., 2021; Meegoda et al., 2018). Several studies revealed that the negative surface charge on NBs is most likely due to the preferential adsorption of hydroxide ions, and thus NBs are more stable at higher pH (Hamamoto et al., 2018; L. Wang et al., 2020). A number of speculative interpretations have been postulated, but neither a complete physical model nor convincing theory on NBs stability has yet to emerge.

The most distinguishing property of NBs is their unusually long lifetime. NBs, once formed, are highly persistent (Zimmerman et al., 2011) and stable for hours (Lou et al., 2000), days (Liu et al., 2013; Ohgaki et al., 2010; Ushikubo et al., 2010b), and even months (Duval et al., 2012; Nirmalkar et al., 2018a). Monitoring NBs suspensions over long periods of time showed that the mean bubble diameter and zeta potential remained approximately unchanged, but the bubble number density gradually decreased with time. On the basis of molecular dynamics simulations, Weijs et al. (2012) had reported earlier

that diffusive shielding stabilizes bulk NBs clusters. More recently, Nirmalkar et al. (2018) suggested the following three possible mechanisms by which NBs can disappear: i) if their surface charge is neutralized; ii) if they contact with a hydrophilic surface such as a glass storage vial; and iii) if they interact with the surface of the solution or near to surface of the solution.

At this point, the impacts of several freshwater background parameters such as pH, temperature, ionic strength, hardness, and the presence of oxidants, salts, and natural organic matter (NOM) on the stability of NBs are still largely unknown. Tyrrell and Attard (2002) reported that bubble size increases as pH decreases and vice versa, and the discrete nature of the bubbles is enhanced because of the increase in surface charge and corresponding repulsion between neighboring sites on the surface of NBs at high pH. NBs may also stabilize themselves through ionic shielding and diffusive shielding. For instance, Ohgaki et al. (2010) showed that the interface of NBs consists of hard hydrogen bonds, like the ones found in ice (i.e., shorter length of hydrogen bond than water with lower frequency O-H vibrations) that can markedly reduce the diffusivity of gas from the NBs. Although some pieces of information are available in literature as summarized in **Table B1**, a consensus has not yet been reached, and information about the impacts of the solution properties on the stability of NBs for a long storage period under typical freshwater conditions remains elusive. The dearth of information is partially because of the lack of analytical techniques to measure NBs concentrations accurately in freshwaters or other natural waters due to interferences from background particles.

The main objective of the present study was to conduct a comprehensive investigation to systematically examine the stability of oxygen NBs in water under various conditions that are closely related to a typical freshwater (e.g., soft water vs. hard water, low specific UV absorbance at 254 nm ($SUVA_{254}$) vs. high $SUVA_{254}$ water, pH, temperature, ionic strength, and the presence of an oxidant). Understanding the impact of water chemistry on the stability of NBs is critical for the development of different applications in aquatic systems. NBs stability was evaluated by monitoring the change in the bubble concentrations and size distribution including average diameter and zeta potential with time. In addition, the formation of hydroxyl radical (•OH) was investigated using disodium terephthalate which forms fluorescent adducts with •OH in the presence of oxygen NBs under the selected conditions.

4.2. Materials and Methods

4.2.1. NBs preparation and storage for 60 days under various conditions

Oxygen NBs were generated in distilled and deionized (DDI) water using a commercially available NBs generator (Nano Bubble Technologies (NBT), Sydney, Australia). Ultra-high-purity oxygen (99.994%) was used as the gas source for preparing oxygen NBs at 4 L/min of oxygen gas flowrate at 60 psi gas pressure. After 90 minutes of NBs generation to ensure that NBs concentration reached the maximum, NBs samples were transferred into 40 mL amber glass vials. The transferred NBs samples were closed with caps with no headspace in the vials. I examined if container materials affected the NBs stability since Nirmalkar et al. (2018) reported that NBs could collapse if they come in contact with the hydrophilic surface of the glass storage vial. However, no significant difference was observed in the NBs concentrations between amber glass vials and polypropylene tubes.

The initial oxygen NBs concentration and dissolved oxygen (DO) concentration were 1.0×10^8 particles/mL and 42.9 mg/L, respectively. DO concentration was measured by placing the probe of a dissolved oxygen meter (Thermo Scientific, Orion 5 Star) directly into the samples. The vials were stored at room temperature except for the temperature effect experiments (i.e., 10 and 30 °C). The initial pH of the NBs samples was 6.5. After 1, 3, 7, 14, 21, 28, 35, 42, and 60 days, the vials were opened and the stability of NBs were monitored by measuring NBs concentrations and size distributions along with DO levels,

zeta potential, pH, UV absorbance at 254 nm, and dissolved organic carbon concentration (DOC).

To examine pH effect, the solution pH was adjusted in the vials at 3, 5, 6.5, and 9 with HCl and NaOH (no buffer used). To test the effect of aromaticity of NOM on the NBs stability, two NOM extracts which were available in our laboratory from a previous study (Song et al., 2009) were used at 5 mg DOC/L: 1.7 L/mg.m for low $SUVA_{254}$ and 4.1 L/mg.m for high $SUVA_{254}$. $SUVA_{254}$, which is the ratio of UV_{254} to DOC, can be used to estimate the percentage of aromatic carbon content of NOM. It is also an indicator of aromaticity and chemical reactivity for aquatic organic matter samples from a wide range of water sources (Karanfil et al., 2002). For the cation and ionic strength effects, 9 mM $CaCl_2$ or NaCl was added to the NBs samples. Hardness was created by adding $CaCl_2$ to achieve 300 mg/L as $CaCO_3$. Also, the combined effect of high $SUVA_{254}$ (4.1 L/mg.m) NOM at 5 mg DOC/L and 3 mM Ca^{2+} as $CaCO_3$ was investigated. Lastly, for the temperature effect, samples were stored at 10, 20, and 30 ^{o}C. Samples for the target temperatures of 10 and 30 °C conditions were kept in a refrigerator and a water bath, respectively. Samples for NBs stability was also examined in the presence of chlorine, a commonly used oxidant during water treatment. All samples and blanks/controls were prepared and analyzed in triplicates or duplicates, and the average values are presented. Overall, my approach was to create the key properties of freshwater by systematically controlling them in DDI and examining the change in NBs levels and characteristics in the water.

4.2.2. Measurement of NBs concentration and zeta potentials

The concentration, mean and mode size, and size distribution of oxygen NBs were measured using a nanoparticle tracking analysis (NTA) instrument (NanoSight NS300, Malvern, UK) (Jadhav and Barigou, 2020; Nirmalkar et al., 2018a). The NanoSight instrument works with particle concentrations in the range of ~10^7–10^9 particles/mL, which is approximately 20–100 particles in the field of view. Before determining the particle size distribution of generated NBs, NanoSight analysis chamber was flushed with 1-2 mL of DDI water to remove any residual from the analysis chamber. After the flush, the syringe was carefully removed while holding the end of the injection line, and 2-3 drops of DDI water were added to the injection line connector to create a water seal that is required to prevent the introduction of larger bubbles when switching between the DDI rinse syringe and the 1 mL NBs sample syringe. After adjusting the quick or standard measurements parameters (e.g., number of captures (5) and duration (60 s), camera level (13-16), and threshold (9-20)), the measurement of NBs was started (see more details in **Table 3.1**). The background nano-sized particle level in the DDI water ranged from 1.6 to 2.0×10^7 particles/mL. The reported NBs concentrations was adjusted by subtracting background particles concentrations and their changes over time are plotted in **Figure B1**. Five captures were taken per sample run, and the average values of these five data points are presented. The standard deviation of NBs size and concentration for each measurement was less than 10%.

The zeta potential was measured to characterize the NBs stability using a Brookhaven 90Plus Particle Size Analyzer. The fundamental zeta potential (ζ) was determined from electrophoretic mobility using the Smoluchowski model or equation that depends on the viscosity, permittivity, and mobility of a solution at absolute temperature (Takahashi, 2005). A 1.6 mL of NBs sample taken from a vial after the designated storage time was added to the sample cell and the zeta potential was measured after measurement parameters (e.g., pH, water type, viscosity, temperature, run time, and cycle time) were properly entered into the software. For each sample, 10 replications were measured for accuracy and quality with less than 5% standard error were achieved. Before measuring each batch of NBs samples, a BI-ZR5 standard solution with the known specific zeta potential was tested to verify the performance of the analyzer.

4.2.3. Determination of •OH radicals in NBs solution

Disodium terephthalate (TP, purchased from Alfa Aesar, > 99%) is a slightly fluorescent probe molecule, but it yields highly fluorescent adducts upon reacting with •OH (Hirano and Kobayashi, 2016; Ishibashi et al., 2000; Page et al., 2010). TP was chosen because it selectively reacts with •OH. TP, a dianion in the aqueous solution, resides in the hydrophilic area and captures only •OH in the bulk solution (Song and O'Shea, 2007). It has been known that the reaction between TP and •OH produces 2-hydroxyterephthalate (TPOH) with a percent yield of 35 % and other adducts (Fang et al., 1996; Žerjav et al., 2020). TPOH (purchased from Sigma Aldrich, 97%) calibration curves (1-1000 nM) were constructed from fluorescence spectra to determine the concentrations of TPOH formed in

NBs solutions. More details on how to determine TP and TPOH are described in Section 3.4.1.

To observe the formation of •OH under selected storage conditions, oxygen NBs solutions were in 500 mL volumetric flasks with 50 µM TP spiked at room temperature (20 °C) with treatments: i) oxygen NBs alone and pH 6.5, ii) NBs at pH 3 (adjusted with HCl), and iii) NBs in the presence of 3 mM Ca^{2+} at pH 6.5. Each solution was transferred into eight 40 mL amber glass vials without headspace and left on the bench top to be sampled at specific times. Vials were opened after designated storage times (i.e., 1, 3, 7, 14, 21, 28, and 35 days) to measure the concentration of oxygen NBs and TPOH. Using a Shimadzu RF5301PC spectrofluorometer, NBs samples were exited at 315 nm and the formation of TPOH was determined from the fluorescence intensity emitted at 425 nm. To the best of my knowledge, this is the first study to prove the formation of •OH in DDI water containing oxygen NBs using TP.

4.2.4. Other Analytical Methods and Minimum Reporting Levels

The measurement methods and minimum reporting limits of water quality parameters and DO was given in the previous Chapter, in **Table 3.4**.

4.3. Results and Discussion

4.3.1. Disappearance of oxygen NBs in DDI water and changes of DO concentration

The disappearance of oxygen NBs in DDI water at room temperature and ambient pH (i.e., pH 6.5) was linear with respect to storage time (**Figure 4.1**). The average

concentrations of NBs in three independent replicates, which represent three distinct vials, are plotted along with standard deviation error bars. Overall, the results showed that the change in NBs concentrations remained within ± 10% in the triplicates. DO concentrations in the stored NBs vials decreased from 42.9 mg/L of the initial supersaturation level over time (**Figure 4.1**). Although the vials were closed tightly with caps and there was no headspace, oxygen was released from the system since DO was supersaturated in water. Almost half of the DO escaped within 24 hours and DO reached its saturated level of 9 mg/L in about 21 days. During the entire period of storage time, the pH of the NBs solutions remained constant. Hamamoto et al. (2018) reported no significant change of pH during storage up to 18 days, but DO decreased from approximately 15 mg/L to 8 mg/L within 7 days and remained constant for the remaining time, which is in agreement with my observations. The excess DO likely escaped through the caps.

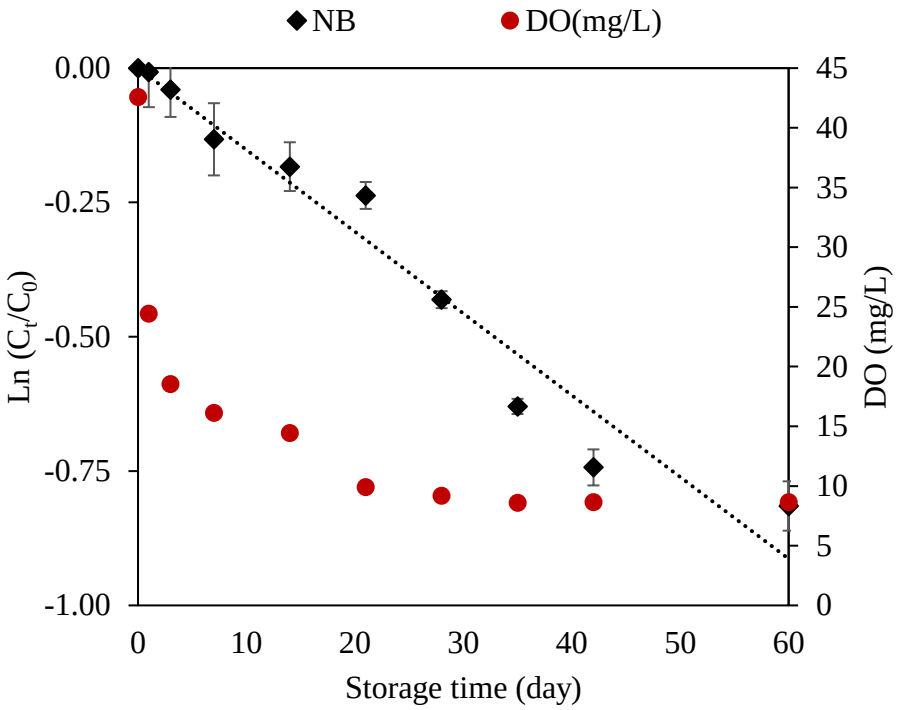

Figure 4.1. Changes in oxygen NBs concentrations in DDI water over storage time at room temperature and pH 6.5 (average of triplicates with standard deviation error bars) along with DO concentrations.

4.3.2. Effect of pH

Until day 3, NBs remained relatively stable regardless of pH (**Figure 4.2** and **Figure B1**). The supersaturated liquid condition or high bubble density may maintain a small concentration gradient between bubble interface and liquid that can enhance the stability of NBs in solutions while reducing the gas transfer rate from NBs to liquid (Meegoda et al., 2018; Ushikubo et al., 2010b). However, the oxygen NBs concentrations at pH 3 and 5 started to drastically decrease from day 7, while those at pH 6.5 and 9 decreased very slowly with increasing storage time. These observations were attributed to the coalescence of the NBs, and their rise in the containers with increasing bubble diameter due to a decrease in negative value of surface charge. The terminal rising velocity (υ) of a spherical bubble can be described by the following equation (Park et al., 2017):

$$\upsilon = \frac{g\rho_L d_e^2}{12\mu_L} \qquad \text{Equation 4.1}$$

where g is the gravitational acceleration, ρ_L is the density of the liquid medium, d_e is the volume-equivalent diameter of the bubble, and μ_L is the viscosity of the liquid medium. Calculated rising velocity in the units of cm/day of bubbles with different diameters at three different temperatures is plotted in **Figure 4.3**. The terminal rising velocity of NBs with a diameter around 100 nm is only 0.08 cm/day at 20 °C. However, if NBs coalesce and form bigger bubbles with a diameter of 300-500 nm, they will begin to rise at 0.7-2.0 cm/day. During the rise, they will likely collide further with other bubbles and grow in size, and eventually the bubbles would reach the top of the 9.5 cm-long vials used in the experiments

and escape. The lower absolute values of zeta potential were observed for day 1 at pH 3 (-8 mV) and pH 5 (-12 mV) than at pH 6 (-22 mV) and pH 9 (-35 mV), would reduce inter-bubble repulsions, promoting successful collisions. **Table 4.1** shows the changes in zeta potential of oxygen NBs during the experiments. However, it appears that even at pH 3 and lower zeta potential values, it takes 3-4 days for NBs to reach the size required to begin to rise in the vials. As a result, there was no significant difference ($p>0.05$) in observed NBs concentrations at different pH for the early period of storage (≤ 7 days).

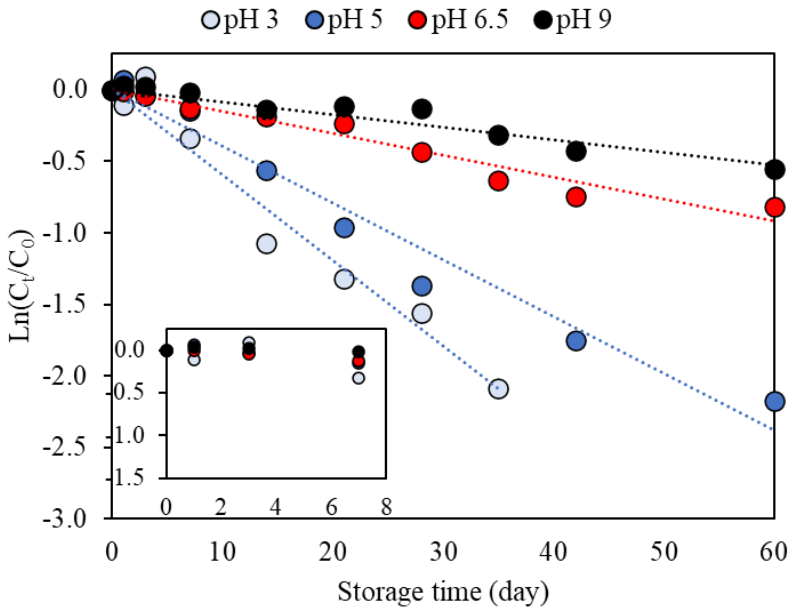

Figure 4.2. Changes in oxygen NBs concentrations over storage time under various pH conditions in DDI water. The inset figure presented NBs concentration changes at different pH values for the early storage duration (≤ 7 days)

Many previous studies revealed that NBs are more stable at high pH (Hamamoto et al., 2018; Jin et al., 2007; Meegoda et al., 2018; L. Wang et al., 2020). For instance, Jin et al. (2007) investigated the pH influence on the formation of stable NBs in aqueous solutions of R-cyclodextrin. They revealed that for a given ionic strength, the NBs were more stable in alkaline solution because the adsorption of more OH^- ions at the gas/water interface enhanced the double layer repulsion, resulting in a repulsive force to prevent bubble aggregation and coalescence. In agreement with their explanations, NBs at pH 9 were more stable than those at pH 3, which was attributed to greater negative charge on the bubble surface, which was supported by the zeta potential measurements at different pH values over time (**Table 4.1**). The absolute value of zeta potential at lower pH decreased considerably with increasing time, while those at pH 9 were even higher than the initial value of the main NBs stock solution at pH 6.5 (-24 mV).

Table 4.1. Changes in zeta potential (mV) of oxygen NBs over 60 days of storage time under various pH values.

Storage time (day)	**pH**			
	3	**5**	**6.5**	**9**
0	NA	NA	-24	NA
1	-8	-12	-22	-35
3	-6	-10	-23	-34
21	-6	-5	-23	-28
28	-2	-5	-24	-31
35	-3	-3	-21	-32
42	0	0	-19	-28
60	NA	NA	-21	-27

NA: Not Available.

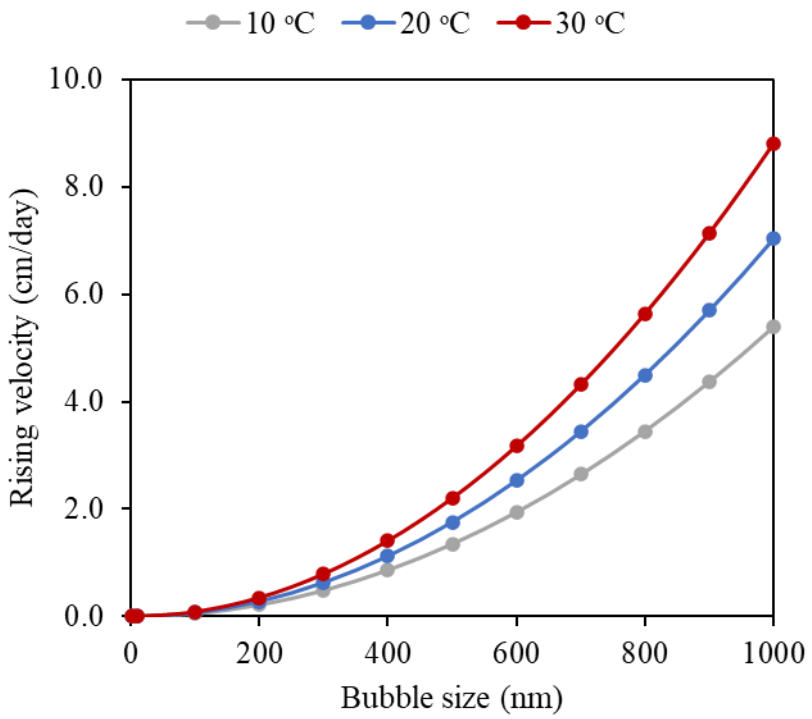

Figure 4.3. The calculated terminal rising velocity (cm/day) versus the diameter (nm) of bubbles at 10, 20, and 30 °C.

The half-lives of oxygen NBs in DDI water at room temperature increased as pH increased (e.g., 12 days at pH 3 and 80 days at pH 9) (**Table 4.2**). It was noted that the bubble concentrations were substantially reduced over time at pH 3, while the diameter of bubbles was not shifted to the range greater than 400 nm (**Figure 4.4**A-C). Once pH was adjusted to 3, the mode of NBs diameter changed slightly from 90 nm to 133 nm. On day 3, an increase of NBs with 286 nm diameter which will have about 0.6 cm/day of rise velocity (**Figure 4.3**) was measured. However, even in day 14, no large bubble with near μm-level diameter was observed. These measurements suggest that oxygen NBs in DDI

water coalesced, grew, moved up very slowly, and finally escaped before or as soon as the vials were opened to collect samples for analysis. Unlike both thermodynamic and kinetic arguments that indicate instability of bulk NBs where the survival time for nano-sized bubbles is predicted to be less than 0.02 s (C. Chen et al., 2020), oxygen NBs in the current study lasted for more than 5 weeks even at low pH. Meegoda et al. (2018) found that the absolute value of zeta potential of bubbles decreased while the bubble size increased. Even though bubble sizes are expected to decrease with time due to gas diffusion, their experimental results indicated increased bubble sizes. They concluded that the increased size was because of their observed decrease in the absolute value of zeta potential and bubble movement due to Brownian motion which may cause bubbles to coalesce over time to form larger bubbles.

In summary, the effect of pH on the oxygen NBs stability was insignificant for a short storage time (3-4 days) probably due to the effects of gradual bubble growth and rise, while the difference in oxygen NBs concentrations at different pH became more noticeable at longer storage time. Moreover, as presented in **Table 4.2**, the half-life of oxygen NBs in pH 9 solutions was almost seven times greater than that of oxygen NBs in pH 3 solutions, highlighting the substantial impact of pH on oxygen NBs stability.

Table 4.2. Oxygen NBs disappearance rate constants and half-lives under various storage conditions in DDI water for 60 days.

Oxygen NBs storage condition		**1st order NBs disappearance rate constant, k (day^{-1})**	**NBs half-life (day)**	**R^2**
pH effect (at 20 ˚C)	pH 3	0.06	12	0.98
	pH 5	0.04	18	0.98
	pH 6.5	0.015	46	0.98
	pH 9	0.009	80	0.95
NOM effect (at pH 6.5 and 20 ˚C)	No NOM added	0.015	46	0.98
	NOM with low $SUVA_{254}$ (1.7 L/mg.m)	0.015	46	0.96
	NOM with high $SUVA_{254}$ (4.1 L/mg.m)	0.041*	17	0.98
Ionic strength, hardness, and cation effect (at pH 6.5 and 20 ˚C)	No cations added	0.015	46	0.98
	9 mM ionic strength (Na^+)	0.147*	5	0.93
	9 mM ionic strength (Ca^{2+})	0.253*	3	0.95
Temperature effect (at pH 6.5)	10 ˚C	0.009	77	0.98
	20 ˚C	0.015	46	0.98
	30 ˚C	0.023	30	0.96
Combined condition (at pH 6.5 and 20 ˚C)	3 mM Ca^{2+}/NOM with high $SUVA_{254}$ (4.1 L/mg.m)	0.221*	3	0.96

* For the conditions showing two apparent (i.e., fast initially and then slow) disappearing phases, only data points that were well fitted to the first linear regression were considered to obtain the disappearance rate constraints and half-lives.

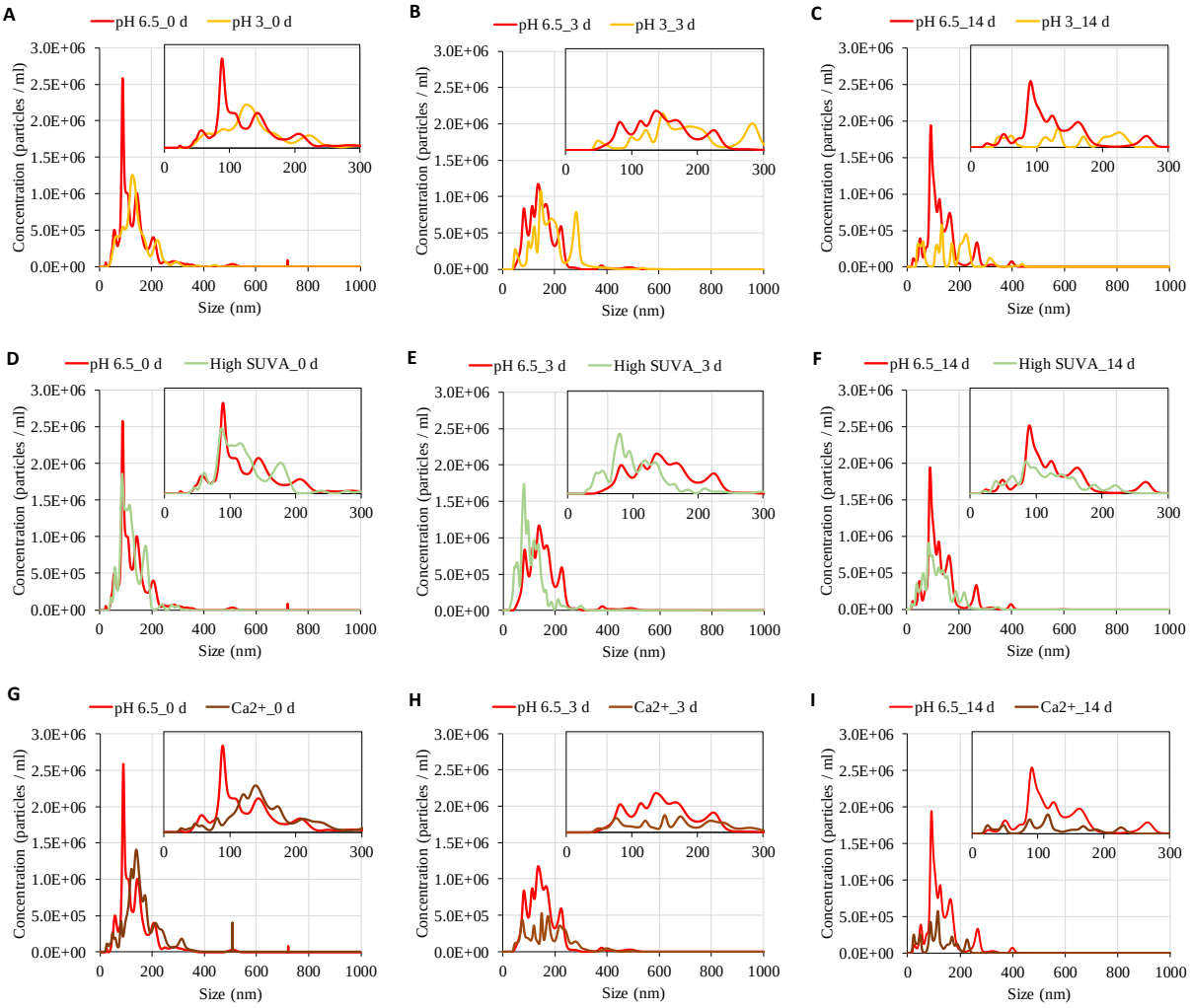

Figure 4.4. Size distributions of oxygen NBs in DDI water (A-C) control at pH 6.5 and pH 3, (D-F) in the presence of and high $SUVA_{254}$ (4.1 L/mg.m at 5 mg/L DOC) NOM, and (G-I) in the presence of Ca^{2+} (3 mM) for 0, 3, and 14 day of storage time. The inset graphs provide a magnified view of the size distribution of NBs, specifically highlighting the portion of NBs with a diameter of less than 300 nm.

4.3.3. Effect of NOM

Amphiphilic NOM macromolecules may interact with NBs surfaces through hydrophobic interactions or adhesion and affect the stability of NBs (e.g., by imparting

negative charge to NBs and thus increasing their overall surface potentials) (Sugano et al., 2017). After NOM was added to the NBs samples at pH 6.5, the magnitude of zeta potential slightly changed from -24 mV to -27 mV and -25 mV with low and high $SUVA_{254}$ NOM, respectively, and then changed in the opposite direction with increasing storage time (**Table 4.3**). NOM with low $SUVA_{254}$ (1.7 L/mg.m) did not significantly affect the oxygen NBs concentrations (**Figure 4.5**), while NOM with high $SUVA_{254}$ (4.1 L/mg.m) resulted in a decrease in the concentration of oxygen NBs, indicating that more hydrophobic NOM with higher aromaticity reduced the oxygen NBs stability in DDI water. The half-life for both NBs with and without low $SUVA_{254}$ NOM in DDI water was 46 days, while the NBs half-life in the presence of high $SUVA_{254}$ NOM dropped to 17 days (**Table 4.2**). One possible explanation is that the more hydrophobic NOM formed a complex with NBs in which NOM can serve as a bridge between NBs. A kind of aggregation of a negatively charged colloid dispersion with an anionic polymer has been reported in a destabilization study of colloids (Black et al., 1965; Lu et al., 2022).

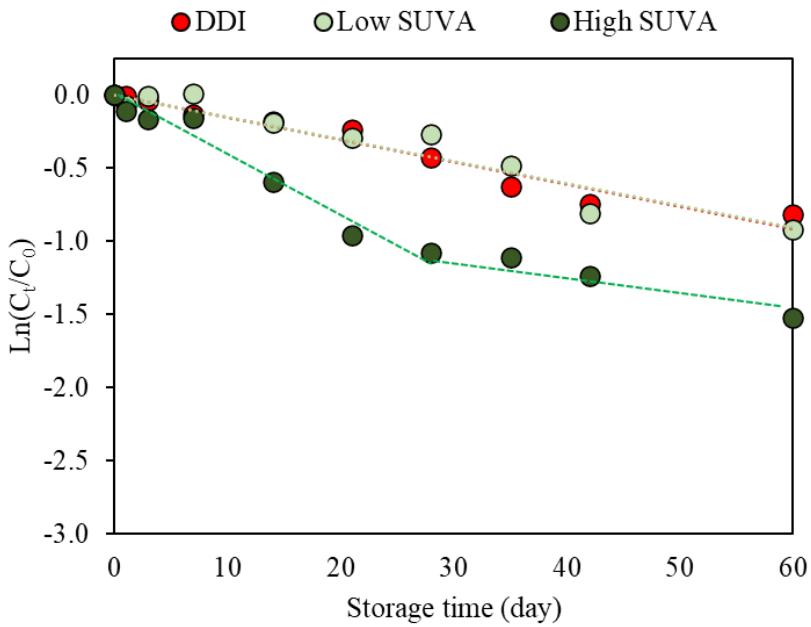

Figure 4.5. Changes in oxygen NBs concentrations in the presence low $SUVA_{254}$ (1.7 L/mg.m) and high $SUVA_{254}$ (4.1 L/mg.m) NOM at 5 mg/L DOC during 60 days of storage time at room temperature.

A linear regression was not well-fitted to the disappearance of oxygen NBs in the presence of high $SUVA_{254}$ NOM showing two apparent decay curves (i.e., fast initially and then slow) (**Figure 4.5**).Therefore, the presence of high $SUVA_{254}$ NOM induced a two-phase behavior in NBs disappearance. The behavior can be attributed to the complex structure of NOM, a heterogeneous compound with varying properties and interactions. Initially, these factors accelerated the disappearance of NBs, possibly due to NOM-induced alterations in NBs properties or interfacial interactions. However, as the initial reactions subsided, the effect of high $SUVA_{254}$ NOM on NBs disappearance gradually diminished. This suggests that the initial rapid decline in NBs concentration was primarily driven by

NOM-induced effects, while the slower subsequent decline was more likely due to the inherent disappearance process of NBs. The disappearance rate constant and half-life for NBs in the presence of high $SUVA_{254}$ NOM were determined using the initial fast decay. It is also noteworthy that by day 21, approximately 60% of NBs disappeared from both treatments with the pH-adjusted at 5 and high $SUVA_{254}$ NOM-added NBs samples, but their zeta potentials were very different from each other (i.e., -5 mV and -22 mV, respectively) (**Table 4.3**). The contrast in zeta potential indicates that different mechanisms were likely involved in NBs interactions in these systems, as discussed above. Although the change of zeta potential is closely related to the stability of NBs, a simple comparison of zeta potential values cannot predict how many NBs would disappear from a system over time, which was also observed by Hamamoto et al. (2018). Like the case of pH 3, the bubble concentrations in the presence of high $SUVA_{254}$ (4.1 L/mg.m) NOM at 5 mg DOC/L during the storage period were substantially reduced over time, while the diameter of bubbles was not shifted to the larger range (**Figure 4.4** D-F compared to A-C). The mode of NBs diameter did not change probably because zeta potential did not change significantly compared to the control with no NOM added. This study represents the first systematic investigation of the effect of NOM type on NBs stability. By comprehensively measuring size, size distribution, concentration, and zeta potential, the study provides valuable insights into the factors governing NBs stability under varying NOM conditions. These findings have the potential to significantly enhance the applicability of NB technology across a wide range of applications.

Table 4.3. Changes in zeta potential (mV) of oxygen NBs over 60 days of storage time in the presence in NOM.

Storage time (day)	NOM	
	DOC (5 mg/L)	
	Low SUVA (1.7 L/mg.m)	High SUVA (4.1 L/mg.m)
0	NA	NA
1	-27	-25
3	-22	-19
21	-24	-22
28	-24	-16
35	-22	-13
42	-19	-14
60	-17	-14

NA: not available

4.3.4. Effect of ionic strength, hardness, and charge of cation

Negatively charged surface potentials of NBs can be affected by positively charged neighbor ions, which was observed as NBs stability decreased with increasing ionic strength (**Figure 4.6**). At 9 mM ionic strength in DDI water, oxygen NBs concentrations decreased nearly immediately unlike the cases of low pH and high $SUVA_{254}$ NOM in which NBs were relatively stable for the initial 3 days of storage. The observation is likely due to differences in the cation concentration that would greatly affect the behavior of negatively charged NBs; the concentration of cationic species, H^+, in DDI water at pH 3 was only 1 mM which is less than the concentrations of Na^+ or Ca^{2+}. The higher ionic strength clearly led to the faster disappearance of oxygen NBs compared to the DDI control. Furthermore, the increasing ionic strength of the solution induced a two-phase behavior in NBs disappearance. This two-phase behavior can be attributed to the immediate effect of cation addition on the negatively charged NBs surface, resulting in an initial rapid decline in NBs concentration. However, as the initial reactions subsided, the disappearance rate of NBs gradually slowed down. In terms of the effect of cationic charge on the NBs stability, Ca^{2+}, a divalent cation, destabilized oxygen NBs more than Na^+, a monovalent cation. The accelerated disappearance of NBs in the presence of Ca^{2+} ions compared to Na^+ ions stem from the distinct nature of their ionic interactions with NBs. Ca^{2+} possess a higher charge density than Na^+, leading to stronger electrostatic interactions with the negatively charged surface of NBs. These interactions induce the aggregation of NBs, resulting in their rapid disappearance from the solution.

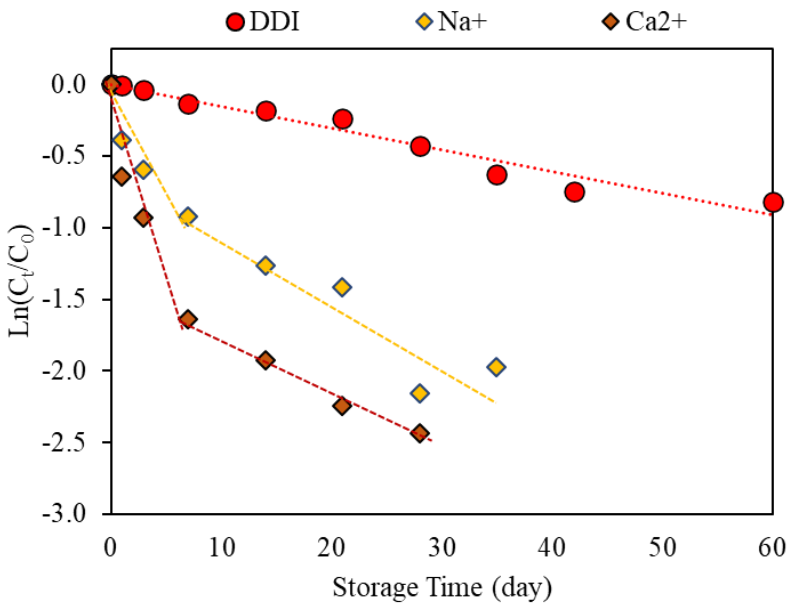

Figure 4.6. Changes in oxygen NBs concentrations in the presence Ca^{2+} and Na^{+} at 9 mM during 60 days of storage time at room temperature.

The magnitude of zeta potential of NBs was reduced more by Ca^{2+} than Na^{+} (**Table 4.4**), indicating that charge density of cation affects the NBs stability. It has been known that high valency cations have the potential to neutralize or completely reverse the bubble charge (Hewage et al., 2021). These results show that NBs are more stable in soft waters than hard waters. The zeta potential change by Ca^{2+} was much faster than that by Na^{+}, and it was neutralized during the storage time (**Table 4.4**).

Table 4.4. Changes in zeta potential (mV) of oxygen NBs in the presence Ca^{2+} and Na^{+} at 9 mM.

Storage time (day)	Ionic Strength	
	9 mM	
	Ca^{2+}	Na^{+}
0	NA	NA
1	-6	-15
3	-6	-13
21	-5	-13
28	-2	-8
35	-1	-4
42	NA	NA
60	NA	NA

NA: Not Available.

Like the case of pH 3, the mode of NBs diameter only slightly moved from 90 nm to 140 nm upon adding Ca^{2+} with a spike around 510 nm (**Figure 4.4**G) probably because of an abrupt change in zeta potentials caused by Ca^{2+}. The bubble size distributions were further investigated in the presence of Ca^{2+} every 10 minutes within a very short (i.e., 60 minutes) period of storage time. The oxygen NBs solution always showed a mode of the bubble diameter at around 90 nm, but the concentration of the 90 nm NBs started decreasing nearly immediately after adding Ca^{2+}. The mode of bubble size shifted to the right (about 10 nm larger for every 10 minutes) and the concentrations of bubbles with diameter ranging 200-400 nm increased (**Figure 4.7**), indicating that Ca^{2+} promoted oxygen NBs coalescing. These results also show that the main disappearance pathway of the oxygen NBs in DDI water was due to their merging to become slightly larger bubbles, rising, and leaving the containers. Again, a linear regression was not well-fitted to the

disappearance of oxygen NBs in the presence of cations (**Figure 4.6**). The disappearance rate constant and half-life for NBs in the presence of Na^+ or Ca^{2+} were determined using the initial fast decay. The calculated half-lives of NBs in the presence of Na^+ and Ca^{2+} were 5 days and 3 days, respectively (**Table 4.2**).

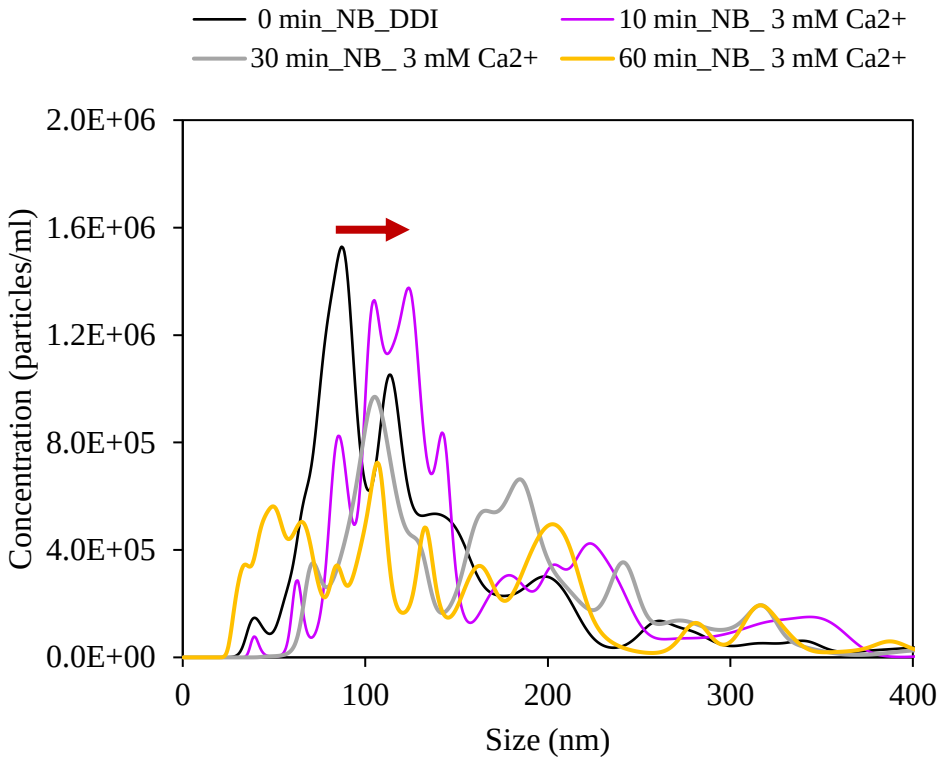

Figure 4.7. Bubble size distributions in the presence of Ca^{2+} (3 mM) within 60 min in DDI water

4.3.5. Effect of temperature

The effect of temperature on the oxygen NBs stability was insignificant for a short storage time (i.e., 14 days) (**Figure 4.8**). The lack of change is probably because of the effect of temperature in the range of 10-30 ˚C on the rise velocity of small-sized bubbles (e.g., bubbles with 100-400 nm range diameter) is relatively small (**Figure 4.3**). The temperature effect would be more significant as the bubble size becomes larger. There was no dramatic difference among oxygen NBs concentrations of the samples stored at three different temperatures until day 14, while the NBs were more stable at lower temperature from day 21. The zeta potentials of NBs solutions stored at 10 ˚C and 20 ˚C were almost constant for 60 days, while the absolute value of zeta potential gradually reduced at 30 ˚C from 24 mV to 17 mV (**Table 4.5**). The half-lives decreased from 77 days at 10 °C to 30 days at 30 °C (**Table 4.2**). At higher temperature due to the kinetic energy, NBs would have more chances to encounter neighbor bubbles, collide or coalesce, and become larger bubbles which may move up and eventually escape from the vials.

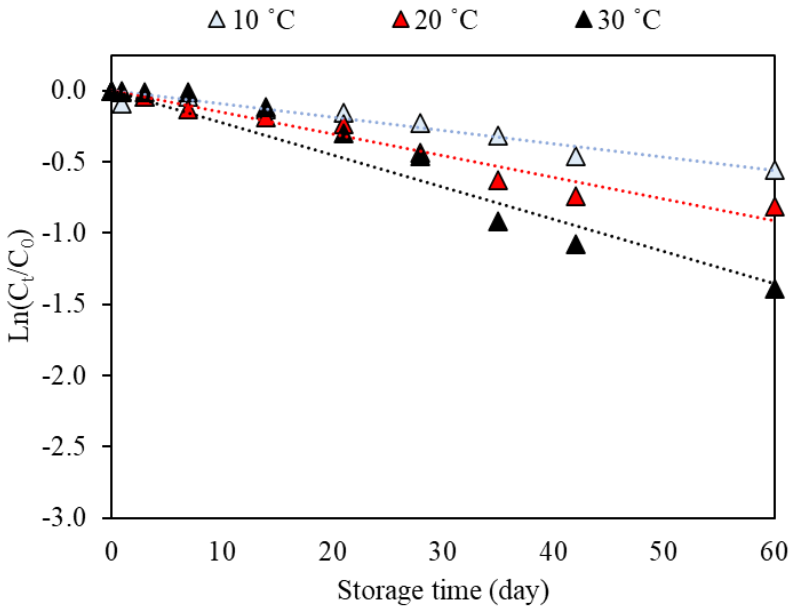

Figure 4.8. Changes in oxygen NBs concentrations during 60 days of storage time at three different temperatures, 10, 20 and 30 ℃.

Table 4.5. Changes in zeta potential (mV) of oxygen NBs at three different temperatures.

Storage time (day)	**Temperature**		
	˚C		
	10	**20**	**30**
0	NA	-24	NA
1	-24	-25	-20
3	-24	-23	-21
21	-25	-22	-21
28	-27	-23	-20
35	-24	-23	-19
42	-24	-21	-17
60	-24	-23	-17

NA: Not Available.

4.3.6. Effect of combined hardness and NOM

The change of NBs concentrations was further investigated under a mixed water chemistry condition, which represents a hard freshwater (**Figure 4.9**). In the presence of both high $SUVA_{254}$ (4.1 L/mg.m) NOM at 5 mg DOC/L and 3 mM Ca^{2+}as $CaCO_3$, NBs started to disappear rapidly at pH 6.5, and no NBs were observed after 7 days. Moreover, the disappearance rates for both combined and Ca^{2+} alone conditions were very close. For individual applications, high $SUVA_{254}$ NOM alone showed less effect on the NBs stability than the only Ca^{2+} treatments. However, when they were combined, high $SUVA_{254}$ NOM made an additional contribution resulting in the complete depletion of NBs in DDI water. Therefore, the results show that oxygen NBs in water with higher hardness and hydrophobic NOM will start to coalesce and escape rapidly from water to atmosphere.

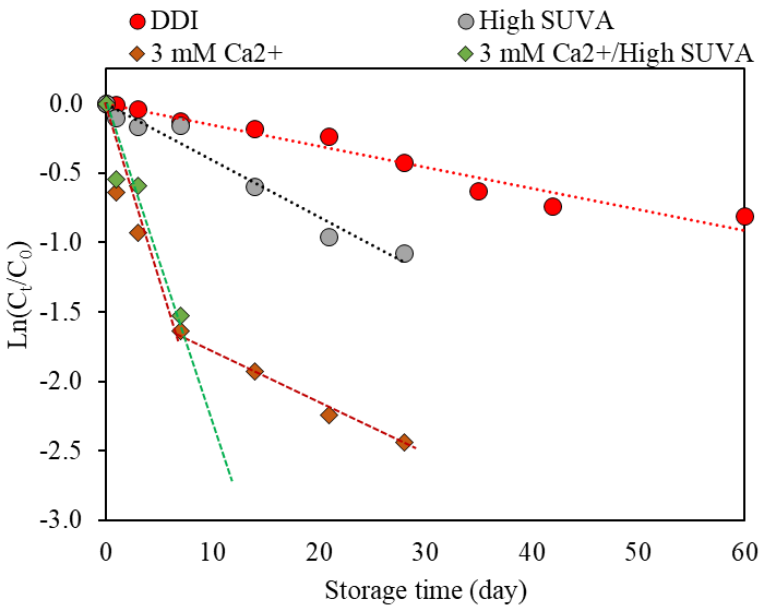

Figure 4.9. Changes in oxygen NBs concentrations over storage time under combined Ca^{2+} (3 mM) with high $SUVA_{254}$ (4.1 L/mg.m at 5 mg/L DOC) NOM conditions in DDI water. It is noted that all NBs disappeared below the detection limit within 14 days of storage in the presence of both Ca^{2+} and high $SUVA_{254}$ NOM.

4.3.7. Effect of chlorine

To examine the impact of oxidant on NBs stability, a set of NBs samples was spiked with 2 mg/L chlorine, which was prepared by diluting a 5% NaOCl solution, and the concentration of NBs were monitored. The oxygen NBs stability was not affected by the presence of chlorine in DDI water (**Figure 4.10**). Although there was a low level (i.e., 0.038 mM) of cationic species, Na^+ from NaOCl solution, that could have facilitated the disappearance of oxygen NBs, the overall disappearance of oxygen NBs was almost identical to that of the control without chlorine. The result is probably because of increasing

pH (up to pH 7.8) by added chlorine, which would cancel out the Na^+ effect on the NBs stability. When they are combined, therefore, no real effect was observed.

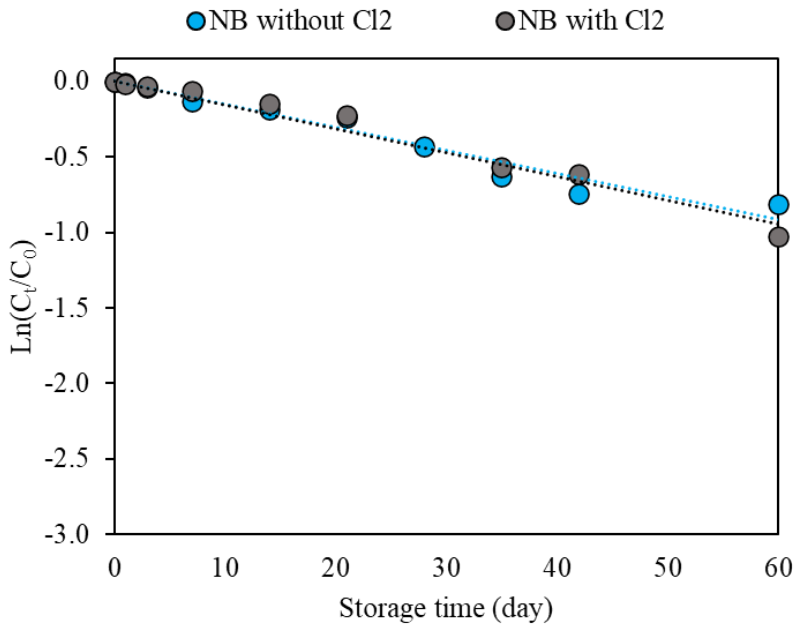

Figure 4.10. Changes in oxygen NBs concentrations in the presence of chlorine (2 mg/L) during 60 days of storage time.

4.3.8. Hydroxyl radical formation in oxygen NBs solutions

NBs have been shown to generate ROS, including •OH, superoxide anion radical (O_2^-), and singlet oxygen ($^1O_2$) during NBs collapse (Atkinson et al., 2019; Minamikawa et al., 2015). Liu et al. (2016) showed by using a sensitive fluorescent probe, 3'-p-(aminophenyl) fluorescein, that without any stimuli (such as H_2O_2, metals, etc.), NBs water continually produced ROS. The collapse of NBs was used to explain the formation of free radicals characterized by electron spin resonance (ESR) spectra (Minamikawa et al., 2015).

To examine the formation and presence of •OH in oxygen NBs solutions, two extreme conditions (i.e., pH 3 and 3 mM Ca^{2+}) where NBs disappeared more rapidly than the other storage conditions were selected and compared to the pH 6.5 condition. During 35 days, approximately 20% and 50% of TP (50 µM of initial concentration) in the oxygen NBs solutions reacted at pH 6.5 and pH 3, respectively (**Table 4.6**). In the presence of Ca^{2+}, about 40% of TP decayed after the same period. However, the formation of TPOH did not correspond to the decay of TP. Only 1-9 nM of TPOH was observed at pH 6.5 and the formation of TPOH in the presence of Ca^{2+} was even lower (**Figure 4.11**). At pH 3, up to 28 nM of TPOH formed as a result of •OH radicals reaction with TP. These major differences between degraded TP and formed TPOH concentrations indicate that collapsed oxygen NBs produce not only produced •OH, but also other ROS which were not included in the study. In addition, TPOH is not the only product from the hydroxylation of TP, because TPOH can further react with ROS such as •OH, O_2^-, and $^1O_2$ if radicals were still available in the vials. Nevertheless, the formation of •OH during the storage of oxygen NBs in DDI water was confirmed by the appearance of TPOH.

Table 4.6. TP degradation under different experiment condition

Storage time (days)	TP in NBs solution at pH 6.5	TP in NBs solution with 3 mM Ca^{2+}	TP in NBs solutions at pH 3
	$[TP]_t/[TP]_0$		
0	1.00	1.00	1.00
1	1.00	0.99	0.83
3	0.93	0.79	0.95
7	0.85	0.71	0.57
14	0.81	0.63	0.64
21	0.87	0.69	0.55
28	0.81	0.62	0.55
35	Not available	0.64	0.50

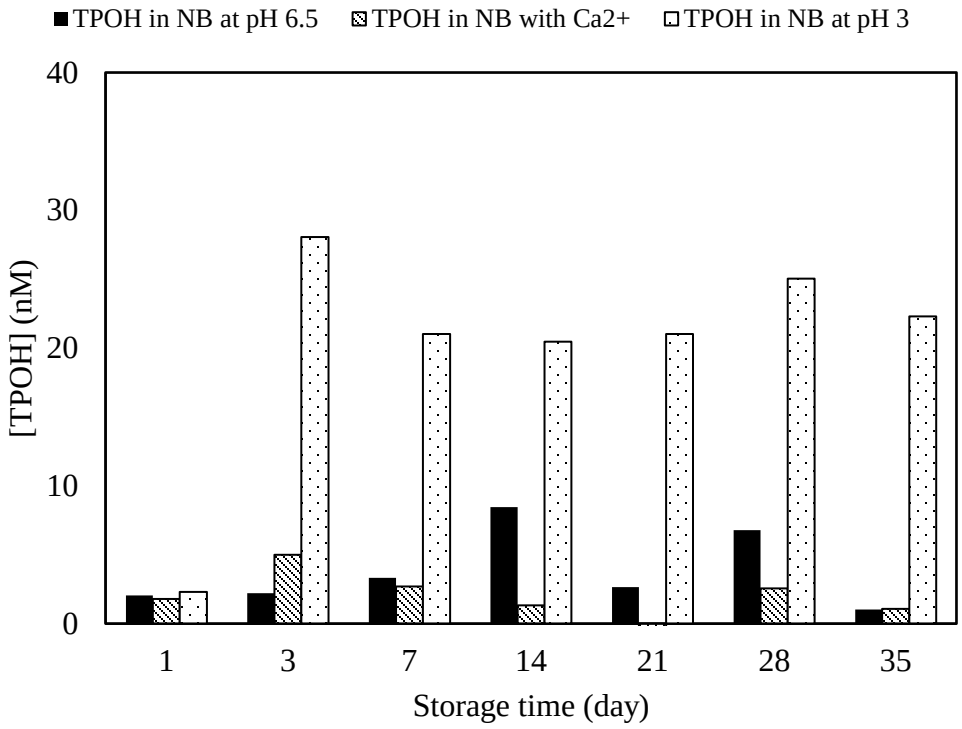

Figure 4.11. The formation of 2-hydroxyterephthalate (TPOH) as a result of the reaction between TP and hydroxyl radical in oxygen NBs solutions under selected storage conditions for 35 days.

Unlike the pH 3 condition, Ca^{2+} likely created more complicated chemistry in the oxygen NBs solutions. Although the fastest disappearance of NBs occurred in the presence of Ca^{2+} among all storage conditions investigated, the formation of TPOH was insignificant. The reason is probably because the collapse of NBs was greatly inhibited by a rapid reduction in the magnitude of zeta potentials in the presence of Ca^{2+} (**Table 4.4**). Such a sudden change of zeta potential may not allow NBs collapse to form •OH. TP may also form a coordination complex with Ca^{2+} (Byler and Farrell, 1989). If such complex reacts with •OH, its hydroxylation product cannot be detected as readily as TPOH.

4.4. Conclusions

The stability of oxygen NBs was investigated under various pH, NOM, cation, hardness, and temperature conditions for 60 days. Calcium was the most influential parameter significantly decreasing NBs levels among all parameters investigated. In the presence of cations (i.e., Ca^{2+}, Na^{+}, and H^{+}), the half-lives of NBs in the solution were in the order of $Ca^{2+} < Na^{+} < H^{+}$. As a result, oxygen NBs were more stable in soft than hard water. Oxygen NBs were relatively stable for 3 days regardless of pH due to very slow rise velocity (<1 cm/day) of coalesced bubbles with their diameter around 200-300 nm. However, NBs disappeared more rapidly at acidic than basic pH, as storage time increased. The formation of hydroxyl radical at pH 3 was also observed. High $SUVA_{254}$ NOM destabilized NBs more than low $SUVA_{254}$ NOM, indicating the impact of hydrophobicity on the NBs stability. The temperature effect on the NBs stability was negligible for a short

storage time; however, the effect of the higher temperature (30 °C) became more apparent at a longer storage time. Different mechanisms, coalescence and collapse, play a role in the NBs disappearance. At the neutral pH in freshwaters, the results obtained in the study suggest that coalescence (growth of bubble size and rise) is the most important mechanism, while at pH 3 NBs collapse also contributes to the disappearance of oxygen NBs from water.

When NBs are released in water bodies, high calcium, high $SUVA_{254}$ NOM, and low pH would significantly reduce the availability of NBs and their residence time in freshwater. Since such parameters can promote NBs coalescing, therefore, the location and depth of bubble release in the treatment systems can also influence NBs concentrations and residence time in natural waters. Furthermore, the results show the importance of conducting NBs studies at environmentally relevant water chemistry conditions, because studies conducted in pure water matrix (e.g., DDI) would not be able to predict the behavior of NBs in freshwaters, because cations and NOM that are commonly present in natural waters greatly affect the NBs fate and reactions in freshwaters.

CHAPTER 5

REMOVAL MECHANISMS OF GEOSMIN AND MIB BY OXYGEN NANOBUBBLES DURING WATER TREATMENT

5.1. Introduction

The presence of taste and odor (T&O) compounds in drinking water has been a significant challenge for water utilities. Geosmin and 2-methylisoborneol (MIB) are naturally produced from the metabolism of the *Cyanobacteria* known as blue-green algae and *Cyanophyta* (Kim and Park, 2021a). These compounds are semivolatile in nature and cause musty and earthy off-flavors (Greenwald et al., 2015). Odor threshold concentrations for geosmin and MIB have been reported to range from 4 to 10 and 9 to 42 ng/L, respectively (Cook et al., 2001; Krasner et al., 1983; Persson, 1983; Peter and von Gunten, 2007; Young et al., 1996).

T&O episodes can occur at any time of the year depending on the climate. A quarter to half of United States (US) water treatment plants using surface water reported problems with T&O compounds related to algae metabolites (Suffet et al., 1996). Their concentrations in raw water ranged from 50 to 150 ng/L in warm climates (i.e., California, Florida, etc. in US) during the summer and autumn months for a short period, while ranging from 10 to 30 ng/L for several months during the summer and autumn, and they dropped below detection levels in winter (Rangel-Mendez and Cannon, 2005). Based on an analysis in Eagle Creek Reservoir (Indianapolis, IN, USA), annual average concentrations of

geosmin and MIB were 13 and 11 ng/L, respectively (Clercin and Druschel, 2019). The concentrations of these compounds increased from spring to summer, especially in the hypolimnion of the reservoir (i.e., the lower layer of water) up to 77 and 112 ng/L for geosmin and MIB, respectively. A survey of 59 drinking water treatment plants in the Great Lakes region showed a widespread occurrence of the two T&O compounds with a number (20%) of utilities reporting annual outbreaks during the summer months with even a higher number (27%) experiencing sporadic episodes (Watson et al., 2008). In certain cases, however, exceptionally high levels of T&O compounds have also been reported. For example, in Lake Hartwell (Anderson, SC), MIB was detected around 2,000 ng/L in the summer of 2014, and geosmin and MIB together were observed at more than 1,250 ng/L the next summer (Huddleston et al., 2016), and they declined significantly after algaecide applications.

Different treatment techniques such as powdered or superfine activated carbon adsorption, membrane filtration, ozonation, electrodialysis, and heterogeneous photocatalysis have been applied for the control of geosmin and MIB levels in drinking water (Fotiou et al., 2016; Guo et al., 2016; Yao et al., 2017; Yaparatne et al., 2018; Zamyadi et al., 2015). Powdered activated carbon (PAC) adsorption, advanced oxidation processes (AOPs), and biofiltration have been effective for the removal of geosmin and MIB (Doederer et al., 2019; Peter and von Gunten, 2007; Srinivasan and Sorial, 2011; Westerhoff et al., 2006; Yao et al., 2017), whereas conventional treatment processes, such as coagulation, sedimentation, filtration, and chlorination, were ineffective (Peter and von Gunten, 2007; Srinivasan and Sorial, 2011; Westerhoff et al., 2006). Note that the removal

of geosmin and MIB that were spiked in filtered water at an initial concentration of 100 ng/L were 40% and 62% by 10 mg/L PAC and 97% and 95% by 2.5 mg/L ozone and 0.5 mg/L H_2O_2, respectively (Kawamura, 2000). Therefore, if T&O events occur seasonally and at low levels, PAC adsorption is one of the best options to effectively control geosmin and MIB. However, dissolved organic matter can reduce the adsorption efficiency of PAC and decrease the removal performance of geosmin and MIB. As a result, the operational cost of PAC application process increases (Chestnutt et al., 2007). On the other hand, in an area with recurring and high levels of T&O compounds, ozonation and AOP can be effective to resolve the T&O challenges. Although AOPs (e.g., ozone, ozone/H_2O_2, UV/ozone, UV/H_2O_2, etc.) are considered a desirable technique for the removal of organic contaminants due to fast reaction rates and unselective hydroxyl radical formation, the required dose, the effect of background constituents, and the plant upgrades to incorporate such processes to existing facilities increase the overall cost (Antonopoulou et al., 2014; Yaparatne et al., 2018).

Nanobubbles have emerged in the past decade as a novel technology for water/wastewater treatment, removal of pollutants from sediments and soils, and other environmental and biomedical applications (Agarwal et al., 2011; Hu and Xia, 2018; Liu et al., 2013; Lukianova-Hleb et al., 2012; Meegoda et al., 2017). However, there is still a lack of information on the fundamentals and application of the technology for water treatment. During the collapse of NBs, reactive oxygen species (e.g., •OH) can be produced (Liu et al., 2016). Hydroxyl radicals have been known as one of the major oxidants for the removal of geosmin and MIB (Xie et al., 2015; Yaparatne et al., 2018). The rate constants

of geosmin and MIB reacting with •OH radicals were known to be 6~8 × 10^9 $M^{-1}s^{-1}$ and 4~5 × 10^9 $M^{-1}s^{-1}$, respectively (Peter and von Gunten, 2007; Xie et al., 2015). To the best of my knowledge, the research is the first systematic study conducted to examine and understand the removal of geosmin and MIB using oxygen NBs under drinking water treatment conditions (Soyluoglu et al., 2022).

The main objectives were to investigate i) the removal efficiency of geosmin and MIB by oxygen NBs under various conditions (e.g., gas flowrate, gas type, pH, alkalinity, hardness, and temperature) in distilled and deionized (DDI) water and natural water matrices, and ii) the removal mechanisms of geosmin and MIB from water using oxygen NBs.

5.2. Material and Methods

5.2.1. Chemicals and water samples

Geosmin and MIB were purchased in powder form from FUJIFILM Wako Chemicals USA Corporation and geosmin-d3 was purchased from Sigma-Aldrich as a neat standard. *tert*-Butyl alcohol (TBA, Sigma Aldrich, ≥99.5%), furfuryl alcohol (FFA, Sigma Aldrich, 98%) and *p*-benzoquinone (PBQ, Thermo Scientific™, ≥98%) were used for the exploration of oxidative removal mechanisms for geosmin and MIB.

The experiments were conducted both in DDI and natural waters. To investigate the removal in natural waters, systematic experiments were conducted using i) Suwannee River NOM purchased from the International Humic Substances Society, and ii) natural waters (A-E) collected from source waters of five drinking water utilities in South Carolina

(SC), USA. Selected water quality parameters for natural water samples are presented in **Table 5.1**.

In DDI experiments, sodium bicarbonate ($NaHCO_3$) and calcium chloride ($CaCl_2$) were used to create alkalinity and hardness, respectively. All chemicals were used as received without further purification.

Table 5.1. Selected water quality parameters of natural waters collected from intake locations of five drinking water utilities in SC.

Parameters	Water A	Water B	Water C	Water D	Water E
pH	7.6	7.3	7.2	7.3	7.4
Chloride (mg/L)	8.1	2.1	3.5	1.3	4.5
Bromide (µg/L)	22	9	10	7	12
Nitrite (µg/L)	<DL				
Nitrate (µg/L)	269	200	930	260	267
Sulfate (mg/L)	3.5	1.2	0.7	0.9	3.6
Alkalinity (mg/L as $CaCO_3$)	29	16	40	24	52
DOC (mg/L)	7.0	1.8	1.9	1.1	3.6
$SUVA_{254}$ (L/mg-m)	3.9	1.4	2.4	2.3	3.2
DN (mg-N/L)	0.4	0.2	0.4	0.2	0.4
Turbidity (NTU)	4.5	3.5	7.5	1.0	3.9
Conductivity (µs/cm)	97	42	46	28	60

DL: detection limit, DOC: dissolved organic carbon, $SUVA_{254}$: specific ultraviolet absorbance at 254 nm, DN: dissolved nitrogen.

5.2.2. NBs generation and characterization

A commercial membrane-based NBs generator (Nano Bubble Technologies, Sydney, Australia) was used to produce NBs for the experiments. The manufacturer's recommended operational parameters for NBs generation were 60 psi for gas pressure and 1-10 L/min for gas flowrate. The operational water flowrate was 68 L/min. The concentration, mean and mode size, and size distribution of oxygen NBs were measured using a nanoparticle tracking analysis (NTA) instrument (NanoSight NS300, Malvern, UK). The zeta potential of oxygen NBs was determined using a Brookhaven 90Plus Particle Size Analyzer. More details can be found in the previous chapter, section 4.2.2.

5.2.3. Microbubble generation

To examine the interactions between oxygen NBs and microbubbles (MBs), micron-sized bubbles (100 to 400 μm) were generated using a flat ceramic ultrafine pore diffuser (Pentair Aquatic Eco-Systems, Inc., Apopka, FL). The gas pressure was set to 50 psi and the flowrate was adjusted at 1-4 L/min.

5.2.4. Geosmin and MIB removal experiments

During each experiment, temperature was controlled by a cooling coil, and pH and dissolved oxygen (DO) concentration were monitored on a real-time basis. When the pump was turned on, a rotameter was fully closed (i.e., gas flow = 0), with the suction and discharge valves that connected to the water container opened. Before injecting gas (e.g., mostly oxygen and air) to generate NBs, 100 ng/L geosmin and 100 ng/L MIB were spiked together in a metal container filled with 65 L DDI water, and water was circulated for two

minutes to create a homogenous solution. Then, a control sample at time=0 was taken from 2-3 inches below the water surface using vials rinsed with circulated water three times. After collecting a sample, a feeding gas was supplied to the NBs generator at 1, 4, or 8 L/min of gas flowrate. For the initial 30 min, water samples were collected every 10 min, and then every 30 min until 120 min and then hourly for the rest of experiments up to six hours. DO, pH, temperature, and NBs concentration were also monitored during the six hours of the total experiment period.

To investigate pH effect on the removal efficiency of geosmin and MIB, HCl and NaOH were used to adjust the pH of water to 3, 5, 6.5, and 10 prior to the addition of geosmin and MIB. To test the effect of hardness, $CaCl_2$ (300 mg/L as $CaCO_3$) was added to water in the container before addition of both geosmin and MIB. For the alkalinity effect, $NaHCO_3$ was used to create 15, 50 and 250 mg/L as $CaCO_3$ alkalinity in water. The water temperature was maintained at 20 °C using a cooling coil connected to a recirculating chiller (PolyScience, Niles, IL) for all experiments, except at 30 °C to explore the temperature effect. Moreover, selected radical scavengers such as TBA, FFA, and PBQ were used to examine the oxidative removal mechanisms of geosmin and MIB.

5.2.5. Geosmin and MIB removal mechanisms in DDI water

Geosmin and MIB can be removed by multiple mechanisms in the NB/DDI water system used in the experiments: i) volatilization facilitated with water circulation plus turbulence caused by continuous gas injection, ii) oxidation by ROS, and iii) sorption losses in the system. Initially, I confirmed that there was no sorption loss of geosmin and MIB in

the system (See section 5.2.7.). To further investigate the removal mechanisms, a series of experiments were designed and conducted in DDI water at pH 6.5 and 20 ^{o}C.

First, geosmin and MIB removal were monitored without oxygen NBs generation (i.e., no continuous gas injection into the system) while water was circulated for 6 h, which was the water circulation (WC) treatment. In the case, geosmin and MIB would be removed from the system only through the volatilization process.

Second, oxygen NBs were generated in the container initially, and the gas injection was stopped. Then, geosmin and MIB were spiked, and NBs were circulated in the system. The NBs circulation (NC) treatment allowed investigation of the effect of oxygen NBs alone. Third, MBs were generated using a diffuser with oxygen fed continuously, where only MBs (i.e., micron-sized bubbles (100 to 400 μm) were present, which was the MB treatment. Fourth, NC was combined with MB where pre-generated NBs were mixed with MBs, which was the NC+MB treatment.

Fifth, the typical NBs operation with oxygen fed continuously at 4 L/min to the system was carried out, which was the 4 L/min O_2 (or NBs regular) treatment, where both NBs and visibly bigger bubbles (i.e., MBs) were present in the system because the production of some MBs was inevitable during NBs generation.

Lastly, a series of experiments were conducted to suppress the oxidation process using bicarbonate (2.5 mM HCO_3^- as 250 mg/L $CaCO_3$ alkalinity), TBA (2 mM), or NOM (Suwannee River NOM at 3 mg/L DOC) which are known to be •OH radical scavengers

(Donham et al., 2014; Grebel et al., 2010; Xie et al., 2015); the results were compared to the 4 L/min O_2 (NBs regular) treatments.

5.2.6. Geosmin and MIB analysis

Geosmin and MIB were quantitatively analyzed using an automated solid-phase microextraction (SPME) method coupled with gas chromatography (GC) and tandem mass spectrometry (GC-MS/MS) on an Agilent 7890B gas chromatograph equipped with a PAL Automated Sample Injector and coupled to a 7000C triple quadrupole mass spectrometer. After a designated reaction time with NBs, 10 mL of collected samples was transferred into 20 mL SPME vial (a glass headspace CTC autosampler vial), and then 3 g NaCl and 100 ng/L of geosmin-d3 as an internal standard were added. Samples were immediately capped with metal screw caps continuing PTFE/silicone septa. All extractions were performed using a PAL automated SPME system with a 50/30 µm divinylbenzene/carboxen/polydimethylsiloxane (DVB/CAR/PDMA) fiber assembly (Supelco). All samples were measured in duplicate, and a new calibration set was analyzed for every batch. The injector was operated at 250 ˚C in splitless mode. Separation was performed on a 30 m × 0.25 mm ID × 0.25 µm (5%-phenyl)-methylpolysiloxane (HP-5MS) column at 1.0 mL/min of research grade helium flow. The temperature program was 40 ˚C, hold for 2 min; up to 220 ˚C at 20 ˚C/min; hold for 4 min. The transfer line temperature was 250 ˚C. Tandem mass spectrometry analysis was performed in the electron ionization (EI) mode and the quantification of target compounds was performed in the multiple reaction monitoring (MRM) mode. Precursor and product ions of MIB, geosmin, and geosmin-d3 are shown in **Table 5.2**.

Table 5.2. Detection information of MIB and geosmin on GC/MS/MS

Compound	Molecular Weight (g/mol)	Precursor ion	Product ion	Retention time (min)
MIB	168.3	95	67, 55	7.40
Geosmin	182.3	112	97, 83	9.04
Geosmin-d3	185.3	115	97	9.02

The detection limits (DL) were estimated for MIB and geosmin by eight consecutive analyses (i.e., one injection per vial for the prepared eight vials) of a mixed standard solution, which included approximately 10 ng/L of MIB and geosmin compounds. DL was calculated by using Equation 5.1.

$$DL = S^* t_{(n-1,\ 1-\alpha)} \qquad \text{Equation 5.1}$$

where S = standard deviation of the replicate analyses, $t_{(n-1,\ 1-\alpha)}$ = student-t value for 1- α with n-1 degrees of freedom. n= number of replicates, and α =0.01 (i.e., confidence level 1- α =0.99). The minimum reporting level (MRL) concentration was established as three times the DL (**Table 5.3**). In practical application, it is the lowest point on the calibration curve that can be quantified. The detection limits for geosmin and MIB were 1.0 and 1.2 ng/L, respectively.

Table 5.3. DLs and MRLs of geosmin and MIB established at 10 ng/L in DDI water

Sample number	MIB (ng/L)	Geosmin (ng/L)
1	10.65	10.76
2	10.28	10.66
3	10.09	11.42
4	10.86	10.54
5	10.30	10.64
6	10.70	10.62
7	9.66	10.32
8	10.79	10.90
Average	10.42	10.73
Std. dev.	0.41	0.32
DL	1.23	0.97
MRL	3.69	2.90

5.2.7. Verification of sorption loss and homogeneity of geosmin and MIB in the NBs generating systems

Prior to conducting any geosmin and MIB removal experiment, it was necessary to ensure that i) there was no loss of geosmin and MIB due to sorption within the system and ii) water in the containers was homogeneously mixed while generating NBs. For the verification, the container was filled with DDI water spiked with 100 ng/L MIB and geosmin. The water was circulated for about 90 seconds to complete two cycles of water circulation in the system. After five min of circulation, geosmin and MIB concentrations at t=0 were measured in samples taken from three different locations to check the homogeneity of the solution (**Figure 5.1**). The water tank was then covered with aluminum

foil and parafilm to reduce potential volatilization of geosmin and MIB. After six hours of holding time, the cover was removed, and water samples were taken from the same locations (as before circulation) to check if there was any sorption loss. To determine if any sorption loss occurred inside the system (e.g., hoses, pump, and connections), after circulating water for 90 seconds and waiting for 5 min, samples were taken again from the same locations to measure the final concentrations of geosmin and MIB.

Table 5.4 shows the results of the sorption and homogeneity experiments. There were no significant differences among the geosmin and MIB concentrations collected from 3 locations in the tank, which suggested a homogeneously well-mixed system. There was also no significant difference in geosmin and MIB concentrations before and after six hours of holding time while minimizing geosmin and MIB by volatilization. The results verified no loss of geosmin and MIB due to sorption and homogeneity of the system while running the experiments. Therefore, any observed geosmin and MIB removal in the presence of NBs could be attributed to either volatilization, or oxidation, or both.

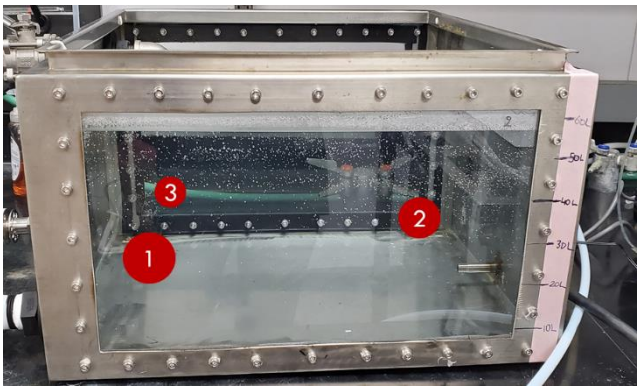

Figure 5.1. Sampling points for the experiments of geosmin and MIB sorption loss and system homogeneity.

Table 5.4. Changes of MIB and geosmin concentrations in the samples collected from three different locations in tank in the absence of NBs before and after 6 h of sitting time.

Condition	Sampling point	MIB (ng/L)	Geosmin (ng/L)
Time=0 h	1	115	110
	2	115	108
	3	111	107
After 6 h (top of tank was covered to minimize volatilization)	1	112	111
	2	114	106
	3	116	109
After 6 h (cover removed and water circulated for 90 sec and waited for 5 min)	1	112	112
	2	114	108
	3	114	109

5.3. Results and Discussion

5.3.1. Effect of gas flowrate and type

The effect of gas flowrate on the removal efficiency of geosmin and MIB in DDI was examined at 1, 4, and 8 L/min oxygen. The initial concentration of geosmin and MIB was 100 ng/L, and their disappearance was monitored for 6 h. During the experiments, temperature (20 °C) and DO (51±1 mg/L) remained relatively constant for the three flowrate conditions (**Figure 5.2**). The average oxygen NBs concentration increased from 4.9×10^7 to 1.2×10^8 particles/mL as gas flowrates increased from 1 to 8 L/min, while the mode of bubble size distribution remained around 100 nm regardless of the gas flowrate (**Figure 5.3**).

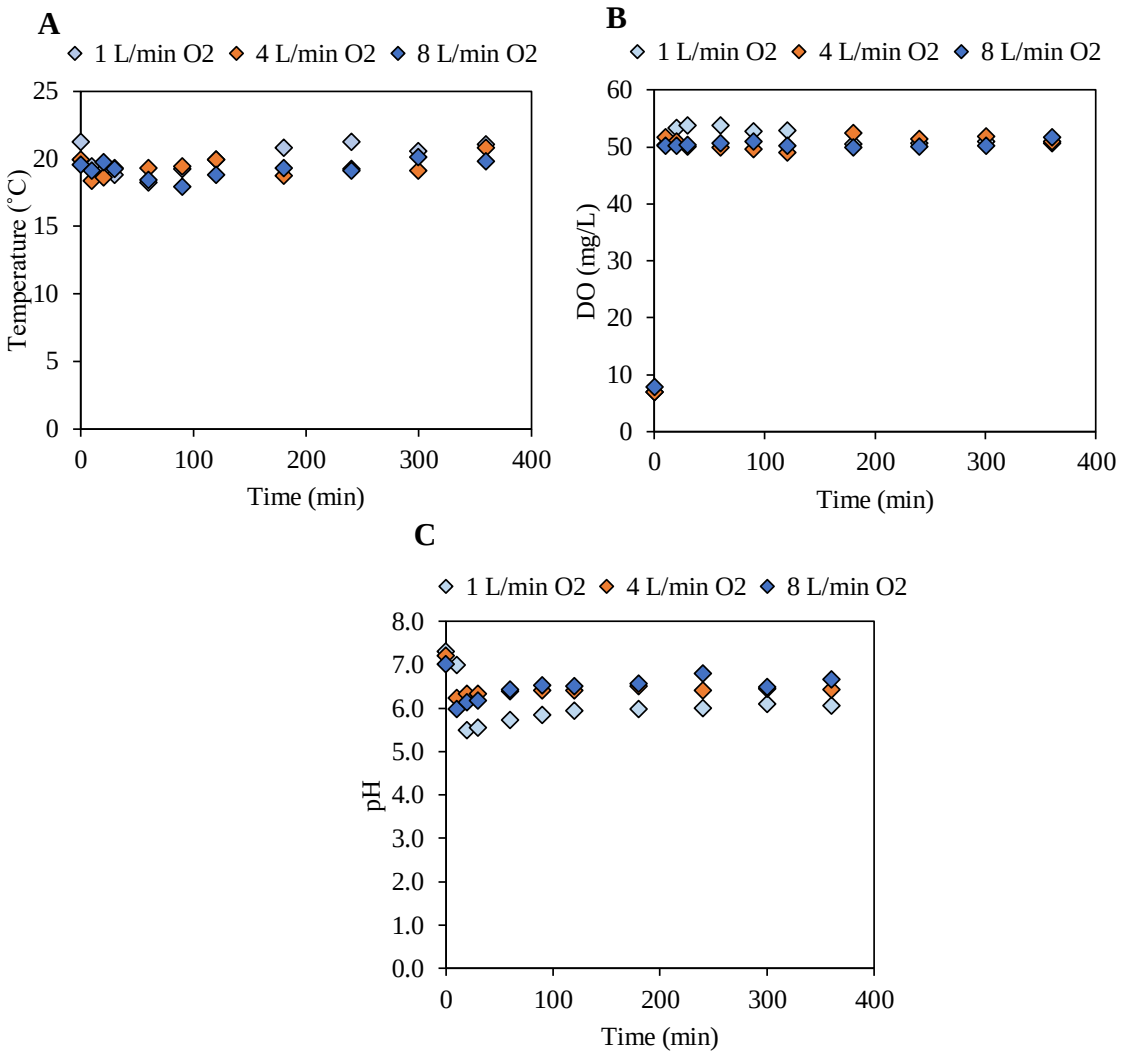

Figure 5.2. Changes of (A) temperature, (B) DO, and (C) pH during 6 h of NBs application at 1, 4, and 8 L/min of oxygen flowrates.

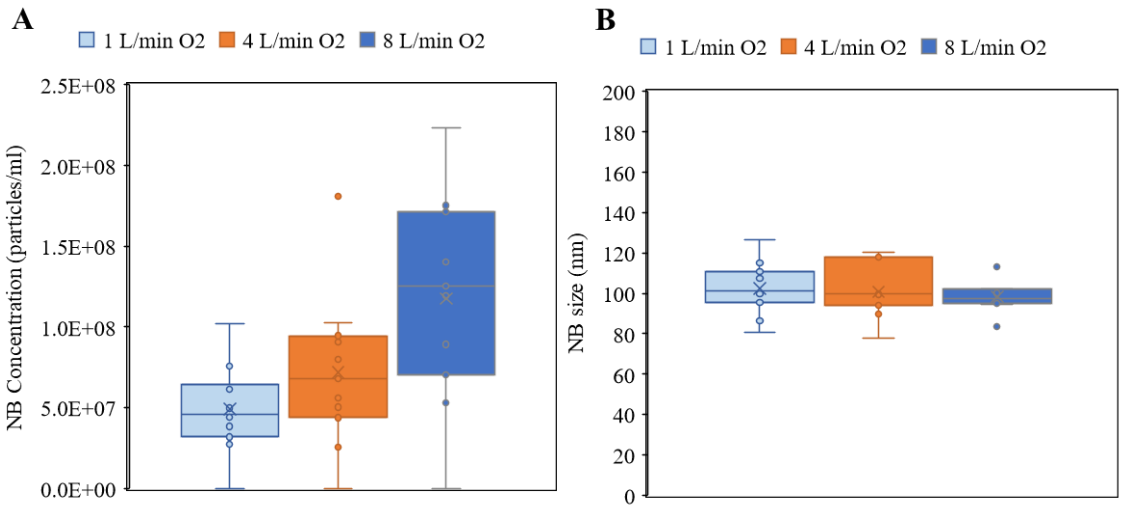

Figure 5.3. Box-and-whisker plots showing (A) variations and average concentrations and (B) the mode of bubble size distribution of oxygen NBs at 1, 4, and 8 L/min of gas flowrates.

Geosmin removal during these experiments were about 8% higher when the gas flowrate increased from 1 to 4 L/min (**Figure 5.4**A). A further increase of the flowrate to 8 L/min did not make any difference in geosmin removal. Therefore, 4 L/min of gas flowrate was selected to further explore geosmin and MIB removal by oxygen NBs. Geosmin removal percentages (~50%) were always higher than those of MIB (~30%) from DDI water by oxygen NBs (**Figure 5.4**). Others have shown that the second order rate constant for the reaction with •OH radical is slightly higher for geosmin (6-8 $\times 10^9$ $M^{-1}s^{-1}$) than MIB (4-5 $\times 10^9$ $M^{-1}s^{-1}$), leading to higher geosmin removal (Westerhoff et al., 2006). In addition, the Henry's law constant (6.75 $\times 10^{-5}$ atm-m^3/mol) of geosmin is higher than that (5.84 $\times 10^{-5}$ atm-m^3/mol) of MIB (Mustapha et al., 2021b). The findings of the study

indicated that geosmin was more readily removed than MIB through both oxidation and volatilization by oxygen NBs.

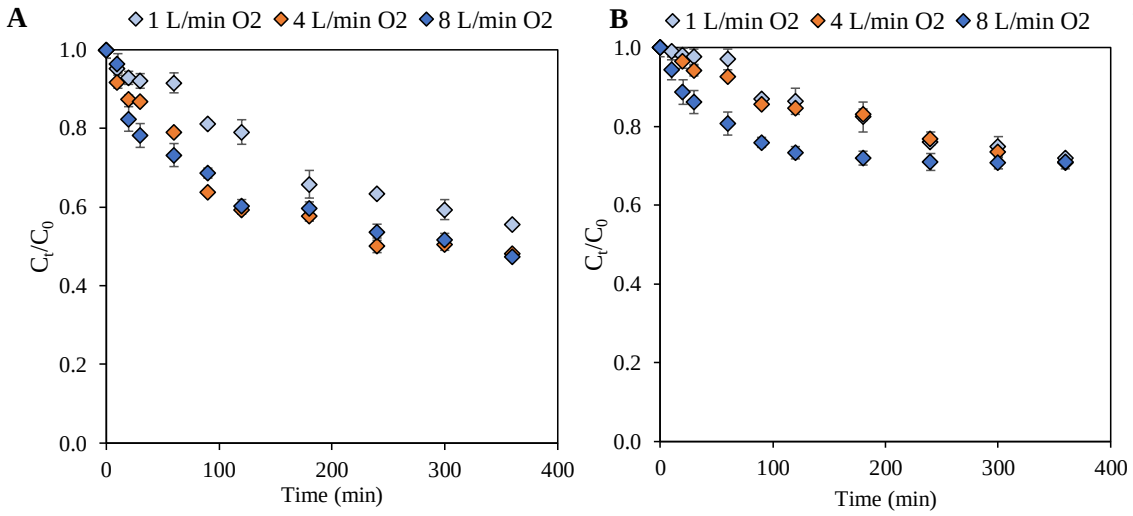

Figure 5.4. Changes in (A) geosmin and (B) MIB concentrations with oxygen NBs at 1, 4, 8 L/min. Error bars represent standard deviations (number of replicates; n=2).

To examine the effect of gas type on geosmin and MIB removal, NBs were generated at 4 L/min with oxygen, air, and nitrogen before spiking geosmin and MIB. While DO (8.0-9.5 mg/L) of the air NBs solution was approximately 20% of DO of the oxygen NBs solution because of the oxygen concentration in air and DO of nitrogen NB was <1 mg/L in solution (**Figure 5.5**), there was no significant difference between oxygen, air, and nitrogen NBs in terms of the mean NBs concentration (about 7.3×10^7 particles/mL) and the mode (about 100 nm) of bubble size distribution (**Figure 5.6**).

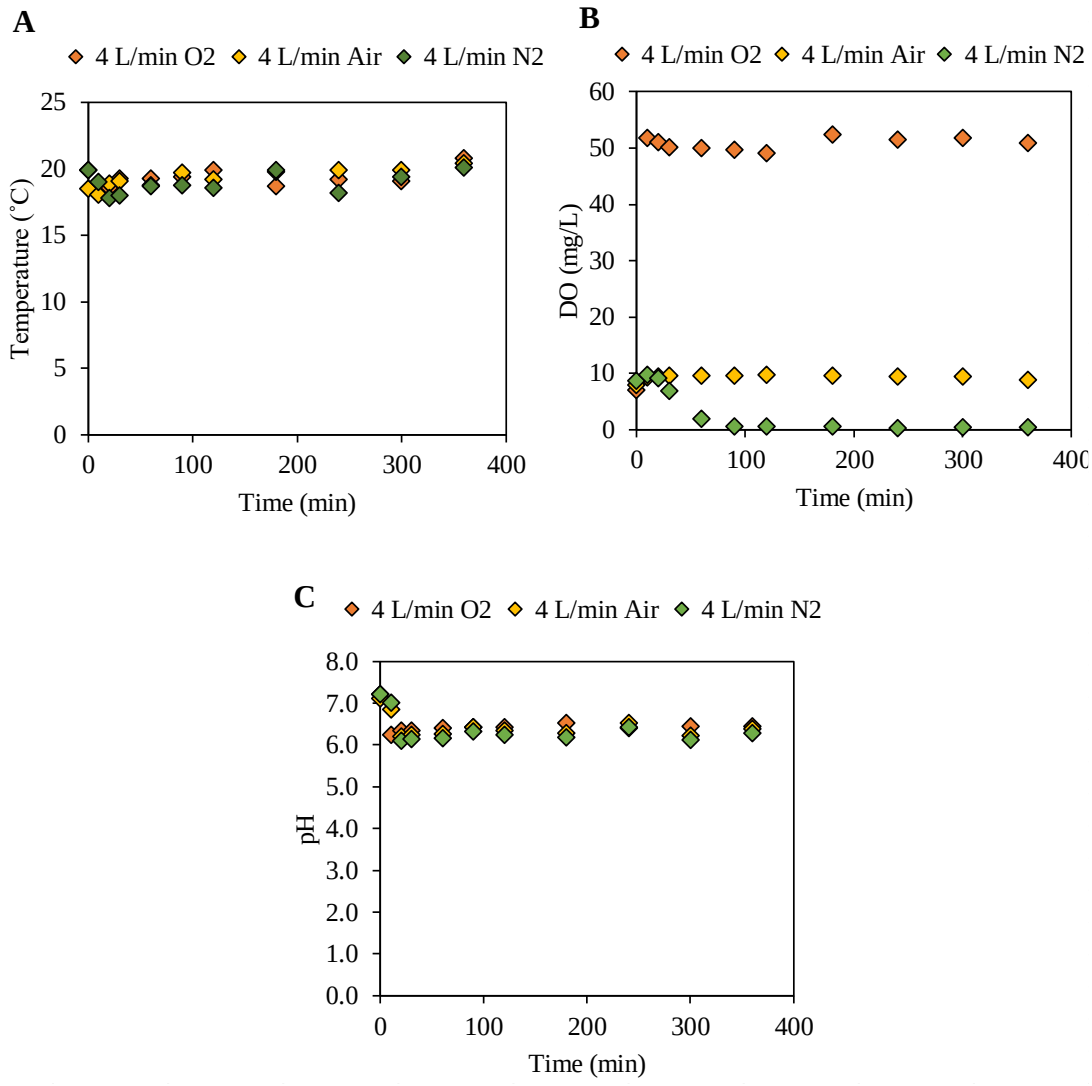

Figure 5.5. Changes of (A) temperature, (B) DO, and (C) pH during 6 h of NBs application of oxygen, air, and nitrogen NBs at a flowrate of 4 L/min.

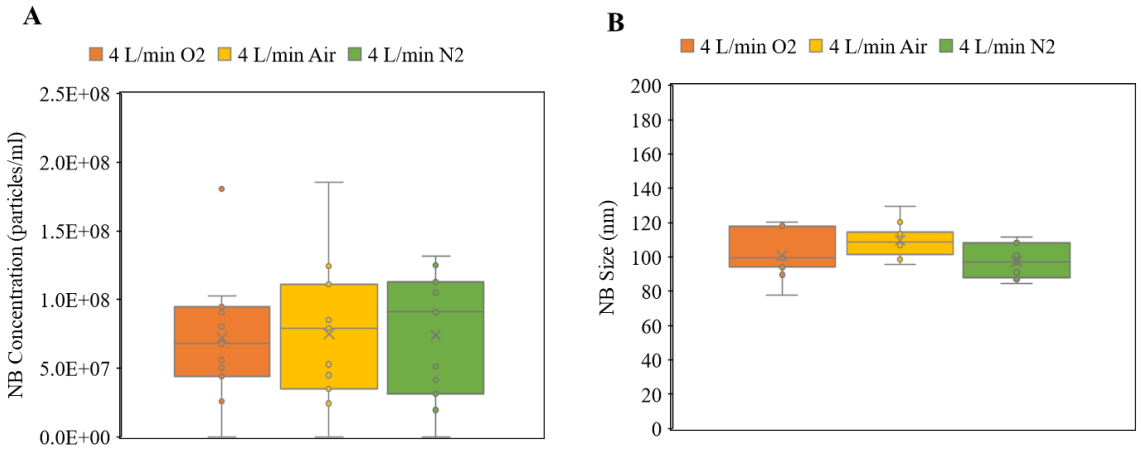

Figure 5.6. Box-and-whisker plots showing (A) variations and average concentrations and (B) the mode of bubble size distribution of oxygen, air and nitrogen NBs at a flowrate of 4 L/min.

Nitrogen and air NBs resulted in lower geosmin and MIB removal (Figures 5.7A and 5.7B, respectively) than oxygen NBs with MIB less affected by gas type than geosmin (**Figure 5.7**A and **Figure 5.7**B), with MIB removal less affected by gas type than geosmin. The removal percentages of geosmin and MIB decreased as the oxygen content of the feed gas decreased from 100% to 0%. Removal percentages of geosmin by nitrogen NBs were 19% for the initial 2 h and 28% after the total 6 h contact time. About 23% of geosmin was removed by air NBs for the initial 2 h, and then further removal (up to 42%) was achieved (**Figure 5.7**A). These removal percentages are lower than those (40% for 2 h and 52% for 6 h) by oxygen NBs, indicating a role for oxidation in the geosmin removal by NBs. Moreover, both oxygen and air NBs achieved about 30% of the maximum MIB removal during 6 h of contact time (**Figure 5.7**B).

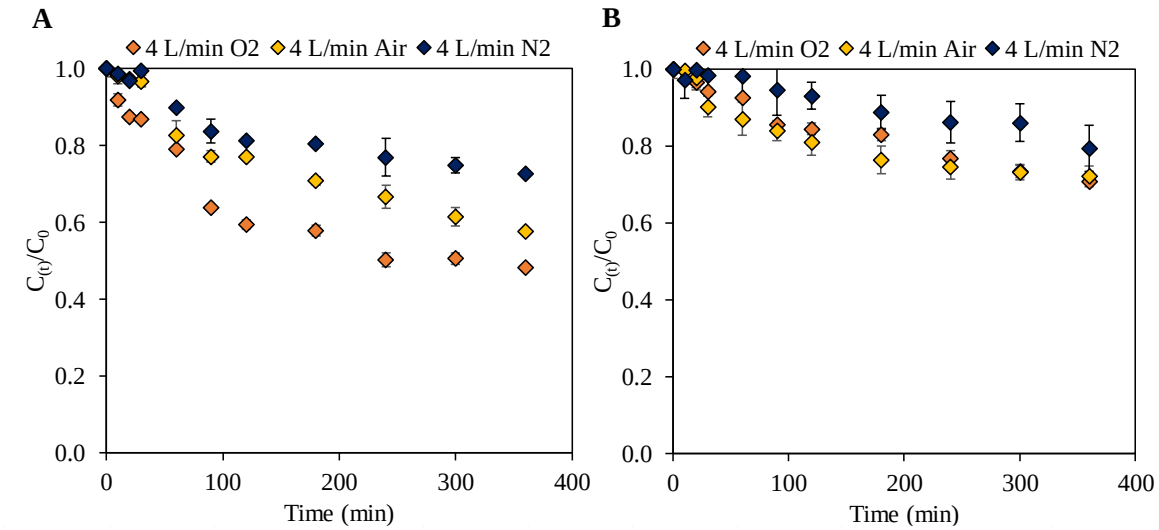

Figure 5.7. Changes in (A) geosmin and (B) MIB concentrations during 6 h of contact with oxygen, air, and nitrogen NBs at 4 L/min. Error bars represent standard deviation (n=4).

5.3.2. Effect of pH

The removal of geosmin and MIB by oxygen NBs was examined at pH 3, 5, 6.5, and 10. Temperature, DO and pH profile during the 6-h experiments are shown in **Figure C1**. Oxygen NBs concentrations depended on water pH because average concentrations increased from 1.48×10^7 to 7.21×10^7 particles/mL as pH increased from 3 to 6.5 (**Figure 5.8**A). The mode of bubble size distributions was around 100 nm (**Figure 5.8**B). Although NBs concentrations decreased at the acidic pH, geosmin and MIB removal were not significantly affected by pH ($p > 0.05$). No statistical difference ($p > 0.05$) in geosmin and MIB removal under different pH conditions was observed for 6 h of contact time, while slightly higher removal of both geosmin and MIB was achieved at pH 6.5 or 10 for the initial 2 h (**Figure 5.9**). MIB removal was not determined at pH 3 due to dehydration of MIB at acidic pH. The known products from MIB dehydration are 2-methyl-2-bornene, 2-

methylenebornane, and 2-methylcamphene which have boiling points 196, -43, and 159 ^{o}C, respectively (Hsieh et al., 2012; Satchwill, 2001; Schumann and Pendleton, 1997). Although dehydration of MIB is reversible, in the open reaction container used in these experiments (**Figure 5.1**), the dehydration products were likely lost from the system by aeration and circulation due to their lower boiling point and continuous reaction in the tank. The irreversible dehydration of MIB was greatly influenced at pH 3. Hsieh et al. (2012) also reported that only 13% of the initial MIB concentration (pH 6.3) can be measured by GC/MS with SPME under acidic conditions. However, there was no problem with measuring geosmin at pH 3 since geosmin is less sensitive to changes on pH and the geosmin dehydration product, argosmin that has similar properties with geosmin [solubility (150.2 ± 4.1 g/ L), K_{ow} (3.70 ± 0.03) and Henry's law constant (6.66×10^{-5} atm. m^3. mol^{-1})] is much less volatile than MIB's dehydration products (Hsieh et al., 2012; Pirbazari et al., 1992). Therefore, it was not lost from the system, thus when pH was adjusted to 7 before analysis, the reaction is completely reversible, making it possible to measure geosmin.

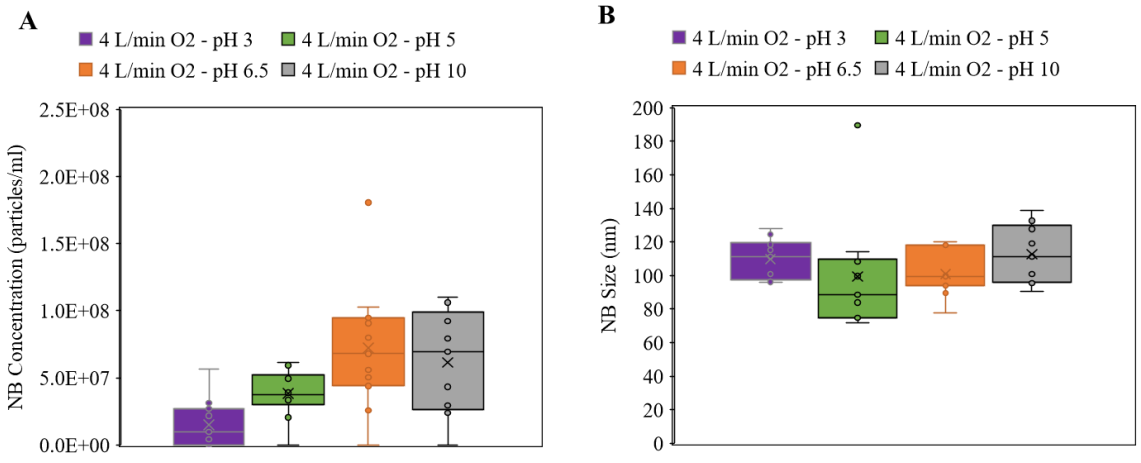

Figure 5.8. Box-and-whisker plots showing (A) variations and average concentrations and (B) the mode of bubble size distribution of oxygen NBs in the range of pH 3 to 10.

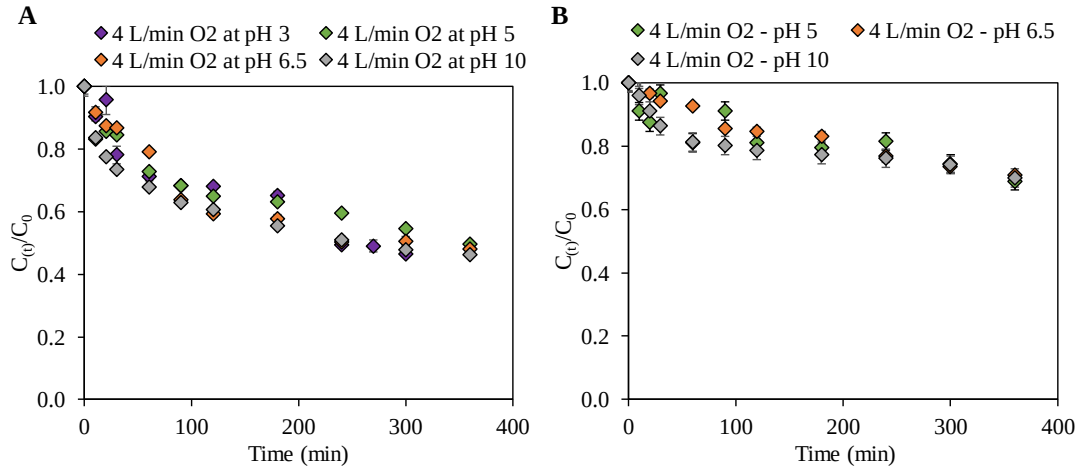

Figure 5.9. Changes in (A) geosmin and (B) MIB concentrations at various pH in DDI water during 6 h of contact with oxygen NBs at 4 L/min. Error bars represent standard deviation (n=2).

5.3.3. Effect of Alkalinity

The presence of alkalinity affected not only the characteristics of oxygen NBs, but also geosmin and MIB removal percentages. $NaHCO_3$ was used to prepare 15, 50 and 250 mg/L (as $CaCO_3$) alkalinity solutions. Previously, it was observed that the presence of cations affected NBs stability (Section 4.3.4 in chapter 4). The absolute value of the zeta potential of NBs solution decreased in the presence of Na^+, and the stability of oxygen NBs decreased. Since the surface of NBs is negatively charged, the absolute value of zeta potential in NBs solution decreased in the presence of cations. As a result, the repulsive force among NBs decreased, and thus the stability of NBs also decreased. Compared to the control, which was DDI with no alkalinity, the average oxygen NBs concentrations decreased up to 50% in the presence of background alkalinity during the NBs generation (**Figure 5.10**A). The mode of bubble size distributions also decreased slightly with increasing alkalinity because of the influence of Na^+ on the stability of oxygen NBs (**Figure 5.10**B).

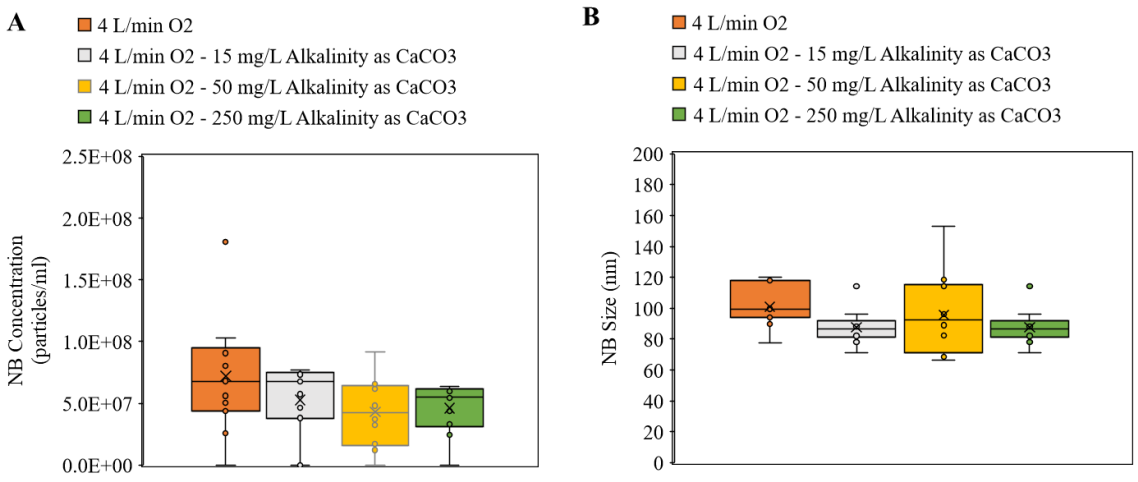

Figure 5.10. Box-and-whisker plots showing (A) variations and average concentrations and (B) the mode of bubble size distribution of oxygen NBs generated at 4 L/min in a range of alkalinity (0,15, 50, and 250 mg/L) as $CaCO_3$.

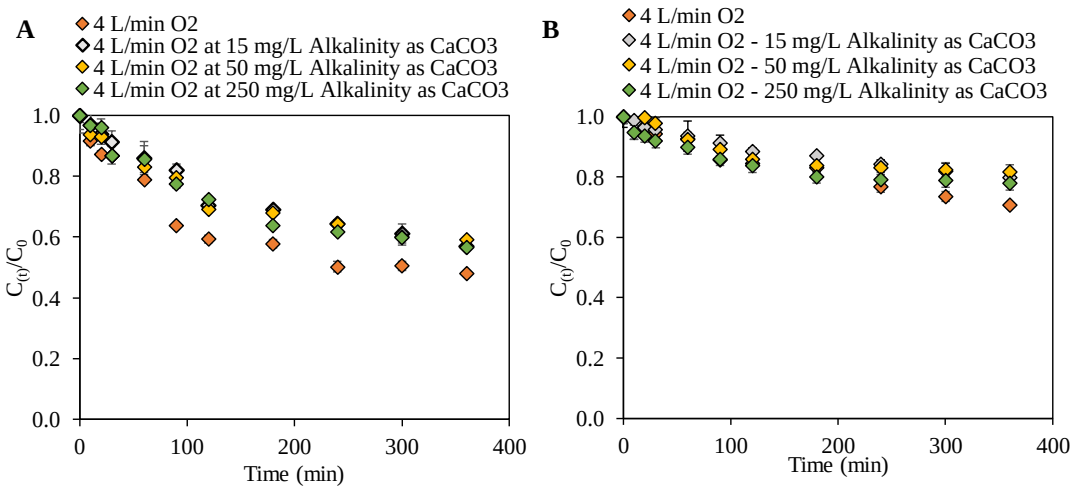

Figure 5.11. Changes in (A) geosmin and (B) MIB concentration under different alkalinity conditions during 6 h of contact with oxygen NBs at 4 L/min.

The presence of background alkalinity decreased geosmin (15%) and MIB (10%) removal and the effects of 15, 50 and 250 mg/L alkalinity were similar (**Figure 5.11**). Bicarbonate is a strong scavenger for •OH radicals (Hoigné and Bader, 1976; Staehelln and Hoigné, 1985); therefore, the oxidative removal pathway of geosmin and MIB by reactive oxygen species (ROS) would be inhibited to some extent by background alkalinity due to reduced oxygen NBs concentrations by the presence of Na^+ and quenched •OH radicals by bicarbonate in the system. The finding is critical for the applications of oxygen NBs in freshwater since a low level (i.e., 15 mg/L) alkalinity in the experiments was sufficient to impede the oxidative removal of geosmin and MIB.

5.3.4. Effect of hardness

To investigate the effect of hardness on geosmin and MIB removal, oxygen NBs were applied in the presence of Ca^{2+} (as 300 mg/L $CaCO_3$) in DDI water to simulate a hard water condition. Compared to the control without Ca^{2+}, available NBs concentrations were lowered by approximately 30%, while the mode of bubble size distributions increased (**Figure 5.12**). The results indicate that NB's negatively charged surface interacted with cations and the absolute value of surface charge decreased. The impact of Ca^{2+} on the stability of oxygen NBs is discussed in Chapter 4.

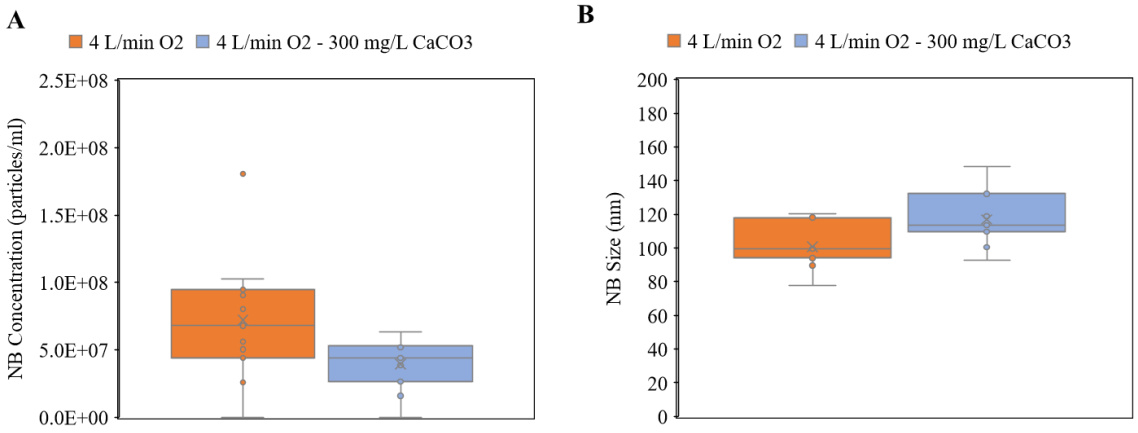

Figure 5.12. Box-and-whisker plots showing (A) variations and average concentrations and (B) the mode of bubble size distribution of oxygen NBs generated at 4 L/min with and without $CaCO_3$ (300 mg/L).

The hard water condition with 6 h of contact time resulted in about 7% lower geosmin removal compared to the control (**Figure 5.13**). For the initial 2 h, the impact of Ca^{2+} was evident (i.e., about 18% less removal than the control) probably because of the immediate influence of Ca^{2+} on the stability of oxygen NBs. Also, the presence of chloride ion (coming from the added $CaCl_2$) plays a role by scavenging •OH radicals that would inhibit the oxidation mechanism (Devi et al., 2013; Grebel et al., 2010; Kiwi et al., 2000; Liao et al., 2001), but the back reaction is very fast. The rate constant for the oxidation of chloride by •OH to Cl atoms is about 10^3 $M^{-1}s^{-1}$ at pH 7, which means that the reaction is very slow. However, the rate constant increases with decreasing pH, so the reaction becomes much faster at lower pH values. Therefore, the quenching of •OH by Cl^- is usually significant for pH ≤3 (von Gunten, 2003b). For these reason, as compared to the effect of alkalinity, the impact of chloride on the geosmin removal was less than bicarbonate, because the •OH radical quenching efficiency of bicarbonate is higher than chloride

(Grebel et al., 2010). On the other hand, MIB removal was not significantly (*p*-value > 0.05) affected by hardness of water, though available NBs concentrations were reduced in the presence of Ca^{2+} (**Figure 5.13**B).

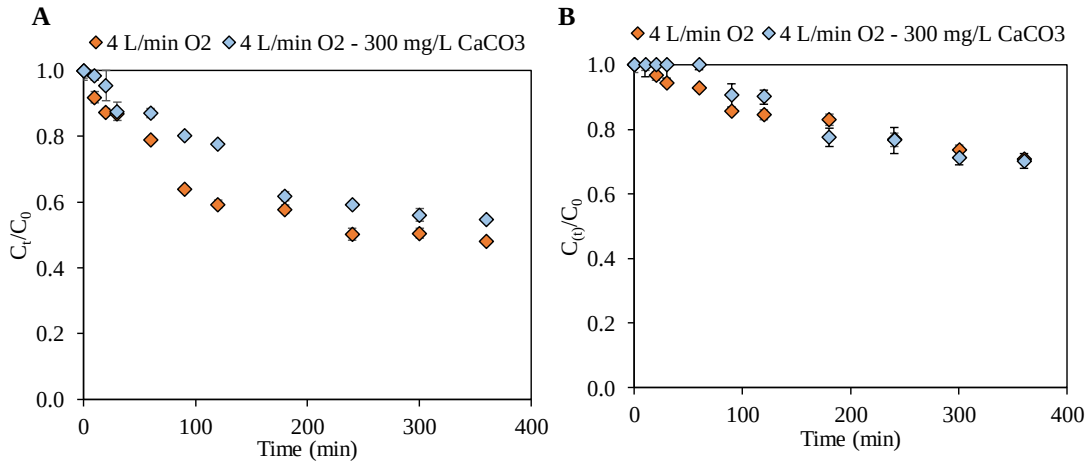

Figure 5.13. Changes in (A) geosmin and (B) MIB concentrations in soft water vs. hardwater during 6 h of contact with oxygen NBs at 4 L/min.

5.3.5. Effect of temperature

As the occurrence of geosmin and MIB increases in summer months due to seasonal algal blooms (Peter et al., 2009; Watson et al., 2008; Westerhoff et al., 2005), the effect of water temperature on the removal percentages of geosmin and MIB were investigated. As temperature increased from 20 °C to 30 °C, DO decreased from about 50 mg/L to 39 mg/L

reflecting the impact on oxygen solubility, while pH remained relatively constant (

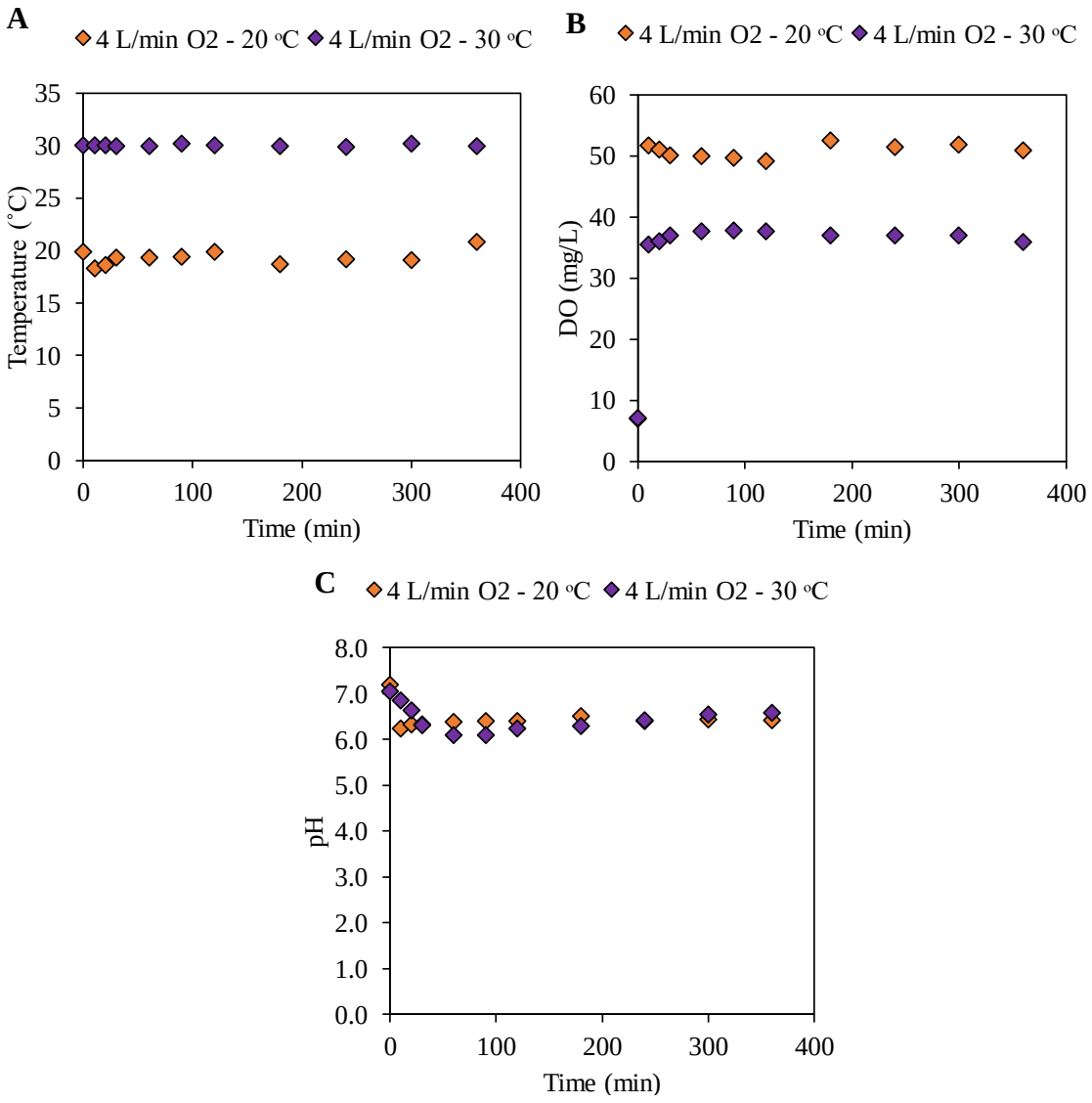

Figure 5.14).

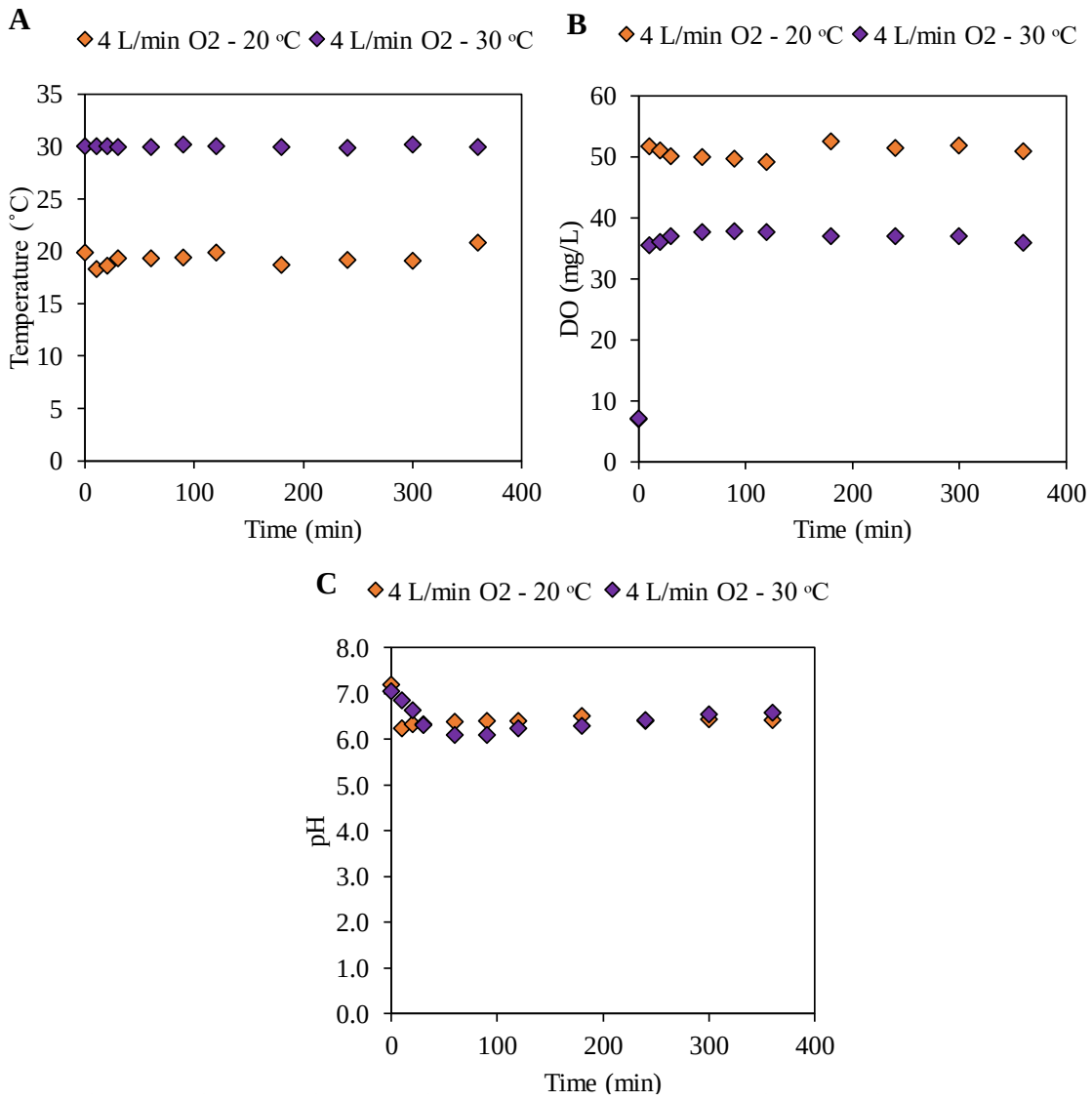

Figure 5.14. Changes of (A) temperature, (B) DO, and (C) pH at different temperature in DDI water during 6 h of contact with oxygen NBs at 4 L/min.

At higher temperature, higher and faster removal of geosmin and MIB was achieved by oxygen NBs (**Figure 5.15**). Approximately 21% of geosmin and 12% of MIB were additionally removed after 6 h of contact time as temperature increased from 20 °C to 30

°C. The enhanced removal of geosmin and MIB was attributed to both increased volatilization (Ömür-Özbek and Dietrich, 2005) and oxidative processes caused by greater production of ROS at higher temperature (Janus et al., 2012; Westerhoff et al., 2006).

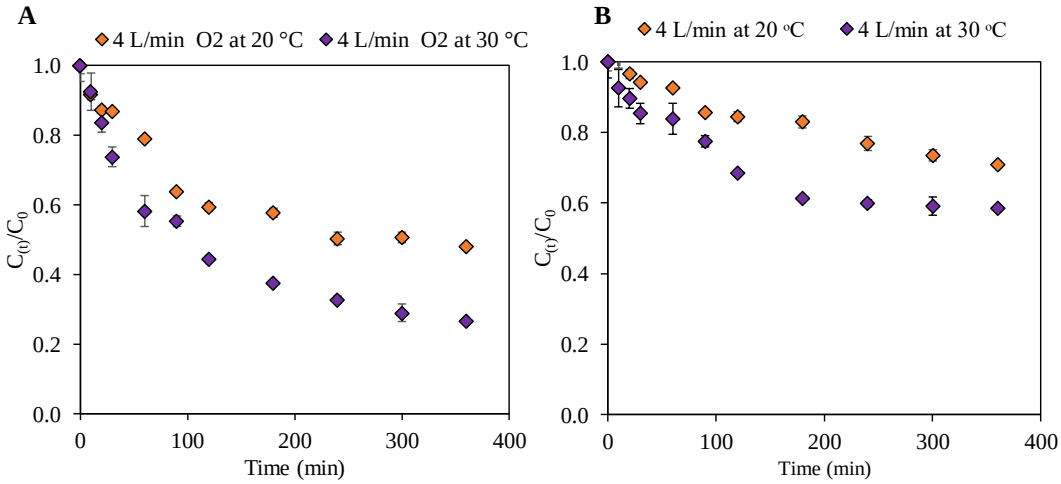

Figure 5.15. Changes in (A) geosmin and (B) MIB concentrations at different temperatures in DDI water during 6 h of contact with oxygen NBs at 4 L/min.

The temperature effect was further investigated along with other parameters such NOM, alkalinity, and pH. In the presence of NOM (Suwannee River NOM with 4.1 L/mg.m $SUVA_{254}$ purchased from International Humic Substances Society and adjusted to 3 mg/L DOC), the removal of geosmin achieved by oxygen NBs was slightly reduced although the difference was not statistically significant ($p > 0.05$), partially because of the radical quenching effect of NOM (Donham et al., 2014) (**Figure 5.16**). The geosmin disappearance rate constants for the initial 2 h by oxygen NBs were 6.2×10^{-5} s^{-1} at 20 °C

and 1.0 × 10^{-4} s^{-1} at 30 °C in the presence of NOM. The NOM effect was more significant for geosmin than MIB at higher temperature and longer reaction time.

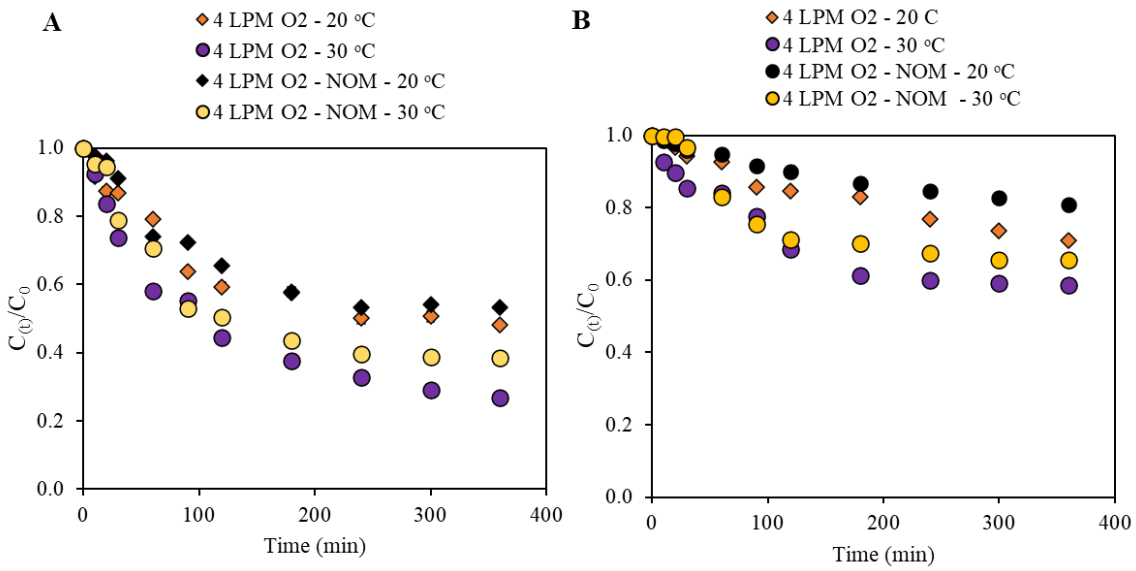

Figure 5.16. Changes in (A) geosmin and (B) MIB concentrations at different temperatures with/without NOM (3 mg/L DOC) in DDI water during 6 h of contact with oxygen NBs at 4 L/min.

Alkalinity significantly reduced the removal percentages of geosmin at both temperatures (i.e., from 7.5 × 10^{-5} s^{-1} to 5.0 × 10^{-5} s^{-1} at 20 °C and from 1.2 × 10^{-4} s^{-1} to 7.7 × 10^{-5} s^{-1} at 30 °C) in the presence of oxygen NBs (**Figure 5.17**). Bicarbonate quenches hydroxyl radicals and thus the oxidative removal pathway is inhibited (Hoigné and Bader, 1976; Staehelln and Hoigné, 1985). Although increasing temperature may enhance both volatilization and oxidation as the removal pathways of geosmin, the presence of 50 mg/L alkalinity as $CaCO_3$ would completely quench all ROS formed from oxygen NBs and thus

stop the oxidative removal pathway. Therefore, alkalinity has a significantly higher impact on the removal than temperature in the range of 20 to 30°C by quenching ROS.

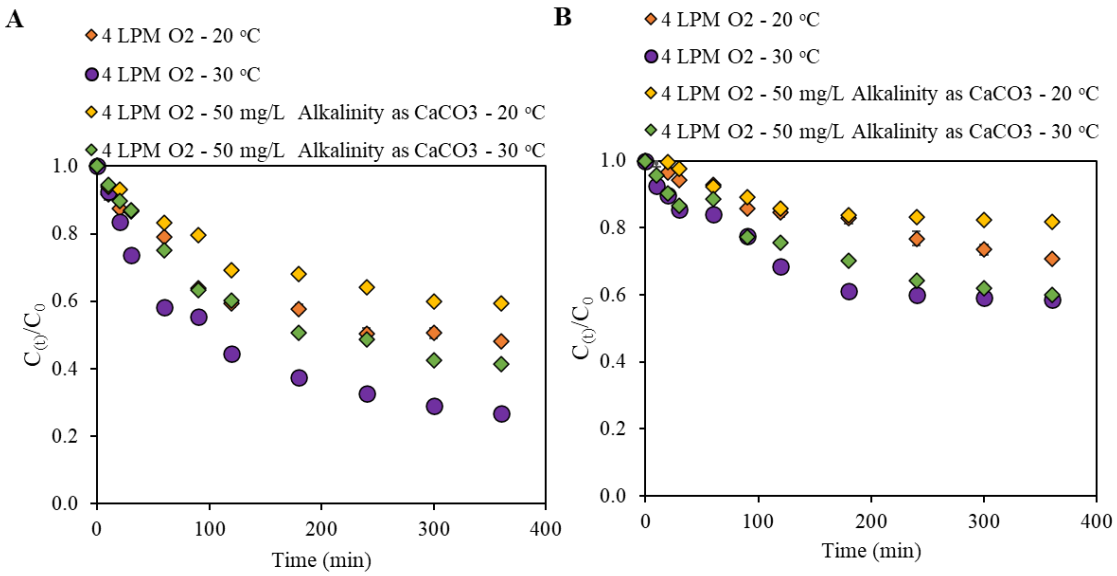

Figure 5.17. Changes in (A) geosmin and (B) MIB concentrations at different temperatures with/without alkalinity (50 mg/L as $CaCO_3$) in DDI water during 6 h of contact with oxygen NBs at 4 L/min.

5.3.6. Rate constant of geosmin and MIB removal by oxygen NBs

First-order disappearance rate constants and half-lives of geosmin and MIB under various conditions were determined from plots of ln C/C_0 vs. time for the initial 2 h of contact time with oxygen NBs (**Table 5.5** and **Figure 5.18**). Due to the time and labor demanding nature of the experiments, it was not feasible to run multiple experiments for all different conditions. However, I did run triplicate experiments for some selected conditions. For example, the rate constants for the removal of geosmin and MIB were

calculated from three independent control experiments at 4 L/min O_2 with the relative standard deviations (RSD) less than 10% (3% and 7% for geosmin and MIB, respectively). RSDs for the 4 L/min N_2 triplicate experiments were 3% and 9% for the removal percentages of geosmin and MIB, respectively. Thus, it was assumed that these low RSDs apply also to the other measurements. The rate constants for 6 h experiments were also derived and presented in **Table C1**. MIB removal percentages were always lower than those of geosmin due to the differences in their physicochemical properties. Lower water solubility (150 mg/L vs. 195 mg/L at 20 °C) and higher volatility (6.66×10^{-5} vs. 5.76×10^{-5} Henry's Law constant and 165 °C vs. 197 °C boiling point) of geosmin (Hafuka et al., 2019; Pirbazari et al., 1992) most likely account for higher removal of geosmin than MIB during the oxygen NBs application. The ratio of geosmin to MIB disappearance rate constants under various conditions in DDI water is shown **Table 5.6**. Further, the second order rate constants for the reactions between •OH radical and geosmin ($k_{OH,\ geosmin} = 9.5 \times 10^9\ M^{-1}s^{-1}$) and MIB ($k_{OH,MIB} = 8.2 \times 10^9\ M^{-1}s^{-1}$) which were derived by Westerhoff et al. (2006) from the time-dependent concentration profiles of residual ozone, MIB, geosmin, and a •OH probe (i.e., *p*-chlorobenzoic acid) and fit to time-dependent concentration profiles using a computer program (AQUASIM) imply a slightly higher oxidation potential for geosmin than MIB. Under all tested conditions, the geosmin disappearance rate was 1.3-3.4 times higher than the MIB disappearance rate (**Table 5.6**).

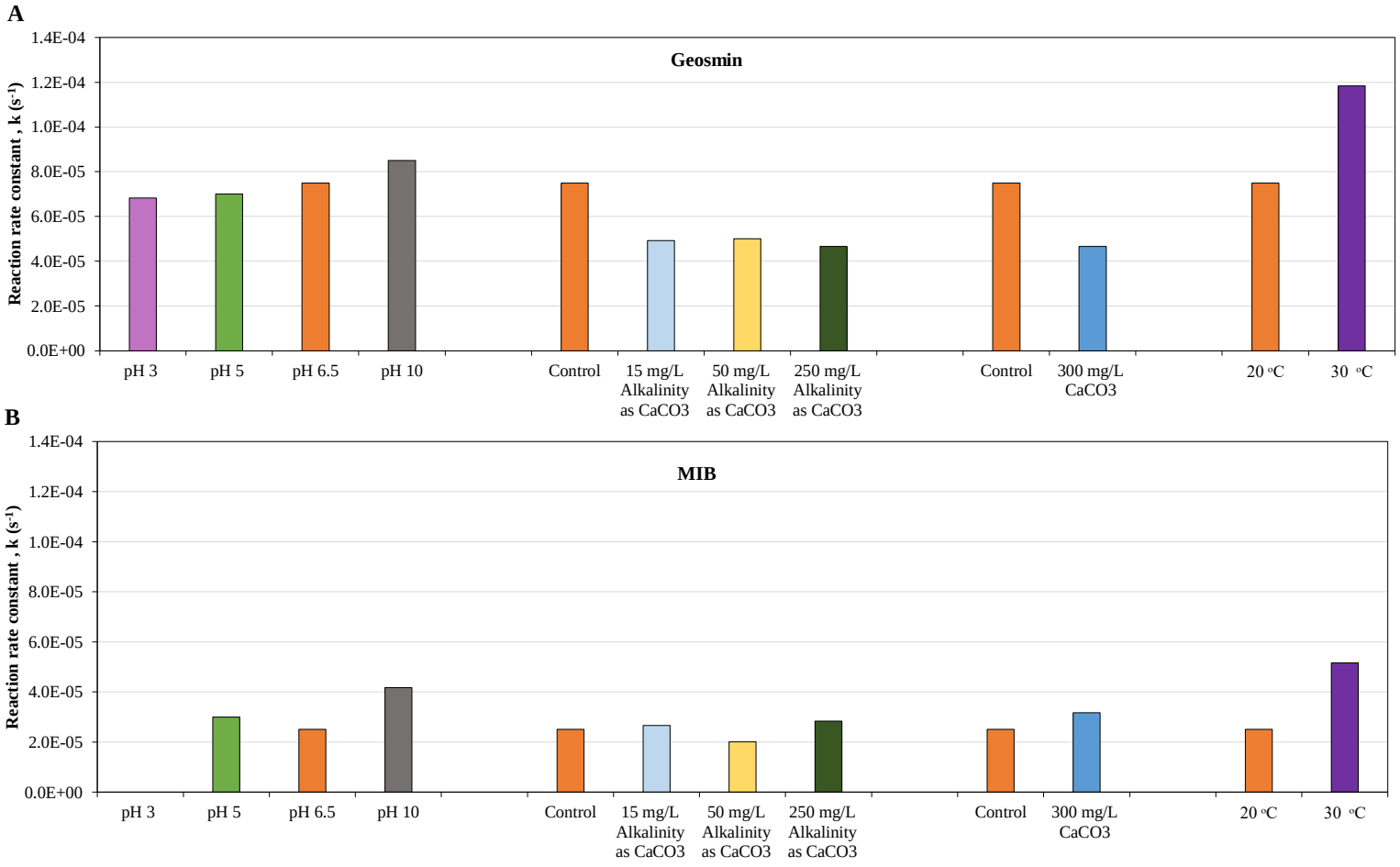

Figure 5.18. Removal rate constants (s^{-1}) for (A) geosmin and (B) MIB under various pH, alkalinity, hardness, and temperature conditions in DDI water during the initial 2 h of contact with oxygen NBs at 4 L/min.

Table 5.5. Geosmin and MIB disappearance rate constants (k in s^{-1}) and half-lives (in h) under various experimental conditions in DDI water for the initial 2 h of the oxygen NBs application.

Parameter	Experimental condition	Geosmin		MIB	
		k (s^{-1})	Half-life (h)	k (s^{-1})	Half-life (h)
Gas type	4 L/min N_2	2.8E-05	6.8	1.0E-05	19.3
	4 L/min O_2	7.5E-05	2.6	2.5E-05	7.7
	4 L/min Air	4.2E-05	4.6	3.2E-05	6.1
Gas flowrate	1 L/min O_2	3.5E-05	5.5	2.0E-05	9.6
	4 L/min O_2	7.5E-05	2.6	2.5E-05	7.7
	8 L/min O_2	7.5E-05	2.6	5.0E-05	3.9
pH	4 L/min O_2 at pH 3	6.8E-05	2.8	Not available	
	4 L/min O_2 at pH 5	7.0E-05	2.8	3.0E-05	6.4
	4 L/min O_2 at pH 6.5 (control)	7.5E-05	2.6	2.5E-05	7.7
	4 L/min O_2 at pH 10	8.5E-05	2.3	4.2E-05	4.6
Alkalinity	4 L/min O_2 (control)	7.5E-05	2.6	2.5E-05	7.7
	4 L/min O_2 at 15 mg/L alkalinity	4.9E-05	3.9	2.7E-05	7.2
	4 L/min O_2 at 50 mg/L alkalinity	5.0E-05	3.9	2.0E-05	9.6
	4 L/min O_2 at 250 mg/L alkalinity	4.7E-05	4.1	2.8E-05	6.8
Hardness	4 L/min O_2 (control)	7.5E-05	2.6	2.5E-05	7.7
	4 L/min O_2 at 300 mg/L as $CaCO_3$	4.7E-05	4.1	3.2E-05	6.1
Temperature	4 L/min O_2 at 20 °C (control)	7.5E-05	2.6	2.5E-05	7.7
	4 L/min O_2 at 30 °C	1.2E-04	1.6	5.2E-05	3.7
	4 L/min O_2 at NOM (3 ppm DOC) at 20 °C	6.2E-05	3.1	1.8E-05	10.5
	4 L/min O_2 at NOM (3 ppm DOC) at 30 °C	1.0E-04	1.9	4.8E-05	4.0
	4 L/min O_2 at 50 mg/L as $CaCO_3$ Alkalinity at 20 °C	5.0E-05	3.9	2.0E-05	9.6
	4 L/min O_2 at 50 mg/L as $CaCO_3$ Alkalinity at 30 °C	7.7E-05	2.5	4.3E-05	4.4

The gas type effect was more evident for the removal of geosmin than MIB. Half-lives of geosmin were 2.6 h, 4.6 h, and 6.8 h at 4 L/min O_2, 4 L/min air and 4 L/min nitrogen, respectively. Nitrogen NBs had a large effect on the half-life of MIB at 19.2 h,

while treatment with air NBs resulted in a half-life of 6.1 h and with oxygen NBs a half-life of 7.7 h. The effect of gas flowrate was more significant on MIB than geosmin removal. As the gas flowrate increased from 1 L/min to 8 L/min, half-lives of MIB decreased from 9.6 h to 3.9 h, while those of geosmin decreased from 5.5 h to 2.6 h. While the pH effect was not significant, both alkalinity and hardness increased half-lives of geosmin and MIB in DDI water. On the other hand, increasing temperature led to decreasing half-lives of both geosmin (from 2.6 to 1.6 h in DDI) and MIB (from 7.7 to 3.7 h in DDI). Also, a similar trend was observed for the effect of NOM and alkalinity under various temperatures, and increasing temperature decreased the half-lives of the compounds.

Among all parameters tested, alkalinity, hardness (added as $CaCl_2$), and low gas flowrate (i.e., 1 L/min O_2) showed the most negative impacts on both geosmin and MIB removal. Under these conditions, half-lives of geosmin and MIB increased up to 2 times as compared to the control condition (i.e., 4 L/min O_2). HCO_3^{--} ion in water serves as •OH radical scavenger (Grebel et al., 2010; Liao et al., 2001), thus the overall removal of geosmin and MIB decreased. Although there were similar concentrations of NBs in nitrogen, air and oxygen gas at 4 L/min gas flowrate (**Figure 5.6**), the presence of higher O_2 level and possible ROS formation likely increased the rate constant and, as a result, nitrogen and air NBs performances on removal efficiency were lower as compared to O_2.

Table 5.6. The ratio of geosmin to MIB disappearance rate constants from **Table 5.5** under various experimental conditions in DDI water for the initial 2 h of the oxygen NBs application

Parameter	**Experiment ID**	**Geosmin/MIB disappearance rate ratio**
		k(s^{-1})
Gas flowrate	1 L/min O_2	1.8
	4 L/min O_2	3.0
	8 L/min O_2	1.5
Gas type	4 L/min O_2	3.0
	4 L/min Air	1.3
pH	4 L/min O_2 - pH 3	-
	4 L/min O_2 - pH 5	2.3
	4 L/min O_2 - pH 6.5	3.0
	4 L/min O_2 - pH 10	2.0
Hardness	4 L/min O_2 (control)	3.0
	4 L/min O_2 - 300 mg/L $CaCO_3$	1.5
Alkalinity	4 L/min O_2 (control)	3.0
	4 L/min O_2 - 15 mg/L as $CaCO_3$ Alkalinity	2.5
	4 L/min O_2 - 50 mg/L as $CaCO_3$ Alkalinity	2.5
	4 L/min O_2 - 250 mg/L as $CaCO_3$ Alkalinity	1.6
Temperature	4 L/min O_2 at 20 ^oC	3.0
	4 L/min O_2 at 30 ^oC	2.3
	4 L/min O_2 at NOM (3 ppm DOC) at 20 ^oC	3.4
	4 L/min O_2 at NOM (3 ppm DOC) at 30 ^oC	2.1
	4 L/min O_2 at 50 mg/L as $CaCO_3$ Alkalinity at 20 ^oC	2.5
	4 L/min O_2 at 50 mg/L as $CaCO_3$ Alkalinity at 30 ^oC	1.8

5.3.7. Geosmin and MIB removal mechanisms in DDI water

Table 5.7 summarizes the removal levels of geosmin and MIB under the conditions described in Section 5.2.5. The removal rate constants for the initial 2 h of contact with oxygen NBs are presented in **Figure 5.19** to show the relative removal trends under various experimental conditions. The difference in both geosmin and MIB removal rate constants between Water circulation (WC) and NB circulation (NC) was statistically insignificant (*p*-value > 0.05), indicating that oxygen NBs alone in the system did not produce any additional removal due to volatilization and oxidation. Neither did microbubbles (MBs) alone (**Figure 5.19** and **Figure 5.20**). I observed that about 20±1% and 10±1% of geosmin and MIB were removed at 1.5 h by WC and MBs, respectively (**Figure 5.20**), which are comparable to the result of the traditional aeration process. Doederer et al. (2019) who conducted pilot scale aeration experiments reported that 2.5 L/min gas flowrate with coarse bubbles decreased geosmin and MIB concentration (C_0: 100 ng/L) by 18 ± 7% and 16 ± 6%, respectively, at 1.2 h of hydraulic retention time (HRT). However, in my study the presence of both oxygen NBs and MBs mixed continuously resulted in higher removal of geosmin than either WC or NC. I hypothesized that the mixture of NBs and MBs can stimulate bubble collapse and produce ROS to promote the oxidative removal process of geosmin and MIB. To test the hypothesis, the removal of geosmin and MIB in the NB/MB mixture system was further examined while shutting down the oxidation pathway. To do so, three different •OH radical scavengers were used (i.e., TBA, bicarbonate, and NOM). In the presence of either TBA or bicarbonate (250 mg/L alkalinity as $CaCO_3$) with a continuous gas injection at 4 L/min, the removal rates of geosmin were not statistically

different (*p*-values > 0.05) from WC, which indicated that the oxidation process was mostly inhibited by these radical quenchers. Although the oxidation process was also suppressed by the presence of NOM, free radical quenching by TBA or bicarbonate was greater than by NOM (i.e., the order of geosmin removal follows NBs regular > NOM > alkalinity > TBA) (**Figure 5.19**) (Donham et al., 2014; Khare, 2016). NOM may have been less effective because the NOM concentration (i.e., 3 mg/L) was lower than either TBA or alkalinity. In comparison to WC (i.e., volatilization process alone), during the regular NBs operating condition (having both volatilization and oxidation processes available), approximately 15% of geosmin and 10% of MIB was additionally removed via the oxidation process via ROS (**Figure 5.20**).

Table 5.7. Summary of a series of experiments and observations conducted to investigate the main removal mechanism of geosmin and MIB in DDI water.

Experiment	Geosmin & MIB removal result	Volatilization	Enhanced Volatilization due to NB/MB mixing	Oxidation due to NB/MB mixing
Water circulation (WC)	Default	+++	**N/A**	**N/A**
NBs circulation (NC)	**NC**≈WC	+++	**N/A**	**N/A**
MB regular	**MB**≈NC≈WC	+++	**N/A**	**N/A**
NC+ MB regular	**(NC+MB)**>MB≈NC≈WC	+++	-	+
4 L/min O_2 (NBs Regular)	**NBs Regular**>(NC+MB)>MB≈NC ≈WC	+++	-	++
NBs regular with alkalinity	NBs regular>NOM >**alkalinity**≈NC≈WC	+++	-	-
NBs regular with TBA	NBs regular>NOM >**TBA**≈alkalinity≈NC≈WC	+++	-	-
NBs regular with NOM	NBs regular>**NOM** >TBA≈alkalinity≈NC≈WC	+++	-	+

+++: primary impact (geosmin up to 40% and MIB up to 20% removal achieved), ++: moderate (geosmin up to 15% and MIB up to 10% removal achieved), +: minimal (<10% for both geosmin and MIB), -: none, N/A: not applicable.

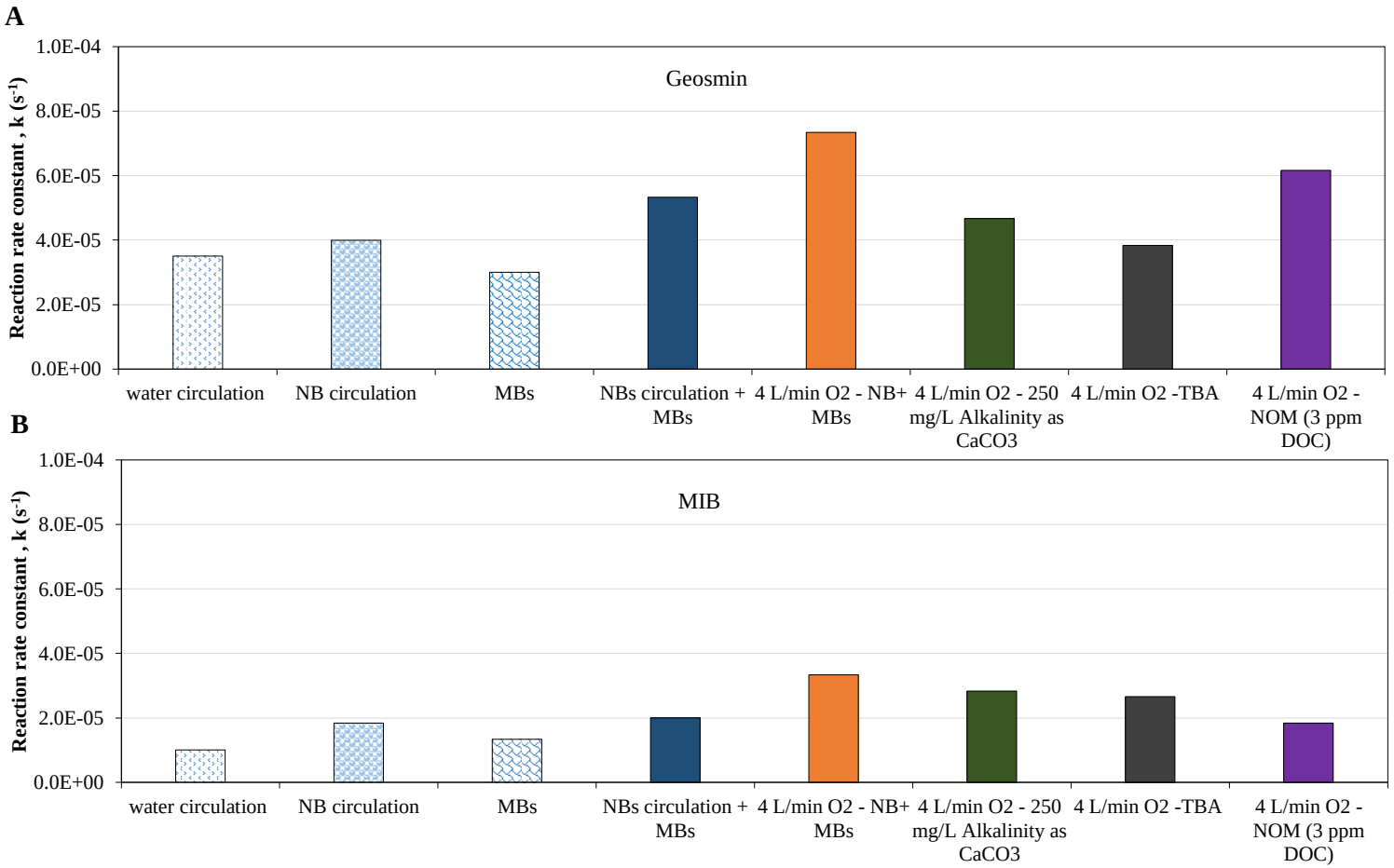

Figure 5.19. Removal rate constants (s^{-1}) for (A) geosmin and (B) MIB under different conditions to systematically explore removal mechanisms during the initial 2 h of contact without (i.e., water circulation) and with oxygen NBs at 4 L/min.

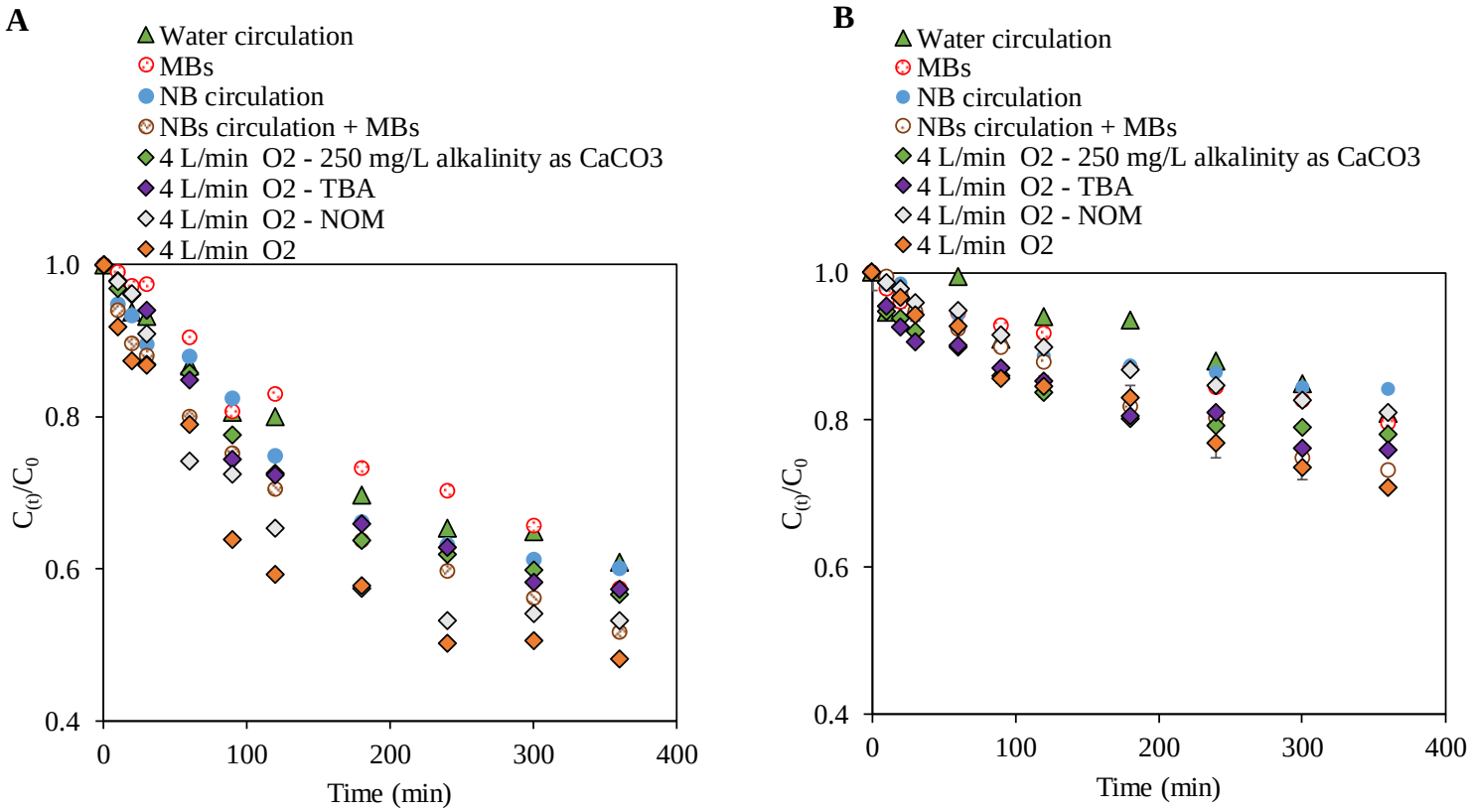

Figure 5.20. Changes in (A) geosmin and (B) MIB concentration under different conditions to systematically explore removal mechanisms during 6 h of contact without (i.e., water circulation) and with oxygen NBs at 4 L/min. Error bars represent standard deviations (n=2).

TBA completely suppressed the oxidative degradation pathway of geosmin. Although TBA quenches mostly •OH radicals, other types of ROS such as singlet oxygen, superoxide radical, etc. may also be quenched (Monteagudo et al., 2011). Therefore, a quenching study with FFA and PBQ was conducted to quench preferentially singlet oxygen and superoxide radical, respectively (Appiani et al., 2017; Fónagy et al., 2021; Liu et al., 2016; Talukdar and Dutta, 2016). To evaluate the effectiveness of various radical scavengers in inhibiting the formation of geosmin and MIB under continuous NBs generation, each specific radical scavenger (i.e., 2 mM TBA, 10 mM FFA, or 0.1 mM PBQ) was individually added to the container before spiking with geosmin and MIB. The concentration changes of geosmin and MIB were then monitored for 6 h.

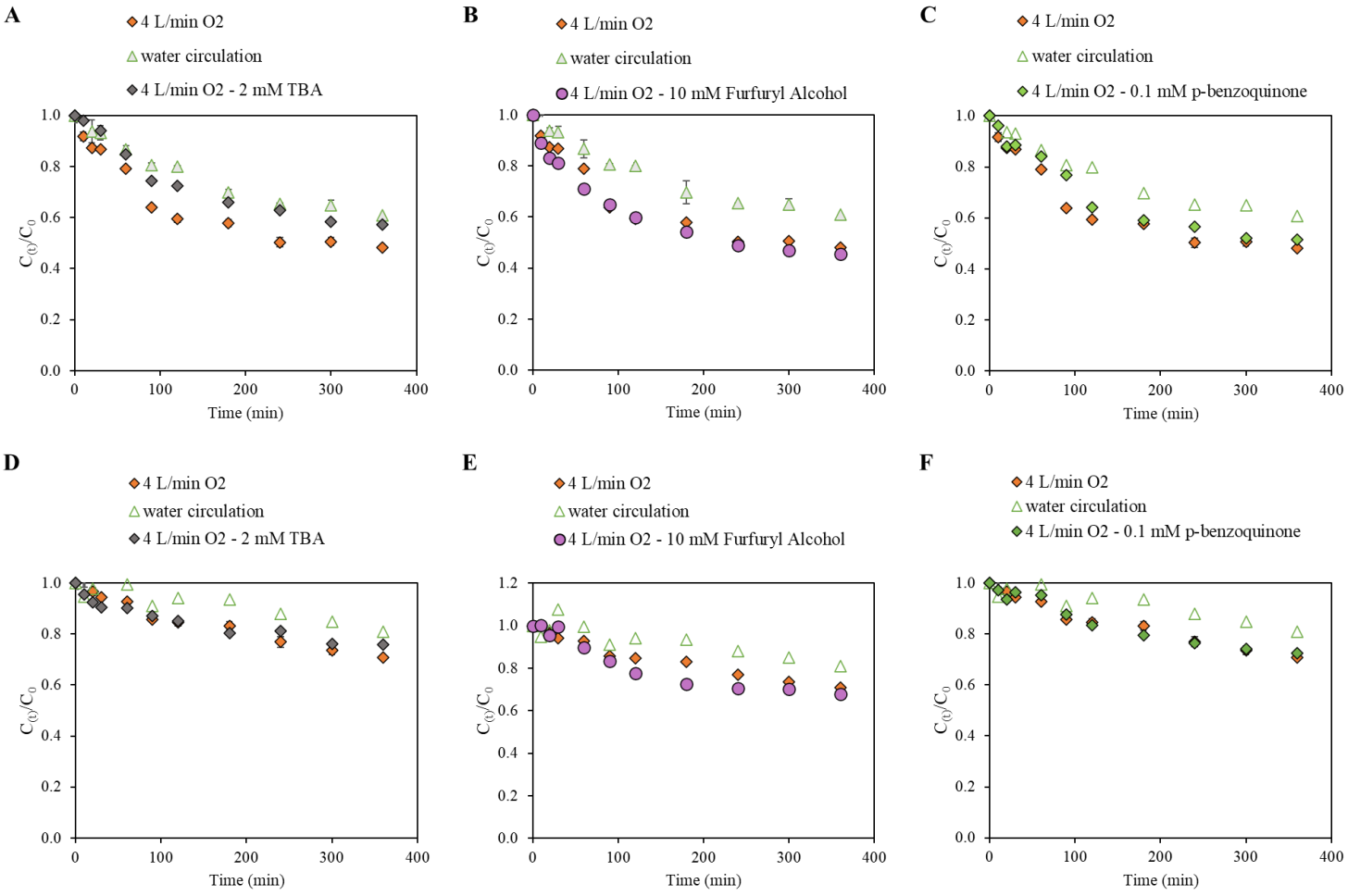

Figure 5.21. Changes in (A-C) geosmin and (D-F) MIB concentration in the presence of TBA, furfuryl alcohol (FFA), and *p*-benzoquinone (PBQ), respectively, to identify responsible ROS during the oxidation removal process. Error bars represent standard deviation (n=2).

Figure 5.21 shows the removal of geosmin and MIB in the presence of the different radical quenching reagents. The effect of FFA and PBQ on the oxidation removal process of geosmin was insignificant (*p*-values > 0.05) compared to TBA, suggesting that there was no oxidative impact by interactions of geosmin and MIB with those preferential ROS (i.e., singlet oxygen and superoxide radical) in the system. Therefore, the removal of geosmin during the oxidation process was likely promoted by •OH radicals alone. The result was consistent with a recent study, where the generation of ROS in NBs suspensions (i.e., O_2, N_2, and CO_2-NBs) was characterized using electron spin resonance spectroscopy; the main ROS generated in the NBs water was •OH radical (Yamaguchi et al., 2021). Overall, these findings indicated that •OH radical was the major ROS for the oxidative degradation of geosmin and MIB by oxygen NBs.

To examine the formation of •OH radicals in my experimental system, a probe molecule, TP, was used. TP was added into the reaction medium as a radical trap that reacts with •OH radicals leading to the formation of stable hydroxyl radical adducts (2-hydroxyterephthalate (TPOH)) with a typical percent yield of 35% in oxygen NBs system (Cheng et al., 2007; Yaparatne et al., 2018). The formation of •OH radicals showed a maximum of 10 nM and an average of 6.9 nM in the oxygen NBs solution at pH 6.5 (See in **Figure 5.22**). Therefore, the additional removal (beyond volatilization) of geosmin observed was likely attributed to the oxidative reaction with •OH radicals in the presence of mixed NBs and MMBs. These results indicate that the presence of MMBs in the system with NBs together induced the formation of •OH radicals. A low level of alkalinity (15

mg/L as $CaCO_3$) was enough to almost completely quench •OH radicals formed from oxygen NBs.

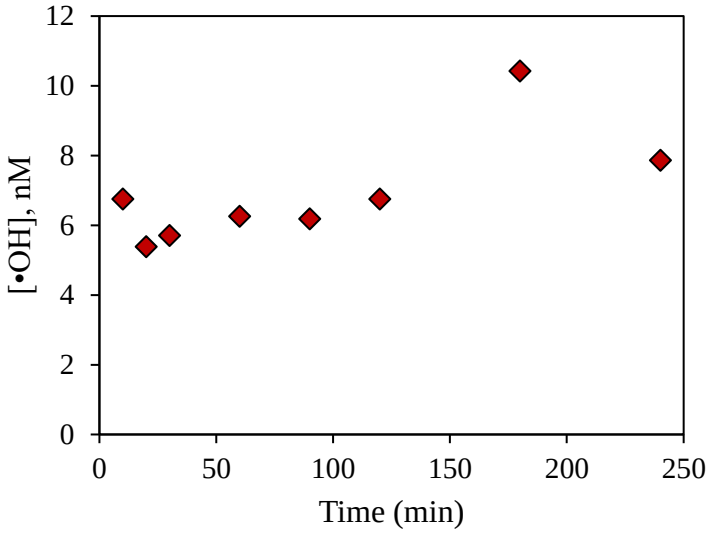

Figure 5.22. The concentration of •OH radicals formed during the oxygen NBs generation at pH 6.5 in DDI.

5.3.8. Geosmin and MIB removal in natural waters

To determine the potential for the use of oxygen NBs in practice, the removal efficiency of geosmin and MIB by oxygen NBs was further investigated in five different natural waters used as source waters for drinking water treatment plants in South Carolina, USA. Unlike DDI water, natural waters contain various components that can inhibit the oxidative removal pathway of geosmin and MIB by quenching ROS. Although the selected natural waters cover a range of water characteristics such as 1.1-7.0 mg/L DOC, 1.4-3.9 L/mg-m $SUVA_{254}$, 1.0-7.5 NTU turbidity, and 28-97 µs/cm conductivity as shown in **Table**

5.1, the removal percentages of geosmin and MIB were not significantly different from one another ($p > 0.05$) (**Figure 5.23**). The removal of geosmin and MIB in these natural waters was not significantly different ($p > 0.05$) from WC (where volatilization is the main removal mechanism), which suggests that the oxidative removal mechanism was considerably inhibited by the components of the natural waters. Among the measured water quality parameters, alkalinity was the most important parameter affecting the removal efficiency of geosmin and MIB while applying oxygen NBs. As discussed above, the oxidation process initiated by •OH radical was completely shut down by ≥ 15 mg/L of alkalinity in DDI water. Measured alkalinity of the natural water samples ranged from 16 to 52 mg/L as $CaCO_3$ (**Table 5.1**). Such levels of alkalinity in tested natural waters would completely inhibit the oxidative degradation process by ROS, and thus the overall removal of geosmin and MIB would be achieved by volatilization alone when using oxygen NBs. In addition, the NOM present in natural waters may have radical scavenging capability to some extent (**Table 5.7**). The removal of geosmin and MIB was greatly influenced by components that can be commonly found in natural waters; the removal percentages of geosmin and MIB in the five different natural waters were not statistically different (*p*-values > 0.05) from WC since the oxidative removal pathway was completely inhibited.

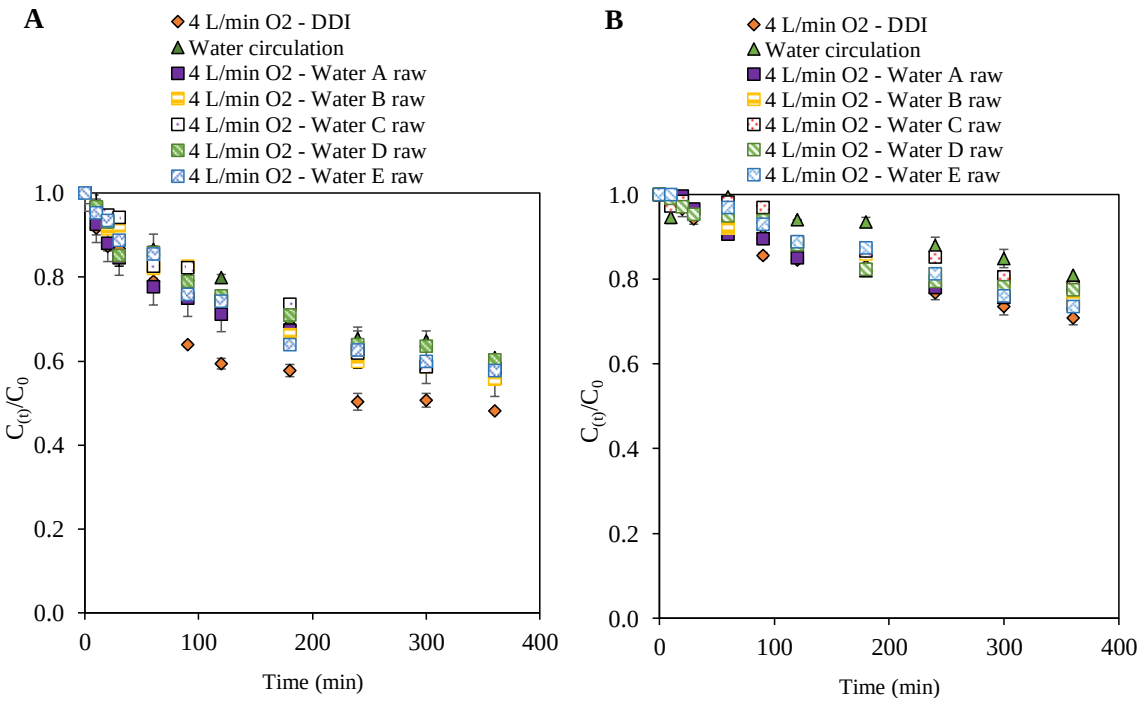

Figure 5.23. Changes in (A) geosmin and (B) MIB concentration in five different natural waters during 6 h of contact with oxygen NBs at 4 L/min. Error bars represent standard deviations (n=2).

Overall, these findings show that volatilization was the main mechanism for the geosmin and MIB removal from natural waters when oxygen NBs were applied. Although •OH radicals are formed by oxygen NB, their levels were too low and were quenched easily by the background alkalinity and NOM, whose concentrations were orders of magnitude higher than those of geosmin and MIB. The low level of •OH radical formation was related to the concentration of NBs generated in water. Although NBs levels may be measured in DDI water, their measurement in natural waters is currently not possible due to the interference from the ubiquitous background particles in natural waters. As a result, usually indirect measures such as dissolved oxygen or oxidation reduction potential (ORP) levels

in water must be used to assess the performance of NBs generators, which do not represent the level of NBs present in water. The limitation is an obstacle for the application and monitoring of using NBs systems in practice. Additional approaches are needed to exploit and take advantage of oxidation pathways in natural waters and drinking water treatment.. Since our NBs generators accommodated the use of ozone gas, I explored ozone NBs and their removal efficiency of geosmin and MIB in the following chapters.

5.4. Conclusions

The removal of geosmin and MIB by NBs and their removal mechanisms were systematically investigated under various operational and environmental conditions. Volatilization was the major removal mechanism of geosmin (~40%) and MIB (~20%) from DDI water, and oxidation by ROS brought additional removal up to ~15% to ~55% for geosmin and ~35% for MIB. However, alkalinity as low as 15 mg/L as $CaCO_3$ significantly decreased the removal of both geosmin and MIB by scavenging free •OH radicals, due to the inhibition of the oxidative removal pathway. The removal of geosmin and MIB was enhanced at a higher temperature because of increased volatilization and oxidative processes, while the removal percentages of geosmin and MIB decreased in the presence of either NOM or $CaCl_2$ in DDI. The effect of pH in the range of 3-10 was insignificant on geosmin and MIB removal using oxygen NBs. Given the differences in water solubility and volatility, geosmin was more readily removed by oxygen NBs than MIB through both oxidation and volatilization removal pathways.

Continuous generating and mixing of NBs and MBs stimulated •OH radical formation and resulted in additional removal of geosmin (~15%) and MIB (10%), while there was no evidence of geosmin/MIB oxidation by either NBs or MBs alone. Free •OH radical was the responsible ROS in the geosmin removal, while no impact of other ROS such as singlet oxygen and superoxide radicals was observed. The role of ROS was not obvious for MIB removal because the overall removal of MIB was lower than that of geosmin.

The removal of geosmin/MIB in natural waters by the oxidation mechanism was considerably suppressed, which was attributed to the ambient alkalinity, NOM, and other components which may work as radical scavengers. The scavenging resulted in lower removal percentages than regular oxygen NBs operation in DDI water, which involved both volatilization and oxidation removal mechanisms; the results from the natural waters were not significantly different (p-values > 0.05) from the water circulation experiments (only volatilization involved). Therefore, additional approaches are needed to exploit and take advantage of oxidation pathway in NBs applications in natural waters for drinking water treatment.

CHAPTER 6

CHARACTERISTICS AND STABILITY OF OZONE NANOBUBBLES IN FRESHWATER CONDITIONS

6.1. Introduction

While oxygen, nitrogen, and air are the most common types of gases studied as NBs, research with ozone NBs is emerging. Ozone is a powerful oxidant and disinfectant that has been widely used in water and wastewater treatment for many years (Hoigné and Bader, 1976).. However, its application is limited by the mass transfer of ozone gas into the liquid phase, which is slow due to the rapid buoyancy of micro- and macrobubbles (Temesgen et al., 2017). In contrast, ozone NBs have a very small size and low buoyancy, allowing them to remain in solution for much longer (Batagoda et al., 2019). The result is faster diffusion and higher ozone concentration in water. Additionally, the smaller size, greater total interfacial surface area, and lower rise velocity of ozone NBs make them uniquely suited for water treatment (Batagoda et al., 2018; D. Li et al., 2014; Temesgen et al., 2017). These properties provide a higher gas holdup capacity (which refers to the volume fraction of gas that can be dispersed and retained within a liquid) and volumetric mass transfer rate, which increases mass transfer while reducing gas consumption and capital costs (Batagoda et al., 2018).

Ozone NBs have been investigated for a variety of applications in recent literature such as sediment remediation, water and wastewater treatment, and agriculture, which were

summarized for a collection of 54-peer-review articles in **Table A1**. However, the majority of ozone studies used the term "micro-nano bubbles" (MNBs), with less than half of these studies actually investigated NBs. Findings from reviewed literature showed that proper characterization of NBs and detailed reporting were generally lacking. Such a limitation must be addressed to be able to document and compare different studies. Seven of the 54 papers mentioned only MBs, and 27 papers did not provide any data or observations regarding the presence of NBs in the solution. Only 21 papers presented data for ozone NBs (i.e., size (<1000 nm) or concentration). Only eight out of the 21 papers reported “NBs concentrations” in the solution (Fan et al., 2021a; Farid et al., 2022; Hu and Xia, 2018; Kim et al., 2021; Maie et al., 2022; Wu et al., 2022; Xia and Hu, 2018; Yang et al., 2023) but without including any information about the background particle levels; therefore, the exact number of NBs was not clear in these studies given the fact that the measurement techniques such as NanoSight and Zetasizer cannot distinguish particles from NBs. For these reasons, the initial solution before NBs generation should be measured and reported as a background. NanoSight (NS300, NS500, or LM-10), Delsa™ Nano C, microscopy, ZetaView and Zetasizer were the most commonly used instruments to characterize bubble size, concentration, and size distribution in ozone NBs studies (Agarwal et al., 2011; Aluthgun Hewage et al., 2021, 2020; Batagoda et al., 2019; Cruz and Flores, 2017; Epelle et al., 2022; Farid et al., 2022; Hashimoto et al., 2021; Hu and Xia, 2018; Jhunkeaw et al., 2020, 2021; Lee et al., 2023; Maie et al., 2022; Xia and Hu, 2018; Zhu et al., 2022). However, less than 15% of the papers reported measurements of ozone NBs concentration and surface charge of ozone NBs in solution, so it is not possible to understand the

characteristics of the ozone NBs present in the experiments. Furthermore, the results of NBs measurements depend on the setting of the instruments used (e.g., camera levels, particle per frame counts etc.). Such details cannot be found in these publications. In addition, only six studies measured and provided the surface charge of ozone NBs in the 21 ozone NBs studies (Aluthgun Hewage et al., 2021, 2020; Batagoda et al., 2019; Hu and Xia, 2018; Hutagalung et al., 2023; Yang et al., 2023). Therefore, it is not possible to distinguish the results in the current literature from O_3 MNBs or NBs.

Understanding the characteristics and fate of ozone NBs in natural waters is critical for their implementation in both natural and engineered systems. There is still limited understanding on the long-term stability of ozone NBs under various freshwater conditions which was shown in Appendix A (**Table A1**). Only one of 54-peer-reviewed studies (**Table A1**) examined the stability of ozone NBs, and it was in just one condition and in ultrapure water at pH 7 - 7.5 for 14-days storage time (Farid et al., 2022). The lack of information suggests a need for further research on ozone NBs characterization and stability under a variety of conditions to comprehensively understand and apply the technology. The main objective of the study was to systematically investigate the characteristics and effects of key water chemistry parameters in freshwaters (e.g., pH, natural organic matter [NOM], carbonate, calcium, and temperature) on the stability of ozone NBs for a relatively long storage period (i.e., 60 days). In addition, the formation of hydroxyl radicals in ozone NBs solutions was examined. To the best of my knowledge, this is the first study to investigate the comprehensive characteristics and stability of ozone NBs in freshwater conditions.

6.2. Material and Methods

6.2.1. Generation of ozone NBs

Oxygen gas was fed to a NANO Ozone Generator (Absolute Ozone, Canada) for ozone generation. The pressure and flowrate of the feed gas were set at 20 psi and 1-4 L/min, respectively, which provided up to 15 g/hour or 10% by weight ozone. A higher gas flow rate provided less dissolved O_3 concentration (i.e., <1 mg/L), but when 1 L/min gas flowrate was applied, the dissolved ozone concentration reached 12.5 mg/L at 19±1.0 ^{o}C. As the flowrate of feed gas through the ozone generator decreases, the concentration of dissolved ozone in the solution will be increased because more of the oxygen in the feed gas is converted to ozone. A low gas flowrate increases the contact time of the ozone generator's oxygen gas, increasing ozone production. Also, ozone is being released slowly from the ozone generator into the solution, increasing its dissolution in the water, which increases the ozone concentration (Cuong et al., 2019; Du and Lin, 2019).

Ozone gas was delivered to an ozone resistant NBs generator to produce ozone NBs in a stainless steel container filled with water (**Figure 6.1**), which was circulated while supplying ozone gas and maintaining the water temperature at 19±1.0 ^{o}C during the ozone NBs generation. Since ozone solubility in water is a function of water temperature, ice bags were placed in the tank to maintain the water temperature at 19±1.0 ^{o}C during the ozone NBs generation.

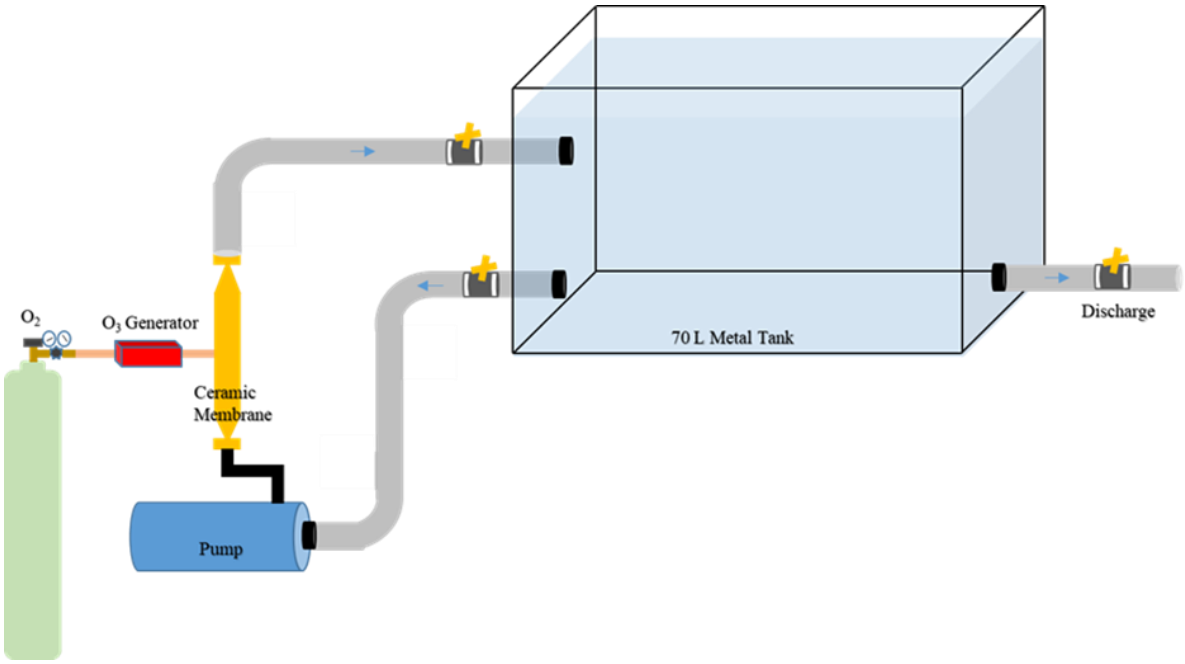

Figure 6.1. Overview of ozone NBs generation system

Ozone concentration was measured using the ozone indigo method (HACH AccuVac ampuls and a colorimeter (DR900)). To test the effect of NBs on the measurement, I ran a quick experiment to test if the presence of ozone NBs influences the measurement. To compare the results of ozone NBs to conventional ozonation side by side, dissolved ozone solutions were also prepared by feeding ozone directly to the water in the tank under the same experimental conditions as discussed above for O_3 NBs. Ozone stock solution was prepared in DDI at 30 mg/L initial concentration. Then, it was spiked in two different beakers; one of them had DDI water in it, and the other one had ozone NBs without any residual ozone after four days of NBs generation. Although there was no measurable dissolved ozone left, the concentration (~10^8 particles/mL) of 4-day old ozone NBs was the same as the concentration of freshly generated ozone NBs. After spiking the

concentrated dissolved ozone solution in both beakers, the target concentration was 1.0 mg/L of dissolved ozone. I was able to measure 1.05 and 1.06 mg/L dissolved ozone in DDI water and ozone NBs solution, respectively. The result confirmed that the presence of ozone NBs did not influence dissolved ozone measurement using the HACH indigo method.

6.2.2. Ozone NBs stability experiments

Ozone NBs were prepared in distilled and deionized (DDI) water at 1 L/min and 4 L/min of oxygen feed gas flowrates to the ozone generator, resulting in dissolved ozone concentrations of 12.5 mg/L and 1 mg/L in water, in addition to ozone NBs, respectively. The ozone NBs generated at the two different flowrates were characterized, and stability experiments under various water chemistry conditions were conducted with ozone NBs generated at 1 L/min.

The NBs generator was operated until the concentration of NBs in water reached the target maximum level (~10^8 NBs/mL), which was verified using a NanoSight (NS300) nanoparticle tracking analyzer (Malvern Instruments Ltd., UK), and then ozone NBs solution was transferred into 40 mL amber glass vials and capped with no headspace for a long-term stability study. More details about measuring the concentrations and size distributions of NBs can be found in Chapter 3. The initial NBs concentration and zeta potential was measured using a Brookhaven 90Plus Particle Size Analyzer, and dissolved ozone was recorded at time zero. The vials were stored at room temperature (19±1.0 ^{o}C)

and the initial pH was around 5.2 ± 0.2. At designated times, vials were opened, and NBs concentration, size distribution, and zeta potential were measured.

To examine pH effects, the solution pH was adjusted in the vials at 3, 5, 7, and 9 with HCl or NaOH at time zero. The effects of NOM, carbonate, calcium, and temperature were examined at pH 7.0±0.5. The NOM effect was investigated at 5 mg/L dissolved organic carbon (DOC) using two NOM extracts which were available in our laboratory from a previous study: 1.7 L/mg.m for low specific ultraviolet absorbance at 254 nm ($SUVA_{254}$) obtained from a surface water (Song et al., 2009) and 4.1 L/mg.m for high $SUVA_{254}$ (Suwannee River NOM from International Humic Substances Society). For calcium effects, calcium chloride ($CaCl_2$) was added to the ozone NBs solution to create 0.3 and 3.0 mM Ca^{2+} (i.e., 30 and 300 mg/L as calcium carbonate ($CaCO_3$), respectively). The effects of carbonate were examined after spiking 0.25 and 2.5 mM sodium bicarbonate ($NaHCO_3$) in pre-generated ozone NBs solutions to create 25 and 250 mg/L as $CaCO_3$, respectively. Finally, for temperature effects, ozone NBs solutions were kept at 10, 20, and 30 ^oC. For selected conditions (i.e., pH 5, 7 and 9, Low $SUVA_{254}$ NOM, and 2.5 mM $NaHCO_3$), longer-term stability (i.e., 255 days) of O_3 NBs were also monitored. All samples and blanks/controls were prepared and analyzed in duplicates and the average values were reported. For the stability experiments, two independent experiments for each condition were conducted, and the average of the results from these two experiments, along with the standard deviation, is presented in the chapter.

6.2.3. The effect of initial terephthalate (TP) concentration on •OH radical formation

To examine the dose of TP required to react with all •OH radicals in the system, 0.5, 1, and 2 mM of TP were applied to both conventional ozonation and ozone NBs solutions. Conventional ozonation, with a dissolved ozone concentration of 1 mg/L, did not show any significant increase in •OH radical formation, even with increasing TP concentrations. On the other hand, ozone NBs enhanced the formation of radicals with increasing initial TP concentration, indicating that more radicals were available in the ozone NBs solution than conventional ozone (**Figure 6.2**A). When the ozone concentration was increased from 1 to 12.5 mg/L, the formation of TPOH also increased with increasing TP concentration from 0.5 to 1 mM for both conventional ozonation and ozone NBs solutions (**Figure 6.2**B). Up to a 70% increase in the •OH radical formation was observed for both conventional ozone and ozone NBs. However, as the dose of TP was further increased to 2 mM, an additional impact on the TPOH formation was not observed for conventional ozone, while the TPOH formation increased for ozone NBs during 30 min contact time. The overall TPOH formation for the ozone NBs reached the same level for the rest of storage time (i.e., 2 days), so TP concentration increase from 1 to 2 mM did not make any additional impact on the •OH radicals quantification. However, during the initial 30 minutes, •OH radical formation showed sensitivity to TP concentration, with noticeable differences between 1 and 2 mM TP. Therefore, 2 mM TP was selected for the quantification of •OH radicals in the following experiments. Similar observations were reported in a previous study for the •OH quantification with TPOH formation. After a certain number of •OH radicals have reacted with TP, newly formed •OH radicals likely

degraded existing TPOH instead of reacting with TP to produce new fluorescent TPOH, especially, when the initial concentration of TP was lower than required amounts (Saran and Summer, 1999).

It was also found that the •OH radical formation in ozone NBs solutions was continuous over time for ozone NBs prepared at higher dissolved ozone concentration of 12.5 mg/L (**Figure 6.2**). Even though there was no residual ozone in the solution during the 2 days (2880 min) of storage time, increasing TPOH formation could be attributed to the ozone diffusion from inside of ozone NBs. Comparing conventional ozonation with ozone NBs for the same initial dissolved ozone concentrations in solution, •OH radical formation from ozone NBs was 1.2 - 1.7 times higher for all tested conditions (**Figure 6.2**). This characteristic can be a further advantage of ozone NBs over conventional ozonation because a longer lasting oxidation may be possible with NBs.

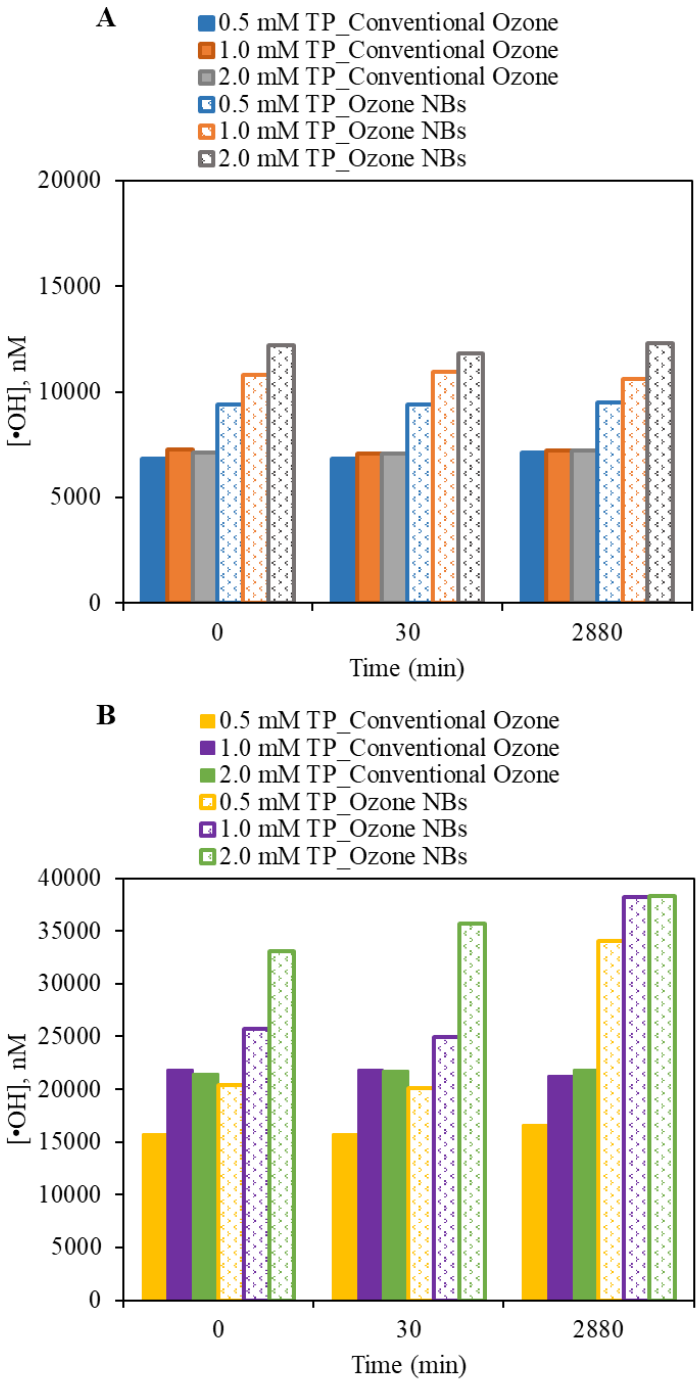

Figure 6.2. The formation of •OH radicals from conventional ozonation and ozone NBs at A) 1 mg/L and B) 12.5 mg/L of initial dissolved ozone concentrations.

6.2.4. Ozone decomposition and •OH radical experiments

Ozone NBs were prepared with 12.5 mg/L dissolved ozone for ozone decomposition and •OH radical formation experiments. The effects of pH (i.e., 3, 5, 7 and 9), NOM (i.e., low and high $SUVA_{254}$ NOM at 5 mg/L), carbonate (i.e., 0.25 and 2.5 mM NaHCO3), and calcium (i.e., 0.3 and 3.0 mM Ca^{2+}) were investigated at 19±1.0 ^{o}C. Each experimental condition was prepared in 1 L amber bottles with fresh O_3 NBs ($[O_3]_0$ = 12.5 mg/L) and then divided into 40 ml vials for the ozone decomposition and •OH radical formation measurements. Then, ozone concentration was measured for each sample at the time of sampling. Right after 2 mM TP was spiked into NBs solution, the solution was shaken one time and measured immediately for •OH radical formation from the calibration curve obtained from fluorescence spectra to determine concentrations of TPOH formed in NBs solutions (**Figure 3.6**). The concentrations of •OH radicals were estimated from the TPOH concentration divided by the yield percentage (31.5 ± 7 %) (Fang et al., 1996; Gonzalez et al., 2018; Žerjav et al., 2020). O_3 levels and the formation of •OH radicals for each experimental condition were recorded and compared side by side.

The generated O_3 NBs were stored at room temperature in vials that were headspace free. After one week, the dissolved ozone level in the solution was measured, and there was no residual ozone. For some conditions, TP was spiked into the solution for 1 and 2-week-aged O_3 NBs; NBs solutions were shaken and put aside. The formation of •OH radical was monitored after 24 and 48-h reaction times.

6.3. Results and Discussion

6.3.1. Impact of NBs generation conditions on characteristics and stability of ozone NBs

Ozone NBs were generated at two different oxygen feed gas flowrates (i.e., 4 and 1 L/min) to the ozone generator, resulting in two different initial dissolved ozone conditions (i.e., 1 and 12.5 mg/L, respectively) present with ozone NBs in water. These two gas flowrates affected the characteristics and stability of ozone NBs. Ozone NBs generated at high initial dissolved ozone concentration showed much higher brightness during ozone NBs counting using NS300 than for the ozone NBs generated at low initial dissolved ozone (**Figure 6.3**). The background dissolved ozone concentration was not a contributing factor to the difference in ozone NBs brightness because after the complete decomposition of dissolved ozone (**Table 6.1**), ozone NBs generated at a higher dissolved ozone level still showed a significantly higher brightness than those generated at low dissolved ozone concentration (**Figure 6.3**B,C and E,F).

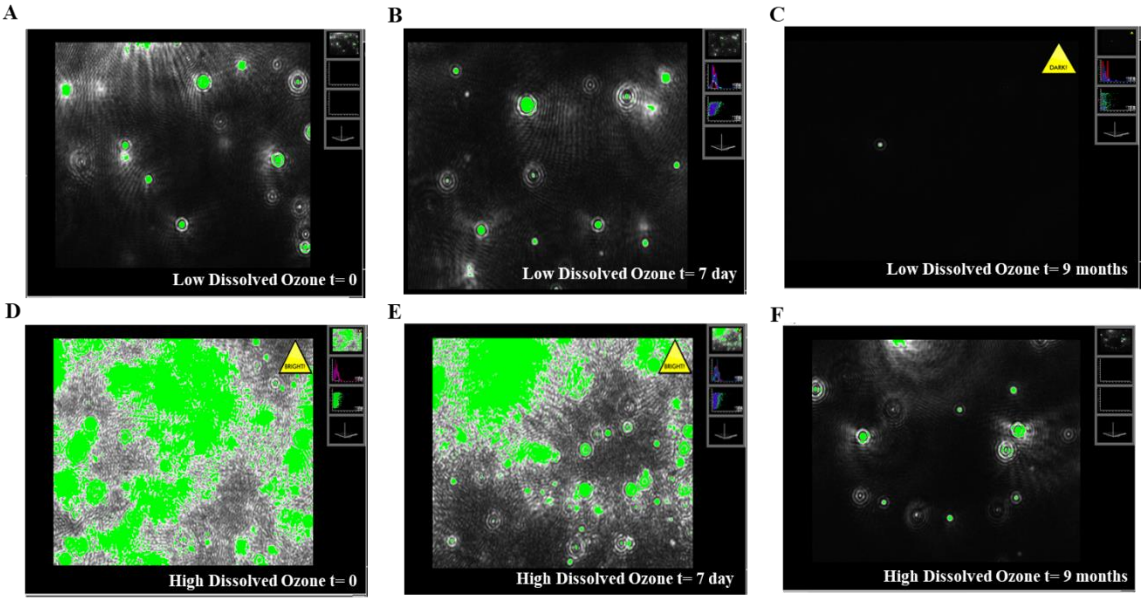

Figure 6.3. The screenshots taken during ozone NBs measurements on NS300 for low dissolved ozone (1 mg/L) at A) Day 0, B) Day 7 and C) 9 months, and for high dissolved ozone (12.5 mg/L) at D) Day 0, E) Day 7 and F) 9 months.

Table 6.1. Dissolved ozone concentration (mg/L) in NBs solutions at pH 5.

Time (min)	Low dissolved ozone	High dissolved ozone
0	1.07	12.50
1	1.03	9.30
5	1.00	10.60
10	0.90	10.00
15	0.85	7.40
20	0.97	7.20
60	0.81	3.70
100	0.56	3.40
140	0.69	1.40
170	0.22	1.40
200	0.05	1.24
230	<DL	0.36
250	<DL	<DL

DL: Detection Limit

Although the initial concentration of ozone NBs for both low and high dissolved ozone conditions were similar (i.e., 1.08×10^8 and 1.10×10^8 particles/mL, respectively), different disappearance rates (**Figure 6.4**A) of ozone NBs and the surface charge change (**Figure 6.4**B) were observed over a long storage time. Ozone NBs generated at high dissolved ozone conditions had more negatively surface charge and exhibited higher stability than ozone NBs generated at low dissolved ozone conditions. The concentration of ozone NBs in the low dissolved ozone solution started to decrease after day 1, while ozone NBs in the high dissolved ozone solution were relatively stable for the first week, then started to decrease slowly with increasing storage time. After 60 days of storage period, the concentration of ozone NBs generated under the high ozone level condition was 23% higher than that of the low ozone condition ($p < 0.05$). The difference in the ozone NBs stability can be attributed to the difference in the change of their surface charge. The size distributions of ozone NBs (most bubbles with diameter < 250 nm) did not drastically change from 0 to 60 days of storage time (**Figure 6.5**). At time=0, there were more NBs ranging from 100 to 250 nm in high dissolved ozone solution, but for 60-day samples, the size distributions under both conditions were very similar and the mode size of ozone NBs shifted from left to right (i.e., from ≈100 nm to ≈150 nm) (**Figure 6.5**).

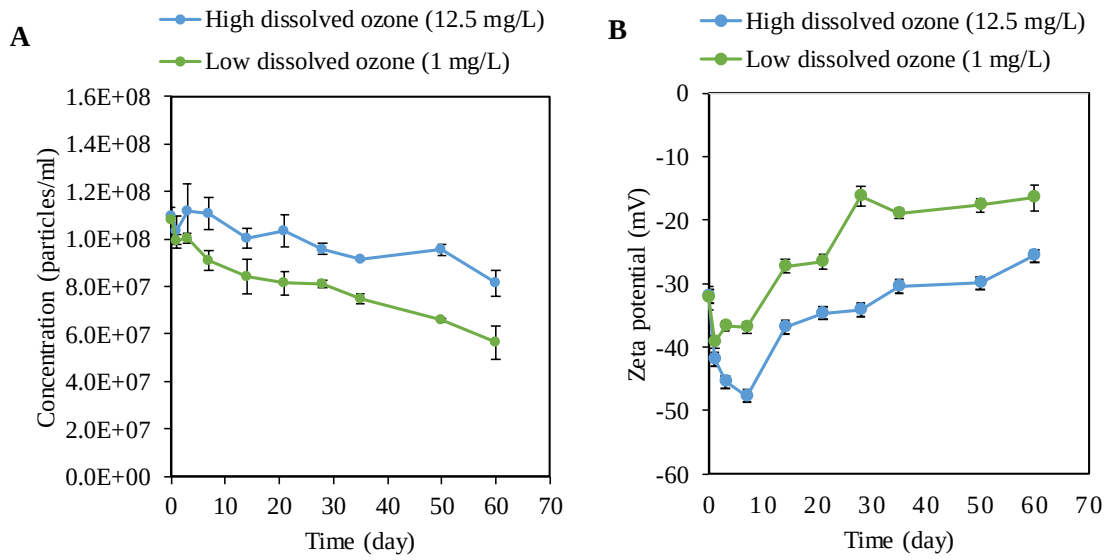

Figure 6.4. Changes of (A) ozone NBs concentrations and (B) surface charge during 60 days of storage time at pH 5.2±0.2 and 19±1.0 ºC.

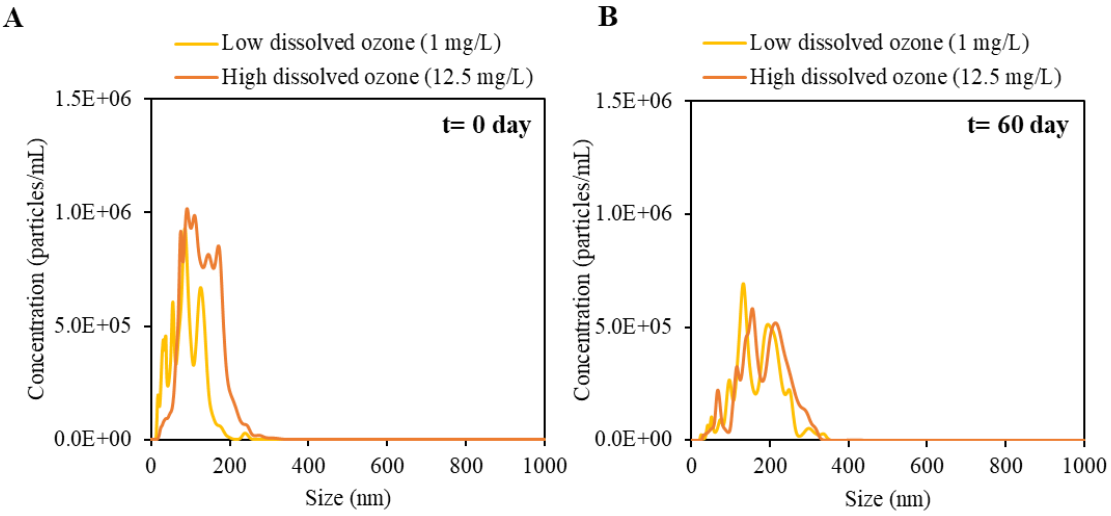

Figure 6.5. The size distributions of ozone NBs under two different feeding gas flowrate conditions in DDI water at (A) t=0 and (B) 60-days

Ozone NBs generated under the two different feed gas flowrate conditions had similar initial zeta potentials (around -32 mV). A sharp decrease of zeta potential was observed for both low and high dissolved ozone solutions during the first 24 h (i.e., -32 to -39 mV and -32 to -42 mV, respectively). After day 1, the zeta potential of the low dissolved ozone solution started to increase to -16 mV by day 60, while that of the high dissolved ozone solution kept decreasing to -48 mV until day 7 and then started to increase to -26 mV. The differences in surface charges of ozone NBs can be related to multiple factors including the presence of dissolved ozone and its decomposition as well as a continuous ozone diffusion from inside of NBs to the solution phase due to the high gas holdup capacity of NBs (Batagoda et al., 2018; Temesgen et al., 2017). Dissolved ozone levels decreased and there was no measurable dissolved ozone (< 0.02 mg/L) in both solutions after 5 hr. Ozone decomposes in water to OH^- ions (Ho et al., 2004), which may increase the magnitude of zeta potential of ozone NBs solutions. Higher dissolved ozone concentration in the solution may promote more negative charges on the surface of NBs, which is probably due to more OH^- at the gas–water interface (Meegoda et al., 2018). Furthermore, ozone can diffuse from NBs into the bulk solution, which can supply additional OH^- ions at the bubble interface. Moreover, at pH 5 less hydrated and more polarized OH^- anions may move to the bubble surface, increasing the magnitude of surface charge (Meegoda et al., 2018; Temesgen et al., 2017). Overall, such factors eventually can enhance ozone NBs stability in water by inhibiting coalescence of NBs for an extended storage period. These results showed for the first time the impact of ozone NBs preparation conditions on their characteristics and stability in water.

6.3.2. Effect of pH

The effect of pH on the ozone NBs stability was investigated at pH 3, 5, 7, and 9. Ozone NBs concentrations and zeta potential changes over the storage time are shown in **Figure 6.6** and **Table 6.3**. Ozone NBs were more stable at higher pH (**Figure 6.6**) and their concentrations decreased slowly at pH 9 with only 10% of ozone NBs disappearing after 60 days, whereas at pH 3 the concentration of ozone NBs started to decrease immediately and reached about 60% of the initial level after the first two weeks, and finally about 40% after 60 days of storage period. The observed stability of ozone NBs was significantly lower at pH 3 than pH 5, 7, or 9 ($p < 0.05$), while the difference between pH 5 and 7 conditions was statistically insignificant ($p > 0.05$).

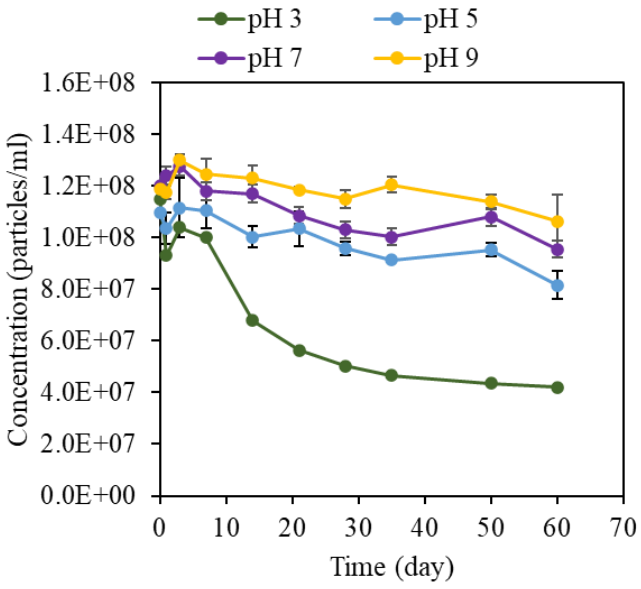

Figure 6.6. Changes in ozone NBs concentrations over storage time under various pH conditions in DDI.

The magnitude of initial surface charge (t = day 0) of ozone NBs solution at pH 3 was lower than those at pH 5, 7 or 9 (**Table 6.3**). Dissolved ozone decomposed spontaneously in the solution and no measurable ozone remained at 5 h in pH 5, 7, and 9 (**Table 6.2**). Since the decomposition of ozone is fast at high pH and produces OH^- ions (Ho et al., 2004), the change in the surface charge of NBs solutions was immediately observed. At pH 5, 7, and 9, ozone decomposition resulted in a prompt increase in the magnitude of surface charge of ozone NBs (**Table 6.3**). The magnitude of zeta potential at pH 3 and 5 increased significantly over the storage time, while it was relatively stable at pH 7 and 9. The repelling forces caused by high magnitude of the negative surface charge would promote stability of negatively charged ozone NBs during a long storage period. Moreover, 65-70% of O_3 NBs were stable at pH 5, 7 and 9 after 255 days storage time (**Table 6.4**). The different pH conditions did not impact the size distribution of ozone NBs at time=0, and the diameter of most bubbles was less than 200 nm (**Figure 6.7**). While the size distribution pattern was not variable with different pH at time=60 day, the mode size of bubble shifted to the right (up to 200 nm of diameter) (**Figure 6.7**).

Table 6.2. Ozone decomposition in O_3 NBs solution at various pH values. DL: detection limit.

Time (min)	Dissolved ozone concentration in NBs solution (mg/L)			
	pH 3	pH 5	pH 7	pH 9
0	12.5	12.5	12.5	12.5
1	9.1	9.3	4.5	1.3
5	9.5	10.6	4.5	0.17
10	10.4	10	3.6	0.03
15	10.7	7.4	1.7	<DL
20	9.6	7.2	1.6	
60	9.6	3.7	0.03	
100	7.1	3.4	<DL	
140	7.0	1.4		
170	6.8	1.4		
200	5.0	1.24		
230	4.4	0.36		
250	3.9	DL		

Table 6.3. Changes in zeta potential values over time under various pH conditions in DDI water.

Day	pH			
	pH 3	pH 5	pH 7	pH 9
0	-21.5	-32.0	-35.4	-42.7
1	-41.1	-41.9	-45.4	-47.9
3	-36.4	-45.5	-43.9	-44.0
7	-42.0	-47.7	-44.1	-44.4
14	-35.1	-36.8	-44.1	-46.7
21	-26.4	-34.6	-41.1	-45.4
28	-25.2	-34.1	-44.1	-43.7
35	-23.1	-30.4	-39.6	-43.1
50	-19.3	-29.9	-45.2	-47.1
60	-15.5	-25.6	-42.2	-44.6

Table 6.4. The long-term stability (t=255 days) of ozone NBs under various conditions.

O_3 NBs (particles/mL)					
Time (day)	**pH 5**	**pH 7**	**pH 9**	**Low $SUVA_{254}$ NOM**	**2.5 mM Carbonate**
0	$1.15x10^8 \pm 1.6x10^6$	$1.24x10^8 \pm 9.7x10^6$	$1.18x10^8 \pm 8.9x10^6$	$1.25x10^8 \pm 8.9x10^6$	$1.29x10^8 \pm 4.3x10^6$
255	$7.45x10^7 \pm 7.3x10^6$	$7.68x10^7 \pm 4.7x10^6$	$8.02x10^7 \pm 2.7x10^6$	$7.18x10^7 \pm 6.4x10^6$	$9.26x10^7 \pm 7.2x10^6$

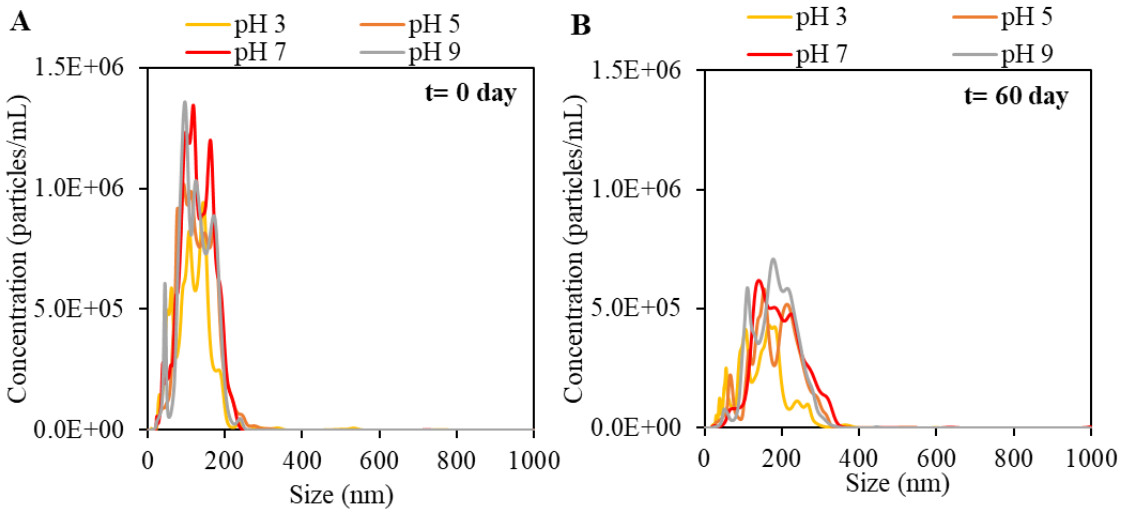

Figure 6.7. The size distributions of ozone NBs under various pH conditions in DDI at (A) t=0 and (B) 60-days.

6.3.3. Effect of NOM

The effects of NOM (i.e., 5 mg-DOC/L) and its aromaticity (i.e., low vs. high $SUVA_{254}$) were also investigated for effects on the stability of ozone NBs at pH 7. There was no significant impact of NOM on the stability of ozone NBs in the presence of low $SUVA_{254}$ NOM (i.e., 1.7 L/mg.m) at 5 mg-DOC/L ($p > 0.05$) with > 80% of NBs remaining after 60 days (**Figure 6.8**). The changes in NBs concentration and surface charge in the presence of low $SUVA_{254}$ NOM were similar to those in the DDI control, even for extended storage time, 255 days (**Table 6.4** and **Table 6.5**). The impact of high $SUVA_{254}$ NOM (i.e., 4.1 L/mg.m) was also insignificant compared to the DDI control until day 35. However, as the storage time increased to 60 days, the concentration of ozone NBs decreased to about 55%, and surface charge increased (**Table 6.5**). As aromaticity (i.e., $SUVA_{254}$) of NOM increased, half-lives of ozone NBs decreased during a relatively long storage period. The more aromatic nature of higher $SUVA_{254}$ NOM may more easily bind to ozone NBs and consequently reduce the stability of NBs. In the previous chapter with oxygen NBs and the same NOM extracts, I observed a clear effect of high $SUVA_{254}$ NOM on the oxygen NBs stability and the difference between low and high $SUVA_{254}$ NOM was distinguishable even over a short storage time (**Figure 4.5**). Furthermore, about 55% of ozone NBs remained in the solution in the presence of the same high $SUVA_{254}$ NOM, while only 20% of oxygen NBs was observed in the solution after 60 days of storage period. The higher negative surface charge of ozone NBs than oxygen NBs can explain the difference.

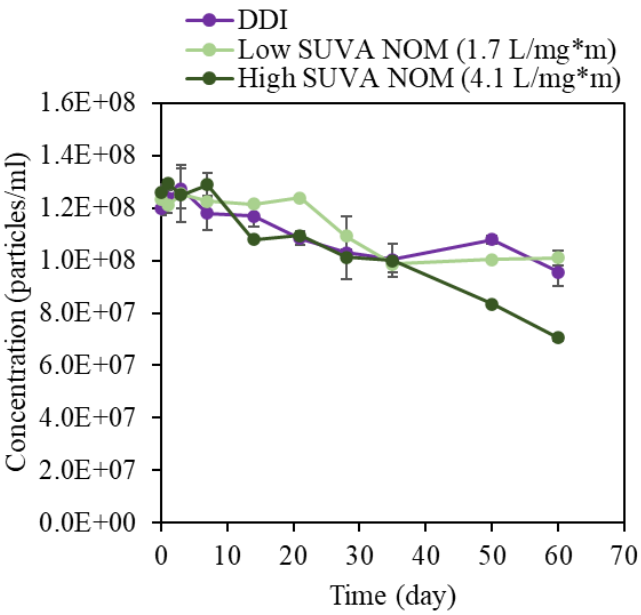

Figure 6.8. Changes in ozone NBs concentrations in the presence low $SUVA_{254}$ (1.7 L/mg.m) and high $SUVA_{254}$ (4.1 L/mg.m) NOM at 5 mg/L DOC and pH 7 in DDI during 60 days of storage time at room temperature.

Table 6.5. Changes in zeta potential values over time under various under various NOM at 5 mg DOC/L conditions.

Day	NOM	
	Low SUVA	High SUVA
0	-34.0	-41.6
1	-43.2	-39.8
3	-42.7	-42.4
7	-42.3	-44.6
14	-43.1	-46.6
21	-43.5	-44.4
28	-40.5	-41.1
35	-37.9	-41.4
50	-37.2	-34.6
60	-35.7	-32.2

6.3.4. Effect of carbonate

The impact of carbonate on the stability of ozone NBs was insignificant compared to pH 3 or high $SUVA_{254}$ NOM (**Figure 6.9**). At 2.5 mM alkalinity (250 mg/L as $CaCO_3$), ozone NBs showed slightly higher stability than at 0.25 mM alkalinity (25 mg/L as $CaCO_3$) and DDI, with less than 10% overall change of the NBs concentration during the storage time. The size distributions of ozone NBs for these three conditions were similar, and the diameter of most bubbles was less than 200 nm at time=0 (**Figure 6.10**A). However, the mode size of ozone NBs in 2.5 mM carbonate solution (i.e., 98.5 nm) was smaller than in DDI and 0.25 mM carbonate solution at time=60 day (i.e., 146.5 and 140.5 nm, respectively) (**Figure 6.10**B), which can be explained by the increase of the negatively charged ions on the surface of the NBs, which can enhance the electrostatic repulsion between neighbor NBs and resulting in the decrease in the size of NBs (D. Li et al., 2014).

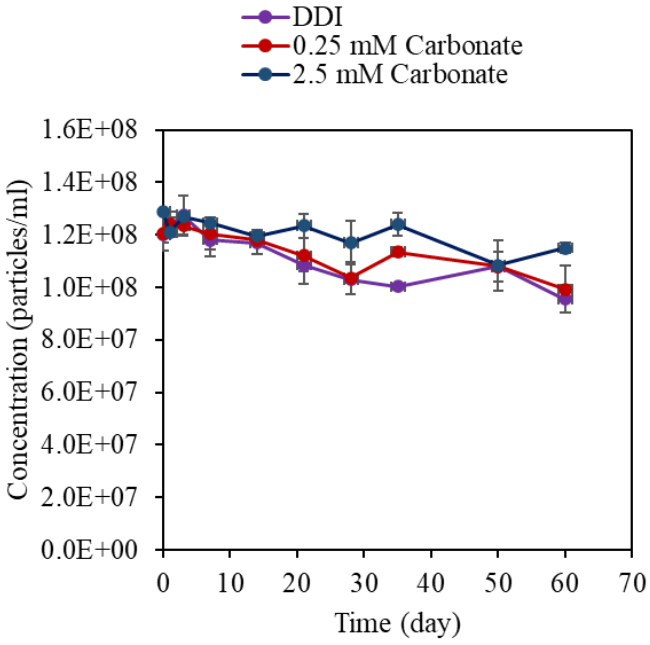

Figure 6.9. Changes in ozone NBs concentrations in the presence of 0.25 (25 mg/L as $CaCO_3$), 2.5 mM (250 mg/L as $CaCO_3$) carbonate, and DDI during 60 days of storage time at room temperature.

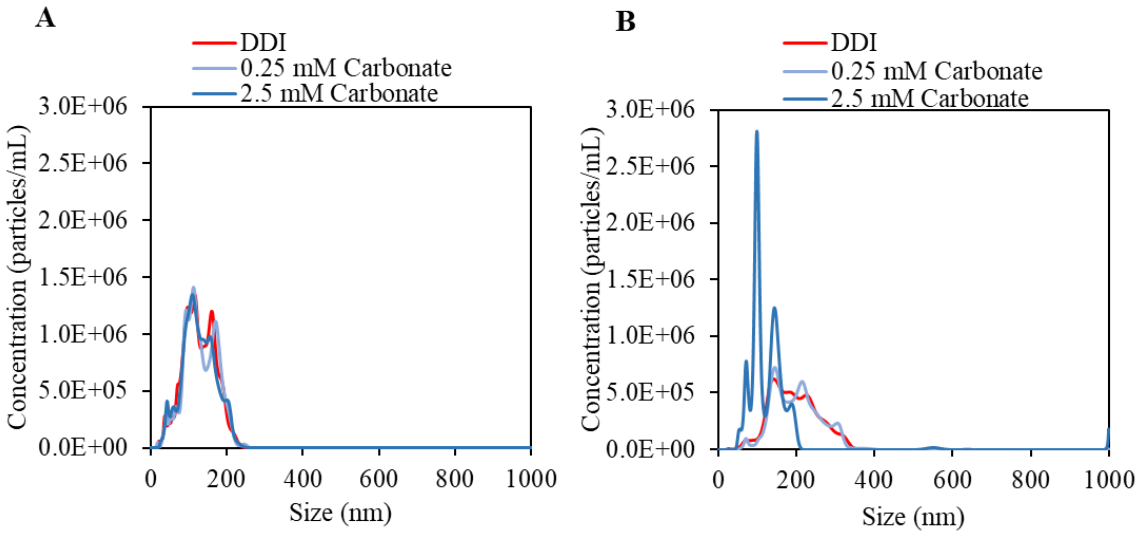

Figure 6.10. The size distributions of ozone NBs under various carbonate levels and DDI alone at (A) t=0 and (B) 60-days.

The magnitude of the surface charge of ozone NBs in 2.5 mM carbonate treatment was also slightly higher than that of the DDI control and 0.25 mM carbonate alkalinity treatment (**Table 6.6**). Ozone decomposition produces HO_3^- and $O_3^{\bullet -}$ in addition to hydroxyl radicals (Elovitz et al., 2000), while $NaHCO_3$ dissociates mainly to HCO_3^- at pH 7. Combinations of these negatively charged species which can affect the surface charge of NBs based on the mobility of counter ions may help ozone NBs persist for longer times in the presence of carbonate (Yildirim et al., 2022). Thus the bubbles become more stable due to these ionic species' formation of a diffusive barrier against gas outflux, which simultaneously lowers the effective value of the liquid-gas surface tension, which prevents fast gas diffusion, and results in an increase in the stability of NBs (Hewage et al., 2021). **Table 6.4** shows that 80% of O_3 NBs (i.e., $9.26x10^7$ NBs/mL) were still present in solution after 255 days of storage time. The finding indicates that typical carbonate levels of natural waters will not have a significant effect on the ozone NBs stability.

Table 6.6. Changes in zeta potential values over time under various carbonate levels.

Day	DDI	0.25 mM	2.5 mM
0	-35.4	-39.7	-44.2
1	-45.4	-44.6	-46.1
3	-43.9	-39.8	-43.3
7	-44.1	-45.6	-49.1
14	-44.1	-41.7	-39.8
21	-41.1	-43.3	-46.0
28	-44.1	-45.9	-48.6
35	-39.6	-43.7	-46.9
50	-45.2	-41.0	-46.7
60	-42.2	-44.1	-48.1

6.3.5. Effect of calcium

To test the effect of calcium on the stability, the concentration changes of ozone NBs were monitored over time in the presence of 0.3 mM and 3.0 mM Ca^{2+}, which correspond to 30 and 300 mg/L as $CaCO_3$ hardness, respectively. As shown in **Figure 6.11**, the presence of 3.0 mM Ca^{2+} (300 mg/L as $CaCO_3$) exhibited an immediate impact on the ozone NBs stability. The initial ozone NBs in solution (i.e., 1.2×10^8 particles/mL) quickly dropped to the background level of DDI water (i.e., ~ 10^7 particles/mL) within one day. The presence of divalent calcium in the solution also decreased the magnitude of surface charge toward zero, and thus directly decreased the repulsive electrostatic forces between negatively charged NBs (Hewage et al., 2021; Nirmalkar et al., 2018b) (**Table 6.7**). As a result, ozone NBs could coalesce to form bigger bubbles and then burst and disappear from the solution in a short time period. Such a disappearance mechanism of ozone NBs in the presence of Ca^{2+} was supported by comparing the size distribution pattern of ozone NBs in 3.0 mM Ca^{2+} solution with those in DDI and 0.3 mM Ca^{2+} solution at time=0 and 60 days. With the immediate decrease in the magnitude of surface charge (i.e., -35.4 and -19.1 mV in DDI and 3.0 mM Ca^{2+} at time=0, respectively.), the concentration of NBs was decreased, and the bubble size distribution shifted to the left for 3.0 mM Ca^{2+} solution at time=0 because larger bubbles would easily escape from the solution (**Figure 6.12**A). On the other hand, 0.3 mM Ca^{2+} (30 mg/L as $CaCO_3$) did not have any significant impact on the stability of ozone NBs until day 21 compared to the DDI control ($p > 0.05$) and then reduced the concentrations of NBs to about 60% remaining after 60 days of storage period. Nevertheless, a significant decrease was observed in the magnitude of surface charge with

the addition of 0.3 mM Ca^{2+} at the beginning of the experiment (**Table 6.7**). While the size distribution of ozone NBs in the presence of 0.3 mM Ca^{2+} was similar to the ozone NBs in DDI, it was shifted to the left after 60 days of storage time with decreasing magnitude of surface charge and number of NBs (**Figure 6.12**B). Additionally, the polydispersity of the NBs size distribution exhibited a notable increase over the extended storage period of 60 days compared to the initial state (t=0). The half-lives of ozone NBs in the presence of 0.3 and 3.0 mM Ca^{2+} were 87 days and 1 day, respectively (**Table 6.10**). Similarly, calcium has been shown to greatly impact the stability of oxygen NBs (Hewage et al., 2021; Soyluoglu et al., 2021). These results showed that ozone NBs stability decreased significantly in waters with high hardness.

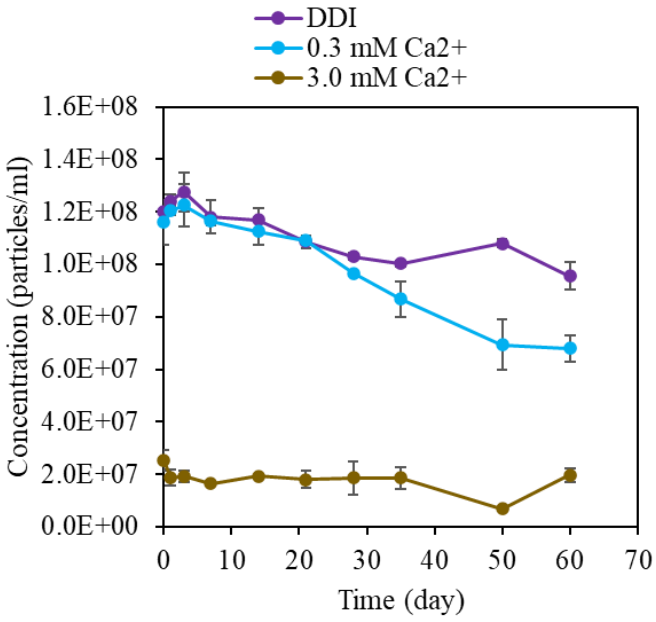

Figure 6.11. Changes in ozone NBs concentrations over storage time under various calcium levels.

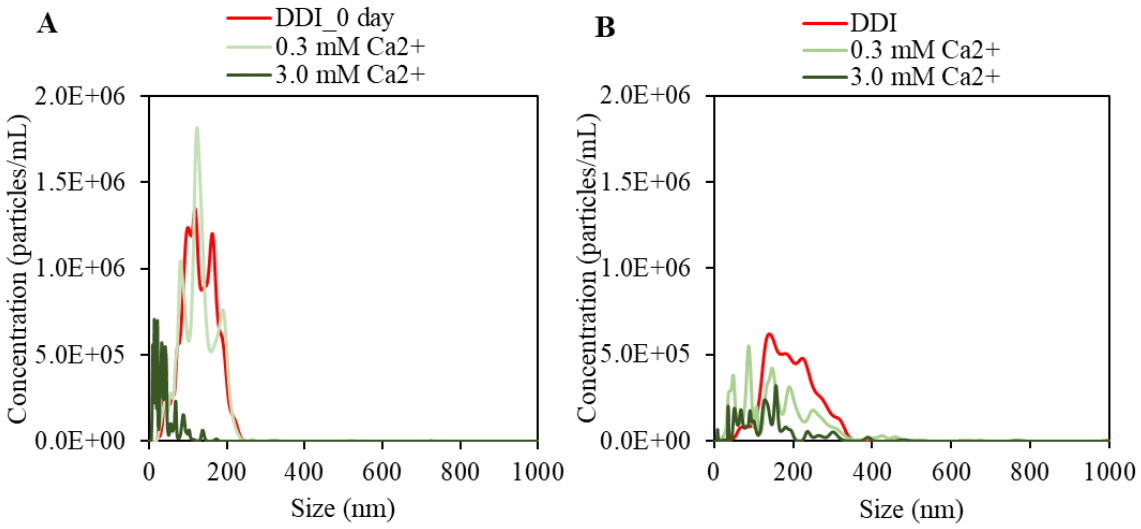

Figure 6.12. The size distributions of ozone NBs under various calcium levels in DDI at (A) t=0 and (B) 60-days.

Table 6.7. Changes in zeta potential values over time under various calcium levels.

Day	DDI	0.3 mM	3.0 mM
0	-35.4	-24.9	-19.1
1	-45.4	-27.7	-16.5
3	-43.9	-25.3	-12.0
7	-44.1	-21.0	-6.9
14	-44.1	-22.7	-5.5
21	-41.1	-18.9	-5.9
28	-44.1	-19.4	-2.9
35	-39.6	-18.7	-1.6
50	-45.2	-16.9	-1.9
60	-42.2	-14.3	-0.6

6.3.6. Effect of temperature

Increasing temperature can enhance the decomposition rate of ozone while decreasing ozone solubility in water (Ershov and Morozov, 2009). With increasing

temperature, rising velocity or the Brownian motion of NBs will increase (**Table 6.9**), enhancing the encounter of neighbor bubbles resulting in collisions and coalescence, thus ozone NBs might be less stable (Jin et al., 2020; Park et al., 2017). Also, the mobility of ions in the solution will be higher, and it can decrease the OH^- ion adsorption on the bubble surface (Meegoda et al., 2018). The possibility of these mechanisms is more reasonable with NBs generated with other gases since their surface charge is less than ozone NBs.

As shown in **Figure 6.13**, the change in ozone NBs levels was not significantly different under three different temperature conditions ($p > 0.05$), and up to 90% of ozone NBs remained after 60 days of storage time, indicating that the effect of Brownian motion change was negligible. In addition, the insignificant temperature effect on the ozone NBs stability was closely related to the surface charge change of ozone NBs. In the range of 10-30 ^oC, the surface charge did not significantly change over time (**Table 6.8**). Ozone NBs at higher temperature showed slightly higher surface charge than at lower temperature, which is likely related to the higher ozone diffusion and decomposition from NBs and increasing reaction rates with increasing temperature (Wang et al., 2021). The hydroxyl anions produced from ozone decomposition could be adsorbed at the gas-water interface, enhancing the magnitude of surface charge and the stability of NBs (Atkinson et al., 2019; Peleg, 1976; Soyluoglu et al., 2021). Higher surface charges enhance the repulsive force between NBs; thus, the coalescence possibility of two NBs is almost negligible in DDI.

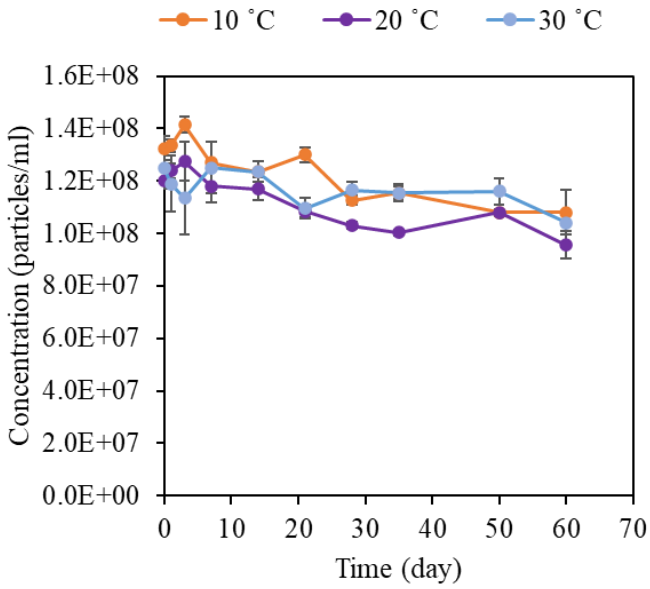

Figure 6.13. Changes in ozone NBs concentrations over storage time under various temperatures.

Table 6.8. Changes in zeta potential values over time under various temperatures.

Day	10 ˚C	20 ˚C	30 ˚C
0	-35.4	-35.4	-35.4
1	-41.3	-45.4	-43.9
3	-40.0	-43.9	-40.7
7	-45.7	-44.1	-47.8
14	-42.5	-44.1	-44.6
21	-40.9	-41.1	-46.1
28	-43.7	-44.1	-45.9
35	-40.0	-41.9	-42.6
50	-42.0	-45.7	-45.0
60	-39.8	-42.5	-41.7

In addition, the size distribution of ozone NBs at the three temperatures was not significantly different from each other during 60 days of storage time (**Figure 6.14**). While

the mode sizes of the ozone NBs were 105 ± 10 nm at time=0, they shifted to the right (i.e., 180 ± 40 nm) for all tested temperatures after 60 days. Therefore, the coalescence possibility can be ignored since NBs have a similar size under all tested conditions, and the stability and surface charge did not change significantly with increasing temperature. Also, the rising velocity of NBs at the three temperatures was calculated, and differences were not statistically different ($p > 0.05$), so NBs will not leave the solution quickly, as shown in **Table 6.9**. Therefore, the combination of change on Brownian motion, and zeta potential can affect the NBs stability, but a significant change was not observed for ozone NBs.

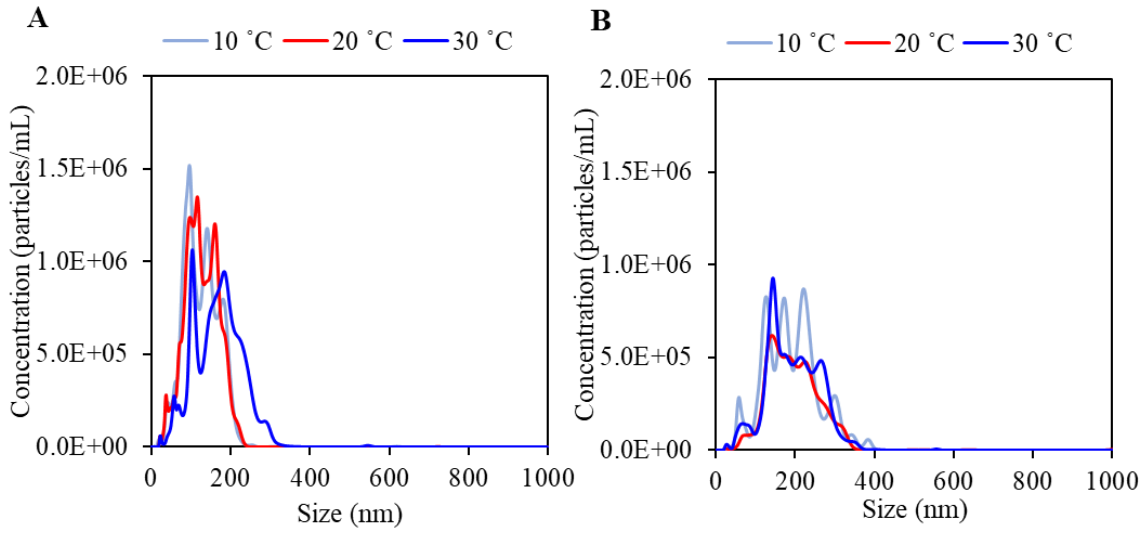

Figure 6.14. The size distributions of ozone NBs under various temperatures in DDI at (A) t=0 and (B) 60-days.

Table 6.9. The calculated rising velocity of ozone NBs at various temperatures.

Temperature	**10 °C**	**20 °C**	**30 °C**	**Rising velocity differences (cm/day)**	
d (nm)	**cm/day**	**cm/day**	**cm/day**	**T_{30}-T_{10}**	**T_{30}-T_{20}**
1	5.4E-06	7.0E-06	8.8E-06	0.00	0.00
10	5.4E-04	7.0E-04	8.8E-04	0.00	0.00
100	0.05	0.07	0.09	0.03	0.02
200	0.22	0.28	0.35	0.14	0.07
300	0.49	0.63	0.79	0.31	0.16
400	0.86	1.13	1.41	0.55	0.28
500	1.35	1.76	2.20	0.85	0.44
600	1.94	2.53	3.17	1.23	0.64
700	2.64	3.45	4.32	1.68	0.87
800	3.45	4.50	5.64	2.19	1.14
900	4.37	5.70	7.14	2.77	1.44
1000	5.39	7.03	8.81	3.42	1.78

6.3.7. Half-lives of ozone NBs in DDI water

The disappearance rates of ozone NBs under different water background conditions were collectively evaluated from the ln C_t/C_0 vs. time plots (**Figure 6.15**). For the two different initial dissolved ozone concentrations (i.e., 1 and 12.5 mg/L), the concentrations of ozone NBs in the solutions at time=0 were very similar (1.08×10^8 and 1.10×10^8 particles/mL, respectively). However, their half-lives were 64 and 165 days, respectively (**Table 6.10**), indicating that the initial dissolved ozone concentration can substantially

affect the stability of ozone NBs, which was due to differences in the NBs characteristics prepared at different ozone concentrations.

The half-lives of ozone NBs increased with increasing pH of the solution. At pH 3, the disappearance rate constant and half-life of ozone NBs at pH 3 were determined using the initial fast decay curve since there were two apparent (i.e., fast initially and then slow) disappearing phases. The disappearance rate for the initial 3 weeks was faster than the rest of the storage period. The same trend was also observed with changes in the surface charge of ozone NBs solutions (**Table 6.3**). As pH increased from 3 to 9, the half-lives increased from 20 to 693 days. (**Table 6.10**). At pH 9, the R^2 value was found to be very low because the concentration of ozone NBs did not change and the average of C_t/C_0 was 0.9987 during the 60 days storage time.

The half-lives of ozone NBs in the presence of NOM decreased with increasing $SUVA_{254}$ of NOM. The presence of low $SUVA_{254}$ NOM did not make a significant impact on the stability of ozone NBs compared to the DDI control (i.e., the half-lives of ozone NBs in DDI and low $SUVA_{254}$ NOM were 193 and 182 days, respectively), while ozone NBs in the presence of high $SUVA_{254}$ NOM disappeared faster (75 day half-life).

As carbonate concentration increased, the half-life of ozone NBs increased with the presence of charged species (i.e., HCO_3^-, CO_3^{2-}, HO_3^-, etc.) in water, which was attributed to the increasing surface charge of ozone NBs. The half-lives of ozone NBs increased from 193 to 267 days with the addition of 0.25 mM alkalinity (**Table 6.10**).

The disappearance rate of ozone NBs was greatly affected by Ca^{2+}. Ozone NBs disappeared very quickly, especially in the presence of 3 mM Ca^{2+}. The half-lives of ozone NBs in the presence of 0.3 and 3.0 mM Ca^{2+} were 86.6 days and 0.5 days, respectively (**Table 6.10**).

The half-lives of ozone NBs in different temperature conditions were not compared, as the differences in NBs levels during the 60-day storage time were not statistically significant ($p>0.05$). Additionally, the calculated half-lives may be misleading, as the differences in NBs concentration during the storage time are less than 5%.

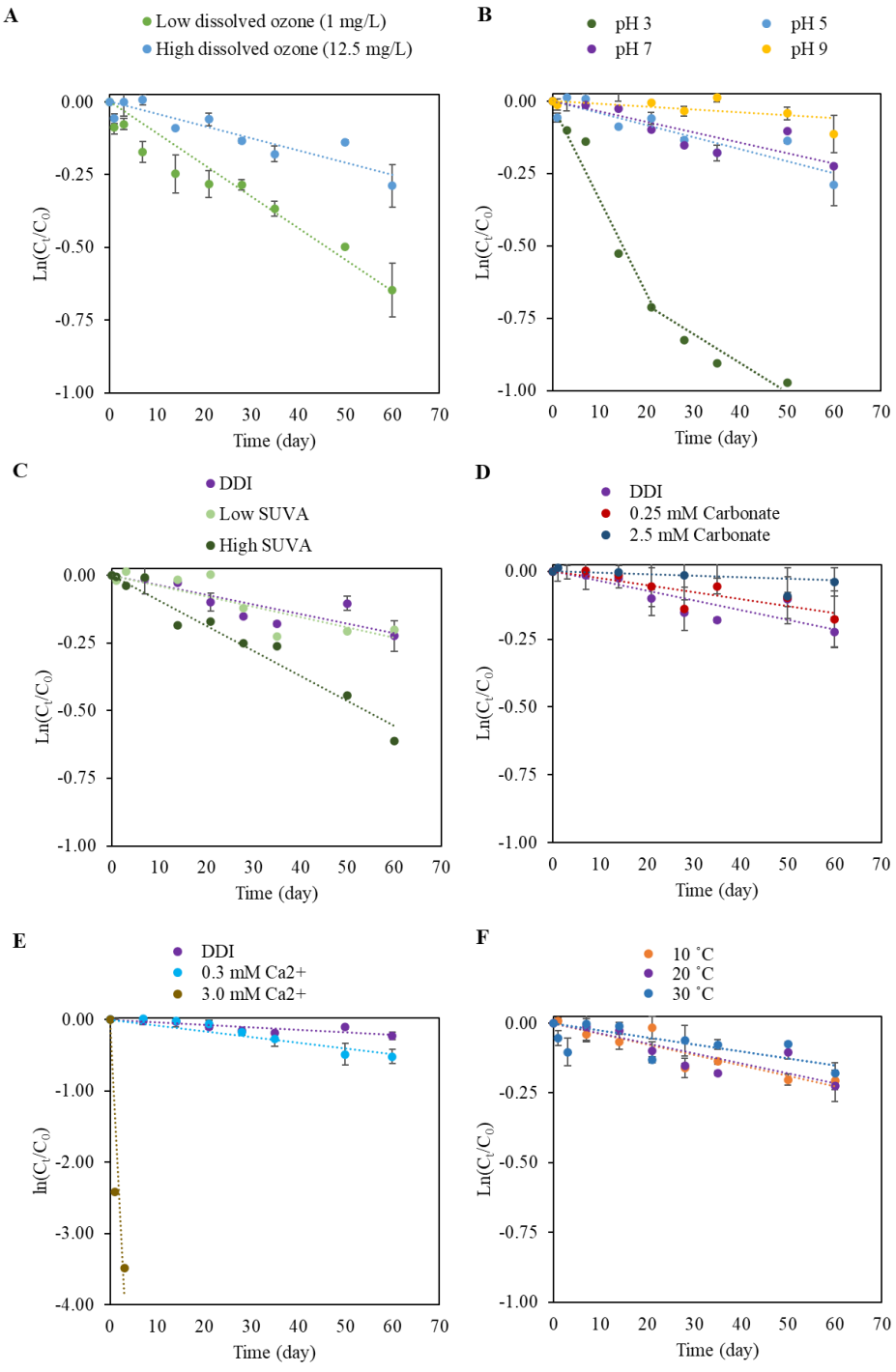

Figure 6.15. Changes of ozone NBs concentrations over storage time under two different feeding gas flowrate (A), pH (B), NOM (C), carbonate (D), calcium (E), and temperature (F) conditions in DDI water.

Table 6.10. Ozone NBs disappearance rate constants and half-lives under various storage conditions for 60 days.

Conditions	Ozone NBs storage condition	1st order NBs disappearance rate constant, k (day^{-1})	NBs half-life (day)	R^2
Initial dissolved ozone concentration effect (at pH 5.1 ± 0.1 and 20 °C)	Low ozone (1 mg/L)	1.08E-02	64	0.92
	High ozone (12.5 mg/L)	4.20E-03	165	0.97
pH effect (at 20 ˚C)	pH 3*	3.40E-02	20	0.99
	pH 5	4.20E-03	165	0.91
	pH 7	3.60E-03	193	0.86
	pH 9	1.00E-03	693	0.30
NOM effect at 5 mg-DOC/L (at pH 7 and 20 ˚C)	No NOM added	3.60E-03	193	0.86
	Low $SUVA_{254}$ NOM (1.7 L/mg.m)	3.80E-03	182	0.87
	High $SUVA_{254}$ NOM (4.1 L/mg.m)	9.30E-03	75	0.98
Carbonate effect (at pH 7 and 20 ˚C)	No carbonate	3.60E-03	193	0.86
	0.25 mM CO_3^{2-}	2.60E-03	267	0.84
	2.5 mM CO_3^{2-}	N.A.**		
Calcium effect (at pH 7 and 20 ˚C)	No calcium	3.60E-03	193	0.86
	0.3 mM Ca^{2+}	8.00E-03	87	0.90
	3.0 mM Ca^{2+}	1.29E+00	1	0.92
Temperature effect (at pH 7)	N.A.**			

*For the conditions showing two apparent disappearing phases (i.e., fast initially and then slow or complete disappearance in the short time), only data points fitted with the linear regression were considered to obtain the disappearance rate constants and half-lives calculations.

** There was less than a 5% difference between the measurements during the 60 days storage time, which is also the variability of the measurement, so disappearance rate was not calculated.

6.3.8. Comparison of ozone decomposition rate and •OH radical formation to conventional ozonation

Conventional ozone delivery methods are limited by the buoyancy of large ozone bubbles, which reduces the amount of ozone that can dissolve in the water. However, ozone injection using NBs can improve the gas holdup capacity of water due to the superior physiochemical properties of NBs, such as their smaller size, slower rising velocity, larger surface area, and longer diffusivity (Agarwal et al., 2011; Chu et al., 2007; Pourkarimi et al., 2017; Temesgen et al., 2017).

Figure 6.16 shows ozone decomposition rates in ozone NBs solution and conventional ozonation. Although the initial dissolved ozone concentration was 12.5 mg/L for both conditions, the ozone decomposition rate of conventional ozonation was faster than that of ozone NBs solutions. Calculated half-lives of dissolved ozone were 41.5 and 21.2 min for ozone NBs solution and conventional ozonation, respectively (**Figure 6.17** and **Table 6.15**). The significant difference in ozone decomposition rates between conventional ozonation and ozone NBs ozonation is due to two factors: (1) the ability of NBs to hold ozone gas in solution for longer periods of time, and (2) the movement of ozone NBs through Brownian motion, which prevents them from rising to the surface of the water and escaping (Batagoda et al., 2018; Kyzas and Mitropoulos, 2021). Given the longer persistence time, when the dissolved ozone is delivered with NBs, the surface of NBs is saturated with diffused gas, slowing the gas diffusion into the liquid. The gas inside the NBs continuously diffuses from the gas-water interface into the liquid, thereby extending the presence of ozone in water (Batagoda et al., 2018). The main drawbacks of

using conventional ozone methods are the lower retention times associated with high buoyancy and the quick ozone decomposition that eliminates residual ozone in water. The limitations mean that conventional ozone treatment often requires high ozone doses to be effective, therefore, ozone treatment may not be able to completely prevent microorganisms from regrowing in the treated water (Batagoda et al., 2018). The longer retention time of dissolved ozone in the ozone NBs solution is advantageous over the conventional ozonation for water treatment purposes, which means that the water can maintain its oxidation potential for longer periods of time. As a result, ozone NBs can achieve higher oxidation efficiency and remove target compounds with lower ozone doses than conventional ozone.

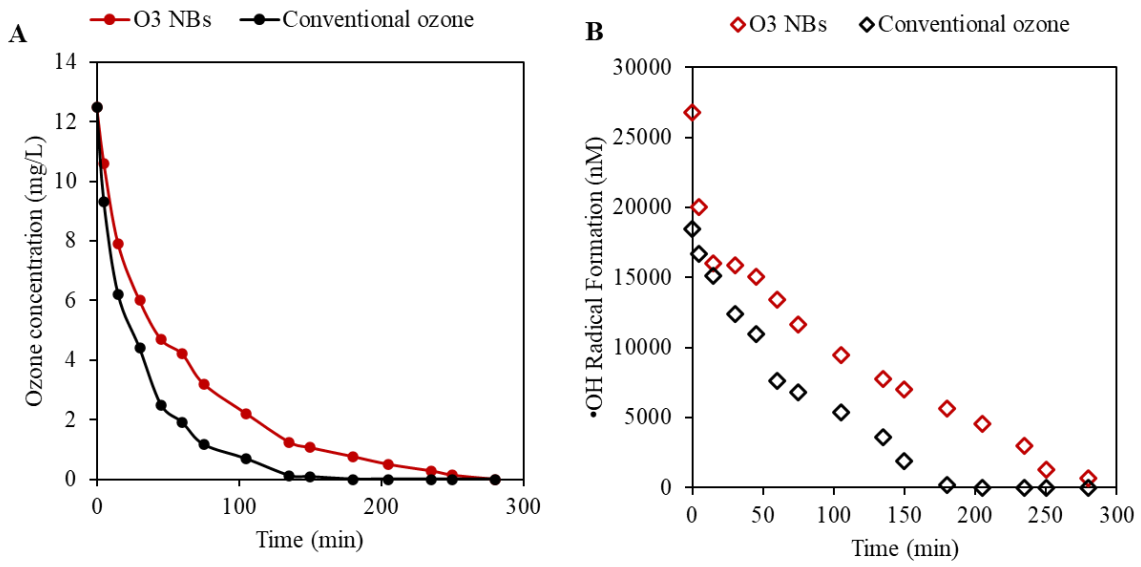

Figure 6.16. Decomposition of ozone (A) and hydroxyl radical formation (B) from ozone NBs solution and conventional ozonation ($[O_3]_0$ = 12.5 mg/L and [TP] = 2 mM at pH 5.2 ± 0.2 and 19±1.0 °C for both conditions).

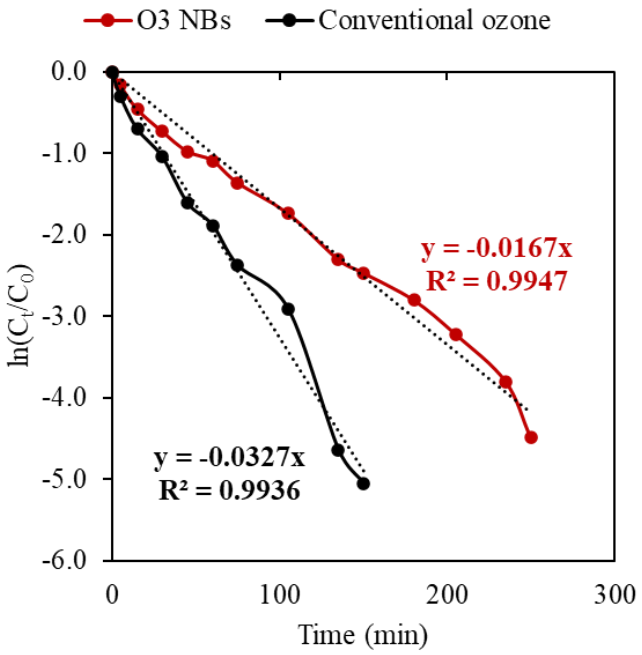

Figure 6.17. First order degradation rates of ozone in ozone NBs solution and conventional ozone.

Table 6.11. The 1st order decomposition rates of O_3 NBs and conventional ozone.

Conditions	Slope (k, min^{-1})	Half-lives (min)
O_3 NBs	0.0167	41.5
Conventional ozone	0.0327	21.2

The formation of •OH radicals for conventional ozonation and ozone NBs solution was also investigated during these experiments (**Figure 6.16**B). At time zero, the formation of •OH from dissolved ozone was ~18,000 nM, while ozone NBs produced a concentration of •OH radicals of 27,000 nM. No more radical formation was observed after 150 min during conventional ozonation, while the radical formation in ozone NBs solution continued. The initial •OH radical formation was mainly caused by different decomposition

rates of dissolved ozone, while the further formation of radicals was attributed to the reactivity of ozone NBs. The residual ozone concentration (**Figure 6.16**A) and the formation of •OH radicals (**Figure 6.16**B, $p < 0.05$) during the conventional ozonation were always lower than in ozone NBs solutions. As a result, the yield of •OH formation from O_3 NBs was significantly higher ($p < 0.05$, up to 25%) than conventional ozonation (e.g., 0.07 and 0.10 molar ratio of •OH to dissolved O_3 for conventional ozone and ozone NBs at time=0, respectively). The observed difference would lead to further oxidation capabilities in ozone NBs solutions. After 300 min, although there was no change on ozone NBs in water, the dissolved ozone was below the detection limits, but further •OH radical formation was observed even after 2 weeks storage time of O_3 NBs (Section 6.2.3 and **Table 6.12**). The results indicate that ozone continued to diffuse from the ozone NBs and its decomposition caused the formation of additional •OH radicals.

Table 6.12. •OH radical formation in 1 and 2 weeks stored O_3 NBs, and then spiked with TP for 24 and 48-h reaction time

24 h reaction time						
•OH radical formation (nM)	**DDI***	**pH 5 2 weeks**	**pH 7 2 weeks**	**pH 9 2 weeks**	**Low SUVA NOM 1 week**	**High SUVA NOM 1 week**
	<DL**	152.2±12	94.9±8.3	86.6± 3.3	201.3±2.5	379.06±17.4
48 h reaction time						
•OH radical formation (nM)	**DDI**	**pH 5 2 weeks**	**pH 7 2 weeks**	**pH 9 2 weeks**	**Low SUVA NOM 1 week**	**High SUVA NOM 1 week**
	<DL	296.3±9.8	95.12±6.3	87.9± 4.5	301.3±6.5	717.64±11.9

*DDI= Conventional ozone solution at pH 5.0-5.5 for comparison with ozone NBs

**DL = 1 nM

6.3.9. Ozone decomposition rate in ozone NBs solution under various freshwater conditions

The individual effects of background water quality parameters on the dissolved ozone decomposition profile are of critical importance in the application of ozone treatment technologies for various objectives. Therefore, the effect of pH (3,5,7, and 9), NOM with high $SUVA_{254}$ (4.1 L/mg.m) and low $SUVA_{254}$ (1.7 L/mg.m), alkalinity/carbonate (i.e., 0.25 and 2.5 mM) and $CaCl_2$ (i.e., 0.3 and 3.0 mM) on ozone decomposition in ozone NBs were investigated.

Since ozone is stable at acid pH, the ozone decomposition rate increased with increasing pH (**Table 6.13**). The half-lives of dissolved ozone in ozone NBs solutions were 1.1 – 2.3 times greater than conventional ozonation under all tested conditions (**Table 6.14**) (Ku et al., 1996). The presence of OH^- ions at high pH promotes the formation of •OH radicals (Elovitz et al., 2000; Gonzalez et al., 2018; Ku et al., 1996; von Gunten, 2003b). A previous study showed that pH-dependent reactions in the ozone decomposition chain cycle involving reaction intermediates such as HO_3^- and $O_3•^-$ increased the rate of ozone consumption as pH increased (Elovitz et al., 2000). It was also reported that the ratio of $[•OH]/[O_3]$ increased with increasing pH due to faster ozone decomposition, but the total •OH exposure remained almost constant. In my study, although there was no residual ozone in the solution detected after 15 min at pH 9 and after 45 min at pH 7 (**Table 6.12**), there was still •OH radical formation in the ozone NBs solutions. Even after 2 weeks storage time, additional 300, 95 and 88 nM •OH radical formation was observed in the pH 5, 7 and 9, respectively (**Table 6.12**).

The presence of NOM enhanced the ozone decomposition rate and the impact of high $SUVA_{254}$ NOM (4.1 L/mg.m) was greater than low $SUVA_{254}$ NOM (1.7 L/mg.m) (**Table 6.13**). Several studies found that during conventional ozonation, the ozone decomposition rate increased with increasing $SUVA_{254}$ or aromaticity of NOM (Croué et al., 1999; Elovitz et al., 2000; Ho et al., 2004; Westerhoff et al., 1999). The number of aromatic carbons was found to be positively related to the ozone consumption and •OH radical rate constant (Liu et al., 2021). The reaction of NOM with •OH radicals may produce carbonaceous radical species that can further react with dissolved oxygen to form superoxide radicals. These superoxide radicals may react quickly with ozone to form •OH radicals again (von Gunten, 2003b). Although there was no residual ozone in solution for my study, 301 and 718 nM •OH radical formation was observed both in low and high $SUVA_{254}$ NOM solution with O_3 NBs, respectively (**Table 6.12** and **Table 6.13**).

Carbonate ions have been shown to serve as a quencher of •OH radicals (Elovitz et al., 2000; Elovitz and von Gunten, 1998; Hoigné and Bader, 1983, 1976; Khuntia et al., 2013) as well as an inhibitor in the cycle of ozone oxidation (Elovitz et al., 2000). Therefore, the ozone decomposition rate decreased in ozone NBs solutions in the presence of carbonate (**Table 6.13**). Compared to the DDI control (i.e., dissolved ozone in DDI water), more residual ozone was observed at both carbonate levels. However, a 10-fold increase in the carbonate concentration did not make a huge impact on ozone decomposition rate.

The ozone decomposition rate increased with increasing calcium levels in ozone NBs solutions (**Table 6.13**). Since $CaCl_2$ was used to prepare calcium solutions, the

increase was likely attributable to chloride rather than calcium because Cl^- is known as an initiator of ozone decomposition, causing a noticeable drop in the amount of ozone in the solution (Devi et al., 2013; Hoigné and Bader, 1976; Liao et al., 2001; Razumovskii et al., 2010). Although Cl^- can react with •OH, the back reaction is very fast. Therefore, the quenching of •OH by Cl^- is usually negligible except at pH ≤3 (von Gunten, 2003a). Moreover, ozone disappeared quickly in 5 and 15 min at 3.0 and 0.3 mM $CaCl_2$, respectively (**Table 6.13**).

Table 6.13. Ozone decomposition (mg/L) in O_3 NBs solution at various conditions.

<table>
<tr><th>Time (min)</th><th>pH 3</th><th>pH 5</th><th>pH 7</th><th>pH 9</th><th>Low SUVA$_{254}$ NOM (1.7 L/mg.m) at 5 mg-DOC/L</th><th>High SUVA$_{254}$ NOM (4.1 L/mg.m) at 5 mg-DOC/L</th><th>0.25 mM Carbonate (25 mg/L as $CaCO_3$)</th><th>2.5 mM Carbonate (250 mg/L as $CaCO_3$)</th><th>0.3 mM Calcium (30 mg/L as $CaCO_3$)</th><th>3.0 mM Calcium (300 mg/L as $CaCO_3$)</th></tr>
<tr><td>0</td><td>12.5</td><td>12.5</td><td>12.5</td><td>12.5</td><td>12.5</td><td>12.5</td><td>12.5</td><td>12.5</td><td>12.5</td><td>12.5</td></tr>
<tr><td>5</td><td>10.1</td><td>9.4</td><td>3.6</td><td>0.2</td><td>2.5</td><td>0.1</td><td>4.0</td><td>4.7</td><td>1.2</td><td>0.2</td></tr>
<tr><td>15</td><td>9.8</td><td>9.3</td><td>1.0</td><td>0.1</td><td>NA</td><td rowspan="10"><DL</td><td>2.1</td><td>2.3</td><td>0.7</td><td rowspan="10"><DL</td></tr>
<tr><td>30</td><td>9.3</td><td>8.5</td><td>0.9</td><td rowspan="9"><DL</td><td>0.1</td><td>1.2</td><td>1.3</td><td rowspan="9"><DL</td></tr>
<tr><td>45</td><td>8.8</td><td>7.4</td><td>0.4</td><td rowspan="9"><DL</td><td>0.3</td><td>0.4</td></tr>
<tr><td>75</td><td>8.4</td><td>5.0</td><td rowspan="8"><DL</td><td rowspan="9"><DL</td><td rowspan="8"><DL</td><td>0.1</td></tr>
<tr><td>105</td><td>7.4</td><td>3.3</td><td rowspan="8"><DL</td></tr>
<tr><td>135</td><td>7.2</td><td>2.8</td></tr>
<tr><td>180</td><td>7.1</td><td>1.2</td></tr>
<tr><td>240</td><td>5.5</td><td>0.5</td></tr>
<tr><td>300</td><td>3.3</td><td>0.3</td></tr>
<tr><td>315</td><td>3.1</td><td><DL</td></tr>
</table>

DL: detection limit (< 0.02 mg/L)

Table 6.14. Half-lives of ozone in ozone NBs vs. conventional ozone solution at various pH values.

O_3 NBs				
	pH 3	pH 5	pH 7	pH 9
Slope	0.004	0.013	0.086	0.379
Half-lives (min)	173.3	55.4	8.1	1.8
Conventional ozone (Ku et al., 1996)				
	pH 3	pH 5	pH 7	pH 9
Slope	0.009	0.023	0.087	0.471
Half-lives (min)	77.0	30.1	8.0	1.5

6.3.10. Comparison of the stability ozone NBs with oxygen NBs

Ozone NBs were much more stable with 4 times larger half-lives than those of oxygen NBs (e.g., ozone NBs (193 days) vs oxygen NBs (46 days) at pH 6.5−7 and 20 ^{o}C) (**Table 6.15**). The differences in surface charge of NBs appeared to play a major role in the behavior (e.g., zeta potentials of ozone and oxygen NBs were -32.0 and -23.6 mV, respectively, at time=0, **Table 6.3** and **Table 4.1**).

The stability of both ozone and oxygen NBs was greatly influenced by Ca^{2+} and pH. The lowest ozone and oxygen NBs stabilities were observed at high calcium and low pH values, indicating the role of cations. The impact of calcium was greater on ozone than oxygen NBs stability. At 3 mM Ca^{2+}, the half-lives of oxygen and ozone NBs were 3 and 0.5 days, respectively. The results suggested that both types of NBs will be more stable in soft than hard waters. Both ozone and oxygen NBs were less stable at acidic pH. As pH

increased from 3 to 9, the half-lives also increased from 20 to 693 days for ozone NBs and from 12 to 80 days for oxygen NBs. High $SUVA_{254}$ NOM destabilized both NBs more than low $SUVA_{254}$ NOM; however, its impact for ozone NBs was not as significant as for oxygen NBs. While 60% of ozone NBs were still available in the high $SUVA_{254}$ NOM solution after 60 days storage time, only 20% of oxygen NBs were. The overall comparison of low and high $SUVA_{254}$ NOM effects was similar in oxygen and ozone NBs. While the half-lives of ozone NBs were 193, 182, and 75 days for DDI water, low $SUVA_{254}$ and high $SUVA_{254}$ NOM, respectively, these values were 46, 46, and 17 days for oxygen NBs. When the relative effect of high to low $SUVA_{254}$ NOM was calculated for both ozone and oxygen NBs, similar ratios were observed, 2.6 and 2.7 respectively. Therefore, it can be explained because ozone NBs showed higher stability under all tested conditions than oxygen NBs, and high $SUVA_{254}$ NOM had more impact on NBs stability than low $SUVA_{254}$ NOM. The temperature effect on both NBs stability was negligible for a short storage time, while the effect of higher temperature (30 ^{o}C) became more apparent only for oxygen NBs at a longer storage time with an adverse effect.

Abundant •OH radical formation was observed in the ozone NBs solutions, while the formation of •OH radical was only detectable in oxygen NBs solutions at pH 3 with very low concentrations (**Figure 4.11**). The findings also suggest that while coalescence (growth of bubble size and rise) was the most important mechanism for the oxygen NBs stability, bubble collapse appeared to play a more important role in the disappearance mechanism of ozone NBs in water.

Table 6.15. The half-lives comparisons of oxygen and ozone NBs under various conditions

Ozone NBs			Oxygen NBs		
Ozone NBs storage condition	**1st order NBs disappearance rate constant, k (day^{-1})**	**NBs half-life (day)**	**Oxygen NBs storage condition**	**1st order NBs disappearance rate constant, k (day^{-1})**	**NBs half-life (day)**
Low ozone (1 mg/L)	1.08E-02	64	-		
High ozone (12.5 mg/L)	4.20E-03	165			
pH 3	3.40E-02	20	pH 3	6.00E-02	12
pH 5	4.20E-03	165	pH 5	4.00E-02	18
pH 7	3.60E-03	193	pH 6.5	1.50E-02	46
pH 9	1.00E-03	693	pH 9	9.00E-03	80
DDI	3.60E-03	193	DDI	1.50E-02	46
Low $SUVA_{254}$ NOM (1.7 L/mg.m)	3.80E-03	182	Low $SUVA_{254}$ NOM (1.7 L/mg.m)	1.50E-02	46
High $SUVA_{254}$ NOM (4.1 L/mg.m)	9.30E-03	75	High $SUVA_{254}$ NOM (4.1 L/mg.m)	0.041	17
DDI	3.60E-03	193	-		
0.25 mM CO_3^{2-}	2.60E-03	267			
2.5 mM CO_3^{2-}	NA				
DDI	3.60E-03	193	DDI	1.50E-02	46
0.3 mM Ca^{2+}	8.00E-03	87	9 mM ionic strength (Na^+)	1.47E-01	5
3.0 mM Ca^{2+}	1.29E+00	0.5	9 mM ionic strength (3 mM Ca^{2+})	2.53E-01	3
10 ˚C	NA		10 ˚C	9.00E-03	77
20 ˚C			20 ˚C	1.50E-02	46
30 ˚C			30 ˚C	2.30E-02	30

6.4. Conclusions

Ozone NBs were very stable due to their high magnitude of surface charge during a long-term storage period. Ozone NBs were generated under two different dissolved ozone concentration conditions (i.e., 1 and 12.5 mg/L) and the characteristics and stability of NBs were significantly different although their initial concentrations of NBs were very similar. As an initial dissolved ozone concentration increased, the stability of ozone NBs also increased. The magnitude of the surface charge of NBs solutions generated at 1 mg/L dissolved ozone decreased faster than that at 12.5 mg/L of initial dissolved ozone, which is likely because of ozone decomposition and continuous ozone diffusion from inside of NBs. These findings suggest the preparation conditions of ozone NBs can make a significant impact on the stability and characteristics of NBs.

The stability of ozone NBs which were generated at 1 L/min were investigated under various freshwater conditions (i.e., different pH, NOM, carbonate, calcium, and temperature conditions) for an extended storage time. The half-lives of ozone NBs follow the order of 3 mM Ca^{2+} < pH 3 < high $SUVA_{254}$ NOM (4.1 L/mg.m) < pH 7 < pH 9, while the effects of carbonate (or alkalinity) and temperature on the stability of ozone NBs were insignificant. Thus, ozone NBs would be stable for up to several months in natural waters depending on the water hardness (i.e., 300 mg/L as $CaCO_3$) and hydrophobicity (or aromaticity) of NOM (i.e., 4.1. L/mg.m). The formation of •OH radicals in ozone NBs solutions was 2 – 3 times higher than conventional ozonation during the same reaction time. A rapid disappearance of ozone NBs in the presence of 3 mM Ca^{2+} (i.e., 0.5 day half-life of ozone NBs at 3.0 mM Ca^{2+} solution while it was 193 days in DDI at pH 7) led to

almost no additional •OH radical formation and the overall concentration of •OH radicals in that solution was comparable to conventional ozonation. The presence of carbonate ions, which are known as radical quenchers, lowered the formation of •OH radicals, but it was not enough to stop the continuous generation of radicals. Also, NBs concentrations were not affected by the presence of carbonate whether its level was low or high in the background.

Not only •OH radicals but also other types of reactive oxygen species, which were not measured in the present study, can also be present in the ozone NBs solution. Therefore, it is expected that the oxidative power of ozone can be substantially enhanced when combined with the NBs technology. Consequently, the required dose of ozone for the similar amount oxidation capacity with •OH radicals could be significantly reduced when ozone NBs are applied. In addition, the presence of small bubbles inside the solution will enhance the gas transfer efficiency with their surface area, long-term stability, and gas holdup capacity in the water. These overall findings will enhance the ozone usage performance with NBs in water treatment.

CHAPTER 7

REMOVAL OF MIB AND GEOSMIN BY OZONE NANOBUBBLES

7.1. Introduction

Reducing T&O problem is an important intermittent challenge for many drinking water treatment utilities. Geosmin and MIB are two major earthy-musty odor compounds commonly detected in natural waters, and conventional water treatment processes are not effective for their removal (Ho et al., 2002; Peter and von Gunten, 2007; Srinivasan and Sorial, 2011; Westerhoff et al., 2006). Although these two compounds are not associated with any health effects, their presence in potable waters can be thought of as unsafe by consumers. Currently, adsorption by powdered activated carbon (PAC) is the most effective and widely used treatment technology for managing the intermittent water quality challenge, but the formation of excessive sludge and increase in operating costs are major drawbacks (Kim and Park, 2021b; Mustapha et al., 2021a; Srinivasan and Sorial, 2011; Yu et al., 2007). Granular activated carbon (GAC) filtration can be also effective (Ridal et al., 2001) but its year around use in filters and the negative impact of NOM on geosmin and MIB removal are some of its important disadvantages (Chen et al., 2019; Cook et al., 2001; Kim and Park, 2021b; Matsui et al., 2013; Mustapha et al., 2021a; Pirbazari et al., 1993; Ridal et al., 2001; Srinivasan and Sorial, 2011; Q. Wang et al., 2020). Competitive adsorption may reduce the capacity of the activated carbon to adsorb geosmin and MIB in the presence of other organic constituents in natural waters.

Ozonation has been considered as a powerful method to destroy organic contaminants in water. For example, an early study found that about 90% of geosmin and 80% of MIB were removed from a surface water with an ozonation dose of 4 mg/L (Glaze et al., 1990). Although ozonation alone is effective in removing geosmin and MIB, a high dosage is required for complete removal (Ho et al., 2004; Kim and Park, 2021b; Liang et al., 2007; Westerhoff et al., 2006). In the presence of bromide in water, a high ozone dosage may result in the formation of an excess amount of regulated bromate in water (Sohn et al., 2006; von Gunten, 2003a; Westerhoff et al., 2006; Yao et al., 2017). Due to its toxicity and adverse health effect on humans, USEPA established a maximum contaminant level of 10 µg/L bromate for a safe drinking water (USEPA, 2010). Ozonation involves reactions of both ozone (direct pathway and selective organic (i.e., mainly double bounds, activate aromatic systems and non-protonated amines) removal) and hydroxyl radicals (•OH, indirect pathway, nonselective organic removal) (Bruchet and Duguet, 2004; von Gunten, 2007). To enhance the ozone oxidation performance, ozone has been applied with H_2O_2 or UV light, which are also known as advanced oxidation processes (Beniwal et al., 2018; Mustapha et al., 2021b; Park et al., 2006; Westerhoff et al., 2006). The addition of H_2O_2 can increase the hydroxyl radical yield by 50% (Fischbacher et al., 2013). The oxidation efficiency of geosmin and MIB during O_3/H_2O_2 process depended on the concentration of O_3 and H_2O_2, temperature, pH and organic matter since these parameters directly change the ozone decomposition and •OH radicals formation rate (Park et al., 2006; Westerhoff et al., 2006). It has been also reported that advanced oxidation with ozone (at 1.5-3 mg/L for 2-3 min of contact time) and UV radiation (at 5,000-6,000 J/m^2) resulted in complete

removal of geosmin and MIB (Collivignarelli and Sorlini, 2004). In a pilot-scale experiment, 200 ng/L of geosmin and MIB decreased below their threshold levels (i.e., 0.1 and 3.85 ng/L, respectively) by pre-ozonation at 1 mg/L followed by GAC filtration (Chen et al., 2019).

Although a number of studies have been conducted on the removal of geosmin and MIB by ozonation alone or coupled with other AOP techniques, there has been no investigation of the application of ozone NBs to destroy the T&O compounds in water matrices. The higher gas holdup capacity in water caused by ozone NBs may lead to elevated levels of •OH radicals formation from the decomposition of ozone. Ozone NBs are known to provide better remediation of groundwater and sediments than conventional systems (Batagoda et al., 2018; Hu and Xia, 2018; Xia and Hu, 2019). More recently, ozone MNBs/NBs were investigated for the remediation of contaminated sediments and groundwater (Aluthgun Hewage et al., 2021; Batagoda et al., 2019; Hu and Xia, 2018), removal of model compounds and micropollutants in water and wastewater (Fan et al., 2021a; Hashimoto et al., 2021; Xia and Hu, 2018), reduction of bacterial pathogens and disinfection in freshwater, wastewater and aquaculture system (Benazir Abate and Flores, 2017; Cruz and Flores, 2017; Dien et al., 2022; Epelle et al., 2022; Huang et al., 2023; Jhunkeaw et al., 2021, 2020; Linh et al., 2022, 2021; Ng et al., 2023; Nghia et al., 2022; Saijai et al., 2019; Seridou and Kalogerakis, 2021; Yang et al., 2023), and anti-microbial effectiveness for fresh vegetables (He et al., 2015; Ushida et al., 2017). Details about the target compounds, experimental conditions, NBs generators and measurements method in these literature studies were summarized in Appendix A, **Table A1**. While several studies

have been reviewed for the application of ozone NBs, there is still a need for further research to address several issues. For example, most of these studies do not provide data on NBs detection, making it unclear whether they are actually NBs or MBs studies. Additionally, because ozone is highly sensitive to changes in water quality parameters such as temperature, pH, NOM, and alkalinity, the experimental and operational conditions need to be clearly stated. Moreover, testing ozone NBs in a side-by-side comparison with conventional ozonation under the same experimental conditions would demonstrate the realistic performance of the technology for further investigation.

The application of ozone NBs technology may significantly enhance the ozonation efficiency, reduce chemical use, and provide opportunities for development of innovative treatment approaches, especially for the removal of geosmin and MIB. The main objective of this phase of my study was to investigate the removal efficiency of geosmin and MIB by ozone NBs in DDI and natural waters under various conditions and compare to the use of conventional dissolved ozone.

7.2. Materials and Methods

7.2.1. Conventional ozone and ozone NBs generation

Ozone NBs were prepared using the membrane NBs generator system (**Figure 6.1**), as described in Section 6.2.1. The dissolved ozone concentration in the solution can be controlled by adjusting the oxygen gas flow rate to the ozone generator. The maximum oxygen gas flow rate is 4 L/min, as specified by the manufacturer. Therefore, the gas flow rate was initially set to 4 L/min to achieve the desired concentration of ozone NBs in the

solution (i.e., 10^8 particles/mL). Once ozone NBs number was confirmed with at least two independent measurements using NanoSight, the gas flow rate was reduced to increase the ozone concentration in the solution. A lower gas flow rate increased the residence time of oxygen molecules in the ozone generator, which resulted in a higher dissolved ozone concentration in the solution. Additionally, slowly releasing ozone from the ozone generator into the solution can increase its dissolution in water, resulting in an even higher ozone concentration (Cuong et al., 2019; Du and Lin, 2019). The target ozone concentrations were 0.5 and 1.0 mg/L for geosmin and MIB removal experiments.

Conventional ozonation was concurrently conducted and used to compare to the ozone NBs experiments. A concentrated ozone stock solution (i.e., 30 mg/L) was prepared in DDI and spiked into bottles to achieve the desired concentrations of 0.5 and 1.0 mg/L. The ozone concentration in each solution was measured using the ozone indigo method (HACH AccuVac ampuls).

7.2.2. Experimental setup and conditions

Geosmin and MIB removal in DDI and natural waters were evaluated using conventional ozone and ozone NBs solutions. The temperature of the solutions was kept at 20±1.0 ^{o}C and the initial pH was around 6.0±0.5 in DDI solutions. When the NBs and ozone levels reached the desired levels, the NBs solution was taken from the tank with a glass beaker and transferred to the 1 L bottle. A 1 L main stock solution was prepared for each experiment and aliquoted into six bottles (133 mL amber bottles), one for each time point. The total contact time for the experiments was 10 minutes, and samples were taken

at 0, 0.25, 1, 2, 5, and 10 minutes for kinetic analysis. The initial geosmin and MIB concentrations were set at 1000 ng/L for the removal experiments because much more radical formation was expected in ozone NBs solutions than oxygen NBs. Therefore, starting with a relatively higher geosmin and MIB level was also preferred to clearly observe degradation kinetics over time.

For natural waters experiments, water was concentrated by using a reverse osmosis (RO) membrane to conduct experiments at the same DOC level and eliminate the dilution of NBs. A small volume of concentrated natural water was spiked into the ozone solutions (i.e., 10 ml in 133 mL), and the dilution ratio was taken into consideration when determining the volume of ozone and ozone NBs to add to the solutions. Ozone levels were measured at least three times before starting experiments to confirm the initial ozone levels at the beginning.

Geosmin and MIB removal, •OH radicals' formation and ozone decomposition experiments were all consistently conducted under the same conditions for both conventional ozone and ozone NBs. The effect of temperature (20 and 30 ^{o}C) was tested in both DDI and natural waters, and solutions were kept in a water bath and temperature was monitored continuously. The effect of calcium with $CaCl_2$ (i.e., 300 mg/L as $CaCO_3$) and alkalinity with $NaHCO_3$ (i.e., 250 mg/L as $CaCO_3$) were tested for geosmin and MIB removal efficiency.

During the kinetic analysis, initially 40 mL of the solution from each bottle was transferred to 50 ml beaker to measure the dissolved ozone concentration at the desired

time point. The remaining solution in the bottle was then quenched immediately for geosmin and MIB analysis. Since the decomposition of ozone forms •OH radicals, the removal of geosmin and MIB would depend on two main oxidants, ozone and •OH radicals during the ozonation experiments. To stop the oxidation of geosmin and MIB caused by ozone and •OH radicals immediately at designated contact times, sodium thiosulfate ($Na_2S_2O_3.5H_2O$) was selected as the quenching agent, and the use of a proper dose was investigated. The initial dose determination of sodium thiosulfate for ozone quenching was selected based on literature data (Qi et al., 2009; Takizawa et al., 1973; Yang et al., 2020). In a previous study, 200 µM of $S_2O_3^{2-}$ was used to quench 0−60 µM ozone (Yang et al. 2020), while in other studies, the molar ratio of $[S_2O_3^{2-}]$:$[O_3]$ was set at greater than 10 (Vel Leitner and Roshani, 2010; Xie et al., 2023; Yang et al., 2020). When sodium thiosulfate was added to the solution, ozone was consumed by thiosulfate forming various reaction products such as $Na_2S_2O_6$, Na_2SO_4, Na_2SO_3 at neutral pH (Takizawa et al., 1973). Based on the information, geosmin and MIB samples were quenched by a dose of sodium thiosulfate solution of 0.1-1.0 mL with a concentration of 0.1 M for 0.5 and 1.0 mg/L (i.e., 10.4 and 20.8 µM ozone, respectively) initial dissolved ozone concentration and the residual remaining ozone during the experiment at different time point. The selected concentration range was tested before the experiments to ensure that it was sufficient to completely quench the ozone in the solution. After the experiments, the quenched samples were immediately prepared for geosmin and MIB analysis. The details of sample preparation are described in Chapter 5.

The •OH radical formation was quantified with 2 mM TP. To determine the concentrations of •OH radicals, TPOH formation was measured at a designated time using a Shimadzu RF5301PC spectrofluorometer. The concentration of •OH radicals were determined in the solution by measuring the fluorescence intensity of TPOH at 425 nm. More detailed information about the methods and calibration curve used to measure TP and TPOH is provided in Chapter 3.

The bromate formation experiments were conducted in natural waters with addition of 250 µg/L bromide. Bromide was first added to the natural waters, and then ozone solutions for both conventional ozone and ozone NBs were injected into the solution for a contact time of 10 minutes. After that, the solutions were quenched with $Na_2S_2O_3.5H_2O$, and samples were analyzed for bromate formation using ion chromatography. The details of the analytical method and the maximum contaminant level (MCL) for bromate are given in **Table 3.4**.

All experiments were performed as independent duplicates, and samples from each data point for geosmin and MIB analysis were measured duplicate (i.e., two-independent vials) on a GC/MS/MS. The final results were presented as the average of the two independent experiments and two duplicate measurements for each sample, with standard deviation. A statistical t-test was used to compare two groups of data to determine if the differences between the results were statistically significant, with p-values (i.e., 0.05) from the analysis.

7.2.3. Excitation emission matrix (EEM) measurements

Excitation-emission matrix (EEM) spectroscopy was used to characterize DOM in the natural waters. DOM is a complex mixture of organic compounds that can come from a variety of sources, such as decaying plants, leaves, and algae (Zark and Dittmar, 2018).

EEM spectroscopy works by exciting DOM molecules with light of different wavelengths and measuring the fluorescence emitted by the molecules. The fluorescence spectrum of a DOM sample is unique and can be used to identify the types of organic compounds present in the sample. It can be used to identify and quantify different DOM components in water, such as humic acids, fulvic acids, and protein-like substances (Chen et al., 2003; Fu et al., 2019). It can also be used to track changes in DOM composition over time and to assess the effectiveness of water treatment processes (Rodríguez-Vidal et al., 2021).

EEM spectra were obtained for different fractions of the DOM, and these spectra were then divided into five different regions based on the fluorescence of the DOM fractions (Chen et al., 2003; Fu et al., 2019). The excitation and emission wavelength boundaries for each organic group were obtained from previous studies (Chen et al., 2003; Fu et al., 2019), and the specific excitation and emission wavelengths of each region are shown in **Table 7.1**.

The DOM fractions were measured using an EEM fluorescence spectrophotometer (Shimadzu, RF-6000). The excitation and emission wavelengths were set to a range of 200-500 nm and 280-550 nm, respectively. Both excitation and emission wavelengths were

scanned simultaneously at intervals of 5 nm and 1 nm, respectively, with a scan speed of 12,000 nm/min.

Before each sample measurement, DDI was measured to establish a baseline and to ensure that the quartz cell was clean. Additionally, EEM fluorescence spectra was normalized to Raman units (R.U.) by using integrated Raman peak area of DDI to calibrate the fluorescence intensity of the sample measurement (Lawaetz and Stedmon, 2009). Water Raman spectra were captured with emission wavelengths ranging from 365 to 430 nm and an excitation wavelength of 350 nm (Lawaetz and Stedmon, 2009). The method also makes it possible to compare quantitative data across different runs and instruments while eliminating signal intensity variations. The EEM results are presented in the unified scale of Raman units.

Table 7.1. Excitation emission regions of the DOM fractions (Adapted from Fu et al., 2019).

Region number	Associated DOM fractions	Excitation/Emission wavelength (nm)
I	Aromatic protein I	220-250/280-330
II	Aromatic protein II	220-250/330-380
III	Fulvic acid-like substances	220-250/380-500
IV	Soluble microbial by-product-like substances	250-280/280-380
V	Humic acid-like substances	250-400/380-500

7.3. Results and Discussion

7.3.1. Ozone mass transfer with ozone NBs and conventional ozone

The ozone mass transfer efficiency of ozone NBs and conventional ozone were compared in 35 L DDI water at a gas flowrate of 1-1.5 L/min. The experimental conditions were the same for both ozone NBs and conventional ozone, with a temperature of 20±1.0 °C and a pH of 6.5±1.0. As shown in **Figure 7.1**, the dissolved ozone level with ozone NBs increased rapidly within 30 seconds and continued to increase throughout the 10-minute reaction time, with continuous gas injection and circulation of water with a pump. The dissolved ozone level reached 16.3 mg/L within 5 minutes, and there was no significant increase in the remaining 5 minutes due to the limitation of the ozone generator. The ozone profile with conventional ozone was completely different from that of ozone NBs. The ozone delivery rate was slow using conventional ozonation, and reached 0.65 mg/L at 10 minutes reaction time under the same experimental and operation conditions as the ozone NBs. Although the same amount of ozone gas was injected into the water, the yield of ozone dissolution was significantly higher with ozone NBs (i.e., 2.2-4.2 mg/L.min) than with conventional ozone (0.07-0.22 mg/L.min).

Previous studies also observed better performance of ozone NBs/MNBs than conventional ozonation (Batagoda et al., 2018; Fan et al., 2021a; Hu and Xia, 2018; Lee et al., 2023; Seridou and Kalogerakis, 2021). Lee et al. (2023) observed that NBs exhibited a 10-fold improvement in ozone dissolution within 30 minutes of bubble generation. While the dissolved ozone concentration in the solution reached 10 mg/L with NBs, it was less

than 1 mg/L with macrobubbles (Lee et al., 2023). Macrobubbles also reached a dissolved ozone concentration of approximately 1 mg/L within 5 minutes, but then remained almost constant at that level. In contrast, NBs showed a continuous increase in dissolved ozone concentration until 25 minutes reaction time, then there was no further increase. In another study, Hu and Xia (2018) showed that while dissolved ozone concentration reached 10.09 mg/L with ozone MNBs within 30 minutes of generation time, the level of ozone with millimeter size bubbles only achieved a dissolved ozone concentration of 0.64 mg/L. The combination of high mass transfer and reduced ozone degradation, attributed to the increased surface area of MNBs, contributes to improved ozonation performance. As a result, less ozone is wasted, and ozone production is less expensive with MNBs than conventional ozonation (Batagoda et al., 2018).

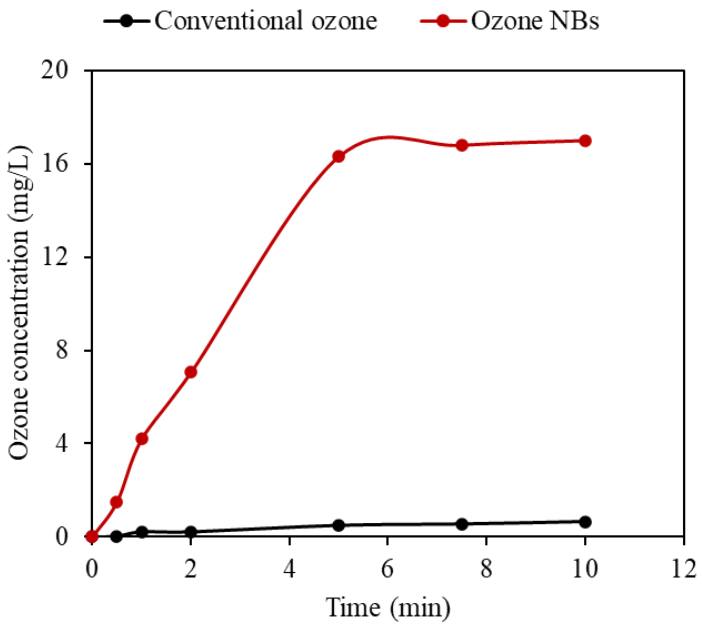

Figure 7.1. Ozone mass transfer with ozone NBs and conventional ozone in DDI at 20±1.0 C and pH 6.5±1.0.

7.3.2. The removal of geosmin and MIB, and •OH radical formation by ozone NBs and conventional ozonation in DDI

The removal of geosmin and MIB by conventional ozonation and ozone NBs ($(NBs)_0$ = 1.10 x 10^8 particles/mL) was examined at 1 mg/L initial dissolved ozone concentration at pH 6.5±0.5 and 20.0±0.1 ^oC. Geosmin and MIB removal during ozonation is primarily driven by •OH radicals rather than ozone, because of 10^9 times higher reaction rate constant of geosmin and MIB reacting with •OH radicals than ozone ($k_{O3,geosmin}$ = 7.5 $M^{-1}s^{-1}$, $k_{O3,MIB}$ = 1.0 $M^{-1}s^{-1}$ and $k_{•OH,geosmin}$ = 9.5 x 10^9 $M^{-1}s^{-1}$, $k_{•OH,MIB}$ = 8.2 x 10^9 $M^{-1}s^{-1}$) (Westerhoff et al., 2006). Therefore, the formation of •OH radicals was examined for the conventional ozone and ozone NBs solutions, with 1 mg/L dissolved ozone in water. The ozone level in the bottles and formation of •OH radicals was observed during the 10-minute reaction time. Since there was no driving force or stimuli, such as organic matter or continuous agitation for ozone decomposition, only a 5% ozone decrease was observed for conventional ozone and no change in the ozone levels in ozone NBs solution (**Figure 7.2**A).

The yield of •OH radicals (the concentration of formed •OH radicals/dissolved ozone concentration) observed with NBs was 1.1-1.5 times higher than conventional ozonation under the same initial ozone levels and experimental conditions (**Figure 7.2**B). The difference was attributed to •OH radicals on ozone NBs surfaces as well as the continuous diffusion of ozone from the NBs and the gas holdup capacity of NBs (Batagoda et al., 2018; Kyzas and Mitropoulos, 2021). Also, the movement of NBs due to Brownian motion will keep them in the solution for a longer time. The longer time enhanced the

surface interaction of NBs with the TP and provided continuous ozone diffusion for further reaction opportunities of TP with •OH radicals, which increased TPOH formation. Also, hydroxide ions on the gas-water interfaces of ozone NBs can further enhance the formation of •OH radicals (Yang et al., 2023).

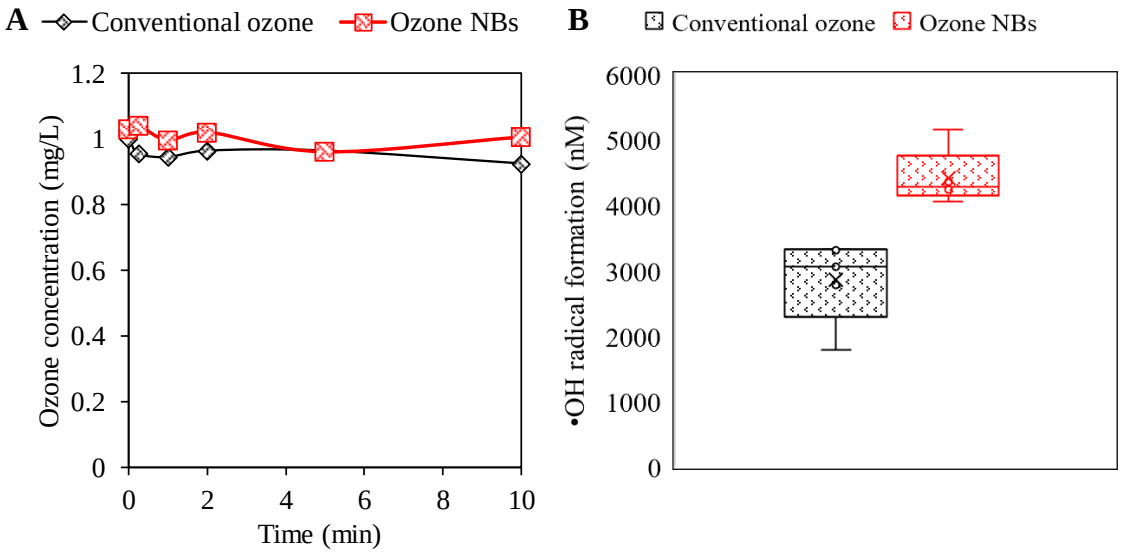

Figure 7.2. The concentration of dissolved ozone and •OH radicals for conventional ozone and ozone NBs. $[O_3]_0$= 1.0 mg/L, $[NBs]_0$ = 1.0 x 10^8 particles/mL, pH 6.5±0.5, T: 20±1.0 ^oC.

The higher production of •OH radicals by ozone NBs compared to conventional ozonation resulted in better removal of geosmin and MIB (**Figure 7.3**). While more than 55% of geosmin was removed by ozone NBs in a very short contact time (i.e., 0.25 min), 45% of geosmin was removed by conventional ozonation under the same experimental conditions. The observed difference shows that ozone NBs can achieve better geosmin and MIB removal in a much shorter contact time than conventional ozonation. The overall removal of geosmin during the 10-minute contact time was >80 and 69% for ozone NBs

and conventional ozonation, respectively. The loss of geosmin and MIB due to volatilization was negligible in the study. The initial reaction with NBs, and further reaction during the 10-minute contact time, showed better performance with higher geosmin degradation rate with NBs. Degradation rate constants of MIB for both ozone and •OH radicals were less than geosmin, so geosmin was more easily removed than MIB by ozone NBs and conventional ozonation (Park et al., 2006; Westerhoff et al., 2006; Xin, 2021). In fact, only 32% of MIB was removed in the first 0.25 min of contact time, which was 13% less than the amount of geosmin removed by conventional ozone. However, over a 10-minute contact time, MIB removal increased to 53%. Ozone NBs were significantly more effective at removing MIB than conventional ozone ($p \leq 0.05$), with a removal efficiency of 73% after 10-minutes of reaction time (**Figure 7.3B**). Immediate geosmin and MIB decrease was observed in a few minutes at the initial part of the reaction time, but then the degradation rate slowed in the previous studies as in the study. For example, a conventional ozonation (0.75-4 mg/L) for 30 min at pH 5.7-8.1 removed 30-130 ng/L geosmin and MIB in nano pure water (Westerhoff et al., 2006). The removal efficiency of geosmin and MIB was more than 90% which happened in a few minutes contact time although the reaction time was 30 minutes. In another study, 72.6% geosmin and 66.4% MIB (500 ng/L of initial doses) in Milli-Q water was removed when 4.19 mg/L of ozone was applied for 20 min at pH 7.3 (Yuan et al., 2013). The results of my study of conventional ozonation were consistent with the general trend observed in the previous studies.

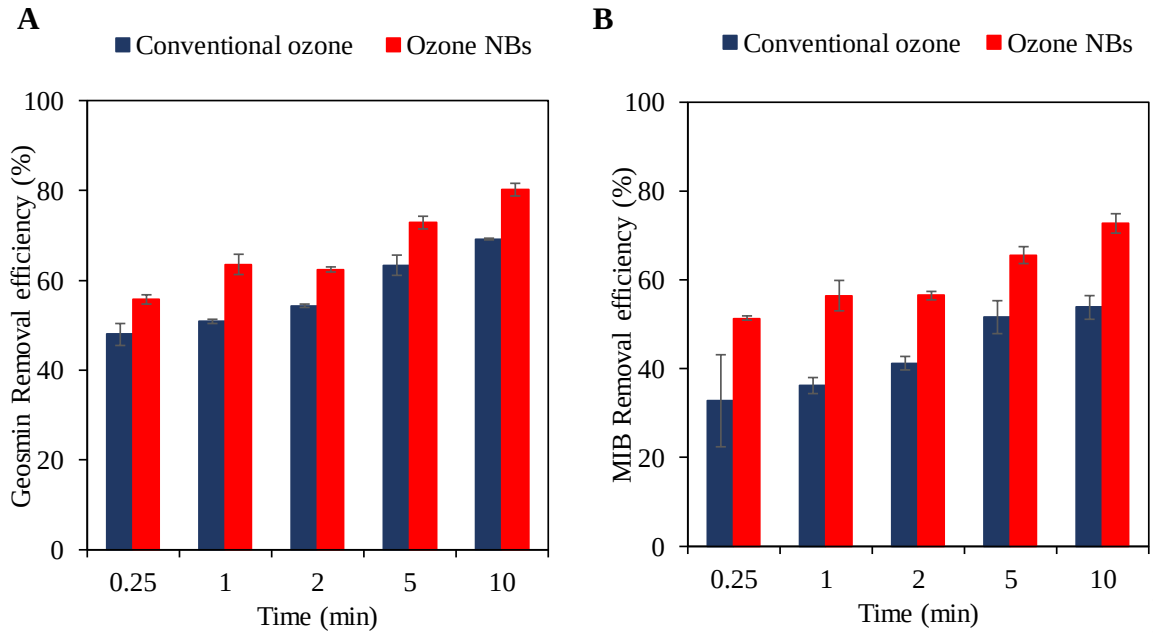

Figure 7.3. Comparison of conventional ozone and ozone NBs: A) Geosmin and B) MIB removal. $[O_3]_0$= 1.0 mg/L, $[geosmin]_0$=1000±5.0 ng/L, $[MIB]_0$=1000±5.0 ng/L, $[NBs]_0$ = 1.0 x 10^8 particles/mL, pH 6.5±0.5, T: 20±1.0 °C. Error bars represent standard deviations (n=4).

7.3.3. The effect of temperature on •OH radical formation, geosmin and MIB removal in DDI

Because the occurrence of geosmin and MIB increases in summer months due to the seasonal algal blooms (Peter et al., 2009; Watson et al., 2008; Westerhoff et al., 2005), the effect of water temperature on the removal percentages of geosmin and MIB were investigated. As temperature increased from 20 °C to 30 °C, the dissolved ozone level decreased from about 1.0 to 0.8 mg/L for conventional ozonation, but remained relatively constant for ozone NBs. The result suggested that the application of ozone NBs can suppress the negative impact of temperature that increases the decomposition of ozone

concentration solution (**Figure 7.4**A). The formation of •OH radicals increased with increasing temperature for both conventional ozone and ozone NBs, but the increase was significantly higher for ozone NBs (shown in **Figure 7.4**B). At 20°C, ozone NBs produced 1.5 times more •OH radicals than conventional ozone. At 30°C, the ratio increased to 1.8.

At 30°C, both conventional ozone and ozone NBs removed more geosmin and MIB than at 20°C. Ozone NBs removed up to 10% geosmin and MIB more after 10 minutes of contact time at 30°C compared to 20°C (**Figure 7.5**A&B). While temperature had a positive impact on the reaction rate of geosmin and MIB removal by conventional ozonation, it increased the removal of both compounds by 5-6%. The enhanced removal of geosmin and MIB at higher temperatures was attributed to the increased production of ROS at higher temperature (Janus et al., 2012; Westerhoff et al., 2006). The calculated rate constants of the geosmin disappearance by conventional ozone and ozone NBs during contact time were 1.3×10^{-3} and 1.9×10^{-3} s^{-1} at 20 °C and 1.7×10^{-3} and 4.6×10^{-3} s^{-1} at 30 °C, respectively. The removal rate constants of MIB also increased at higher temperature from 9.4×10^{-4} to 9.6×10^{-4} s^{-1} and 1.4×10^{-3} and 3.3×10^{-3} s^{-1} for conventional ozone and ozone NBs, respectively. As discussed in the previous sections, geosmin was more readily degradable than MIB and geosmin removal rate constants were 1.4 - 1.7 times higher than MIB for all tested conditions. The result suggests that both conventional ozone and ozone NBs were more effective at removing geosmin and MIB from water at higher temperatures. Although conventional ozone and ozone NBs treatments can significantly decrease geosmin and MIB concentrations, the residual levels still exceeded the established threshold concentrations (i.e., 4-20 ng/L). In the absence of downstream treatment

processes capable of further reducing these compounds, extending the ozone contact time and increasing ozone dosage can be implemented to achieve adequate removal. Ozone NBs were also more effective at removing geosmin and MIB than conventional ozone at both temperatures.

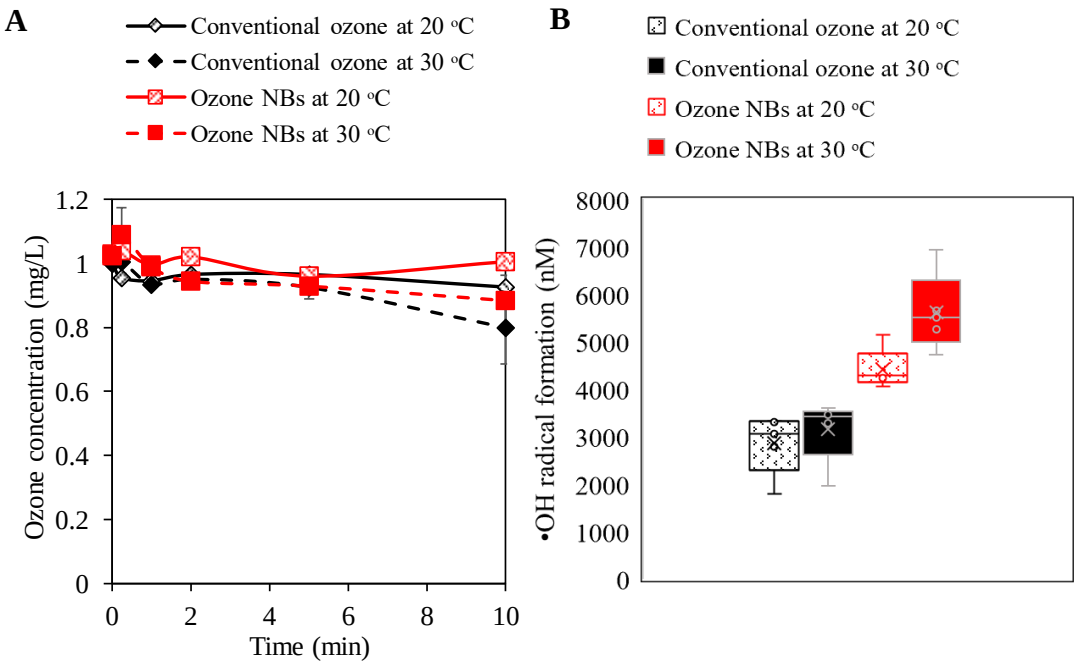

Figure 7.4. The effect of temperature, 20 vs. 30°C, on ozone concentration and •OH radicals formation for conventional ozone and ozone NBs. $[O_3]_0$= 1.0 mg/L, $[NBs]_0$ = 1.0 x 10^8 particles/mL, pH 6.5±0.5. Error bars represent standard deviations (n=4).

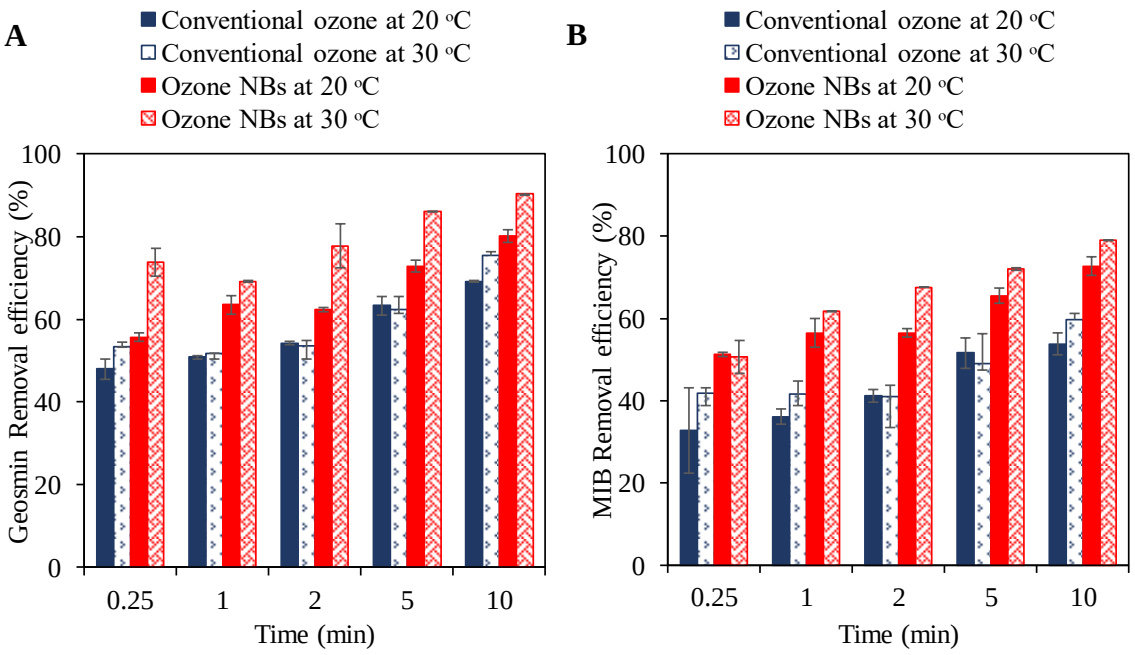

Figure 7.5. The effect of temperature on A) geosmin and B) MIB removal by conventional ozone and ozone NBs. $[O_3]_0$= 1.0 mg/L, $[geosmin]_0$=1000±5.0 ng/L, $[MIB]_0$=1000±5.0 ng/L, $[NBs]_0$ = 1.0 x 10^8 particles/mL, pH 6.5±0.5, T: 20±1.0 & 30±1.0 °C. Error bars represent standard deviations (n=4).

7.3.4. The removal of MIB and geosmin, and •OH radical formation by ozone NBs and conventional ozonation in natural water

The removal efficiency of geosmin and MIB by ozone NBs was further investigated in natural water. The characteristics of the natural water selected was shown in

Table 7.2. The presence of different components in natural water such as organic matter, alkalinity, chloride, etc. can change the efficiency of conventional ozone and ozone NBs treatment. These components can consume ozone and reduce the formation of radicals, which can inhibit the removal of geosmin and MIB. However, organic matter can

also react with •OH radicals to form carbon-centered radicals. These radicals can then react with oxygen to form superoxide radicals, which can quickly react with ozone to form •OH radicals again (von Gunten, 2003b). It is difficult to say whether NOM fractions promote or inhibit reactions because their effects vary depending on the specific NOM fractions and other factors (von Gunten, 2003b). Therefore, the conventional ozone and ozone NBs were compared for geosmin and MIB removal in natural water under the same experimental conditions. The DOC value of water was 2.3 mg/L, and ozone level was adjusted to 1.0 mg/L (0.43 mg dissolved O_3/mg DOC ratio) at pH 7.3±0.3 and temperature 20±1.0 ^{o}C.

Ozone decomposition and the formation of •OH radical in a natural water during 10-min contract time are plotted in **Figure 7.6**. The initial ozone concentration was the same for both conventional ozone and ozone NBs, 1.02 mg/L. Over time, the ozone concentration decreased in both conventional ozone and ozone NBs, but the ozone concentration in ozone NBs decreased at a slower rate, and there was 0.01-0.16 mg/L difference in 5-min conduct time. After 5 minutes, there was no residual ozone in either conventional ozone or ozone NBs. As shown in **Figure 7.6**B, ozone NBs produced more •OH radicals (i.e., 1.6 times) than conventional ozonation. Therefore, ozone NBs were more effective at removing geosmin and MIB from natural water than conventional ozonation (**Figure 7.7**). During a 10-minute reaction time, ozone NBs removed 70-87% of geosmin and 54-76% of MIB, while conventional ozonation removed 50-75% of geosmin and 40-63% of MIB. In addition, ozone NBs were faster at removing geosmin and MIB than conventional ozonation. In the first 15 seconds of the experiment, ozone NBs removed more than 70% of geosmin and more than 50% of MIB, while conventional ozone only

removed 50% of geosmin and 40% of MIB, which was also observed for •OH radical formation.

Table 7.2. Natural water characteristics which were used for experiments.

Parameters	**Unit**	**Values**
pH	-	7.3
Dissolved Organic Carbon (DOC)	mg/L	2.34
UV_{254}	cm^{-}	0.04
Bromide	µg/L	21
Geosmin	ng/L	8
MIB	ng/L	4
Total Hardness	mg/L as $CaCO_3$	25
Iron	mg/L	<0.01
Manganese	mg/L	<0.01
Chloride	mg/L	7.7
Nitrite	mg/L	0.01
Nitrate	mg/L	0.16
Sulfate	mg/L	3.03
Total Nitrogen (TN)	mg-N/L	0.24
Turbidity	NTU	< 1
Alkalinity	mg/L as $CaCO_3$	20

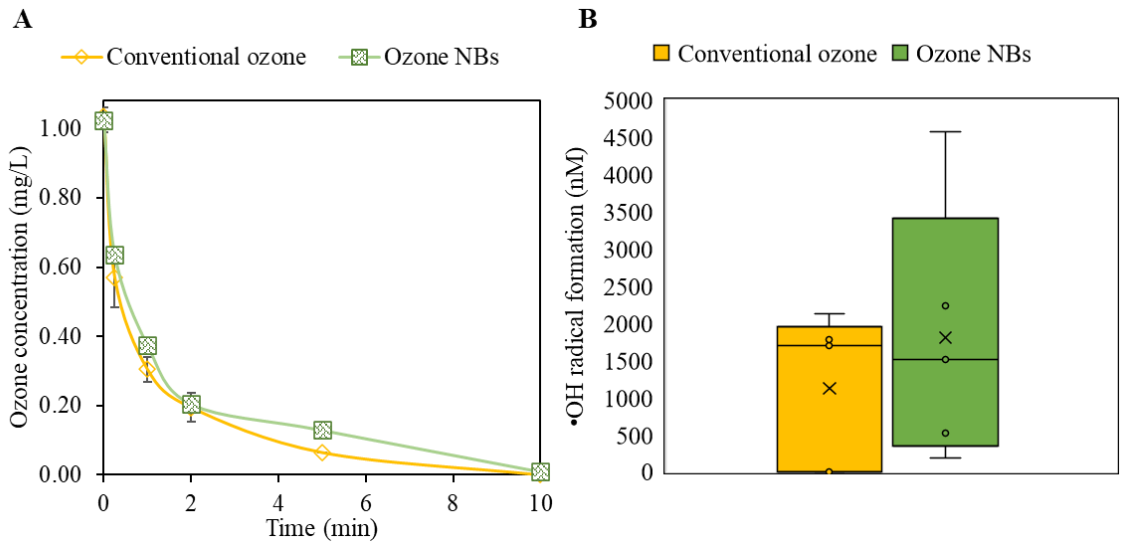

Figure 7.6. The effect of natural water on (A) ozone concentration and (B) •OH radicals formation in time for conventional ozone and ozone NBs. $[O_3]_0$= 1.0 mg/L, $[NBs]_0$ = 1.0 x 10^8 particles/mL, pH 7.3±0.3, T: 20±1.0 °C. Error bars represent standard deviations (n=2).

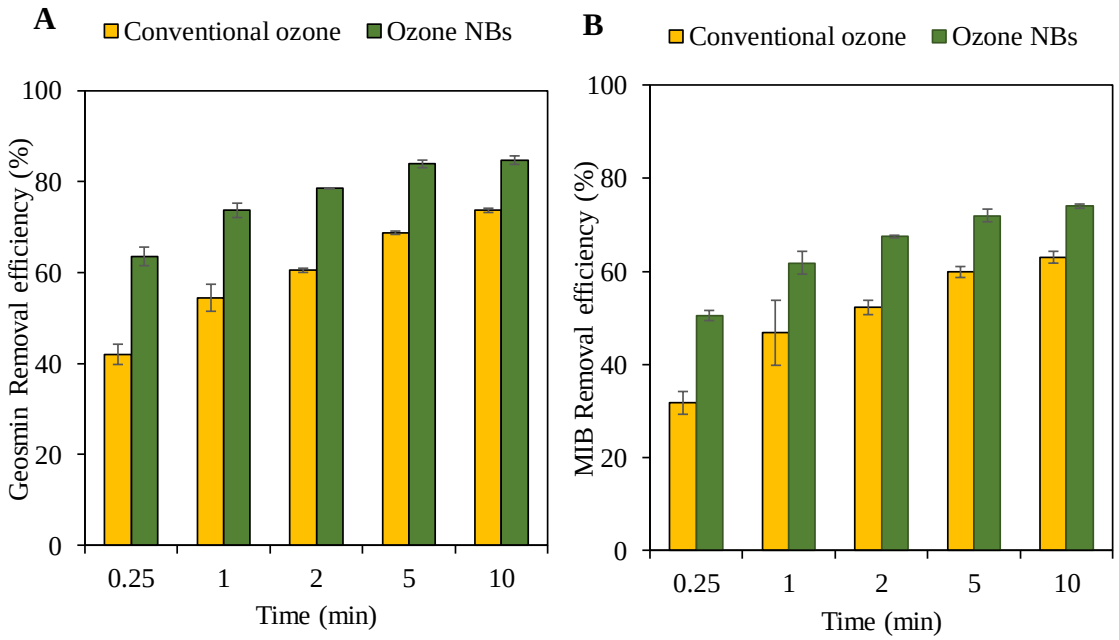

Figure 7.7. Comparison of conventional ozone and ozone NBs: A) Geosmin and B) MIB removal in natural water. $[O_3]_0$= 1.0 mg/L, [DOC]= 2.3 mg/L, $[geosmin]_0$=1000±5.0 ng/L, $[MIB]_0$=1000±5.0 ng/L, $[NBs]_0$ = 1.0 x 10^8 particles/mL, pH 7.3±0.3, T: 20±1.0 °C. Error bars represent standard deviations (n=4).

7.3.4.1.The effect of temperature on geosmin and MIB removal in natural water

The effect of temperature on geosmin and MIB removal efficiencies were also tested in natural water. The results indicated that ozone decomposition increased with elevated temperature, and there was no residual ozone after 5 minutes of reaction in the natural water (**Figure 7.8**) (Elovitz et al., 2000; Eriksson, 2005; Ershov and Morozov, 2009; Westerhoff et al., 2006). The effect of fast ozone decay on geosmin and MIB removal was similar to the behavior in DDI conditions. Moreover, increasing the temperature from 20 to 30°C increased geosmin and MIB removal by up to 10% for both conventional ozone and ozone NBs (**Figure 7.9**.) Since the experiments were conducted in headspace-free bottles, the volatilization in 10-min short contact time was negligible, and the difference in removal was attributed to further oxidation of the compounds. Ozone NBs maintained their removal advantage (i.e., 10-15% more) under both conditions. Based on these findings, it was concluded that higher temperature provided additional benefits to both conventional ozone and ozone NBs. Therefore, the rest of the experiments were conducted at 30°C.

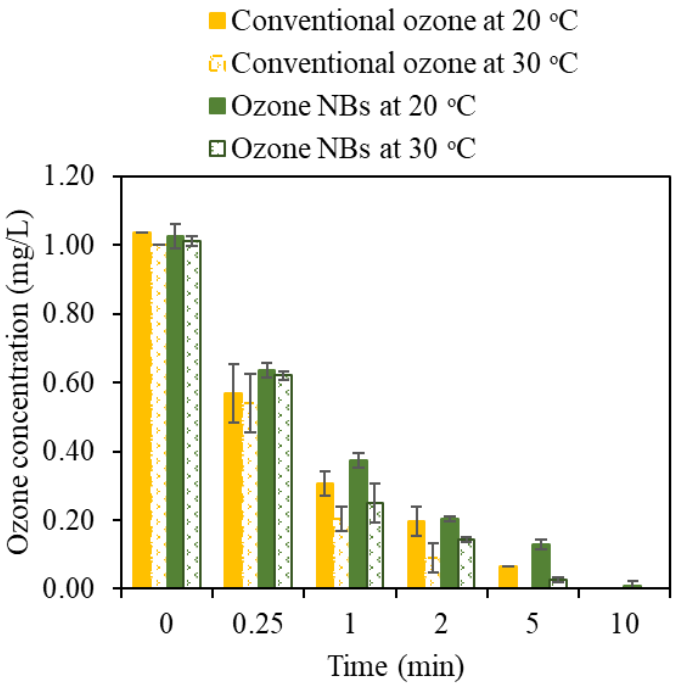

Figure 7.8. The effect of temperature on ozone decomposition by conventional ozone and ozone NBs in natural water. $[O_3]_0$= 1.0 mg/L, [DOC]= 2.3 mg/L, $[NBs]_0$ = 1.0 x 10^8 particles/mL, pH 7.3±0.3, T: 20±1.0 & 30±1.0 °C. Error bars represent standard deviations (n=4).

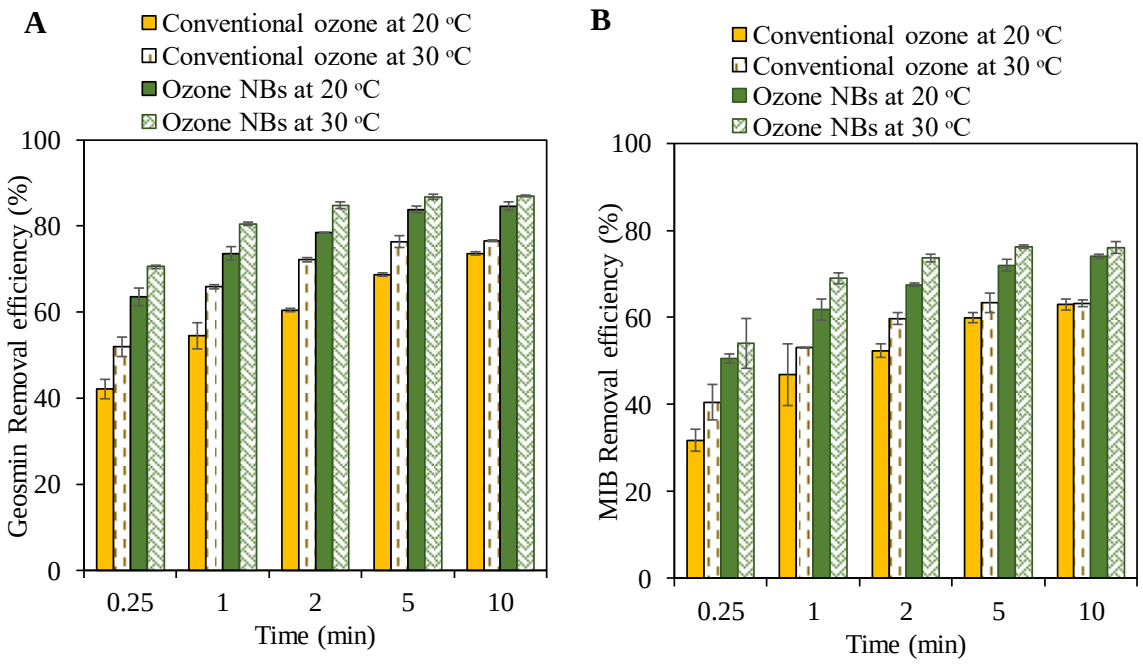

Figure 7.9. The effect of temperature on A) geosmin and B) MIB removal by conventional ozone and ozone NBs in natural water. $[O_3]_0$= 1.0 mg/L, [DOC]= 2.3 mg/L, $[geosmin]_0$=1000±5.0 ng/L, $[MIB]_0$=1000±5.0 ng/L, $[NBs]_0$ = 1.0 x 10^8 particles/mL, pH 7.3±0.3, T: 20±1.0 & 30±1.0 °C. Error bars represent standard deviations (n=4).

7.3.5. The effect of different natural water sources on geosmin and MIB removal

Ozone and •OH radicals formed during the ozone decomposition can breakdown organic contaminants (Hoigné and Bader, 1979; Staehelln and Hoigné, 1985; von Sonntag and von Gunten, 2012). Ozone application increases the percentage of low-molecular-weight organics (<1 kDa) and decreases the amount of high-molecular-weight organics (>100 kDa) in organic matter (Fu et al., 2019). Although DOC mineralization is limited, ozone can significantly change the composition of DOM and produce biodegradable organic carbon. The most common low-molecular-weight organic byproducts are

carboxylic acids, aldehydes, and ketones (Remucal et al., 2020; Siddique et al., 2022; von Gunten, 2003b). These changes can be monitored by measuring the change in fluorescence and specific UV absorbance of organic matter. Therefore, the characterization of organic matter in natural water can further impede the removal efficiency of geosmin and MIB by consuming the oxidant. Therefore, two natural waters were characterized, and their properties are given in **Table 7.3**. Water A was a raw water source and Water B was a treated water source, which were collected from two different natural water sources in the South Carolina region. Although they were raw and treated water, they have similar specific UV_{254} absorbance at the same DOC level, and their inorganic content was similar.

The DOM fractions of the two waters were characterized with an EEM fluorescence. As shown in **Figure 7.10**, although these two waters had the same DOC value and similar UV_{254} absorbance, their fractions differed. Also, detailed EEM results of two waters are shown in **Table D1**. The fluorescence intensity of each region and their percentages were given to identify the main characteristics of the organic matter. While Water A had the highest percentage for region 1 (R1), which consists of aromatic protein (i.e., tyrosine), the fulvic acid region (R3) was the dominant fraction in Water B (**Figure 7.11**). The fluorescence response of these two waters after conventional ozone and ozone NBs treatment was monitored. As shown in **Figure 7.12**, conventional ozone and ozone NBs effectively broke down the organic matter in the five specific regions. The residual organic matter compositions showed similar trends for both treatments (**Figure 7.13**). Both conventional ozone and ozone NBs effectively broke down the NOM fractions with 75-90% and 75-83% efficiency, respectively, However, the removal of humic acid-like region

was less than other components in NOM with removal percentages of 62-65% for both conventional ozone and ozone NBs, which is likely due to the complex, dispersed, and heterogeneous structure of humic acid (Xie et al., 2023). The slower degradation of humic acid than fulvic acid compounds has been observed in previous oxidation studies (Rajca and Bodzek, 2013; Xie et al., 2023).

Table 7.3. The characteristics of natural waters which were used for experiments.

Parameters	**Unit**	**Water A**	**Water B**
pH	-	7.3±0.3	
Dissolved Organic Carbon (DOC)	mg/L	2.3±0.1	
UV_{254}	cm^{-}	0.040	0.041
Bromide	µg/L	21	27
Chloride	mg/L	7.7	4.2
Nitrite	mg/L	0.01	
Sulfate	mg/L	3.03	19
Turbidity	NTU	< 1	
Alkalinity	mg/L as $CaCO_3$	20	25

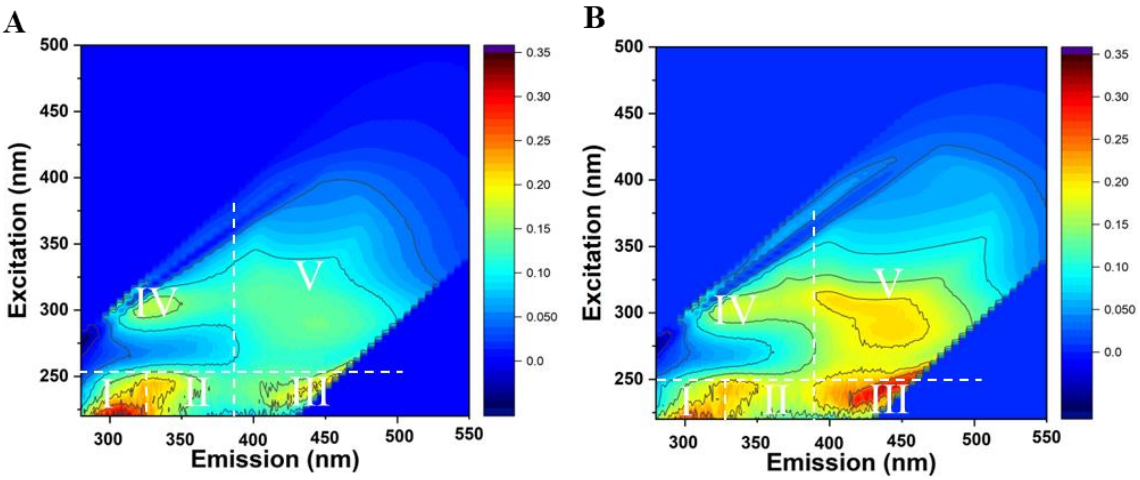

Figure 7.10. EEM of two natural waters, A) Water A and B) Water B (**I**, aromatic protein I; **II**, aromatic protein II; **III**, fulvic acid-like substances; **IV**, soluble microbial by-product-like substances; **V**, humic acid-like substances)

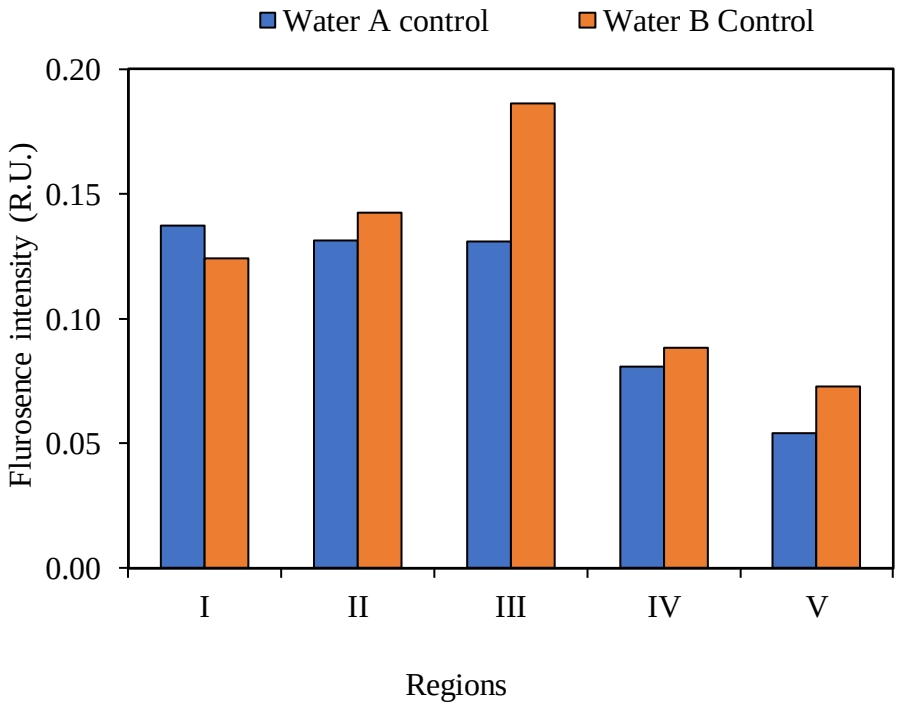

Figure 7.11. Comparison of organic matter fractions of two waters.

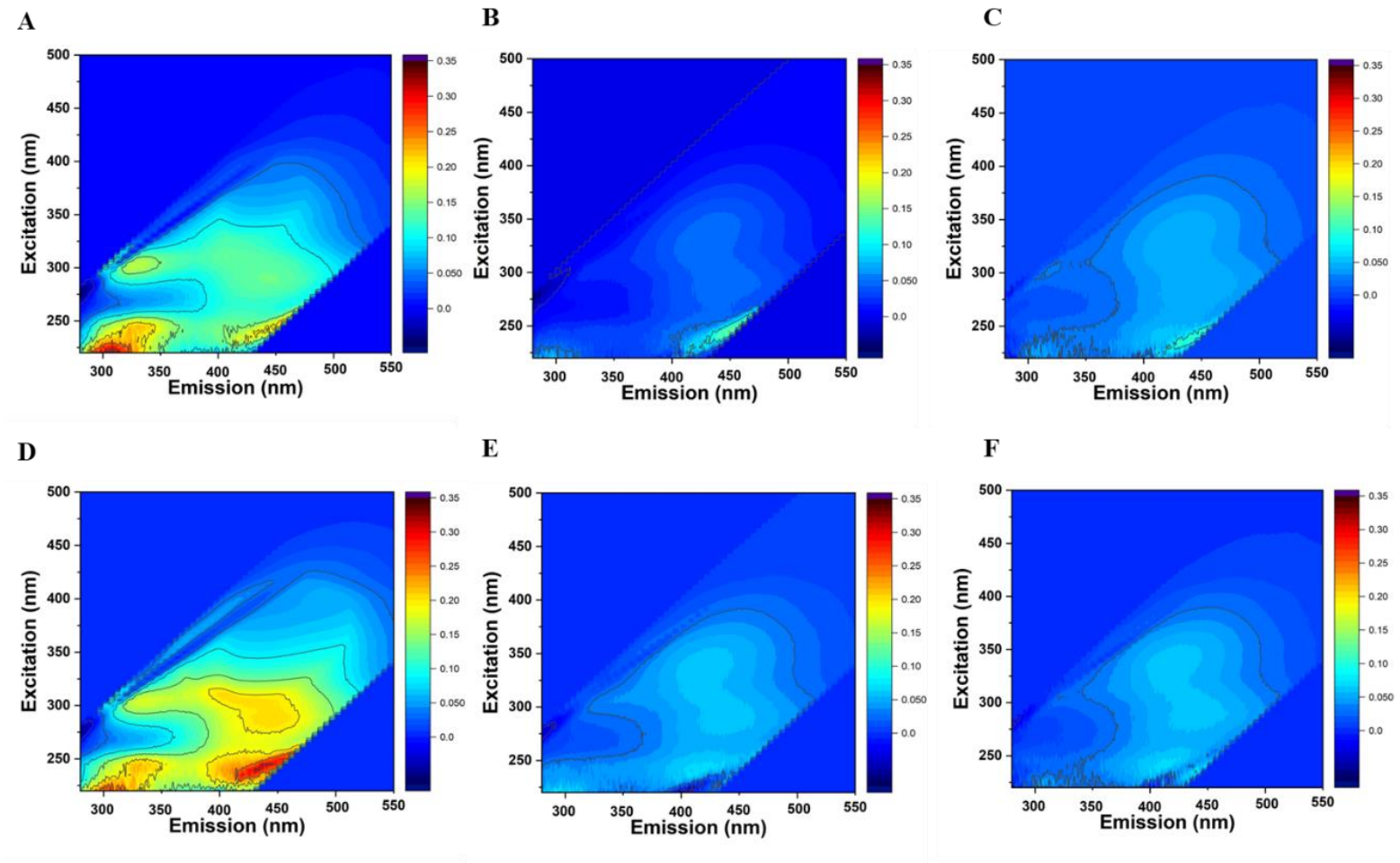

Figure 7.12. EEM of two natural waters, (A-C) Water A and (D-F) Water B for control, conventional ozone and ozone NBs solutions, respectively.

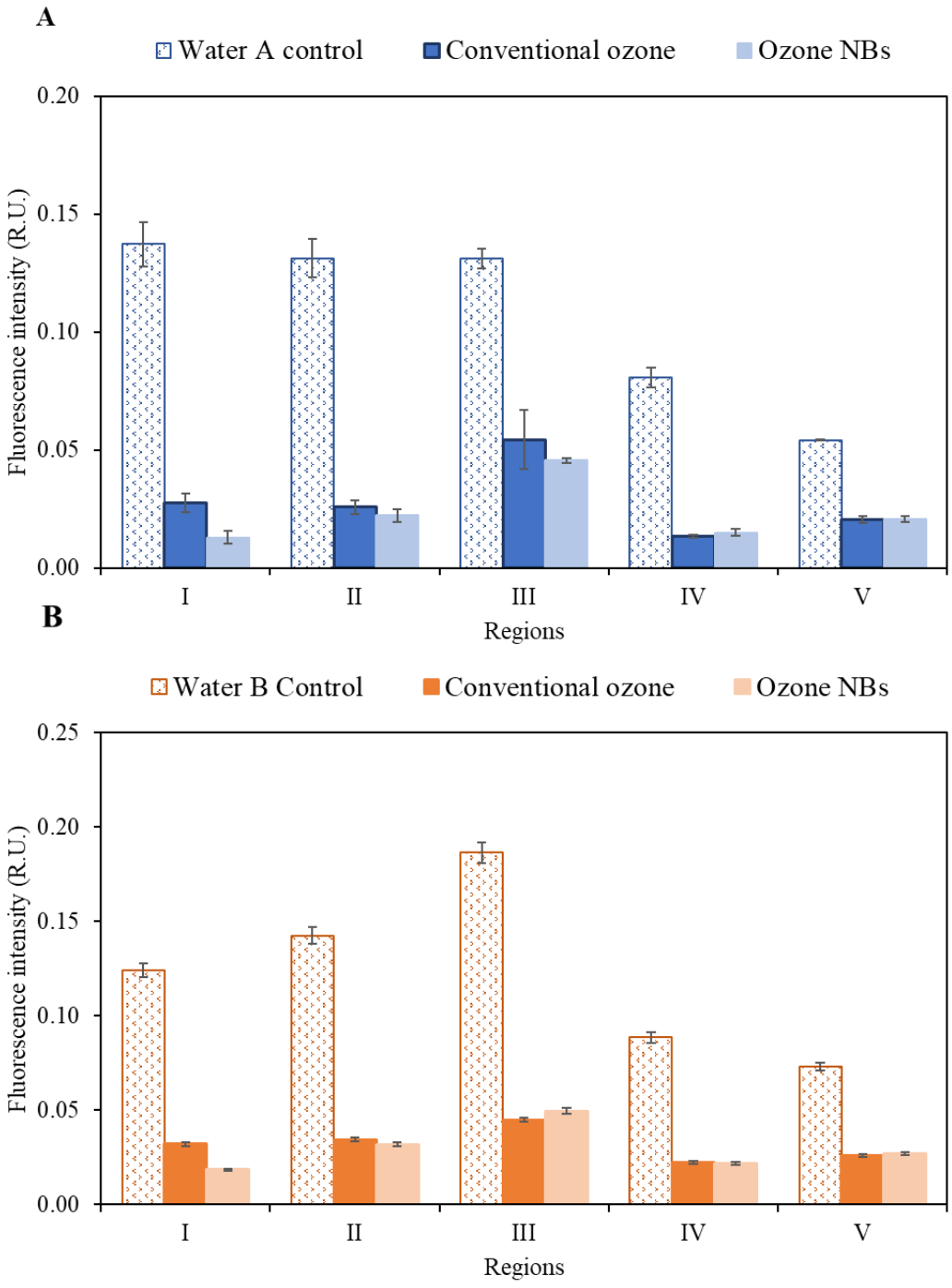

Figure 7.13. The change of EEM spectra of two natural waters, A) Water A and B) Water B for control, conventional ozone and ozone NBs solutions, respectively.

There was no significant difference ($p > 0.05$) in geosmin and MIB removal between water A and water B for either conventional ozone or ozone NBs with an initial dissolved ozone level of 1.0 mg/L at pH 7.3±0.3 and 30±1.0°C (**Figure 7.14**). Ozone NBs showed higher removal performance than conventional ozonation for both waters under the same experimental conditions. The difference in DOM characteristics did not have a significant impact on ozone decomposition and target compound removal. While up to 87% geosmin was removed by ozone NBs in 10 minutes for Water A, it increased to 91% for Water B. A similar trend was observed for conventional ozonation with increasing removal from 75 to 80%. The same trend was also observed for MIB for both conventional ozone and ozone NBs. These results showed that the difference in background chloride, carbonate, sulfate, and aromatic regions in the two waters did not make a statistically significant difference ($p > 0.05$) in geosmin and MIB removal. The lack of an observed difference is likely because the level of DOC, $SUVA_{254}$ and background alkalinity were similar in these two waters. Water B was used for further experiments to test the effect of different parameters on the treatment performance.

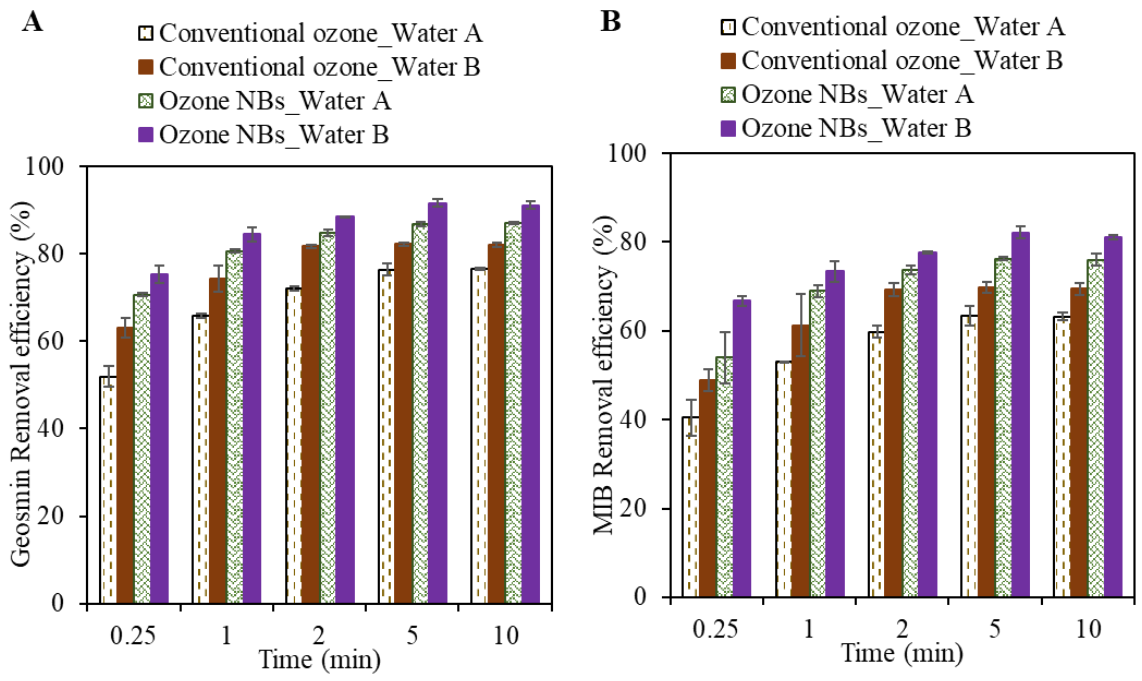

Figure 7.14. The effect of natural waters' aromatic fractions on A) geosmin and B) MIB removal by conventional ozone and ozone NBs in natural water. $[O_3]_0$= 1.0 mg/L, [DOC]= 2.3 mg/L, $[geosmin]_0$=1000±5.0 ng/L, $[MIB]_0$=1000±5.0 ng/L, $[NBs]_0$ = 1.0 x 10^8 particles/mL, pH 7.3±0.3, T: 30±1.0 °C. Error bars represent standard deviations (n=2).

7.3.6. The effect of ozone dose on geosmin and MIB removal in natural water

The ozone dose is one of the most important parameters for removing target compounds by ozonation (von Gunten, 2003a; Westerhoff et al., 2006). To investigate the removal of geosmin and MIB under limited oxidant conditions, the initial ozone dose was set to 0.5 mg/L to compare to previous experiments with 1.0 mg/L dissolved ozone level for conventional ozone and ozone NBs. Dissolved ozone concentration was not detected at a 2-minute reaction time for conventional ozone and 5 minutes for ozone NBs (**Figure 7.15**). Decreasing the ozone dose (i.e., 0.22 mg O_3/mg DOC) significantly ($p<0.05$)

reduced the removal efficiency of geosmin and MIB. While up to 80% geosmin and 69% MIB removal were observed for conventional ozonation with 1.0 mg/L initial ozone dose, removal were decreased to 40-46% for both compounds (**Figure 7.16**). On the other hand, there were still 10-20% more geosmin (i.e., 64%) and MIB (i.e., 51%) removal with ozone NBs than conventional ozonation. At 1.0 mg/L ozone in the solution, the difference between geosmin removal by conventional ozone and ozone NBs was around 10%. However, under the limited oxidant conditions, ozone NBs showed their advantages over conventional ozone more clearly. The observed results can be attributed to the impact of surface interaction on NBs. In the condition where the dissolved ozone level was reduced by half, the ozone NBs level remained similar as at 1.0 mg/L dissolved ozone condition (i.e., $1.0 * 10^8$ particles/mL). The result suggested that the additional removal capacity provided by NBs was maintained at different ozone levels. As a result, while the decreasing ozone concentration had a drastic impact on the removal efficiency by conventional ozone, the ozone NBs continued to perform well and exhibited higher removal efficiency than conventional ozone.

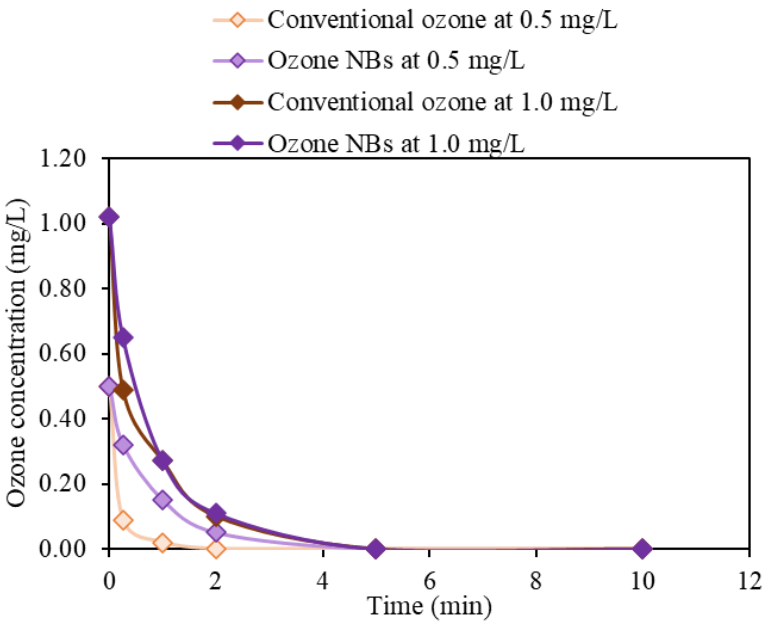

Figure 7.15. The effect of ozone dose, 0.5 and 1.0 mg/L, on ozone decomposition by conventional ozone and ozone NBs in natural water. [DOC]= 2.3 mg/L, $[NBs]_0 = 1.0 \times 10^8$ particles/mL, pH 7.3±0.3, T: 30±1.0 °C.

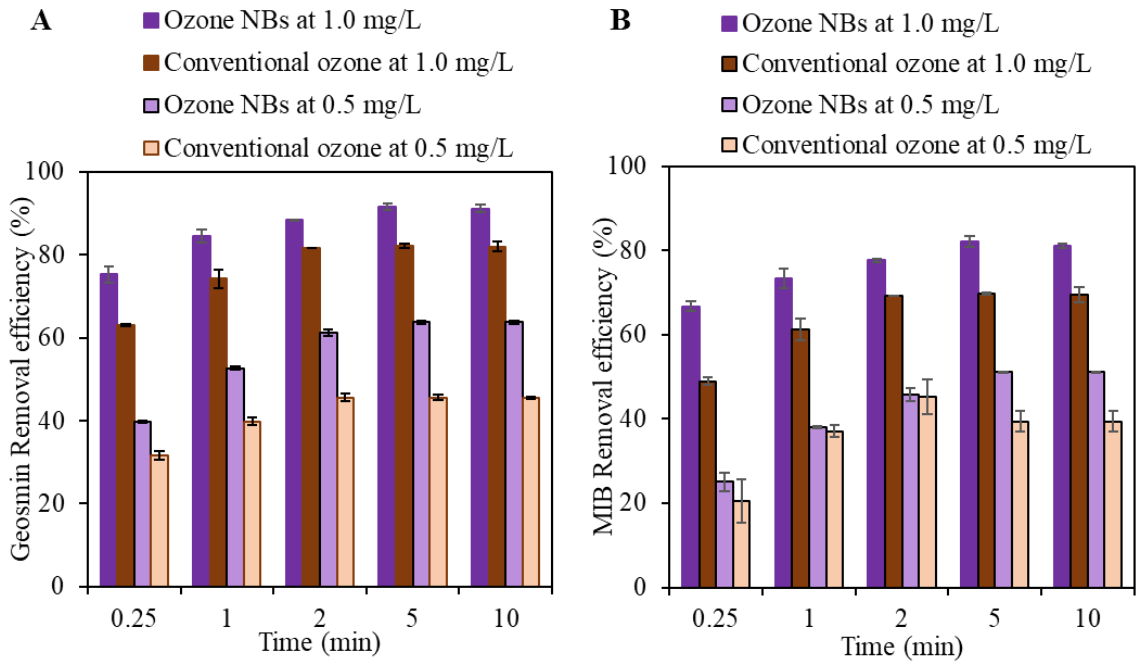

Figure 7.16. The effect of ozone dose on A) geosmin and B) MIB removal by conventional ozone and ozone NBs in natural water. [DOC]= 2.3 mg/L, $[geosmin]_0$=1000±5.0 ng/L, $[MIB]_0$=1000±5.0 ng/L, $[NBs]_0$ = 1.0 x 10^8 particles/mL, pH 7.3±0.3, T: 30±1.0 °C. Error bars represent standard deviations (n=2&4).

7.3.7. The effect of alkalinity on the removal of geosmin and MIB in natural water

Ozone stability is significantly impacted by alkalinity. Both bicarbonate (HCO_3^-) and carbonate (CO_3^{2-}) in water can act as inhibitors of the ozone decomposition cycle by scavenging •OH radicals to form oxidation products (Elovitz and von Gunten, 1999; Grebel et al., 2010; Ho et al., 2004; Liao et al., 2001; Westerhoff et al., 2006). To investigate the effect of alkalinity on ozone stability, further experiments were conducted with 2.5 mM carbonate (as 250 mg/L $CaCO_3$ alkalinity) spiked in natural water (Water B) at a dissolved ozone concentration of 1.0 mg/L. The addition of alkalinity slowed the ozone

decomposition profile with 0.05-0.20 mg/L more dissolved ozone than under the regular condition (raw water with no additional alkalinity) during the 10-min reaction time (**Figure 7.17**).

Adding 250 mg/L $CaCO_3$ alkalinity to natural water decreased the removal of geosmin and MIB by both conventional ozone and ozone NBs. The removal efficiency of geosmin by conventional ozone decreased from 82% to 71% (**Figure 7.18**A). The effect was less on ozone NBs with 84% of geosmin removal (i.e., 6-7% decrease), and there was still a significant difference between ozone NBs and conventional ozonation. Alkalinity had the greatest impact on the first sampling points at 0.25 minutes for all tested conditions. While there was 17-24% more removal in under the regular condition (before the addition of alkalinity) than 250 mg/L $CaCO_3$ alkalinity condition at 0.25 min, the gap was decreased to 8-12 % at 10-minutes reaction. The initial reaction of alkalinity with ozone slowed down the reaction, but further ozone concentration levels in the solution enhanced the removal performances.

A similar trend was also observed for MIB removal, but the effect of alkalinity on MIB removal was greater than geosmin. The overall removal in the 10-minute contact time was decreased from 69 and 81% to 56 and 71% for conventional ozone and ozone NBs, respectively (**Figure 7.18**B). In a previous study, geosmin and MIB removal was decreased with increasing alkalinity from 0 to 200 mg/L as $CaCO_3$ during conventional ozonation (Ho et al., 2004). With a 120 ng/L initial geosmin concentration, while less than 10 ng/L geosmin was detected in water at 2 mg/L ozone (DOC= 2 mg/L), the removal percentage decreased and the residual geosmin was 30 ng/L at 200 mg/L alkalinity (Ho et al., 2004).

The effect of alkalinity in water had more impact on the MIB removal, as the residual MIB level was increased from 5-10 ng/L to 40 ng/L for the initial 94 ng/L MIB levels (Ho et al., 2004). In another study, increasing alkalinity from 0 to 2.5 mM decreased the •OH-exposure [it was indirectly determined by monitoring the decrease of an ozone-resistant probe compound, ρ-chlorobenzoic acid] by 50% at 1 mg/L dissolved ozone with 1.3±0.08 mg/L DOC level at pH 7.82±0.1 (Elovitz et al., 2000). Based on these findings, the overall trends that I observed were similar to previous studies for conventional ozonation. However, ozone NBs showed better performance than conventional ozonation under all tested conditions.

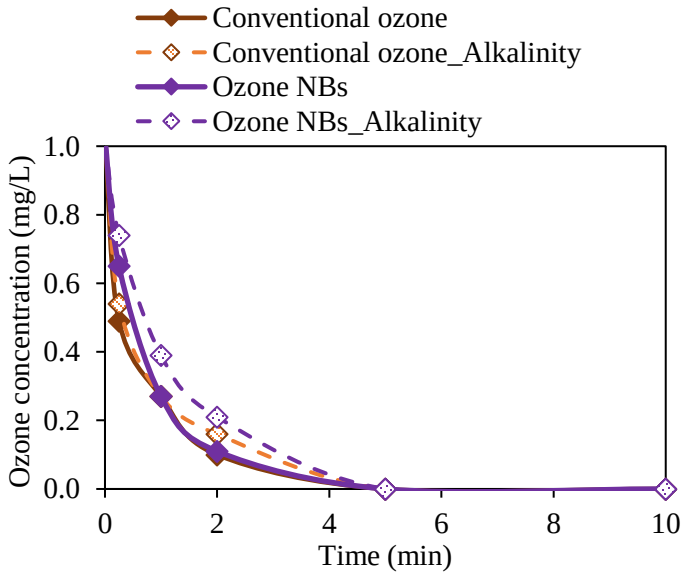

Figure 7.17. The effect of alkalinity at 2.5 mM carbonate (as 250 mg/L $CaCO_3$ alkalinity) on ozone concentration in conventional ozone and ozone NBs in natural water. [DOC]= 2.3 mg/L, $[geosmin]_0$=1000±5.0 ng/L, $[MIB]_0$=1000±5.0 ng/L, $[NBs]_0$ = 1.0 x 10^8 particles/mL, pH 7.3±0.3, T: 30±1.0 °C.

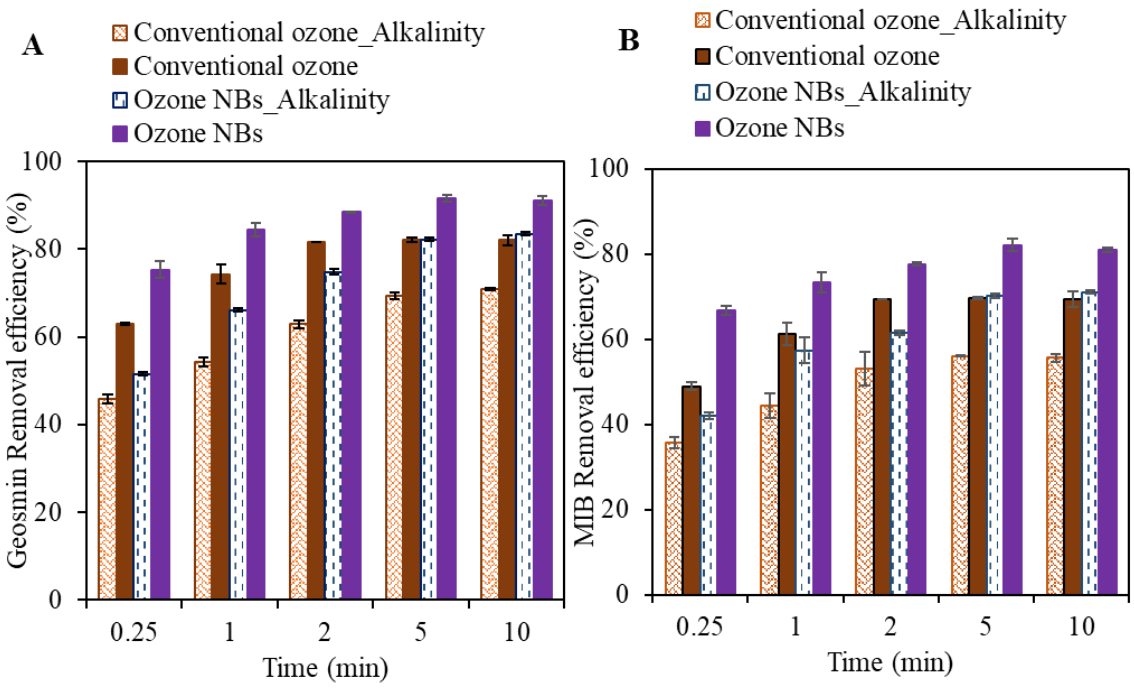

Figure 7.18. The effect of alkalinity at 2.5 mM carbonate (as 250 mg/L $CaCO_3$ alkalinity) on A) geosmin and B) MIB removal by conventional ozone and ozone NBs in natural water. [DOC]= 2.3 mg/L, $[geosmin]_0$=1000±5.0 ng/L, $[MIB]_0$=1000±5.0 ng/L, $[NBs]_0$ = 1.0 x 10^8 particles/mL, pH 7.3±0.3, T: 30±1.0 °C. Error bars represent standard deviations (n=4).

7.3.8. The effect of hardness on the removal of geosmin and MIB in natural water by ozone NBs

Calcium was found to be the most significant parameter affecting the stability of ozone NBs (**Figure 6.11** in Chapter 6). Therefore, its effect on the geosmin and MIB removal was also tested in natural water with the addition of 3.0 mM $CaCl_2$ (as 300 mg/L $CaCO_3$ hardness) (**Figure 7.19**). Calcium decreased the concentration of ozone NBs from 1.10 x 10^8 particles/mL to 4.05 x 10^7 particles/mL. The addition of $CaCl_2$ also introduced 6.0 mM Cl^- to the solution. Chloride is known to be an initiator of ozone decomposition,

which can lead to a shorter ozone lifetime in the solution, which was shown in the previous chapter with the initial high ozone dose (12.5 mg/L ozone) decomposition profile (**Table 6.13**) (Devi et al., 2013; Hoigné and Bader, 1976; Liao et al., 2001; Razumovskii et al., 2010). Since Ca^{2+} facilitates the disappearance of NBs and Cl^- serves as a promoter for ozone decomposition, their combined effect on geosmin and MIB removal was investigated. Although Cl^- can react with •OH radicals and consume them, the reverse reaction happens very quickly. Therefore, unless at pH 3, the quenching of •OH by Cl^- is typically insignificant (von Gunten, 2003b). **Figure 7.19** showed that there was no significant effect of both Ca^{2+} and Cl^- on the removal of geosmin and MIB by ozone NBs ($p>0.05$). There were only 1-3% removal differences for geosmin and MIB within the 10 minutes of reaction time. Therefore, it can be concluded that the high hardness levels had no direct impact on the removal performance of the target compounds.

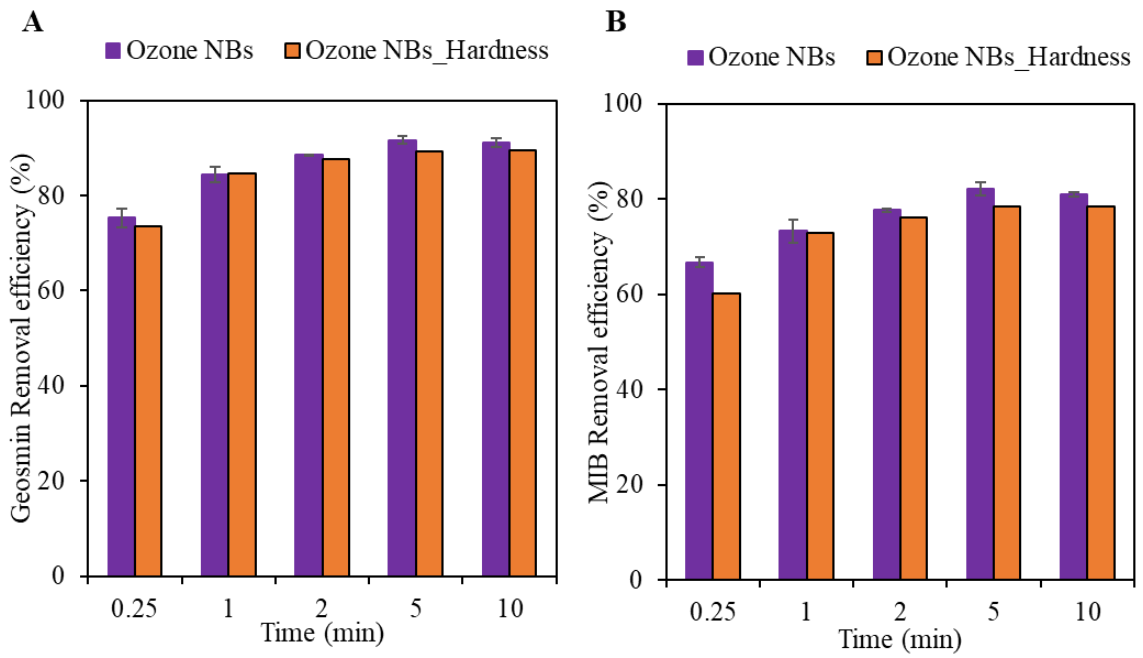

Figure 7.19. The effect of hardness at 3.0 mM calcium (as 300 mg/L $CaCO_3$ hardness) on A) geosmin and B) MIB removal by ozone NBs in natural water. [DOC]= 2.3 mg/L, $[geosmin]_0$=1000±5.0 ng/L, $[MIB]_0$=1000±5.0 ng/L, $[NBs]_0$ = 1.0 x 10^8 particles/mL, pH 7.3±0.3, T: 30±1.0 °C. Error bars represent standard deviations (n=2&4).

7.3.9. Bromate formation with conventional ozone and ozone NBs

The formation of bromate in ozone application is a concern for water treatment plants. Therefore, the effect of ozone NBs on bromate formation was tested in ambient condition and by adding additional 250 µg/L of bromide to natural waters, A and B at 1.0 mg/L dissolved ozone (i.e., 0.43 mg ozone/mg DOC). Both waters had less than 30 µg/L of bromide (**Table 7.3**), and the bromate formation was below the detection limit (5.0 µg/L). When the initial bromide level was increased, the bromate formation for each natural water was 8.5±1.0 µg/L, which was less than the USEPA regulation limit (10 µg/L) (Sohn et al., 2006; USEPA, 2010; von Gunten, 2003b; Westerhoff et al., 2006). Since the ozone

NBs solution contained more •OH radicals, their further impact on bromate formation was considered (von Gunten, 2003a). However, the presence of organic matter in the background and its further reaction with ozone and •OH radicals controlled the main reaction mechanisms in these experiments, and it was also shown in the previous studies (Jahan et al., 2021; von Gunten, 2003a). Therefore, the formation of bromate with conventional ozone and ozone NBs with two different natural waters can be attributed to the dissolved ozone level in this study.

$$[BrO_3]=1.6 \times 10^{-6}[DOC]^{-1.3}[Br]^{0.73}[O_{3,0}]^{1.57}[pH]^{5.8}[t]^{0.28} \qquad \text{Equation 7.1.}$$

In addition, Westerhoff et al. (2006) developed a model to predict bromate formation in natural water (Equation 7.1.). The model included critical parameters such as DOC, bromide, initial ozone dose, pH, and contact time. DOC in mg/L, bromide in µg/L, ozone dose ($O_{3,0}$) mg/L, time (t) in minutes. However, the temperature in the model was kept constant at 20 °C. When the parameters from the experiments in my study were plugged into the model equation, the predicted bromate formation was 6.0 µg/L. The difference of 2-3 µg/L can be attributed to the difference in temperature (i.e., 30 °C) and organic matter composition. The model predicts that increasing the ozone dose, bromide concentration, pH, or contact time can increase the formation of bromate for both conventional ozone and ozone NBs. Therefore, it is important to monitor these parameters continuously during the ozone application for water treatment.

7.4. Conclusions

The removal of geosmin and MIB by conventional ozone and ozone NBs was investigated under various conditions in DDI and natural waters at 1.0 mg/L dissolved ozone. Oxidative degradation of geosmin and MIB by •OH radicals was the main mechanism for both conventional ozonation and ozone NBs. While more than 80% of geosmin and 73% of MIB were removed by ozone NBs in a 10-min contact time in DDI at 20 ºC, only 69% of geosmin and 54% of MIB were removed by conventional ozonation. Higher •OH radical formation from ozone NBs accounts for these removal differences. The removal differences between conventional ozone and ozone NBs were also observed in natural waters.

The removal efficacy of geosmin and MIB for both treatments improved as the temperature increased in DDI and natural waters from 20 to 30 ºC. At 20 ^{o}C, ozone NBs formed 1.5 times more •OH radicals compared to conventional ozone, but the ratio increased to 1.8 at 30 ^{o}C. Higher reductions of geosmin and MIB were achieved at 30 °C by using ozone NBs and conventional ozone. After 10 minutes of contact time, ozone NBs removed an additional 15% of geosmin and 14% of MIB at 30°C. While temperature increased the reaction rate of geosmin and MIB removal by conventional ozonation, it resulted in only an additional 5-6% reduction for both compounds. Additionally, ozone NBs and conventional ozonation removed 10% more geosmin and MIB from natural water at 30°C than at 20°C.

As the initial ozone dose was decreased from 1.0 to 0.5 mg/L dissolved ozone, the removal of geosmin and MIB by conventional ozonation decreased from 82% for geosmin and 69% for MIB to 45 and 39%, respectively. However, ozone NBs removed 10-20% more geosmin and MIB than conventional ozone. The benefits of NBs over traditional ozone became more apparent when the ozone dose was reduced, which was because the number of NBs in the water remained constant, even when the ozone dose was reduced. As a result, the additional removal provided by NBs remained the same although the ozone level decreased.

The removal of geosmin and MIB was not significantly affected by the different aromatic fractions in natural waters. Both conventional ozone and ozone NBs effectively removed geosmin and MIB in two natural waters, and the reduction of aromatic regions intensity in organic matter was observed for both treatments by EEM measurement. The addition of calcium (300 mg/L as $CaCO_3$) affected the NBs concentration but did not decrease the geosmin and MIB removal by ozone NBs. The addition of alkalinity (250 mg/L as $CaCO_3$) decreased the removal efficiencies of geosmin and MIB, but the impact on ozone NBs performance was less than conventional ozonation. More geosmin removal was observed than MIB under all tested conditions. Additionally, the formation of bromate with a bromide level of 250 µg/L was less than the established regulatory limit by the USEPA (i.e., 10 µg/L) for both conventional ozone and ozone NBs.

Overall, in both DDI and natural waters, ozone NBs outperformed conventional ozonation. Ozone NBs can be more efficient than conventional ozonation at controlling taste and odor problems during water treatment. NBs can be used to treat water with a

lower ozone dose, which can reduce the cost and the energy requirement of the treatment process.

CHAPTER 8

CONCLUSIONS AND RECOMMENDATIONS

The study investigated the characteristics and stability of nanobubbles and their efficiency and mechanisms of removing geosmin and MIB from natural waters. The results of this study provided several important to the fundamental understanding of the new technology for various applications. The important conclusions from different portions of the study and the overall recommendations are summarized as follows.

Stability of oxygen nanobubbles under freshwater conditions

The concentration of oxygen NBs in the solution was $1x10^8$ particles/mL, with a surface charge of -24 mV at pH 6.5 in DDI. The majority of NBs had a diameter of less than 200 nm. Calcium was the most influential parameter, significantly decreasing the NBs levels among the other tested parameters pH, NOM, Na^+, and temperature during 60 days of storage period. Therefore, oxygen NBs would be less stable in hard than soft waters. Oxygen NBs were stable for 3 days independent of pH, but as storage time extended, they disappeared more quickly at acidic than at basic pH values. The presence of increasing H^+ ions in solution decreased the stability of the negatively charged oxygen NBs at longer storage times. The formation of •OH radicals by oxygen NBs was very low, with concentrations reaching up to 9 nM at pH 6.5 and up to 28 nM at pH 3. High $SUVA_{254}$ NOM destabilized oxygen NBs more than low $SUVA_{254}$ NOM. While the effect of temperature was insignificant for a short storage time (14 days), the impact of higher

temperature became more noticeable at longer storage times. The findings showed that coalescence (increase in bubble size and rise) was the most significant mechanism for the loss of NBs from freshwaters at high hardness levels, while NBs collapse also played a role in the disappearance of oxygen NBs from water at pH 3.

Removal of geosmin and MIB by oxygen nanobubbles during water treatment

The performance of oxygen NBs for the removal of geosmin and MIB from water was systematically evaluated under a variety of operational and water chemistry conditions. The major removal mechanism for geosmin (40%) and MIB (20%) was volatilization. Mixing NBs with microbubbles (MBs) stimulated the formation of •OH radicals, resulting in additional removal of geosmin (~55%) and MIB (30%). The result demonstrates the impact of MBs with NBs, as there was no evidence of geosmin/MIB oxidation by oxygen NBs alone. Singlet oxygen and superoxide radicals did not appear to play a significant role.

Alkalinity decreased the removal percentages of both geosmin and MIB by scavenging •OH radicals and inhibiting the oxidative removal pathway. The removal percentages of geosmin and MIB increased at higher temperatures due to increased volatilization and oxidative processes. However, the removal percentages decreased in the presence of either NOM or hardness, while they were not significantly affected by pH in the range of 3-10. Geosmin was more readily removed by oxygen NBs than MIB through both oxidation and volatilization. In natural waters, the oxidation mechanism for the

removal of geosmin/MIB was significantly suppressed by alkalinity, hardness, NOM, and other components that may act as radical scavengers.

Characteristics and stability of ozone nanobubbles in freshwater conditions

Ozone NBs were significantly more stable than oxygen NBs, exhibiting a four-fold longer half-life (193 days vs. 46 days, respectively, at pH 6.5-7.0 and 20°C), with a similar initial NBs concentration in solution (1.0-1.1×10^8 particles/mL). The difference in surface charge between the two types of NBs appeared to play a major role in this behavior. Ozone NBs had a more negative zeta potential (−32.0 mV) than oxygen NBs (−23.6 mV) at time zero, which makes them less likely to coalesce. Ozone NBs were generated under two different dissolved ozone concentration conditions (i.e., 1 and 12.5 mg/L, respectively), and the characteristics and stability of NBs were significantly different, although their initial concentrations of NBs were very similar. Ozone NBs generated at 12.5 mg/L dissolved ozone were more stable than those at 1 mg/L during long-term storage. The magnitude of the surface charge of ozone NBs solutions generated at 12.5 mg/L dissolved ozone decreased more slowly than that at 1.0 mg/L dissolved ozone. Therefore, the preparation conditions of ozone NBs can significantly impact their stability and characteristics.

The half-lives of ozone NBs decreased in the following the order: 3 mM Ca^{2+} < pH 3 < high $SUVA_{254}$ NOM (4.1 L/mg.m) < pH 7 < pH 9. The effects of carbonate (or alkalinity) and temperature on the stability of ozone NBs were negligible. Therefore, ozone NBs would be stable in waters for up to several months (i.e., 255 days), depending on the

water hardness (i.e., 300 mg/L as $CaCO_3$) and hydrophobicity (or aromaticity) of NOM (i.e., 4.1 L/mg·m). Also, the half-life of dissolved ozone in the solutions in ozone NBs was 1.1 - 2.3 longer than conventional ozonation under the same experimental conditions. In addition, the formation of •OH radicals and yield of •OH radicals at the same ozone dose were greater with ozone NBs than conventional ozone. Although there was no residual ozone in the solution, ozone NBs continued their reactivity and further oxidation capability with additional •OH radical formation during the storage time (i.e., 1-2 weeks).

Removal of geosmin and MIB by ozone nanobubbles

The application of ozone NBs for ozone delivery significantly improved the mass transfer (2.2-4.2 mg/L.min and 0.07-0.22 mg/L.min for ozone NBs and conventional ozone during 10 min, respectively) and half-life of ozone (i.e., more than 2 times) in water. Ozone NBs were more effective than conventional ozonation at removing geosmin and MIB, two compounds that can cause earthy or musty odors in water. In deionized water (DDI), ozone NBs removed more than 80% of geosmin and 73% of MIB in 10 minutes, while conventional ozonation only removed 69% of geosmin and 54% of MIB. The higher removal efficiency of ozone NBs is due to the formation of more •OH radicals, which is a non-selective strong oxidant. The removal efficiency of geosmin and MIB improved for both treatments as the temperature increased from 20°C to 30°C, in both DDI and natural waters. At 30°C, ozone NBs removed 91-95 % of geosmin and 79-81% of MIB in DDI and natural water after 10 minutes of contact time, while conventional ozonation only removed 80-82% of geosmin and 60-69% of MIB.

Ozone NBs also showed 10-20% more geosmin and MIB removal compared to conventional ozone when the initial dissolved ozone dose was decreased from 1.0 ((O_3/DOC) = 0.43) to 0.5 mg/L ((O_3/DOC) = 0.22) in natural waters. Since the number of ozone NBs were similar (i.e., $1.0x10^8$ particles/mL) at 0.5 and 1.0 mg/L ozone experiments, the additional removal capacity provided by NBs was maintained at various ozone concentrations. Consequently, ozone NBs are more efficient and can perform better than conventional ozonation to control taste and odor issues during water treatment, especially when the amount of available oxidant is reduced. The differences in the composition of NOM between the two natural waters did not significantly ($p>0.05$) affect the decomposition of ozone or the removal of geosmin and MIB by either ozone NBs or conventional ozonation. These can be attributed to the similar water background compositions such as DOC and $SUVA_{254}$ values of the two waters (i.e., DOC = 2.3±0.1 mg/L and UV_{254}= 0.040-0.041 cm^{-1}), as these were two of the most important parameters that influenced the reaction of ozone and •OH radicals with NOM. In addition to the removal of geosmin and MIB, ozone NBs were more effective than conventional ozone at degrading different fractions of NOM. On the other hand, the presence of alkalinity (250 mg/L as $CaCO_3$) reduced the removal efficiencies of geosmin and MIB due to the scavenging effect of alkalinity, but its impact on removal by ozone NBs (decreased from 91% and 81% to 84% and 71%, respectively) was less than observed for conventional ozonation (decreased from 82% and 69% to 71% and 56%, respectively). However, the addition of calcium (300 mg/L as $CaCO_3$) did not appear to reduce the effectiveness of NBs at removing geosmin and MIB, even though it affected the NBs concentration. The

result suggests that calcium may interfere with the formation or stability of NBs, but it does not affect their ability to oxidize geosmin and MIB. More geosmin removal was observed than MIB under all tested conditions. Additionally, the formation of bromate with an initial 250 µg/L bromide level was compared for ozone NBs and conventional ozone in natural water. The formation was less than the established regulatory limit by USEPA (i.e., 10 µg/L) for both ozone NBs and conventional ozone.

Overall, ozone NBs performed better than conventional ozonation in DDI and natural waters. The longer retention time of dissolved ozone in ozone NBs solution is a significant advantage over conventional ozonation for water treatment purposes. Ozone NBs solution provides higher oxidation capability while requiring a lower ozone dose to achieve the same target compound removal. Thus, ozone NBs can be used effectively to control taste and odor issues during water treatment.

Recommendations for Practical Applications and Future Research

The terms "MNBs" and "NBs" are often used interchangeably in the literature, even though they refer to different types of bubbles. Additionally, some studies start with MNBs but end up with only MBs. It is important to distinguish between NBs and MBs, as they have different physicochemical and chemical properties. For example, ozone NBs persist in water for longer periods of time and have prolonged oxidation efficiency for the remediation of both organic and inorganic contaminants compared to MBs.

More details in the description of NBs generation (method used, gas flowrate, pressure, etc.) along with more comprehensive characterization of NBs (e.g., concentration, size distribution, surface charge), the presence of MBs vs. NBs should be provided in publications to allow a better comparison of findings from different studies. Studies should be conducted with freshwater and wastewater samples, not only in DDI water, and the relevancy of observations and findings should be linked to representative practical applications.

New, sensitive, NB-selective, and accurate techniques and methods are required to measure NBs in natural waters where background particulate materials are ubiquitous. Currently, the ability to measure NBs in natural waters is limited, and NBs applications rely on indirect parameters such as dissolved ozone or dissolved oxygen concentrations. New measurement methods are critical to directly monitor the concentrations and fate of NBs, as well as the production and performance of NBs generators, in real time and in-situ.

The effectiveness of ozone NBs should be evaluated for removing a wider range of organic contaminants from water including emerging contaminants and deactivating microbial pathogens. The formation and quantification of ROS, superoxide ($O_2^{\bullet -}$), •OH radicals, hydrogen peroxide (H_2O_2), singlet oxygen ($^1O_2$), especially •OH radicals, should be investigated under a variety of conditions. The impact of ozone NBs on other water treatment processes should be further understood. For example, the impact of ozone NBs on filters, biofilters, GAC adsorbers, AOPs and/or other disinfection processes should be investigated. Oxygen NBs can be a good source of oxygen for the bottom of lakes to mitigate anoxic conditions, or to degrade compounds that are susceptible to aerobic degradation. NBs production from other gases (e.g., H_2, CO_2) should be evaluated for different environmental applications.

Although NBs technologies can make a positive impact on water treatment, more research is needed on the impact and fate of NBs in natural waters, through water treatment processes and distribution systems before they can be widely adopted. Since NBs are stable and can remain in natural waters for a long time, there is a possibility that they could pass through treatment processes and enter distribution systems. However, given their negative surface charge, they can be removed through conventional water treatment processes such as coagulation, flocculation, and sedimentation when NB technology is applied at the source waters and/or beginning of the treatment plant.

More research is needed to assess the compatibility of ozone NBs with other water treatment processes. There is a great need to demonstrate NBs at pilot-scale and full-scale applications for water treatment. Well documented and characterized studies are missing

in literature. Such research will help to demonstrate the feasibility of using NBs at a large scale and to identify any potential challenges and the long-term environmental impact of NBs for water treatment. Life cycle assessment of NBs applications should be performed.

NBs have the potential to be a valuable novel technology for water treatment. With more research addressing the recommendations listed above and others, the development and commercialization of NBs can be accelerated for water treatment, which will help to improve the quality and safety of our drinking water.

APPENDICES

Appendix A: Supporting information for Chapter 2

Table A1. Ozone NBs literature review

References	Title	Tested in	Target contaminant	Bubble generator	Bubble analyzer	Bubble size (nm)	NBs concentration (particles/mL)	Zeta potential (mV)	Stability of ozone NBs (days)	•OH radical
(Agarwal et al., 2011)	Principle and applications of microbubble and nanobubble technology for water treatment	NA	NA	Decompression, gas–water circulation, venturi-type and ultrasonication	Laser diffraction particle size analyzer and scanning electron microscopy (SEM)	NA	NA	NA	NA	NA
(Nishimura et al., 2014)	Nanoscale smooth interface maintained metallisation of polyimide using low concentration ozone micro–nano bubbles dispersed in water	Water	Surface modification of Polyimide	A microcracked ceramic filter	NA	NA	NA	NA	NA	NA
(Kawara et al., 2014)	The Influences of pepsin concentrations and pH levels on the disinfective activity of ozone nanobubble water against *Helicobacter pylori*	Distilled water	*Helicobacter pylori* bacterium	Bubble from" REO Research Institute, Higashi Matsushima, Japan"	NA	NA	NA	NA	NA	NA

References	Title	Tested in	Target contaminant	Bubble generator	Bubble analyzer	Bubble size (nm)	NBs concentration (particles/mL)	Zeta potential (mV)	Stability of ozone NBs (days)	•OH radical
(He et al., 2015)	Research on the feasibility of spraying micro/nano bubble ozonated water for airborne disease prevention	NA	*Alternaria solani Sorauer* and *Cladosporium fulvum* (tomato airborne disease)	Micro/nano bubble generator (Benzhou Technology Co. Ltd., Beijing, China)	NA	NA	NA	NA	NA	NA
(Xia and Hu, 2015)	Remediation of organics contaminated groundwater by ozone micro-nano bubble	Deionized (DI) water & surface water & groundwater	Methyl orange	Spiral liquid flow type combined with pressurized dissolution type	NA	NA	NA	NA	NA	NA
(Meegoda and Batagoda, 2016)	A new technology to decontaminate sediments using ultrasound with ozone nano bubbles	Soil/Sediment	Polycyclic aromatic hydrocarbon (PAH) contaminated sediment	NA	NA	NA	NA	NA	NA	NA
(Ushida et al., 2017)	Antimicrobial effectiveness of ultra-fine ozone-rich bubble mixtures for fresh vegetables using an alternating flow	DDI water	Chinese cabbage wash	UFB generator (Nano-Aqua MN-20, TECH Corporation Co. Ltd., Japan) **&** FB generator (OM1-C200, Aura Tech Co. Ltd., Japan)	NanoSight LM1-HS, Japan Quantum Design Co. Ltd., Japan **&** A microscope (VH-8000, Keyence Co. Ltd., Japan) for FBs	UFBs: 110 **&** FBs: 20 - 80 x 10^3	NA	NA	NA	NA

References	Title	Tested in	Target contaminant	Bubble generator	Bubble analyzer	Bubble size (nm)	NBs concentration (particles/mL)	Zeta potential (mV)	Stability of ozone NBs (days)	•OH radical
(Meegoda et al., 2017)	Briefing: In situ decontamination of sediments using ozone nanobubbles and ultrasound	Sediment	Contaminated river sediments	NA	NA	NA	NA	NA	NA	NA
(Tekile et al., 2017)	applications of ozone micro- and nanobubble technologies in water and wastewater treatment: review	Water and wastewater		NA	NA	NA	NA	NA	NA	NA
(Sung et al., 2017)	Dissolution enhancement and mathematical modeling of removal of residual trichloroethene in sands by ozonation during flushing with micro-nanobubble solution	Soil with Non-aqueous-phase-liquid (NAPL).	Trichloroethene (TCE)	MNBs generator from AS-MA II, Riverforest Inc., USA	Dynamic Light Scattering (Delsa™ Nano C, Beckman Coulter Inc., USA)	< 50, and 60 - 150	NA	NA	NA	NA
(Cruz and Flores, 2017)	Reduction of coliforms presents in domestic residual waters by air-ozone micro-nanobubbles in Carhuaz city, Peru.	Domestic wastewater	Total and fecal coliform	MNBs generator patented by Dr. Eng. Jhonny Valverde Flores	Optic microscope	$7x10^3$	NA	NA	NA	NA
(Menendez and Flores, 2017)	Reduction of hospital wastewater through micro-nano ozone-air bubbles	Hospital wastewater	Organic matter	NA	A trinocular microscope MOD BM-120T-LED	24	NA	NA	NA	NA

References	Title	Tested in	Target contaminant	Bubble generator	Bubble analyzer	Bubble size (nm)	NBs concentration (particles/mL)	Zeta potential (mV)	Stability of ozone NBs (days)	•OH radical
(Salguero and Flores, 2017)	Reduction of the biochemical oxygen demand of the water samples from the lower basin of the Chillon river by means of air-ozone micronanobubbles, Ventanilla - Callao	River water samples	BOD5	MNBs generator patented by Dr. Eng. Jhonny Valverde Flores	NA	24	NA	NA	NA	NA
(Benazir Abate and Flores, 2017)	Reduction of *Thermotolerant Coliforms* present in the sea water by means of micro-nanobubbles of air-ozone of the beach Los Pavos, Lima, Peru	Marine water samples	*Thermotolerant coliforms*	MNBs generator patented by Dr. Eng. Jhonny Valverde Flores	NA	$7x10^3$	NA	NA	NA	NA
(Hu and Xia, 2018)	Application of ozone micro-nano-bubbles to groundwater remediation	DI water& An organics-contaminated site in Niiza, Japan	Methyl orange and TCE	Spiral liquid flow-type MNB generator (Eco-20, Taikohgiken Ltd., Nishi-ku, Kumamoto, Japan).	NanoSight LM-10, (Malvern, UK)	247 ± 9	$4.5 \times 10^7 \pm 1.5 \times 10^6$	(-18) - (-22)	It was just checked for 3 hr, not for longer storage time	NA
(Batagoda et al., 2018)	Nano-ozone bubbles for drinking water treatment	NA	NA	Fluid oscillation or mechanical vibration, venturi, and ceramic diffusers	NA	NA	NA	NA	NA	NA
(Jiang et al., 2018)	Simultaneous desulfurization and denitrification method using O_3 and NO micro-nano bubbles system	NA	Desulfurization and denitrification	Yunnan Xiazhi XZCP-K-0.75	NA	NA	NA	NA	NA	NA

References	Title	Tested in	Target contaminant	Bubble generator	Bubble analyzer	Bubble size (nm)	NBs concentration (particles/mL)	Zeta potential (mV)	Stability of ozone NBs (days)	•OH radical
(Xia and Hu, 2018)	Treatment of Organics Contaminated Wastewater by Ozone Micro-Nano-Bubbles	Wastewater	Methylene blue, COD, Benzene, Chlorobenzene, Nitrobenzene, p(o)-Nitrochlorobenzene	A spiral liquid flow-type micro-nano-bubble generator (ASUPU ASK3, Asupu Co., Ltd., Suntogun, Shizuoka, Japan)	A Nanoparticle Tracking Analyzer (NanoSight LM-10, Malvern, UK).	265	$2.3x10^8$	NA	NA	NA
(Yasui et al., 2019)	Mechanism of OH radical production from ozone bubbles in water after stopping cavitation	Water	NA	NA	NA	NA	NA	NA	NA	NA
(Batagoda et al., 2019)	Remediation of heavy-metal-contaminated sediments in USA using ultrasound and ozone nanobubbles	Soil/Sediment	Polycyclic aromatic hydrocarbons, polychlorinated biphenyl, chromium, nickel (Ni), cadmium (Cd) and mercury (Hg).	Micro–nano-bubble nozzle (model BT-50FR, Riverforest Corporation, USA)	Malvern Zetasizer Nano	100–200	NA	(-24)-(-27)	NA	NA
(Saijai et al., 2019)	sterilization effects of ozone fine (micro/nano) bubble water	Tap water	*Escherichia coli*	RMUTL micro/nanobubble generator (RMUTL-KVM-10)	NA	NA	NA	NA	NA	NA

References	Title	Tested in	Target contaminant	Bubble generator	Bubble analyzer	Bubble size (nm)	NBs concentration (particles/mL)	Zeta potential (mV)	Stability of ozone NBs (days)	•OH radical
(Aluthgun Hewage et al., 2020)	In situ remediation of sediments contaminated with organic pollutants using ultrasound and ozone nanobubbles	*p*-Terphenyl-contaminated sediments	*p*-Terphenyl	MBs-NBs nozzle (Model BT-50FR; Riverforest Corporation)	The Malvern NanoZetasizer with Folded Capillary Zeta Cells (model DTS1070)	100–300	NA	(-14)–(-25)	NA	NA
(Maie et al., 2020)	Removal of 1,4-dioxane in groundwater using ozone nanobubbles	Groundwater	1,4-Dioxane	NBs generator (AzNano10, Anzaikantetsu Inc., Japan)	NA	NA	NA	NA	NA	NA
(Jhunkeaw et al., 2020)	Ozone nanobubble treatment effectively reduced pathogenic Gram positive 1 and negative bacteria in freshwater and safe for tilapia	Tap water and fish cultured water	The Gram-positive bacterium *Streptococcus agalactiae* and Gram-negative bacterium *Aeromonas veronii*	NBs generator (model: aQua+075MO; maker: AquaPro Solutions Pte Ltd, Singapore)	NanoSight NS300 (Malvern Panalytical Ltd) for O_2 and air. *O_3 NBs were not measured due to its oxidation effect on NS300.*	NA	NA	NA	NA	NA
(Kwon et al., 2020)	Remediation of NAPL-contaminated porous media using micro-nano ozone bubbles: Bench-scale experiments	Tap water	n-decane	KET-1, Korea EMB Technology Co., Ltd., Incheon City, Korea	Microscope	$4.9 \pm 3.3\times10^{3}$	2.8×10^{8}	NA	NA	NA

References	Title	Tested in	Target contaminant	Bubble generator	Bubble analyzer	Bubble size (nm)	NBs concentration (particles/mL)	Zeta potential (mV)	Stability of ozone NBs (days)	•OH radical
(Fan et al., 2020)	Solubilization and stabilization for prolonged reactivity of ozone using micro-nano bubbles and ozone-saturated solvent: A promising enhancement for ozonation	DDI	p-chlorophenol	MNBs generator (Xiazhichun, China)	A Multisizer 4e counter (Beckman Coulter, USA)	$3.38 \pm 0.73\times10^{3}$	$2.41 \pm 1.45 \times 10^{5}$	NA	NA	Methanol capturing method
(Fan et al., 2021a)	An integrated approach using ozone nanobubble and cyclodextrin inclusion complexation to enhance the removal of micropollutants	DI water	4-chlorophenol	Pressurized dissolution type NBs generator (Model XZCP-K-0.75, Xiazhichun, China)	A Coulter Multisizer 4e (Beckman Coulter, Brea, USA).	580	2.16×10^{5}	NA	NA	A formaldehyde capturing method
(Hui, 2021)	Assessment of ozone micro-nano bubble technology for freshwater cooling towers in HVAC systems	NA	NA	NA	NA	NA	NA	NA	NA	NA
(Seridou and Kalogerakis, 2021)	Disinfection applications of ozone micro- and nanobubbles	NA	NA	NA	NA	NA	NA	NA	NA	NA

References	Title	Tested in	Target contaminant	Bubble generator	Bubble analyzer	Bubble size (nm)	NBs concentration (particles/mL)	Zeta potential (mV)	Stability of ozone NBs (days)	•OH radical
(Takahashi et al., 2021)	Free-radical generation from bulk nanobubbles in aqueous electrolyte solutions: ESR spin-trap observation of microbubble-treated water	Ultrapure water	NA	MBs generator (A01N; Dan-Takuma Technologies Inc.).	A particle counting spectrometer for liquids (LiQuilaz-E20; Particle Measuring Systems Inc.)	10 and 50×10^3	NA	NA	NA	ESR (JES-X330; JEOL Ltd.) with spin-trap reagent, DMPO
(Linh et al., 2021)	Ozone nanobubble modulates the innate defense system of Nile tilapia (*Oreochromis niloticus*) against *Streptococcus agalactiae*	Chlorine-free water	The bacterial isolate *S. agalactiae* 2803	NBs generator (model: aQua+075MO; maker: AquaPro Solutions Pte Ltd, Singapore)	NA	NA	NA	NA	NA	NA
(Jhunkeaw et al., 2021)	Ozone nanobubble treatment in freshwater effectively reduced pathogenic fish bacteria and is safe for Nile tilapia (*Oreochromis niloticus*)	Tap water and fish cultured water	*Streptococcus agalactiae* or *Aeromonas veronii*	NBs generator (model: aQua+075MO; maker: AquaPro Solutions Pte Ltd, Singapore)	NanoSight NS300 (Malvern Panalytical Ltd) for O_2 and air. *O_3 NBs were not measured due to its high reactivity.*	130	*not ozone*, 2-3 $\times 10^7$	NA	NA	NA

References	Title	Tested in	Target contaminant	Bubble generator	Bubble analyzer	Bubble size (nm)	NBs concentration (particles/mL)	Zeta potential (mV)	Stability of ozone NBs (days)	•OH radical
(Hashimoto et al., 2021)	Reduction of ozone dosage by using ozone in ultrafine bubbles to reduce sludge volume	Activated sludge	Bacteria	A spiral, liquid-flow-type UFB generator (model Buvitas HYK-25, Ligaric Co., Ltd.,Japan)	NS500, Malvern Panalytical Co., Ltd., UK	120	NA	NA	NA	NA
(Aluthgun Hewage et al., 2021)	Remediation of contaminated sediments containing both organic and inorganic chemicals using ultrasound and ozone nanobubbles	Passaic River sediment	p-terphenyl and chromium	The BT-50FR micro-nano-sized nozzle	The Malvern Zetasizer Nano ZS	30 - 300	NA	-22.77	NA	NA
(Kim et al., 2021)	Removal of tetramethylammonium hydroxide (TMAH) in semiconductor wastewater using the nano-ozone H_2O_2 process	Semiconductor wastewater	Tetramethylammonium hydroxide	A custom-made nano-size bubble generator (OHR, Tokyo, Japan)	NanoSight	133 - 144	5.25×10^9	NA	NA	4-CBA
(Temesgen and Han, 2021)	Ultrafine bubbles as an augmenting agent for ozone-based advanced oxidation	DI water	NA	NB generation system	NA	$58x10^3$ and 897 (measured for O_2 NBs since ozone is reactive)	NA	NA	NA	pCBA

References	Title	Tested in	Target contaminant	Bubble generator	Bubble analyzer	Bubble size (nm)	NBs concentration (particles/mL)	Zeta potential (mV)	Stability of ozone NBs (days)	•OH radical
(Sakr et al., 2022)	A critical review of the recent developments in micro–nano bubbles applications for domestic and industrial wastewater treatment	NA	NA	NA	NA	NA	NA	NA	NA	NA
(Zhou et al., 2022)	Degradation mechanism of micro-nanobubble technology for organic pollutants in aqueous solutions	NA	NPnEOs, (nonionic surfactant)	NA	NA	NA	NA	NA	NA	NA
(Nghia et al., 2022)	Effect of nanobubbles (oxygen, ozone) on the Pacific white shrimp (*Penaeus vannamei*), *Vibrio parahaemolyticus* and water quality under lab conditions	Saline water	The gram-negative bacterium *Vibrio parahaemolyticus*	aQua+75MO (AquaPro Solutions, Singapore, Singapore)	NA	168.9 ± 73.8 (not measured, taken from manufacturer website)	$1.04 \times 10^9 \pm 2.6 \times 10^8$ particles/mL (not measured, was taken from manufacturer website)	NA	NA	NA
(Farid et al., 2022)	Hybrid nanobubble-forward osmosis system for aquaculture wastewater treatment and reuse	Ultrapure water	Pharmaceutical Chemicals [Oxytetracycline	aQua+75MO (AquaPro Solutions, Singapore, Singapore)	NanoSight LM-10HS (Salisbury, UK)	145	7.8×10^7	NA	14 days in ultrapure water at pH 7 - 7.5	NA
(Dien et al., 2022)	Impacts of oxygen and ozone nanobubbles on bacteriophage in aquaculture system	Dechlorinated tap water	*Aeromonas hydrophila*-specific phage, pAh6.2TG	NA	NA	NA	NA	NA	NA	NA

References	Title	Tested in	Target contaminant	Bubble generator	Bubble analyzer	Bubble size (nm)	NBs concentration (particles/mL)	Zeta potential (mV)	Stability of ozone NBs (days)	•OH radical
(Zhu et al., 2022)	Interfacial mechanism of the synergy of biochar adsorption and catalytic ozone micro-nano-bubbles for the removal of 2,4-dichlorophenoxyacetic acid in water	DI water	2,4-dichlorophenoxyacetic acid (2,4-D)	MNBs generator (Xingheng Technology Co. Ltd., Shanghai)	Zetasizer Nano ZS (Malvern)	156	NA	NA	NA	EPR
(Epelle et al., 2022)	Microbial inactivation: gaseous or aqueous ozonation?	Water and air	*Escherichia coli* NTCC1290 and *Pseudomonas aeruginosa* NCTC10332, *Staphylococcus aureus* ATCC25923 and *Streptococcus mutans*, and *Candida albicans* and *Aspergillus fumigatus*	An electrolysis oxygen radical generator (EORGTM Novus Clean Tech Ltd)	Malvern Zetasizer Nano ZEN5600	0.8-7000	NA	-10	NA	NA
(Pal et al., 2022)	Nanobubble ozonation for waterbody rejuvenation at different locations in India: A holistic and sustainable approach	Water	Total soluble solids (TSS), biochemical oxygen demand (BOD), and chemical oxygen demand (COD)	ANBG system of Accelerated Cleaning System (The shear force)	NA	<5000	NA	NA	NA	NA

References	Title	Tested in	Target contaminant	Bubble generator	Bubble analyzer	Bubble size (nm)	NBs concentration (particles/mL)	Zeta potential (mV)	Stability of ozone NBs (days)	•OH radical
(Wu et al., 2022)	Nanobubble technology enhanced ozonation process for ammonia removal	Artificial wastewater	Ammonia	NBs generator (KMT, Nikuni Co., Ltd., Kanagawa, Japan)	ZetaView PMX 120 (Particle Metrix, Meerbusch, Germany)	<200	2.2×10^7	NA	NA	NA
(Linh et al., 2022)	Pre-treatment of Nile tilapia (*Oreochromis niloticus*) with ozone nanobubbles improve efficacy of heat-killed *Streptococcus agalactiae* immersion vaccine	Dechlorinated tap water	*Streptococcus agalactiae*	NA	NA	NA	NA	NA	NA	NA
(Maie et al., 2022)	Using oxygen/ozone nanobubbles for in situ oxidation of dissolved hydrogen sulfide at a residential tunnel-construction site	Industrial wastewater and sewage water	Hydrogen sulfide	Anzai Kantetsu Co., Ltd. (Japan)	NanoSight NS300 analyzer (Malvern, UK)	106	1.93×10^9	NA	NA	NA
(Ng et al., 2023)	Assessment of ozone nanobubble technology to reduce freshwater algae	Water from a fishpond with jade perch	A diatom species, *Nitzschia sp*	aQua + 075M, AquaPro Solutions Pte Ltd., Singapore	NA	NA	NA	NA	NA	NA
(Ponce-robles et al., 2023)	Full-scale o_3/micro-nano bubbles system based advanced oxidation as alternative tertiary treatment in WWTP effluents	Wastewater	12 pharmaceuticals	A non-commercial prototype composed of an MNBs bubble injector	NA	NA	NA	NA	NA	NA

References	Title	Tested in	Target contaminant	Bubble generator	Bubble analyzer	Bubble size (nm)	NBs concentration (particles/mL)	Zeta potential (mV)	Stability of ozone NBs (days)	•OH radical
(Wei et al., 2023)	Study on treatment of basic yellow 28 dye wastewater by micro-nano bubble ozone catalytic oxidation	Simulated printing and dyeing wastewater	COD	Aeration disk	NA	20-30 x 10^3	NA	NA	NA	NA
(Yang et al., 2023)	Mechanism for enhancing the ozonation process of micro- and nanobubbles: bubble behavior and interface reaction	DI water	*Escherichia coli*	MNB generator (OM4-MDG-045H, Aura Tec Co., Ltd., Japan)	A nanoparticle tracking video microscope (ZetaView, Particle Metrix, Germany)	151.9	1.56×10^7	-30	NA	Fluorescence Spectrophotometry and EPR
(Huang et al., 2023)	Effect of ozone nanobubbles on the microbial ecology of pond water and safety for jade perch (*Scortum barcoo*)	Pond water	*Heterotrophic bacteria*	aQua+075MO, AquaPro Solutions Pte Ltd., Singapore	NA	NA	NA	NA	NA	NA
(Lee et al., 2023)	Oxidative power loss control in ozonation: nanobubble and ultrasonic cavitation	Water	Rhodamine B	A pressurized dissolution-type NBs generator	Zetasizer nano, Malvern Panalytical, UK	270-520	NA	NA	NA	A fluorescence spectrometer (coumarin)
(Hutagalung et al., 2023)	Combination of ozone-based advanced oxidation process and nanobubbles generation toward textile wastewater recovery	Textile wastewater	Ammonia and TSS	Orifice Plate (Nanobubbles Karya Indonesia)	Zetasizer Pro Blue, Malvern	216.9	NA	−21.08 ± 0.35	NA	NA

References	Title	Tested in	Target contaminant	Bubble generator	Bubble analyzer	Bubble size (nm)	NBs concentration (particles/mL)	Zeta potential (mV)	Stability of ozone NBs (days)	•OH radical
(Xie et al., 2023)	Effect of dissolved organic matter on selective oxidation of toluene by ozone micro-nano bubble water	Tap water	Toluene	HG-WNF-1, Hangzhou Guiguan Company, China	NA	NA	NA	NA	NA	pCBA

NA= Not Available

Appendix B: Supporting information for Chapter 4

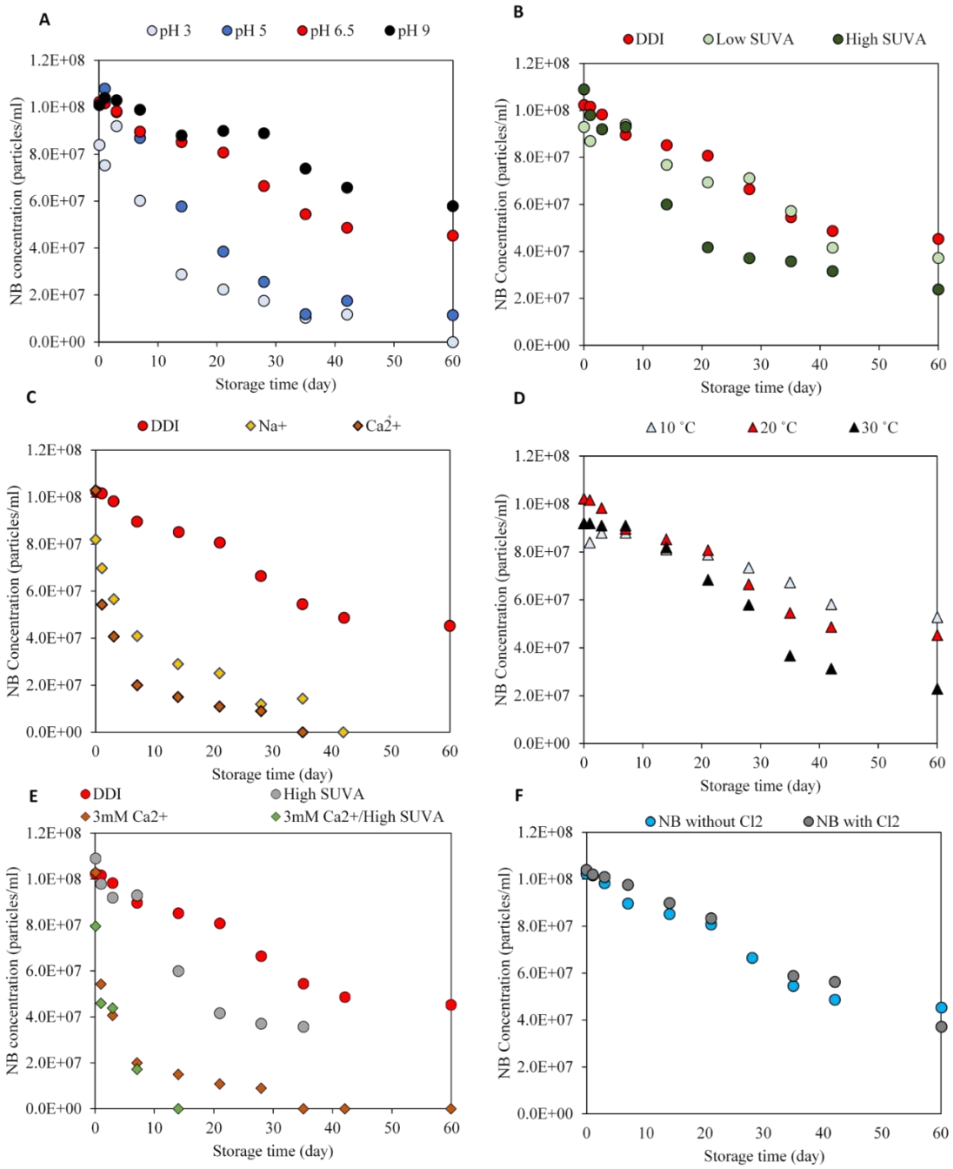

Figure B1. Changes in oxygen NBs concentrations over storage time under various pH (A), NOM (B), cations (C), temperature (D), combined Ca^{2+} (3 mM) with high $SUVA_{254}$ (4.1 L/mg.m at 5 mg/L DOC) NOM (E), and 2 mg/L chlorine (F) conditions in DDI water.

Table B1. Summary of micro- and nanobubble stability in ultrapure or distilled water from the literature

References	NBs Generator	NBs Analyzer	Gas type	Parameters investigated	Storage conditions and period	Findings
Ushikubo et al., 2010	a micro-bubble generator (OM4-GP-040, Aura Tec Co. Ltd., Japan)	a green laser (532 nm laser) Zetasizer Nano ZS particle size analyzer (ZEN3500, Sysmex Co., Japan)	oxygen	bubble-size distribution, DO, zeta potential, and proton spin–lattice relaxation time	not specified for 6 days	NBs were detected using a dynamic light scattering (DLS) on the 6th day after generation
Liu et al., 2013	a micro-bubble generator (OM4-GP-040, Aura Tec Co. Ltd., Japan)	NanoSight-LM10 (Quantum Design Inc., Japan), Zeta Potential Analyzer (Zeecom, Microtech Co. Ltd., Japan)	nitrogen	bubble-size distribution, pH, and DO	not specified for 7 days	the total number of bubbles and size of the main bubbles decreased with storage time, and almost no NBs were observed in day 7.
(Oh and Kim, 2017)	a gas−liquid mixing method with a linear actuator	NanoSight LM10-HSBFT14 with a 405 nm blue laser (Quantum Design Korea, Korea), ζ-potential analyzer (ZetaPALS, Brookhaven Instruments, USA)	carbon dioxide	bubble-size distribution, ATR-FTIR, and zeta potential	4 mL clear glass vials for 24 hr	i) 15% decreased over 24 h (3.5 E8 to 2.9 E8 particles/mL), ii) mean diameter increased from 89 to 110 nm
Hamamoto et al., 2018	a pressurized dissolution NBs generator (FZIN-10-I, IDEC Co., Ltd., Japan)	resonant mass measurement (Archimedes, Malvern Instruments Ltd.), ZetaCAD (CAD Instruments, France)	oxygen	turbidity, pH, DO, bubble concentration, bubble-size distribution, and ζ potential	airtight 50 mL polypropylene bottles without any headspace at 25 °C for 18 days	i) For NBs at higher pH, significant changes in the bubble-size distributions and concentrations were not observed, even 18 days from the production, ii) NBs in higher pH were more stable in water because the surface charge of the NBs became more negative, iii) There were no significant changes of pH during the stored periods (up to 18 days), but DO decreased to approximately 8 mg/L, suggesting O_2 diffusion from the NBs water through the polypropylene bottles.

References	NBs Generator	NBs Analyzer	Gas type	Parameters investigated	Storage conditions and period	Findings
Meegoda et al., 2018	a hydrodynamic cavitation generator with BT-50FR micro- and nano-sized nozzle	Malvern Zetasizer Nano ZS	air, oxygen, nitrogen, and ozone	bubble-size (diameter), pH, temperature, ion concentration, and zeta potential	not specified for 7 days	i) Ozone NBs had highest magnitude negative zeta potential value followed by oxygen, air, and nitrogen. ii) Magnitude of negative zeta potential values decreased with increased solution temperatures. There was no significant change in bubble size with temperatures. iii) With increased NaCl concentrations from 0.01 to 1 M, magnitude negative zeta potential value decreased, while the bubble diameter increased from 500 nm to 680 nm. iv) At neutral pH and above, O_2 bubble size remained smaller in the nanosize range for 1 week. However, for a solution pH of 4, bubbles were much bigger in the microsize range at the time of generation and very rapidly increased in size, and after a week.
Nirmalkar et al., 2018	a ultrasonic (US) cavitation generator with a 20 kHz probe-type US processor (AUTOTUNE SERIES 750 W model, Sonics & Materials)	NanoSight LM10 instrument (Malvern Instruments, UK), ZEN5600 Zetasizer Nano ZSP (Malvern Instruments)	no additional gas injected	bubble-size distribution, bubble number density, pH, DO, zeta potential, and the presence of salt (NaCl) and surfactant (SDS)	airtight 20 mL glass vials in a fridge for 6-11 months	i) The high zeta potential in alkaline solutions is evidence of strong electrostatic interaction providing stability to the system and, thus, alkaline solutions are a more favorable medium for the formation and stability of nanobubbles than acidic solutions. ii) Exponential decay in the number of nanobubbles, with approximately 50−70% disappearing in the first 50 days stored at -18°C. Then, the bubble decay slows down considerably and the rest (30-50%) of bubbles was still observed after 170 days in the less concentrated samples and after 330 days in the most concentrated sample. iii) The mean bubble diameter remains constant over time, and zeta potential also remained unchanged over these periods of sample monitoring.

References	NBs Generator	NBs Analyzer	Gas type	Parameters investigated	Storage conditions and period	Findings
Wang et al., 2019	a periodic pressure change device	Zetasizer Nano ZS (Malvern Instrument Ltd. UK)	nitrogen, oxygen, and carbon dioxide	bubble-size distribution and zeta potential	sealed in vial with parafilm and stored at low temperature	i) N2 NBs were stable more than 48 h and the negative zeta potential experienced no significant change over 48 h. ii) The stability of N_2 and O_2 nanobubbles were better than CO_2 nanobubbles in terms of bubble size changes over time.
(Ke et al., 2019)	compression−de compression method (i.e., pressurizing gas into the solution and then slowly depressurizing it)	NS 300 (Malvern, UK)	nitrogen and krypton (kr)	bubble-size distribution	not specified	The concentration of bulk NBs in alkaline is much higher than in other solutions (neutral and acidic or with NaCl).
Michailidi et al., 2020	a hydrodynamic cavitation generator	Malvern Zetasizer Nano ZS	air and oxygen	bubble-size distribution, pH, NaCl, zeta potential and Electron paramagnetic resonance (EPR)	not specified for 3 months	The mechanism of bulk NBs' generation and their extremely long-time stability can be attributed mainly to the hydrogen bonding interactions. The formation of a diffusion layer, by absorption of OH^- due to electrostatic interaction, contributing to negative surface charge, whereas the interaction of ions with the surface hydroxylic groups provide the equilibrium between the protonation and deprotonation of water and finally the formation of a stable interface layer.
Wang et al., 2020	a nanobubbles generator (Zhongnong Tianlu micro-nano bubble water technology Co. Ltd, China)	NS 500 (Malvern Instrument Ltd. UK), Zetasizer Nano ZS (Malvern Instrument Ltd. UK)	oxygen	bubble-size distribution, pH, and zeta potential	500 mL glass photoreactor	i) O_2 NBs concentrations remained constant for 4 h. ii) The nanobubbles concentration increased from 0.76 to 3.78×10^8 particles/mL with increasing pH value from 3.2 to 11.0, while the mean size decreased from 205 nm to 138 nm as the pH value increased. iii) Higher zeta potential (negative) showed higher stability of oxygen NBs at higher pH.

References	NBs Generator	NBs Analyzer	Gas type	Parameters investigated	Storage conditions and period	Findings
Hewage et al., 2021	a hydrodynamic cavitation generator with BT-50FR micro- and nano-sized nozzle	Malvern Zetasizer Nano ZS	not specified (maybe no gas injected)	bubble-size (diameter), pH, DO, ion concentration (NaCl, Na_2SO_4, Na_3PO_4, $CaCl_2$, and $FeCl_3$), and zeta potential	not specified for 7 days	All the samples were stable for 1 week with no significant deviation in either bubble size or zeta potential values. The variation of size and zeta potential among six samples can be attributed to the solution properties and was mainly dependent on solution pH and the cation valency.

Appendix C: Supporting information for Chapter 5

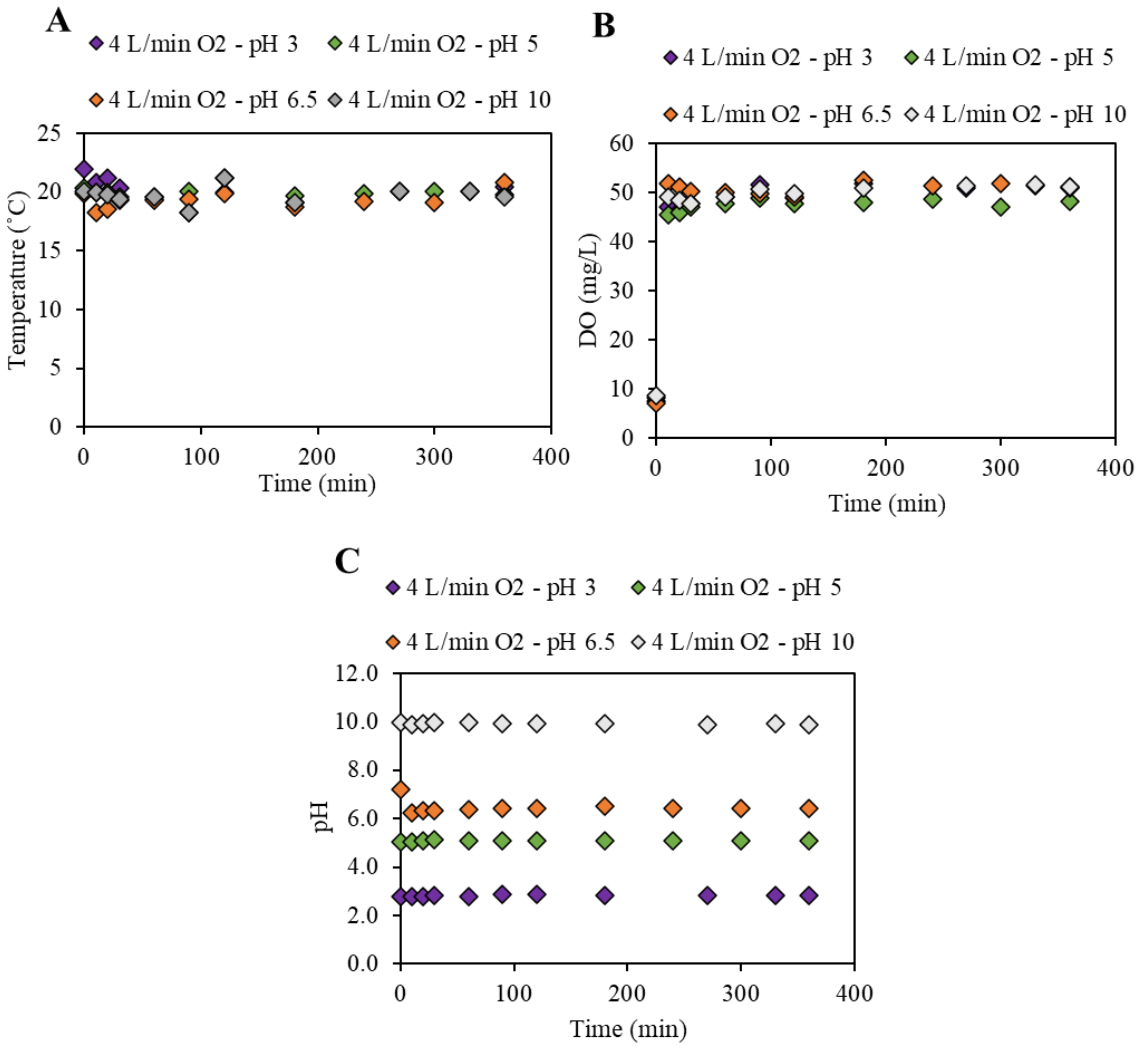

Figure C1. Changes of temperature (A), DO (B), and pH (C) during 6 h of NBs application of oxygen, air and nitrogen NBs at 4 L/min of gas flowrates.

Table C1. Geosmin and MIB disappearance rate constants (k in s-1) and half-lives (in h) under various experimental conditions in DDI water for the initial 6 h of the oxygen NBs application.

Parameter	Experimental condition	Geosmin		MIB	
		k (s^{-1})	Half-life (h)	k (s^{-1})	Half-life (h)
Gas type	4 L/min N_2	2.00E-05	9.63	1.06E-05	18.16
	4 L/min O_2	4.17E-05	4.6	1.83E-05	10.5
	4 L/min Air	2.83E-05	6.8	1.83E-05	10.5
Gas flowrate	1 L/min O_2	3.00E-05	6.4	1.67E-05	11.6
	4 L/min O_2	4.17E-05	4.6	1.83E-05	10.5
	8 L/min O_2	4.17E-05	4.6	2.17E-05	8.9
pH	4 L/min O_2 at pH 3	4.67E-05	4.1	Not available	
	4 L/min O_2 at pH 5	3.67E-05	5.3	1.83E-05	10.5
	4 L/min O_2 at pH 6.5 (control)	4.17E-05	4.6	1.83E-05	10.5
	4 L/min O_2 at pH 10	4.50E-05	4.3	2.00E-05	9.6
Alkalinity	4 L/min O_2 (control)	4.17E-05	4.6	1.83E-05	10.5
	4 L/min O_2 at 15 mg/L alkalinity	3.00E-05	6.4	1.17E-05	16.5
	4 L/min O_2 at 50 mg/L alkalinity	3.00E-05	6.4	1.17E-05	16.5
	4 L/min O_2 at 250 mg/L alkalinity	3.17E-05	6.1	1.50E-05	12.8
Hardness	4 L/min O_2 (control)	4.17E-05	4.6	1.83E-05	10.5
	4 L/min O_2 at 300 mg/L as $CaCO_3$	3.33E-05	5.8	1.83E-05	10.5
Temperature	4 L/min O_2 at 20 °C (control)	4.17E-05	4.6	1.83E-05	10.5
	4 L/min O_2 at 30 °C	7.33E-05	2.6	5.17E-05	3.7

Appendix D: Supporting information for Chapter 7

Table D1. Detailed EEM data with the intensity of each region for two waters.

Water A					
	Aromatic Protein	Aromatic Protein	Fulvic acid-like	Soluble microbial byproduct-like	Humic acid-like
	R1	R2	R3	R4	R5
Total Sum of Intensity	77.0	72.2	106.7	91.9	327.8
Total number of cell	561	550	814	1138	6052
Intensity / Cell number *	0.14	0.13	0.13	0.08	0.05
% *	25.7	24.6	24.5	15.1	10.1
Water B					
	Aromatic Protein	Aromatic Protein	Fulvic acid-like	Soluble microbial byproduct-like	Humic acid-like
	R1	R2	R3	R4	R5
Total Sum of Intensity	69.6	78.3	151.6	100.6	441.2
Total number of cell	561	550	814	1138	6052
Intensity / Cell number *	0.12	0.14	0.19	0.09	0.07
% *	20.2	23.2	30.3	14.4	11.9

REFERENCES

5310 Total Organic Carbon, n.d. , in: Standard Methods For the Examination of Water and Wastewater. https://doi.org/10.2105/SMWW.2882.104

5910 UV-Absorbing Organic Constituents, n.d. , in: Standard Methods For the Examination of Water and Wastewater. https://doi.org/10.2105/SMWW.2882.113

Achar, J.C., Nam, G., Jung, J., Klammler, H., Mohamed, M.M., 2020. Microbubble ozonation of the antioxidant butylated hydroxytoluene: Degradation kinetics and toxicity reduction. Environ. Res. 186, 109496. https://doi.org/10.1016/j.envres.2020.109496

Agarwal, A., Ng, W.J., Liu, Y., 2011. Principle and applications of microbubble and nanobubble technology for water treatment. Chemosphere 84, 1175–1180. https://doi.org/10.1016/j.chemosphere.2011.05.054

Agus, E., Lim, M.H., Zhang, L., Sedlak, D.L., 2011. Odorous compounds in municipal wastewater effluent and potable water reuse systems. Environ. Sci. Technol. 45, 9347–9355. https://doi.org/10.1021/es202594z

Ahmed, A.K.A., Shi, X., Hua, L., Manzueta, L., Qing, W., Marhaba, T., Zhang, W., 2018a. Influences of air, oxygen, nitrogen, and carbon dioxide nanobubbles on seed germination and plant growth. J. Agric. Food Chem. 66, 5117–5124. https://doi.org/10.1021/acs.jafc.8b00333

Ahmed, A.K.A., Sun, C., Hua, L., Zhang, Z., Zhang, Y., Marhaba, T., Zhang, W., 2018b. Colloidal properties of air, oxygen, and nitrogen nanobubbles in water: Effects of Ionic strength, natural organic matters, and surfactants. Environ. Eng. Sci. 35, 720–727. https://doi.org/10.1089/ees.2017.0377

Alheshibri, M., Qian, J., Jehannin, M., Craig, V.S.J., 2016. A history of nanobubbles. Langmuir 32, 11086–11100. https://doi.org/10.1021/acs.langmuir.6b02489

Aluthgun Hewage, S., Batagoda, J.H., Meegoda, J.N., 2021. Remediation of contaminated sediments containing both organic and inorganic chemicals using ultrasound and ozone nanobubbles. Environ. Pollut. 274, 116538. https://doi.org/10.1016/j.envpol.2021.116538

Aluthgun Hewage, S., Batagoda, J.H., Meegoda, J.N., 2020. In situ remediation of sediments contaminated with organic pollutants using ultrasound and ozone nanobubbles. Environ. Eng. Sci. 37, 521–534. https://doi.org/10.1089/ees.2019.0497

American Public Health Association, American Water Works Association, W.E.F., 2023. 4500-H+ pH, in: Lipps WC, Braun-Howland EB, B. TE (Ed.), Standard Methods For the Examination of Water and Wastewater. Washington DC: APHA Press. https://doi.org/10.2105/SMWW.2882.082

Antonopoulou, M., Evgenidou, E., Lambropoulou, D., Konstantinou, I., 2014. A review on advanced oxidation processes for the removal of taste and odor compounds from aqueous media. Water Res. 53, 215–234. https://doi.org/10.1016/j.watres.2014.01.028

Appiani, E., Ossola, R., Latch, D.E., Erickson, P.R., McNeill, K., 2017. Aqueous singlet oxygen reaction kinetics of furfuryl alcohol: Effect of temperature, pH, and salt content. Environ. Sci. Process. Impacts 19, 507–516. https://doi.org/10.1039/c6em00646a

Atkinson, A.J., Apul, O.G., Schneider, O., Garcia-Segura, S., Westerhof, P., 2019. Nanobubble technologies offer opportunities to improve water treatment. Acc. Chem. Res. 52, 1196–1205. https://doi.org/10.1021/acs.accounts.8b00606

Attard, P., 2014. The stability of nanobubbles. Eur. Phys. J. Spec. Top. 223, 893–914. https://doi.org/10.1140/epjst/e2013-01817-0

Batagoda, J.H., Hewage, S.D.A., Meegoda, J.N., 2019. Remediation of heavy-metal-contaminated sediments in USA using ultrasound and ozone nanobubbles. J. Environ. Eng. Sci. 14, 130–138. https://doi.org/10.1680/jenes.18.00012

Batagoda, J.H., Hewage, S.D.A., Meegoda, J.N., 2018. Nano-ozone bubbles for drinking water treatment. J. Environ. Eng. Sci. 14, 57–66. https://doi.org/10.1680/jenes.18.00015

Benazir Abate, T., Flores, J.V., 2017. Reduction of thermotolerant coliforms present in the sea water by means of micro-nanobubbles of air-ozone of the beach los pavos, Lima, Peru. Chem. Eng. Trans. 60, 313–318. https://doi.org/10.3303/CET1760053

Beniwal, D., Taylor-Edmonds, L., Armour, J., Andrews, R.C., 2018. Ozone/peroxide advanced oxidation in combination with biofiltration for taste and odour control and organics removal. Chemosphere 212, 272–281. https://doi.org/10.1016/j.chemosphere.2018.08.015

Black, A.P., Birkner, F.B., Morgan, J.J., 1965. Destabilization of dilute clay suspensions with labeled polymers. J. AWWA 57, 1547–1560. https://doi.org/https://doi.org/10.1002/j.1551-8833.1965.tb01542.x

Botana, L.M., 2016. Toxicological Perspective on Climate Change: Aquatic Toxins. Chem. Res. Toxicol. 29, 619–625. https://doi.org/10.1021/acs.chemrestox.6b00020

Bouaifi, M., Roustan, M., 1998. Bubble size and mass transfer coefficients in dual-impeller agitated reactors. Can. J. Chem. Eng. 76, 390–397. https://doi.org/10.1002/cjce.5450760307

Bruchet, A., Duguet, J.P., 2004. Role of oxidants and disinfectants on the removal, masking and generation of tastes and odours. Water Sci. Technol. a J. Int. Assoc. Water Pollut. Res. 49, 297–306.

Bu, X., Alheshibri, M., 2021. The effect of ultrasound on bulk and surface nanobubbles: A review of the current status. Ultrason. Sonochem. 76, 105629. https://doi.org/10.1016/j.ultsonch.2021.105629

Bui, T.T., Nguyen, D.C., Han, M., 2019. Average size and zeta potential of nanobubbles in different reagent solutions. J. Nanoparticle Res. 21. https://doi.org/10.1007/s11051-019-4618-y

Buxton, G. V, Greenstock, C.L., Helman, W.P., Ross, A.B., 1988. Critical review of rate constants for reactions of hydrated electrons, hydrogen atoms and hydroxyl radicals (·OH/·O− in aqueous solution. J. Phys. Chem. Ref. Data 17, 513–886. https://doi.org/10.1063/1.555805

Byler, D.M., Farrell, H.M., 1989. Infrared spectroscopic evidence for calcium ion interaction with carboxylate groups of casein. J. Dairy Sci. 72, 1719–1723. https://doi.org/10.3168/jds.S0022-0302(89)79287-0

Caire-Maurisier, F., Aymes-Chodur, C., Jandard, V., Bourrel, A., Yagoubi, N., 2019. Effects of electron beam sterilization on polyethylene terephthalate: Physico-chemical modifications and formation of non-volatile organic extractables. Ann. Pharm. Fr. 77, 276–285. https://doi.org/10.1016/j.pharma.2019.02.001

Calgaroto, S., Wilberg, K.Q., Rubio, J., 2014. On the nanobubbles interfacial properties and future applications in flotation. Miner. Eng. 60, 33–40. https://doi.org/10.1016/j.mineng.2014.02.002

Chapra, S.C., Boehlert, B., Fant, C., Bierman, V.J., Henderson, J., Mills, D., Mas, D.M.L., Rennels, L., Jantarasami, L., Martinich, J., Strzepek, K.M., Paerl, H.W., 2017. Climate Change impacts on harmful algal blooms in U.S. freshwaters: A screening-level assessment. Environ. Sci. Technol. 51, 8933–8943. https://doi.org/10.1021/acs.est.7b01498

Chen, C., Li, J., Zhang, X., 2020. The existence and stability of bulk nanobubbles: A long-standing dispute on the experimentally observed mesoscopic inhomogeneities in aqueous solutions. Commun. Theor. Phys. 72. https://doi.org/10.1088/1572-9494/ab6183

Chen, M., Peng, L., Qiu, J., Luo, K., Liu, D., Han, P., 2020. Monitoring of an ethanol-water exchange process to produce bulk nanobubbles based on dynamic light scattering. Langmuir 36, 10069–10073. https://doi.org/10.1021/acs.langmuir.0c01170

Chen, S., Dong, B., Gao, K., Li, T., 2019. Pilot study on advanced treatment of geosmin and 2-MIB with O_3/GAC. Water Sci. Technol. Water Supply 19, 1253–1263. https://doi.org/10.2166/ws.2018.184

Chen, W., Westerhoff, P., Leenheer, J.A., Booksh, K., 2003. Fluorescence excitation-emission matrix regional integration to quantify spectra for dissolved organic matter.

Environ. Sci. Technol. 37, 5701–5710. https://doi.org/10.1021/es034354c

Cheng, Z., Zhou, H., Yin, J., Yu, L., 2007. Electron spin resonance estimation of hydroxyl radical scavenging capacity for lipophilic antioxidants. J. Agric. Food Chem. 55, 3325–3333. https://doi.org/10.1021/jf0634808

Chestnutt, T.E., Bach, M.T., Mazyck, D.W., 2007. Improvement of thermal reactivation of activated carbon for the removal of 2-methylisoborneol. Water Res. 41, 79–86. https://doi.org/10.1016/j.watres.2006.09.010

Chu, L.B., Xing, X.H., Yu, A.F., Zhou, Y.N., Sun, X.L., Jurcik, B., 2007. Enhanced ozonation of simulated dyestuff wastewater by microbubbles. Chemosphere 68, 1854–1860. https://doi.org/10.1016/j.chemosphere.2007.03.014

Clercin, N.A., Druschel, G.K., 2019. Influence of Environmental Factors on the Production of MIB and Geosmin Metabolites by Bacteria in a Eutrophic Reservoir. Water Resour. Res. 55, 5413–5430. https://doi.org/10.1029/2018WR023651

Collivignarelli, C., Sorlini, S., 2004. AOPs with ozone and UV radiation in drinking water: Contaminants removal and effects on disinfection byproducts formation. Water Sci. Technol. 49, 51–56. https://doi.org/10.2166/wst.2004.0218

Cook, D., Newcombe, G., Sztajnbok, P., 2001. The application of powdered activated carbon for MIB and geosmin removal: Predicting PAC doses in four raw waters. Water Res. 35, 1325–1333. https://doi.org/10.1016/S0043-1354(00)00363-8

Croué, J.-P., Violleau, D., Bodaire, C., Legube, B., 1999. Removal of hydrophobic and hydrophilic constituents by anion exchange resin. water Sci. Technol. 40, 207–214. https://doi.org/10.2166/wst.1999.0478

Cruz, R., Flores, J.V., 2017. Reduction of coliforms presents in domestic residual waters by air-ozone micro-nanobubbles in Carhuaz city, Peru 1, 59–72.

Cuong, L.C., Nghi, N.H., Dieu, T.V., Oanh, D.T.Y., Vuong, D.D., 2019. Influence of oxygen concentration, feed gas flow rate and air humidity on the output of ozone produced by corona discharge. Vietnam J. Chem. 57, 604–608. https://doi.org/10.1002/vjch.201900095

Devi, L.G., Munikrishnappa, C., Nagaraj, B., Rajashekhar, K.E., 2013. Effect of chloride and sulfate ions on the advanced photo Fenton and modified photo Fenton degradation process of Alizarin Red S. J. Mol. Catal. A Chem. 374–375, 125–131. https://doi.org/10.1016/j.molcata.2013.03.023

Dien, L.T., Linh, N.V., Mai, T.T., Senapin, S., St-Hilaire, S., Rodkhum, C., Dong, H.T., 2022. Impacts of oxygen and ozone nanobubbles on bacteriophage in aquaculture system. Aquaculture 551, 737894. https://doi.org/10.1016/j.aquaculture.2022.737894

Doederer, K., Gale, D., Keller, J., 2019. Effective removal of MIB and geosmin using MBBR for drinking water treatment. Water Res. 149, 440–447.

https://doi.org/10.1016/j.watres.2018.11.034

Donham, J.E., Rosenfeldt, E.J., Wigginton, K.R., 2014. Photometric hydroxyl radical scavenging analysis of standard natural organic matter isolates. Environ. Sci. Process. Impacts 16, 764–769. https://doi.org/10.1039/c3em00663h

Du, Z., Lin, X., 2019. Characteristic research on the generation of ozone using dielectric barrier discharge. IOP Conf. Ser. Earth Environ. Sci. 295. https://doi.org/10.1088/1755-1315/295/4/042079

Duval, E., Adichtchev, S., Sirotkin, S., Mermet, A., 2012. Long-lived submicrometric bubbles in very diluted alkali halide water solutions. Phys. Chem. Chem. Phys. 14, 4125–4132. https://doi.org/10.1039/C2CP22858K

Elovitz, M.S., von Gunten, U., 1999. Hydroxyl radical/ozone ratios during ozonation processes. I. The Rct Concept. Ozone Sci. \& Eng. 21, 239–260. https://doi.org/10.1080/01919519908547239

Elovitz, M.S., von Gunten, U., Kaiser, H.P., 2000. Hydroxyl radical/ozone ratios during ozonation processes. II. The effect of temperature, pH, alkalinity, and DOM properties. Ozone Sci. Eng. 22, 123–150. https://doi.org/10.1080/01919510008547216

Epelle, E.I., Emmerson, A., Nekrasova, M., Macfarlane, A., Cusack, M., Burns, A., Mackay, W., Yaseen, M., 2022. Microbial inactivation: Gaseous or aqueous ozonation? Ind. Eng. Chem. Res. 61, 9600–9610. https://doi.org/10.1021/acs.iecr.2c01551

Eriksson, M., 2005. Ozone chemistry in aqueous solution - ozone decomposition and stabilisation. Royal Institute of Technology.

Ershov, B.G., Morozov, P.A., 2009. The kinetics of ozone decomposition in water, the influence of pH and temperature. Russ. J. Phys. Chem. A 83, 1295–1299. https://doi.org/10.1134/S0036024409080093

Fan, W., An, W. Gang, Huo, M. xin, Yang, W., Zhu, S. yi, Lin, S. shan, 2020. Solubilization and stabilization for prolonged reactivity of ozone using micro-nano bubbles and ozone-saturated solvent: A promising enhancement for ozonation. Sep. Purif. Technol. 238, 116484. https://doi.org/10.1016/j.seppur.2019.116484

Fan, W., An, W., Huo, M., Xiao, D., Lyu, T., Cui, J., 2021a. An integrated approach using ozone nanobubble and cyclodextrin inclusion complexation to enhance the removal of micropollutants. Water Res. 196, 117039. https://doi.org/10.1016/j.watres.2021.117039

Fan, W., Desai, P., Zimmerman, W.B., Duan, Y., Crittenden, J.C., Wang, C., Huo, M., 2021b. Optical density inferences in aqueous solution with embedded micro/nano bubbles: A reminder for the emerging green bubble cleantech. J. Clean. Prod. 294,

126258. https://doi.org/10.1016/j.jclepro.2021.126258

Fang, X., Mark, G., von Sonntag, C., 1996. •OH radical formation by ultrasound in aqueous solutions: Part I: The chemistry underlying the terephthalate dosimeter. Ultrason. Sonochem. 3, 57–63. https://doi.org/10.1016/1350-4177(95)00032-1

Farid, M.U., Choi, P.J., Kharraz, J.A., Lao, J.Y., St-Hilaire, S., Ruan, Y., Lam, P.K.S., An, A.K., 2022. Hybrid nanobubble-forward osmosis system for aquaculture wastewater treatment and reuse. Chem. Eng. J. 435, 135164. https://doi.org/10.1016/j.cej.2022.135164

Favvas, E.P., Kyzas, G.Z., Efthimiadou, E.K., Mitropoulos, A.C., 2021. Bulk nanobubbles, generation methods and potential applications. Curr. Opin. Colloid Interface Sci. 54, 101455. https://doi.org/10.1016/j.cocis.2021.101455

Fischbacher, A., von Sonntag, J., von Sonntag, C., Schmidt, T.C., 2013. The •OH radical yield in the H_2O_2 + O_3 (peroxone) reaction. Environ. Sci. Technol. 47, 9959–9964. https://doi.org/10.1021/es402305r

Fischbacher geb Jarocki, A., 2017. Formation and quantification of •OH in oxidative water treatment. Universität Duisburg-Essen.

Fónagy, O., Szabó-Bárdos, E., Horváth, O., 2021. 1,4-Benzoquinone and 1,4-hydroquinone based determination of electron and superoxide radical formed in heterogeneous photocatalytic systems. J. Photochem. Photobiol. A Chem. 407. https://doi.org/10.1016/j.jphotochem.2020.113057

Fotiou, T., Triantis, T.M., Kaloudis, T., O'Shea, K.E., Dionysiou, D.D., Hiskia, A., 2016. Assessment of the roles of reactive oxygen species in the UV and visible light photocatalytic degradation of cyanotoxins and water taste and odor compounds using C-TiO_2. Water Res. 90, 52–61. https://doi.org/10.1016/j.watres.2015.12.006

Fu, L., Wu, C., Zhou, Y., Zuo, J., Song, G., Tan, Y., 2019. Ozonation reactivity characteristics of dissolved organic matter in secondary petrochemical wastewater by single ozone, ozone/H_2O_2, and ozone/catalyst. Chemosphere 233, 34–43. https://doi.org/10.1016/j.chemosphere.2019.05.207

Ger, K.A., Hansson, L.A., Lürling, M., 2014. Understanding cyanobacteria-zooplankton interactions in a more eutrophic world. Freshw. Biol. 59, 1783–1798. https://doi.org/10.1111/fwb.12393

Glaze, W.H., Schep, R.A., Chauncey, W., Ruth, E.C., Zarnoch, J.J., Aieta, E.M., Tate, C.H., McGuire, M.J., 1990. Evaluating oxidants for the removal of model taste and odor compounds from a municipal water supply. J. Am. Water Work. Assoc. 82, 79–84.

Gonzalez, D.H., Kuang, X.M., Scott, J.A., Rocha, G.O., Paulson, S.E., 2018. Terephthalate probe for hydroxyl radicals: Yield of 2-hydroxyterephthalic acid and transition metal

interference. Anal. Lett. 51, 2488–2497.
https://doi.org/10.1080/00032719.2018.1431246

Grebel, J.E., Pignatello, J.J., Mitch, W.A., 2010. Effect of halide ions and carbonates on organic contaminant degradation by hydroxyl radical-based advanced oxidation processes in saline waters. Environ. Sci. Technol. 44, 6822–6828. https://doi.org/10.1021/es1010225

Greenwald, M.J., Redding, A.M., Cannon, F.S., 2015. A rapid kinetic dye test to predict the adsorption of 2-methylisoborneol onto granular activated carbons and to identify the influence of pore volume distributions. Water Res. 68, 784–792. https://doi.org/10.1016/j.watres.2014.10.022

Guo, Q., Yang, K., Yu, J., Wang, C., Wen, X., Zhang, L., Yang, M., Xia, P., Zhang, D., 2016. Simultaneous removal of multiple odorants from source water suffering from septic and musty odors: Verification in a full-scale water treatment plant with ozonation. Water Res. 100, 1–6. https://doi.org/10.1016/j.watres.2016.05.017

Guo, Z., Wang, X., Wang, H., Hu, B., Lei, Z., Kobayashi, M., Adachi, Y., Shimizu, K., Zhang, Z., 2019. Effects of nanobubble water on the growth of: Lactobacillus acidophilus 1028 and its lactic acid production. RSC Adv. 9, 30760–30767. https://doi.org/10.1039/c9ra05868k

Gurung, A., Dahl, O., Jansson, K., 2016. The fundamental phenomena of nanobubbles and their behavior in wastewater treatment technologies. Geosystem Eng. 19, 133–142. https://doi.org/10.1080/12269328.2016.1153987

Hafuka, A., Nagasato, T., Yamamura, H., 2019. Application of graphene oxide for adsorption removal of geosmin and 2-methylisoborneol in the presence of natural organic matter. Int. J. Environ. Res. Public Health 16, 1–8.
https://doi.org/10.3390/ijerph16111907

Hamamoto, S., Takemura, T., Suzuki, K., Nishimura, T., 2018. Effects of pH on nano-bubble stability and transport in saturated porous media. J. Contam. Hydrol. 208, 61–67. https://doi.org/10.1016/j.jconhyd.2017.12.001

Hansen, H.H.W.B., Cha, H., Ouyang, L., Zhang, J., Jin, B., Stratton, H., Nguyen, N.T., An, H., 2023. Nanobubble technologies: Applications in therapy from molecular to cellular level. Biotechnol. Adv. 63, 108091.
https://doi.org/10.1016/j.biotechadv.2022.108091

Hashimoto, K., Kubota, N., Okuda, T., Nakai, S., Nishijima, W., Motoshige, H., 2021. Reduction of ozone dosage by using ozone in ultrafine bubbles to reduce sludge volume. Chemosphere 274, 129922.
https://doi.org/10.1016/j.chemosphere.2021.129922

Hayakumo, S., Arakawa, S., Takahashi, M., Kondo, K., Mano, Y., Izumi, Y., 2014. Effects of ozone nano-bubble water on periodontopathic bacteria and oral cells - In vitro

studies. Sci. Technol. Adv. Mater. 15. https://doi.org/10.1088/1468-6996/15/5/055003

Hayashi, H., Akamine, S., Ichiki, R., Kanazawa, S., 2016. Comparison of OH radical concentration generated by underwater discharge using two methods. Int. J. Plasma Environ. Sci. Technol. 10, 24–28.

He, H., Zheng, L., Li, Y., Song, W., 2015. Research on the feasibility of spraying micro/nano bubble ozonated water for airborne disease prevention. Ozone Sci. Eng. 37, 78–84. https://doi.org/10.1080/01919512.2014.913473

Hewage, S.A., Kewalramani, J., Meegoda, J.N., 2021. Stability of nanobubbles in different salts solutions. Colloids Surfaces A Physicochem. Eng. Asp. 609, 125669. https://doi.org/10.1016/j.colsurfa.2020.125669

Hirano, K., Kobayashi, T., 2016. Coumarin fluorometry to quantitatively detectable •OH radicals in ultrasound aqueous medium. Ultrason. Sonochem. 30, 18–27. https://doi.org/10.1016/j.ultsonch.2015.11.020

Ho, L., Croué, J.P., Newcombe, G., 2004. The effect of water quality and NOM character on the ozonation of MIB and geosmin. Water Sci. Technol. 49, 249–255. https://doi.org/10.2166/wst.2004.0583

Ho, L., Newcombe, G., Croué, J.P., 2002. Influence of the character of NOM on the ozonation of MIB and geosmin. Water Res. 36, 511–518. https://doi.org/10.1016/S0043-1354(01)00253-6

Hoigné, J., Bader, H., 1983. Rate constants of reactions of ozone with organic and inorganic compounds in water-I. Non-dissociating organic compounds. Water Res. 17, 173–183. https://doi.org/10.1016/0043-1354(83)90098-2

Hoigné, J., Bader, H., 1979. Ozonation of Water: "oxidation-competition values" of different types of waters used in Switzerland. Ozone Sci. \& Eng. 1, 357–372. https://doi.org/10.1080/01919512.1979.10684571

Hoigné, J., Bader, H., 1976. The role of hydroxyl radical reactions in ozonation processes in aqueous solutions. Water Res. 10, 377–386. https://doi.org/10.1016/0043-1354(76)90055-5

Hosokawa, Y., Tanaka, L., Sano, T., Ohnishi, T., Shinozaki, K., Minami, S., Kaneko, M., 2002. ESR detection of •OH radicals generated inside cells by X-ray and evaluation of the cytotoxicity of DMPO. Oral Radiol. 18, 113–117. https://doi.org/10.1007/bf02493251

Hsieh, W.H., Hung, W.N., Wang, G.S., Hsieh, S.T., Lin, T.F., 2012. Effect of pH on the analysis of 2-MIB and geosmin in water. Water. Air. Soil Pollut. 223, 715–721. https://doi.org/10.1007/s11270-011-0896-4

Hu, L., Xia, Z., 2018. Application of ozone micro-nano-bubbles to groundwater

remediation. J. Hazard. Mater. 342, 446–453. https://doi.org/10.1016/j.jhazmat.2017.08.030

Huang, Q., Ng, P.H., Marques, A.R.P., Cheng, T.H., Man, K.Y., Lim, K.Z., MacKinnon, B., Huang, L., Zhang, J., Jahangiri, L., Furtado, W., Hasib, F.M.Y., Zhong, L., Kam, H.Y., Lam, C.T., Liu, H., Yang, Y., Cai, W., Brettell, D., St-Hilaire, S., 2023. Effect of ozone nanobubbles on the microbial ecology of pond water and safety for jade perch (Scortum barcoo). Aquaculture 576, 739866. https://doi.org/10.1016/j.aquaculture.2023.739866

Huddleston, M., Rodgers, J.H., Wardlaw, K., Geer, T., Calomeni, A., Barrington, J., Melton, D., Chastain, J., Bowen, M., Spacil, M., 2016. Adaptive water resource management for taste and odor control for the Anderson Regional Joint Water System. South Carolina Am. Water Work. Assoc. Water Environ. Assoc. South Carolina.

Hui, I.D.S.C.M., 2021. Assessment of ozone micro-nano bubble technology for fresh water cooling towers in HVAC systems 1–18.

Hutagalung, S.S., Rafryanto, A.F., Sun, W., Juliasih, N., Aditia, S., Jiang, J., Arramel, Dipojono, H.K., Suhardi, S.H., Rochman, N.T., Kurniadi, D., 2023. Combination of ozone-based advanced oxidation process and nanobubbles generation toward textile wastewater recovery. Front. Environ. Sci. 11, 1–11. https://doi.org/10.3389/fenvs.2023.1154739

Ishibashi, K.I., Fujishima, A., Watanabe, T., Hashimoto, K., 2000. Detection of active oxidative species in TiO_2 photocatalysis using the fluorescence technique. Electrochem. commun. 2, 207–210. https://doi.org/10.1016/S1388-2481(00)00006-0

Jabesa, A., Ghosh, P., 2016. Removal of diethyl phthalate from water by ozone microbubbles in a pilot plant. J. Environ. Manage. 180, 476–484. https://doi.org/10.1016/j.jenvman.2016.05.072

Jadhav, A.J., Barigou, M., 2020. Bulk nanobubbles or not nanobubbles: That is the question. Langmuir 36, 1699–1708. https://doi.org/10.1021/acs.langmuir.9b03532

Jahan, B.N., Li, L., Pagilla, K.R., 2021. Fate and reduction of bromate formed in advanced water treatment ozonation systems: A critical review. Chemosphere 266, 128964. https://doi.org/10.1016/j.chemosphere.2020.128964

Janus, M., Kusiak-Nejman, E., Morawski, A.W., 2012. Influence of water temperature on the photocatalytic activity of titanium dioxide. React. Kinet. Mech. Catal. 106, 289–295. https://doi.org/10.1007/s11144-012-0432-6

Jhunkeaw, C., Khongcharoen, N., Rungrueng, N., Sangpo, P., Panphut, W., Thapinta, A., Senapin, S., St-Hilaire, S., Dong, H.T., 2021. Ozone nanobubble treatment in freshwater effectively reduced pathogenic fish bacteria and is safe for Nile tilapia (Oreochromis niloticus). Aquaculture 534, 736286.

https://doi.org/10.1016/j.aquaculture.2020.736286

Jhunkeaw, C., Khongcharoen, N., Rungrueng, N., Sangpo, P., Panphut, W., Thapinta, A., Senapin, S., St-Hilaire, S., Dong, H.T., 2020. Ozone nanobubble treatment effectively reduced pathogenic Gram positive and negative bacteria in freshwater and safe for tilapia. bioRxiv 1–21. https://doi.org/10.1101/2020.06.07.138297

Jiang, D., Sun, H., Xia, H., Yang, G., Li, D., 2018. Simultaneous desulfurization and denitrification method using O_3 and NO micro-nano bubbles systemthe. IOP Conf. Ser. Earth Environ. Sci. 170, 0–6. https://doi.org/10.1088/1755-1315/170/5/052006

Jin, F., Li, J., Ye, X., Wu, C., 2007. Effects of pH and ionic strength on the stability of nanobubbles in aqueous solutions of α-Cyclodextrin. J. Phys. Chem. B 111, 11745–11749. https://doi.org/10.1021/jp074260f

Jin, J., Wang, R., Tang, J., Yang, L., Feng, Z., Xu, C., Yang, F., Gu, N., 2020. Dynamic tracking of bulk nanobubbles from microbubbles shrinkage to collapse. Colloids Surfaces A Physicochem. Eng. Asp. 589, 124430. https://doi.org/10.1016/j.colsurfa.2020.124430

John, A., Carra, I., Jefferson, B., Jodkowska, M., Brookes, A., Jarvis, P., 2022. Are microbubbles magic or just small?A direct comparison of hydroxyl radical generation between microbubble and conventional bubble ozonation under typical operational conditions. Chem. Eng. J. 435, 134854. https://doi.org/10.1016/j.cej.2022.134854

Jüttner, F., Watson, S.B., 2007. Biochemical and ecological control of geosmin and 2-methylisoborneol in source waters. Appl. Environ. Microbiol. 73, 4395–4406. https://doi.org/10.1128/AEM.02250-06

Karanfil, T., Schlautman, M.A., Erdogan, I., 2002. Survey of DOC and UV measurement practices with implications for SUVA determination. J. / Am. Water Work. Assoc. 94, 68–80.

Kawamura, S., 2000. Integrated design and operation of water treatment facilities, 2nd ed. ed. John Wiley & Sons, New York.

Kawara, F., Inoue, J., Takenaka, M., Hoshi, N., Masuda, A., Nishiumi, S., Kutsumi, H., Azuma, T., Ohdaira, T., 2014. The influences of pepsin concentrations and pH levels on the disinfective activity of ozone nanobubble water against helicobacter pylori. Digestion 90, 10–17. https://doi.org/10.1159/000358286

Ke, S., Xiao, W., Quan, N., Dong, Y., Zhang, L., Hu, J., 2019. Formation and stability of bulk nanobubbles in different solutions. Langmuir 35, 5250–5256. https://doi.org/10.1021/acs.langmuir.9b00144

Khan, P., Zhu, W., Huang, F., Gao, W., Khan, N.A., 2020. Micro-nanobubble technology and water-related application. Water Sci. Technol. Water Supply 20, 2021–2035. https://doi.org/10.2166/ws.2020.121

Khare, M., 2016. Reactivity of hydroxyl radical : mechanistic insight into the reactivity with dissolved organic matter. Michigan Technological University.

Khuntia, S., Majumder, S.K., Ghosh, P., 2015. Quantitative prediction of generation of hydroxyl radicals from ozone microbubbles. Chem. Eng. Res. Des. 98, 231–239. https://doi.org/10.1016/j.cherd.2015.04.003

Khuntia, S., Majumder, S.K., Ghosh, P., 2014. Oxidation of As(III) to As(V) using ozone microbubbles. Chemosphere 97, 120–124. https://doi.org/10.1016/j.chemosphere.2013.10.046

Khuntia, S., Majumder, S.K., Ghosh, P., 2013. Removal of ammonia from water by ozone microbubbles. Ind. Eng. Chem. Res. 52, 318–326. https://doi.org/10.1021/ie302212p

Kim, K.T., Park, Y.G., 2021a. Geosmin and 2-MIB removal by full-scale drinkingwater treatment processes in the Republic of Korea. Water 13. https://doi.org/10.3390/w13050628

Kim, T.K., Kim, T., Lee, I., Choi, K., Zoh, K.D., 2021. Removal of tetramethylammonium hydroxide (TMAH) in semiconductor wastewater using the nano-ozone H_2O_2 process. J. Hazard. Mater. 409, 123759. https://doi.org/10.1016/j.jhazmat.2020.123759

Kiwi, J., Lopez, A., Nadtochenko, V., 2000. Mechanism and kinetics of the •OH-radical intervention during Fenton oxidation in the presence of a significant amount of radical scavenger (Cl-). Environ. Sci. Technol. 34, 2162–2168. https://doi.org/10.1021/es991406i

Krasner, S.W., Hwang, C.J., McGuire, M.J., 1983. A Standard Method for Quantification of earthy-musty odorants in water, sediments, and algal cultures. Water Sci. Technol. 15, 127–138. https://doi.org/10.2166/wst.1983.0137

Ku, Y., Su, W.J., Shen, Y.S., 1996. Decomposition kinetics of ozone in aqueous solution. Ind. Eng. Chem. Res. 35, 3369–3374. https://doi.org/10.1021/ie9503959

Kwon, H., Mohamed, M.M., Annable, M.D., Kim, H., 2020. Remediation of NAPL-contaminated porous media using micro-nano ozone bubbles: Bench-scale experiments. J. Contam. Hydrol. 228, 103563 . https://doi.org/10.1016/j.jconhyd.2019.103563

Kyzas, G.Z., Mitropoulos, A.C., 2021. From bubbles to nanobubbles. Nanomaterials 11. https://doi.org/10.3390/nano11102592

Lawaetz, A.J., Stedmon, C.A., 2009. Fluorescence intensity calibration using the Raman scatter peak of water. Appl. Spectrosc. 63, 936–940. https://doi.org/10.1366/000370209788964548

Lee, S., Anwer, H., Park, J.W., 2023. Oxidative power loss control in ozonation: Nanobubble and ultrasonic cavitation. J. Hazard. Mater. 455, 131530.

https://doi.org/10.1016/j.jhazmat.2023.131530

Lehman, P.W., Kurobe, T., Lesmeister, S., Baxa, D., Tung, A., Teh, S.J., 2017. Impacts of the 2014 severe drought on the Microcystis bloom in San Francisco Estuary. Harmful Algae 63, 94–108. https://doi.org/10.1016/j.hal.2017.01.011

Lewitus, A.J., Horner, R.A., Caron, D.A., Garcia-Mendoza, E., Hickey, B.M., Hunter, M., Huppert, D.D., Kudela, R.M., Langlois, G.W., Largier, J.L., Lessard, E.J., RaLonde, R., Jack Rensel, J.E., Strutton, P.G., Trainer, V.L., Tweddle, J.F., 2012. Harmful algal blooms along the North American west coast region: History, trends, causes, and impacts. Harmful Algae 19, 133–159. https://doi.org/10.1016/j.hal.2012.06.009

Li, D., Jing, D., Pan, Y., Wang, W., Zhao, X., 2014. Coalescence and stability analysis of surface nanobubbles on the polystyrene/water interface. Langmuir 30, 6079–6088. https://doi.org/10.1021/la501262a

Li, H., Hu, L., Song, D., Al-Tabbaa, A., 2014. Subsurface transport behavior of micro-nano bubbles and potential applications for groundwater remediation. Int. J. Environ. Res. Public Health 11, 473–486. https://doi.org/10.3390/ijerph110100473

Li, P., Takahashi, M., Chiba, K., 2009. Enhanced free-radical generation by shrinking microbubbles using a copper catalyst. Chemosphere 77, 1157–1160. https://doi.org/10.1016/j.chemosphere.2009.07.062

Liang, C., Wang, D., Chen, J., Zhu, L., Yang, M., 2007. Kinetics analysis on the ozonation of MIB and geosmin. Ozone Sci. Eng. 29, 185–189. https://doi.org/10.1080/01919510701294197

Liao, C.H., Kang, S.F., Wu, F.A., 2001. Hydroxyl radical scavenging role of chloride and bicarbonate ions in the H_2O_2/UV process. Chemosphere. https://doi.org/10.1016/S0045-6535(00)00278-2

Linh, N.V., Dien, L.T., Panphut, W., Thapinta, A., Senapin, S., St-Hilaire, S., Rodkhum, C., Dong, H.T., 2021. Ozone nanobubble modulates the innate defense system of Nile tilapia (Oreochromis niloticus) against Streptococcus agalactiae. Fish Shellfish Immunol. 112, 64–73. https://doi.org/10.1016/j.fsi.2021.02.015

Linh, N.V., Dien, L.T., Sangpo, P., Senapin, S., Thapinta, A., Panphut, W., St-Hilaire, S., Rodkhum, C., Dong, H.T., 2022. Pre-treatment of Nile tilapia (Oreochromis niloticus) with ozone nanobubbles improve efficacy of heat-killed Streptococcus agalactiae immersion vaccine. Fish Shellfish Immunol. 123, 229–237. https://doi.org/10.1016/j.fsi.2022.03.007

Liu, S., Kawagoe, Y., Makino, Y., Oshita, S., 2013. Effects of nanobubbles on the physicochemical properties of water: The basis for peculiar properties of water containing nanobubbles. Chem. Eng. Sci. 93, 250–256. https://doi.org/10.1016/j.ces.2013.02.004

Liu, S., Oshita, S., Kawabata, S., Makino, Y., Yoshimoto, T., 2016. Identification of ROS produced by nanobubbles and their positive and negative effects on vegetable seed germination. Langmuir 32, 11295–11302. https://doi.org/10.1021/acs.langmuir.6b01621

Liu, Z., Demeestere, K., Hulle, S. Van, 2021. Comparison and performance assessment of ozone-based AOPs in view of trace organic contaminants abatement in water and wastewater: A review. J. Environ. Chem. Eng. 9, 105599. https://doi.org/10.1016/j.jece.2021.105599

Lou, S.-T., Ouyang, Z.-Q., Zhang, Y., Li, X.-J., Hu, J., Li, M.-Q., Yang, F.-J., 2000. Nanobubbles on solid surface imaged by atomic force microscopy. J. Vac. Sci. \& Technol. B Microelectron. Nanom. Struct. Process. Meas. Phenom. 18, 2573–2575. https://doi.org/10.1116/1.1289925

Lu, J., Huang, X., Zhang, Z., Pang, H., Chen, K., Xia, H., Sui, Y., Chen, R., Zhao, Z., 2022. Co-coagulation of micro-nano bubbles (MNBs) for enhanced drinking water treatment: A study on the efficiency and mechanism of a novel cleaning process. Water Res. 226, 119245. https://doi.org/10.1016/j.watres.2022.119245

Lukianova-Hleb, E.Y., Belyanin, A., Kashinath, S., Wu, X., Lapotko, D.O., 2012. Plasmonic nanobubble-enhanced endosomal escape processes for selective and guided intracellular delivery of chemotherapy to drug-resistant cancer cells. Biomaterials 33, 1821–1826. https://doi.org/10.1016/j.biomaterials.2011.11.015.

Lukianova-Hleb, E.Y., Ren, X., Sawant, R.R., Wu, X., Torchilin, V.P., Lapotko, D.O., 2014. On-demand intracellular amplification of chemoradiation with cancer-specific plasmonic nanobubbles. Nat. Med. 20, 778–784. https://doi.org/10.1038/nm.3484

Lürling, M., Van Oosterhout, F., Faassen, E., 2017. Eutrophication and warming boost cyanobacterial biomass and microcystins. Toxins (Basel). 9, 1–16. https://doi.org/10.3390/toxins9020064

Lyu, T., Wu, S., Mortimer, R.J.G., Pan, G., 2019. Nanobubble Technology in Environmental Engineering: Revolutionization Potential and Challenges. Environ. Sci. Technol. 53, 7175–7176. https://doi.org/10.1021/acs.est.9b02821

Maie, N., Anzai, S., Tokai, K., Kakino, W., Taruya, H., Ninomiya, H., 2022. Using oxygen/ozone nanobubbles for in situ oxidation of dissolved hydrogen sulfide at a residential tunnel-construction site. J. Environ. Manage. 302, 114068. https://doi.org/10.1016/j.jenvman.2021.114068

Maie, N., Kakino, W., Anzai, S., Taruya, H., 2020. Removal of 1 , 4-dioxane in groundwater using ozone nanobubbles. J. Med. Hyg. use ozone 27(4), 140–145.

Manning, G.S., 2020. On the thermodynamic stability of bubbles, immiscible droplets, and cavities. Phys. Chem. Chem. Phys. 22, 17523–17531. https://doi.org/10.1039/d0cp02517h

Matsui, Y., Nakao, S., Taniguchi, T., Matsushita, T., 2013. Geosmin and 2-methylisoborneol removal using superfine powdered activated carbon: Shell adsorption and branched-pore kinetic model analysis and optimal particle size. Water Res. 47, 2873–2880. https://doi.org/10.1016/j.watres.2013.02.046

Matsumoto, M., Tanaka, K., 2008. Nano bubble-size dependence of surface tension and inside pressure. Fluid Dyn. Res. 40, 546–553. https://doi.org/10.1016/j.fluiddyn.2007.12.006

Matthews, R.W., 1980. The radiation chemistry of the terephthalate dosimeter. radiat. Res. Soc. 83, 27–41.

Matuszek, K., Pankalla, E., Grymel, A., Latos, P., Chrobok, A., 2020. Studies on the solubility of terephthalic acid in ionic liquids. Molecules 25, 1–10. https://doi.org/10.3390/molecules25010080

Meegoda, J.N., Aluthgun Hewage, S., Batagoda, J.H., 2018. Stability of nanobubbles. Environ. Eng. Sci. 35, 1216–1227. https://doi.org/10.1089/ees.2018.0203

Meegoda, J.N., Batagoda, J.H., 2016. A New Technology to Decontaminate Sediments Using Ultrasound with Ozone Nano Bubbles. [Conference proceeding] Geo-Chicago 2016: Sustainable Waste Management and Remediation, GSP 273, 235–244. https://doi.org/10.1061/9780784480168

Meegoda, J.N., Batagoda, J.H., Aluthgun-Hewage, S., 2017. Briefing: In situ decontamination of sediments using ozone nanobubbles and ultrasound. J. Environ. Eng. Sci. 12, 1–3. https://doi.org/10.1680/jenes.17.00006

Menendez, D., Flores, J.V., 2017. Reduction of hospital wastewater through micro-nano ozone-air bubbles. J. Nanotechnol. 1, 59–72.

Michailidi, E.D., Bomis, G., Varoutoglou, A., Kyzas, G.Z., Mitrikas, G., Mitropoulos, A.C., Efthimiadou, E.K., Favvas, E.P., 2020. Bulk nanobubbles: Production and investigation of their formation/stability mechanism. J. Colloid Interface Sci. 564, 371–380. https://doi.org/10.1016/j.jcis.2019.12.093

Millero, F.J., 2001. The physical chemistry of natural waters. Wiley-Interscience Ser. Geochemistry.

Minamikawa, K., Takahashi, M., Makino, T., Tago, K., Hayatsu, M., 2015. Irrigation with oxygen-nanobubble water can reduce methane emission and arsenic dissolution in a flooded rice paddy. Environ. Res. Lett. 10. https://doi.org/10.1088/1748-9326/10/8/084012

Monteagudo, J.M., Durán, A., San Martin, I., Carnicer, A., 2011. Roles of different intermediate active species in the mineralization reactions of phenolic pollutants under a UV-A/C photo-Fenton process. Appl. Catal. B Environ. 106, 242–249. https://doi.org/10.1016/j.apcatb.2011.05.034

Mustapha, S., Tijani, J.O., Ndamitso, M., Abdulkareem, A.S., Shuaib, D.T., Mohammed, A.K., 2021a. A critical review on geosmin and 2-methylisoborneol in water: Sources, effects, detection, and removal techniques, Environmental Monitoring and Assessment. https://doi.org/10.1007/s10661-021-08980-9

Mustapha, S., Tijani, J.O., Ndamitso, M., Abdulkareem, A.S., Shuaib, D.T., Mohammed, A.K., 2021b. A critical review on geosmin and 2-methylisoborneol in water: sources, effects, detection, and removal techniques, Environmental Monitoring and Assessment. https://doi.org/10.1007/s10661-021-08980-9

Neta, P., Huie, R.E., Ross, A.B., 1988. Rate constants for reactions of inorganic radicals in aqueous solution. J. Phys. Chem. Ref. Data 17, 1027–1284. https://doi.org/10.1063/1.555808

Ng, P.H., Huang, Q., Huang, L., Cheng, T.H., Man, K.Y., Cheng, K.P., Marques, P., Rita, A., Zhang, J., St-hilaire, S., 2023. Assessment of ozone nanobubble technology to reduce freshwater algae. Aquac. Res. 2023. https://doi.org/https://doi.org/10.1155/2023/9539102

Nghia, N.H., Nguyen, N.T., Binh, P.T., May, L.T., Huy, T.T., Giang, P.T., St-Hilaire, S., Van, P.T., 2022. Effect of nanobubbles (oxygen, ozone) on the Pacific white shrimp (Penaeus vannamei), Vibrio parahaemolyticus and water quality under lab conditions. Fish. Aquat. Sci. 25, 429–440. https://doi.org/10.47853/FAS.2022.e39

Nirmalkar, N., Pacek, A.W., Barigou, M., 2018a. On the existence and stability of bulk nanobubbles. Langmuir 34, 10964–10973. https://doi.org/10.1021/acs.langmuir.8b01163

Nirmalkar, N., Pacek, A.W., Barigou, M., 2018b. Interpreting the interfacial and colloidal stability of bulk nanobubbles. Soft Matter 14, 9643–9656. https://doi.org/10.1039/c8sm01949e

Nishimura, Y., Watanabe, S., Tashiro, K., Umeda, Y., Honma, H., Yamashita, T., 2014. Nanoscale smooth interface maintained metallisation of polyimide using low concentration ozone micro-nano bubbles dispersed in water. Trans. Inst. Met. Finish. 92, 52–58. https://doi.org/10.1179/imf.2014.92.1.52

Nobbmann, U., 2016. DLS or NTA ?. Malvern Panalytical. URL https://www.materials-talks.com/2016/09/15/nta-or-dls/ (accessed 11.27.21).

Oh, S.H., Kim, J.M., 2017. Generation and stability of bulk nanobubbles. Langmuir 33, 3818–3823. https://doi.org/10.1021/acs.langmuir.7b00510

Ohgaki, K., Khanh, N.Q., Joden, Y., Tsuji, A., Nakagawa, T., 2010. Physicochemical approach to nanobubble solutions. Chem. Eng. Sci. 65, 1296–1300. https://doi.org/10.1016/j.ces.2009.10.003

Ömür-Özbek, P., Dietrich, A.M., 2005. Determination of temperature-dependent Henry's

law constants of odorous contaminants and their application to human perception. Environ. Sci. Technol. 39, 3957–3963. https://doi.org/10.1021/es0480264

Paerl, H.W., Otten, T.G., Kudela, R., 2018. Mitigating the expansion of harmful algal blooms across the freshwater-to-marine continuum. Environ. Sci. Technol. 52, 5519–5529. https://doi.org/10.1021/acs.est.7b05950

Page, S.E., Arnold, W.A., McNeill, K., 2010. Terephthalate as a probe for photochemically generated hydroxyl radical. J. Environ. Monit. 12 9, 1658–1665.

Pal, P., Joshi, A., Anantharaman, H., 2022. Nanobubble ozonation for waterbody rejuvenation at different locations in India: A holistic and sustainable approach. Results Eng. 16, 100725. https://doi.org/10.1016/j.rineng.2022.100725

Park, G., Yu, M., Koo, J.Y., Joe, W.H., Kim, H., 2006. Oxidation of geosmin and MIB in water using O_3/H_2O_2: Kinetic evaluation. Water Sci. Technol. Water Supply 6, 63–69. https://doi.org/10.2166/ws.2006.051

Park, S.H., Park, C., Lee, J.Y., Lee, B., 2017. A simple parameterization for the rising velocity of bubbles in a liquid pool. Nucl. Eng. Technol. 49, 692–699. https://doi.org/10.1016/j.net.2016.12.006

Pei, S., You, S., Ma, J., Chen, X., Ren, N., 2020. Electron Spin Resonance evidence for electro-generated hydroxyl radicals. Environ. Sci. Technol. 54, 13333–13343.

https://doi.org/10.1021/acs.est.0c05287

Peleg, M., 1976. The chemistry of ozone in the treatment of water. Water Res. 10, 361–365. https://doi.org/10.1016/0043-1354(76)90052-X

Persson, P.-E., 1983. Off-flavours in aquatic ecosystems – An introduction. Water Sci. Technol. 15, 1–11. https://doi.org/10.2166/wst.1983.0125

Peter, A., Köster, O., Schildknecht, A., von Gunten, U., 2009. Occurrence of dissolved and particle-bound taste and odor compounds in Swiss lake waters. Water Res. 43, 2191–2200. https://doi.org/10.1016/j.watres.2009.02.016

Peter, A., von Gunten, U., 2007. Oxidation kinetics of selected taste and odor compounds during ozonation of drinking water. Environ. Sci. Technol. 41, 626–631. https://doi.org/10.1021/es061687b

Pirbazari, M., Borow, H.S., Craig, S., Ravindran, V., McGuire, M.J., 1992. Physical chemical characterization of five earthy musty-smelling compounds. Water Sci. Technol. 25, 81–88. https://doi.org/10.2166/wst.1992.0038

Pirbazari, M., Ravindran, V., Badriyha, B.N., Craig, S., McGuire, M.J., 1993. GAC adsorber design protocol for the removal of off-flavors. Water Res. 27, 1153–1166. https://doi.org/10.1016/0043-1354(93)90007-5

Pirillo, V., Pollegioni, L., Molla, G., 2021. Analytical methods for the investigation of

enzyme-catalyzed degradation of polyethylene terephthalate. FEBS J. 288, 4730–4745. https://doi.org/10.1111/febs.15850

Ponce-robles, L., Pagán-Muñoz, A., Lara-Guillén, A.J., Masdemont-Hernández, B., Munuera-Pérez, T., Nortes-Tortosa, P.A., Alarcón-Cabañero, J.J.A.-C., 2023. Full-scale o_3/micro-nano bubbles system based advanced oxidation as alternative tertiary treatment in WWTP effluents 1–18.

Pourkarimi, Z., Rezai, B., Noaparast, M., 2017. Effective parameters on generation of nanobubbles by cavitation method for froth flotation applications. Physicochem. Probl. Miner. Process. 53, 920–942. https://doi.org/10.5277/ppmp170220

Qi, F., Xu, B., Chen, Z., Ma, J., Sun, D., Zhang, L., 2009. Efficiency and products investigations on the ozonation of 2-methylisoborneol in drinking water. Water Environ. Res. 81, 2411–2419. https://doi.org/10.2175/106143009x425933

Rajca, M., Bodzek, M., 2013. Kinetics of fulvic and humic acids photodegradation in water solutions. Sep. Purif. Technol. 120, 35–42. https://doi.org/10.1016/j.seppur.2013.09.019

Rangel-Mendez, J.R., Cannon, F.S., 2005. Improved activated carbon by thermal treatment in methane and steam: Physicochemical influences on MIB sorption capacity. Carbon N. Y. 43, 467–479. https://doi.org/10.1016/j.carbon.2004.09.031

Ravichandran, S.A., Rajan, V.P., Aravind, P.V., Seenivasan, A., Prakash, D.G., Ramakrishnan, K., 2016. Characterization of terephthalic acid monomer recycled from post-consumer PET polymer bottles. Macromol. Symp. 361, 30–33. https://doi.org/10.1002/masy.201400269

Razumovskii, S.D., Konstantinova, M.L., Grinevich, T. V., Korovina, G. V., Zaitsev, V.Y., 2010. Mechanism and kinetics of the reaction of ozone with sodium chloride in aqueous solutions. Kinet. Catal. 51, 492–496. https://doi.org/10.1134/S0023158410040051

Remucal, C.K., Salhi, E., Walpen, N., Von Gunten, U., 2020. Molecular-level transformation of dissolved organic matter during oxidation by ozone and hydroxyl radical. Environ. Sci. Technol. 54, 10351–10360. https://doi.org/10.1021/acs.est.0c03052

Rezazadeh, A., Thomsen, K., Gavala, H.N., Skiadas, I. V., Fosbøl, P.L., 2021. Solubility and freezing points of disodium terephthalate in water-ethylene glycol mixtures. J. Chem. Eng. Data 66, 2143–2152. https://doi.org/10.1021/acs.jced.1c00052

Ridal, J., Brownlee, B., McKenna, G., Levac, N., 2001. Removal of taste and odour compounds by conventional granular activated carbon filtration. Water Qual. J. 36, 43–54.

Rodríguez-Vidal, F.J., García-Valverde, M., Ortega-Azabache, B., González-Martínez, Á.,

Bellido-Fernández, A., 2021. Using excitation-emission matrix fluorescence to evaluate the performance of water treatment plants for dissolved organic matter removal. Spectrochim. Acta - Part A Mol. Biomol. Spectrosc. 249. https://doi.org/10.1016/j.saa.2020.119298

Rosa, A.F., Rubio, J., 2018. On the role of nanobubbles in particle–bubble adhesion for the flotation of quartz and apatitic minerals. Miner. Eng. 127, 178–184. https://doi.org/10.1016/j.mineng.2018.08.020

Saijai, S., Thonglek, V., Yoshikawa, K., 2019. Sterilization effects of ozone fine (micro/nano) bubble water. Int. J. Plasma Environ. Sci. Technol. 12, 55–58.

Sakr, M., Mohamed, M.M., Maraqa, M.A., Hamouda, M.A., Aly Hassan, A., Ali, J., Jung, J., 2022. A critical review of the recent developments in micro–nano bubbles applications for domestic and industrial wastewater treatment. Alexandria Eng. J. 61, 6591–6612. https://doi.org/10.1016/j.aej.2021.11.041

Salguero, J., Flores, J.V., 2017. Reduction of the biochemical oxygen demand of the water samples from the lower basin of the Chillon River by means of Air-Ozone MicroNanobubbles, Ventanilla - Callao 1, 59–72.

Saran, M., Summer, K.H., 1999. Assaying for hydroxyl radicals: Hydroxylated terephthalate is a superior fluorescence marker than hydroxylated benzoate. Free Radic. Res. 31, 429–436. https://doi.org/10.1080/10715769900300991

Satchwill, T., 2001. Drinking water taste and odor: Compound identification and treatment. ProQuest Diss. Theses 156. https://doi.org/10.11575/PRISM/21711

Schumann, R., Pendleton, P., 1997. Dehydration products of 2-methylisoborneol. Water Res. 31, 1243–1246. https://doi.org/10.1016/S0043-1354(96)00330-2

Seridou, P., Kalogerakis, N., 2021. Disinfection applications of ozone micro- and nanobubbles. Environ. Sci. Nano 8, 3493–3510. https://doi.org/10.1039/d1en00700a

Siddique, M.S., Xiong, X., Yang, H., Maqbool, T., Graham, N., Yu, W., 2022. Dynamic variations in DOM and DBPs formation potential during surface water treatment by ozonation-nanofiltration: Using spectroscopic indices approach. Chem. Eng. J. 427. https://doi.org/10.1016/j.cej.2021.132010

Sohn, J., Amy, G., Yoon, Y., 2006. Bromide ion incorporation into brominated disinfection by-products. Water. Air. Soil Pollut. 174, 265–277. https://doi.org/10.1007/s11270-006-9104-3

Song, H., Orr, O., Hong, Y., Karanfil, T., 2009. Isolation and fractionation of natural organic matter: Evaluation of reverse osmosis performance and impact of fractionation parameters. Environ. Monit. Assess. 153, 307–321. https://doi.org/10.1007/s10661-008-0357-8

Song, W., O'Shea, K.E., 2007. Ultrasonically induced degradation of 2-methylisoborneol

and geosmin. Water Res. 41, 2672–2678. https://doi.org/10.1016/j.watres.2007.02.041

Soyluoglu, M., Kim, D., Zaker, Y., Karanfil, T., 2022. Removal mechanisms of geosmin and MIB by oxygen nanobubbles during water treatment. Chem. Eng. J. 443, 136535. https://doi.org/10.1016/j.cej.2022.136535

Soyluoglu, M., Kim, D., Zaker, Y., Karanfil, T., 2021. Stability of oxygen nanobubbles under freshwater conditions. Water Res. 206, 117749. https://doi.org/10.1016/j.watres.2021.117749

Srinivasan, R., Sorial, G.A., 2011. Treatment of taste and odor causing compounds 2-methyl isoborneol and geosmin in drinking water: A critical review. J. Environ. Sci. 23, 1–13. https://doi.org/10.1016/S1001-0742(10)60367-1

Staehelln, J., Hoigné, J., 1985. Decomposition of Ozone in Water in the Presence of Organic Solutes Acting as Promoters and Inhibitors of Radical Chain Reactions. Environ. Sci. Technol. 19, 1206–1213.

Suffet, I.H., Corado, A., Chou, D., McGuire, M.J., Butterworth, S., 1996. AWWA taste and odor survey. J. Am. Water Work. Assoc. 88, 168–180.

Sugano, K., Miyoshi, Y., Inazato, S., 2017. Study of ultrafine bubble stabilization by organic material adhesion. Japanese J. Multiph. Flow 31, 299–306. https://doi.org/10.3811/jjmf.31.299

Sun, Y., Xie, G., Peng, Y., Xia, W., Sha, J., 2016. Stability theories of nanobubbles at solid-liquid interface: A review. Colloids Surfaces A Physicochem. Eng. Asp. 495, 176–186. https://doi.org/10.1016/j.colsurfa.2016.01.050

Sun, Z., Chen, X., Yang, K., Zhu, N., Lou, Z., 2020. The progressive steps for TPH stripping and the decomposition of oil refinery sludge using microbubble ozonation. Sci. Total Environ. 712, 135631. https://doi.org/10.1016/j.scitotenv.2019.135631

Sung, M., Teng, C.H., Yang, T.H., 2017. Dissolution enhancement and mathematical modeling of removal of residual trichloroethene in sands by ozonation during flushing with micro-nano-bubble solution. J. Contam. Hydrol. 202, 1–10. https://doi.org/10.1016/j.jconhyd.2017.03.008

Takahashi, M., 2005. ζ Potential of microbubbles in aqueous solutions: Electrical properties of the gas - Water interface. J. Phys. Chem. B 109, 21858–21864. https://doi.org/10.1021/jp0445270

Takahashi, M., Chiba, K., Li, P., 2007. Free-radical generation from collapsing microbubbles in the absence of a dynamic stimulus. J. Phys. Chem. B 111, 1343–1347. https://doi.org/10.1021/jp0669254

Takahashi, M., Shirai, Y., Sugawa, S., 2021. Free-Radical Generation from bulk nanobubbles in aqueous electrolyte solutions: ESR spin-trap observation of

microbubble-treated water. Langmuir 37, 5005–5011. https://doi.org/10.1021/acs.langmuir.1c00469

Takizawa, M., Okuwaki, A., Okabe, T., 1973. The chemical behavior of low valence sulfur compounds. VIII. The oxidation of sodium thiosulfate with ozone. Bull. Chem. Soc. Jpn. 46, 3785–3789.

Talukdar, S., Dutta, R.K., 2016. A mechanistic approach for superoxide radicals and singlet oxygen mediated enhanced photocatalytic dye degradation by selenium doped ZnS nanoparticles. RSC Adv. 6, 928–936. https://doi.org/10.1039/c5ra17940h

Tekile, A., Kim, I., Lee, J.-Y., 2017. Applications of ozone micro- and nanobubble technologies in water and wastewater treatment: Review. J. Korean Soc. Water Wastewater 31, 481–490. https://doi.org/10.11001/jksww.2017.31.6.481

Temesgen, T., Bui, T.T., Han, M., Kim, T. il, Park, H., 2017. Micro and nanobubble technologies as a new horizon for water-treatment techniques: A review. Adv. Colloid Interface Sci. 246, 40–51. https://doi.org/10.1016/j.cis.2017.06.011

Temesgen, T., Han, M., 2021. Ultrafine bubbles as an augmenting agent for ozone-based advanced oxidation. Water Sci. Technol. 84, 3705–3715. https://doi.org/10.2166/wst.2021.475

Ulanski, P., von Sonntag, C., 1999. The •OH radical-induced chain reactions of methanol with hydrogen peroxide and with peroxodisulfate. J. Chem. Soc. Perkin Trans. 2 2, 165–168. https://doi.org/10.1039/a808543i

Ulatowski, K., Sobieszuk, P., Mróz, A., Ciach, T., 2019. Stability of nanobubbles generated in water using porous membrane system. Chem. Eng. Process. - Process Intensif. 136, 62–71. https://doi.org/10.1016/j.cep.2018.12.010

USEPA, 2010. Comprehensive disinfectants and disinfection byproducts rules (stage 1 and stage 2): Quick Reference Guide. U. S. Environ. Prot. Agency 816-F, 4.

Ushida, A., Koyama, T., Nakamoto, Y., Narumi, T., Sato, T., Hasegawa, T., 2017. Antimicrobial effectiveness of ultra-fine ozone-rich bubble mixtures for fresh vegetables using an alternating flow. J. Food Eng. 206, 48–56. https://doi.org/10.1016/j.jfoodeng.2017.03.003

Ushikubo, F.Y., Enari, M., Furukawa, T., Nakagawa, R., Makino, Y., Kawagoe, Y., Oshita, S., 2010a. Zeta-potential of micro- and/or nano-bubbles in water produced by some kinds of gases. IFAC Proc. Vol. 3. https://doi.org/10.3182/20101206-3-jp-3009.00050

Ushikubo, F.Y., Furukawa, T., Nakagawa, R., Enari, M., Makino, Y., Kawagoe, Y., Shiina, T., Oshita, S., 2010b. Evidence of the existence and the stability of nano-bubbles in water. Colloids Surfaces A Physicochem. Eng. Asp. 361, 31–37. https://doi.org/10.1016/j.colsurfa.2010.03.005

Vel Leitner, N.K., Roshani, B., 2010. Kinetic of benzotriazole oxidation by ozone and hydroxyl radical. Water Res. 44, 2058–2066. https://doi.org/10.1016/j.watres.2009.12.018

von Gunten, U., 2007. The basics of oxidants in water treatment. Part B: Ozone reactions. Water Sci. Technol. 55, 25–29. https://doi.org/10.2166/wst.2007.382

von Gunten, U., 2003a. Ozonation of drinking water: Part I. Oxidation kinetics and product formation. Water Res. 37, 1443–1467. https://doi.org/https://doi.org/10.1016/S0043-1354(02)00457-8

von Gunten, U., 2003b. Ozonation of drinking water: Part II. Disinfection and by-product formation in presence of bromide, iodide or chlorine. Water Res. 37, 1469–1487. https://doi.org/10.1016/S0043-1354(02)00458-X

von Sonntag, C., von Gunten, U., 2012. Chemistry of ozone in water and wastewater treatment: From basic principles to applications. https://doi.org/10.2166/9781780400839

Wang, L., Ali, J., Wang, Z., Oladoja, N.A., Cheng, R., Zhang, C., Mailhot, G., Pan, G., 2020. Oxygen nanobubbles enhanced photodegradation of oxytetracycline under visible light: Synergistic effect and mechanism. Chem. Eng. J. 388. https://doi.org/10.1016/j.cej.2020.124227

Wang, Q., Zhao, H., Qi, N., Qin, Y., Zhang, X., Li, Y., 2019. Generation and stability of size-adjustable bulk nanobubbles based on periodic pressure change. Sci. Rep. 9, 1–9. https://doi.org/10.1038/s41598-018-38066-5

Wang, Q., Zietzschmann, F., Yu, J., Hofman, R., An, W., Yang, M., Rietveld, L.C., 2020. Projecting competition between 2-methylisoborneol and natural organic matter in adsorption onto activated carbon from ozonated source waters. Water Res. 173, 115574. https://doi.org/10.1016/j.watres.2020.115574

Wang, Y., Guo, Z., Tan, T., Ji, Y., Hu, J., Zhang, Y., 2021. The effects of nanobubbles on the assembly of glucagon amyloid fibrils. Soft Matter 17, 3486–3493. https://doi.org/10.1039/d0sm02279a

Wang, Y., Wang, S., Sun, J., Dai, H., Zhang, B., Xiang, W., Hu, Z., Li, P., Yang, J., Zhang, W., 2021. Nanobubbles promote nutrient utilization and plant growth in rice by upregulating nutrient uptake genes and stimulating growth hormone production. Sci. Total Environ. 800, 149627. https://doi.org/10.1016/j.scitotenv.2021.149627

Watson, S.B., Ridal, J., Boyer, G.L., 2008. Taste and odour and cyanobacterial toxins: Impairment, prediction, and management in the Great Lakes. Can. J. Fish. Aquat. Sci. 65, 1779–1796. https://doi.org/10.1139/F08-084

Wei, J., Sha, H., Wang, R., 2023. Study on Treatment of Basic Yellow 28 dye Wastewater by Micro-nano Bubble Ozone Catalytic Oxidation. Environ. Eng. Res. 28, 0–2.

https://doi.org/10.4491/eer.2022.606

Weijs, J.H., Seddon, J.R.T., Lohse, D., 2012. Diffusive Shielding Stabilizes Bulk Nanobubble Clusters. ChemPhysChem 13, 2197–2204.

https://doi.org/https://doi.org/10.1002/cphc.201100807

Wells, M.L., Trainer, V.L., Smayda, T.J., Karlson, B.S.O., Trick, C.G., Kudela, R.M., Ishikawa, A., Bernard, S., Wulff, A., Anderson, D.M., Cochlan, W.P., 2015. Harmful algal blooms and climate change: Learning from the past and present to forecast the future. Harmful Algae 49, 68–93. https://doi.org/10.1016/j.hal.2015.07.009

Wert, E.C., Korak, J.A., Trenholm, R.A., Rosario-Ortiz, F.L., 2014. Effect of oxidant exposure on the release of intracellular microcystin, MIB, and geosmin from three cyanobacteria species. Water Res. 52, 251–259. https://doi.org/10.1016/j.watres.2013.11.001

Westerhoff, P., Aiken, G., Amy, G., DeBroux, J., 1999. Relationships between the structure of natural organic matter and its reactivity towards molecular ozone and hydroxyl radicals. Water Res. 33, 2265–2276. https://doi.org/10.1016/S0043-1354(98)00447-3

Westerhoff, P., Nalinakumari, B., Pei, P., 2006. Kinetics of MIB and geosmin oxidation during ozonation. Ozone Sci. Eng. 28, 277–286. https://doi.org/10.1080/01919510600892836

Westerhoff, P., Rodriguez-Hernandez, M., Baker, L., Sommerfeld, M., 2005. Seasonal occurrence and degradation of 2-methylisoborneol in water supply reservoirs. Water Res. 39, 4899–4912. https://doi.org/10.1016/j.watres.2005.06.038

White, E.R., Mecklenburg, M., Singer, S.B., Aloni, S., Regan, B.C., 2011. Imaging nanobubbles in water with scanning transmission electron microscopy. Appl. Phys. Express 4. https://doi.org/10.1143/APEX.4.055201

Wickham, J., Stehman, S., Gass, L., Dewitz, J., Sorenson, D., Granneman, B., Ross, R., Baer, L., 2019. An ecological function approach to managing harmful cyanobacteria in three Oregon lakes: Beyond Water quality advisories and total maximum daily loads (TMDLs). Adv. Ecol. Res. 60, 1–24. https://doi.org/10.3390/w11061125.Submit

Wu, J., Zhang, K., Cen, C., Wu, X., Mao, R., Zheng, Y., 2021. Role of bulk nanobubbles in removing organic pollutants in wastewater treatment. AMB Express 11. https://doi.org/10.1186/s13568-021-01254-0

Wu, Y., Lyu, T., Yue, B., Tonoli, E., Verderio, E.A.M., Ma, Y., Pan, G., 2019. Enhancement of tomato plant growth and productivity in organic farming by agri-nanotechnology using nanobubble oxygation. J. Agric. Food Chem. 67, 10823–10831. https://doi.org/10.1021/acs.jafc.9b04117

Wu, Y., Tian, W., Zhang, Y., Fan, W., Liu, F., Zhao, J., Wang, M., Liu, Y., Lyu, T., 2022.

Nanobubble technology enhanced ozonation process for ammonia removal. water 14, 1–10. https://doi.org/10.3390/w14121865

Xia, Z., Hu, L., 2019. Theoretical model for micro-nano-bubbles mass transfer during contaminant treatment. J. Environ. Eng. Sci. 14, 157–167. https://doi.org/10.1680/jenes.18.00039

Xia, Z., Hu, L., 2018. Treatment of organics contaminated wastewater by ozone micro-nano-bubbles. Water 11. https://doi.org/10.3390/w11010055

Xia, Z., Hu, L., 2015. Remediation of organics contaminated groundwater by ozone micro-nano bubble. 15th Asian Reg. Conf. Soil Mech. Geotech. Eng. ARC 2015 New Innov. Sustain. 1978–1981. https://doi.org/10.3208/jgssp.TC215-06

Xie, P., Ma, J., Liu, W., Zou, J., Yue, S., Li, X., Wiesner, M.R., Fang, J., 2015. Removal of 2-MIB and geosmin using UV/persulfate: Contributions of hydroxyl and sulfate radicals. Water Res. 69, 223–233. https://doi.org/10.1016/j.watres.2014.11.029

Xie, Z., Shentu, J., Long, Y., Lu, L., Shen, D., Qi, S., 2023. Effect of dissolved organic matter on selective oxidation of toluene by ozone micro-nano bubble water. Chemosphere 325. https://doi.org/10.1016/j.chemosphere.2023.138400

Xin, Z., 2021. Comparison of geosmin and 2-methylisoborneol removal by conventional ozonation and co-treatment of potassium ferrate and peroxymonosulfate. The University of Western Ontario.

Xue, S., Zhang, Y., Marhaba, T., Zhang, W., 2022. Aeration and dissolution behavior of oxygen nanobubbles in water. J. Colloid Interface Sci. 609, 584–591. https://doi.org/10.1016/j.jcis.2021.11.061

Yamaguchi, M., Ma, T., Tadaki, D., Hirano-Iwata, A., Watanabe, Y., Kanetaka, H., Fujimori, H., Takemoto, E., Niwano, M., 2021. Bactericidal activity of bulk nanobubbles through active oxygen species generation. Langmuir 37, 9883–9891. https://doi.org/10.1021/acs.langmuir.1c01578

Yang, J., Luo, C., Li, T., Cao, J., Dong, W., Li, J., Ma, J., 2020. Superfast degradation of refractory organic contaminants by ozone activated with thiosulfate: Efficiency and mechanisms. Water Res. 176. https://doi.org/10.1016/j.watres.2020.115751

Yang, X., Chen, L., Oshita, S., Fan, W., Liu, S., 2023. Mechanism for enhancing the ozonation process of micro- and nanobubbles: Bubble behavior and interface reaction. Environ. Sci. Technol. Water. https://doi.org/10.1021/acsestwater.3c00031

Yang, X., Liu, Z., Manhaeghe, D., Yang, Y., Hogie, J., Demeestere, K., Van Hulle, S.W.H., 2021. Intensified ozonation in packed bubble columns for water treatment: Focus on mass transfer and humic acids removal. Chemosphere 283. https://doi.org/10.1016/j.chemosphere.2021.131217

Yao, W., Qu, Q., von Gunten, U., Chen, C., Yu, G., Wang, Y., 2017. Comparison of

methylisoborneol and geosmin abatement in surface water by conventional ozonation and an electro-peroxone process. Water Res. 108, 373–382. https://doi.org/10.1016/j.watres.2016.11.014

Yaparatne, S., Tripp, C.P., Amirbahman, A., 2018. Photodegradation of taste and odor compounds in water in the presence of immobilized TiO_2-SiO_2 photocatalysts. J. Hazard. Mater. 346, 208–217. https://doi.org/10.1016/j.jhazmat.2017.12.029

Yasui, K., Tuziuti, T., Kanematsu, W., 2019. Mechanism of •OH radical production from ozone bubbles in water after stopping cavitation. Ultrason. Sonochem. 58, 104707. https://doi.org/10.1016/j.ultsonch.2019.104707

Yasui, K., Tuziuti, T., Kanematsu, W., 2018. Mysteries of bulk nanobubbles (ultrafine bubbles); Stability and radical formation. Ultrason. Sonochem. 48, 259–266. https://doi.org/10.1016/j.ultsonch.2018.05.038

Yildirim, T., Yaparatne, S., Graf, J., Garcia-Segura, S., Apul, O., 2022. Electrostatic forces and higher order curvature terms of Young–Laplace equation on nanobubble stability in water. npj Clean Water 5, 4–6. https://doi.org/10.1038/s41545-022-00163-4

Yin, T., Wang, P., Zheng, R., Zheng, B., Cheng, D., Zhang, X., Shuai, X., 2012. Nanobubbles for enhanced ultrasound imaging of tumors. Int. J. Nanomedicine 7, 895–904. https://doi.org/10.2147/IJN.S28830

Young, W.F., Horth, H., Crane, R., Ogden, T., Arnott, M., 1996. Taste and odour threshold concentrations of potential potable water contaminants. Water Res. 30, 331–340. https://doi.org/10.1016/0043-1354(95)00173-5

Yu, J., Yang, M., Lin, T.F., Guo, Z., Zhang, Y., Gu, J., Zhang, S., 2007. Effects of surface characteristics of activated carbon on the adsorption of 2-methylisobornel (MIB) and geosmin from natural water. Sep. Purif. Technol. 56, 363–370. https://doi.org/10.1016/j.seppur.2007.01.039

Yuan, B., Xu, D., Li, F., Fu, M.L., 2013. Removal efficiency and possible pathway of odor compounds (2-methylisoborneol and geosmin) by ozonation. Sep. Purif. Technol. 117, 53–58. https://doi.org/10.1016/j.seppur.2013.04.029

Zamyadi, A., Henderson, R., Stuetz, R., Hofmann, R., Ho, L., Newcombe, G., 2015. Fate of geosmin and 2-methylisoborneol in full-scale water treatment plants. Water Res. 83, 171–183. https://doi.org/10.1016/j.watres.2015.06.038

Zark, M., Dittmar, T., 2018. Universal molecular structures in natural dissolved organic matter. Nat. Commun. 9, 1–8. https://doi.org/10.1038/s41467-018-05665-9

Žerjav, G., Albreht, A., Vovk, I., Pintar, A., 2020. Revisiting terephthalic acid and coumarin as probes for photoluminescent determination of hydroxyl radical formation rate in heterogeneous photocatalysis. Appl. Catal. A Gen. 598. https://doi.org/10.1016/j.apcata.2020.117566

Zhang, Xy., Wang, Qs., Wu, Zx., Tao, Dp., 2020. An experimental study on size distribution and zeta potential of bulk cavitation nanobubbles. Int. J. Miner. Metall. Mater. 27, 152–161. https://doi.org/10.1007/s12613-019-1936-0

Zhou, L., Wang, S., Zhang, L., Hu, J., 2021. Generation and stability of bulk nanobubbles: A review and perspective. Curr. Opin. Colloid Interface Sci. 53, 101439. https://doi.org/10.1016/j.cocis.2021.101439

Zhou, S., Marcelino, K.R., Wongkiew, S., Sun, L., Guo, W., Khanal, S.K., Lu, H., 2022. Untapped potential: Applying microbubble and nanobubble technology in water and wastewater treatment and ecological restoration. Environ. Sci. Technol. Eng. 2, 1558–1573. https://doi.org/10.1021/acsestengg.2c00117

Zhou, Y., Cao, D., Zhang, X., 2022. Degradation mechanism of micro-nanobubble technology for organic pollutants in aqueous solutions. Nanomaterials 12. https://doi.org/10.3390/nano12152654

Zhu, J., An, H., Alheshibri, M., Liu, L., Terpstra, P.M.J., Liu, G., Craig, V.S.J., 2016. Cleaning with bulk nanobubbles. Langmuir 32, 11203–11211.

https://doi.org/10.1021/acs.langmuir.6b01004

Zhu, X., Wang, B., Kang, J., Shen, J., Yan, P., Li, X., Yuan, L., Zhao, S., Cheng, Y., Li, Y., Zuo, J., Chen, Z., 2022. Interfacial mechanism of the synergy of biochar adsorption and catalytic ozone micro-nano-bubbles for the removal of 2,4-dichlorophenoxyacetic acid in water. Sep. Purif. Technol. 299, 121777. https://doi.org/10.1016/j.seppur.2022.121777

Zimmerman, W.B., Tesař, V., Bandulasena, H.C.H., 2011. Towards energy efficient nanobubble generation with fluidic oscillation. Curr. Opin. Colloid Interface Sci. 16, 350–356. https://doi.org/10.1016/j.cocis.2011.01.010